School of Chemical, Environmental and Mining Engineering

Gas-liquid two-phase flow in inclined pipes

By

Valente Hernandez Perez

Thesis submitted to The University of Nottingham

for the degree of Doctor of Philosophy,

September 2007

Abstract

In order to understand the behaviour of two-phase flow in inclined pipes, an extensive programme of work has been undertaken using the Inclinable Facility in the laboratories of the School of Chemical, Environmental and Mining Engineering at the University of Nottingham. The test pipe (6.5 m long) could be positioned at angles between -20° downwards and vertical upwards. Two pipe diameters were used; namely 38 mm and 67 mm. The fluids used were air and water. Superficial velocities for air ranged from 0.15 to 8.9 m/s and from 0.04 m/s to 0.7 m/s for water. Time series of liquid holdup (using capacitance probes) and pressure drop (differential pressure transducer) were measured. In addition, a high speed video system was used in order to obtain image sequence of the flow under different selected conditions.

It was found that for upward inclined flow most of the experiments fall within the slug flow regime whereas for inclined downward flow the dominant flow pattern is stratified flow. For horizontal flow, the flow regime depends more on the gas and liquid superficial velocities. Data for liquid holdup, pressure drop, frequency and translational velocity of periodical structures are reported. Comparisons with literature correlations and data are performed as well. Frequency was found to be strongly affected by inclination angle and a correlation has been proposed.

An effect of the pipe diameter is also found under certain flow conditions mainly on the liquid holdup, pressure drop and structure velocity. Increase of pipe diameter displaces the bubbly-slug transition to the right hand side on the flow pattern map for inclined flow, and for horizontal pipe the stratified-slug transition is moved up.

In addition, a CFD code has been used to successfully model the hydrodynamics of the slug flow pattern, using the Volume of Fluid model based on the Euler-Euler approach. The modeling results are validated with the experiments and also provide more detailed information on the flow such as the velocity field.

Acknowledgements

I would like to express my gratitude to Prof. Barry Azzopardi for his supervision. His guidance and his trust also outside of the supervision of this work have given me uncommon opportunities. I would like to acknowledge Dr. H. P. Morvan for his technical suggestions on the CFD modelling. I am also grateful to Marco Da Silva for the support with the wire-mesh experiments.

My sincere thanks also to the technical staff of SChEME. In particular, I thank the technicians of the workshop in laboratory 3 (Mel, Mick, Fred, Phil, Marion, Reg and Jim). In particular I would like to thank Fred Anderton who developed the capacitance probes among other arrangements.

Special thanks to Vas, Ryu, Karl, Bayo, Paiza, Giorgio, Mario, Sadanah for the great times we shared. Many thanks to all my colleagues in the Research Postgraduate room B06 that have finished and started the experience of a PhD during my time at Nottingham University. They have been giving me friendship, encouragement, understanding and much help in academia. I wish them a successful career in their future.

Thanks to the Mexican Council for Science and Technology (CoNaCyT) for providing me the financial support to carry out my PhD. Thanks to Secretaria de Educación Publica (SEP) Mexico for financial support. In addition, this work has been undertaken within the Joint Project on Transient Multiphase Flows.

Finally but not less I would like to thank all my family and friends for their constant support and contact while far away.

Table of contents

List of figures

List of tables

Chapter 1

Introduction

Multiphase flows are of great interest to a large variety of industries. The power generation, nuclear reactor technology, food production, chemical process, petroleum, aerospace and automotive industries are all driving forces in this complex field. This work is concerned only with gas-liquid flows in inclined pipes with particular interest towards oil and gas industry applications.

1.1 Multiphase flow in pipes

The mixtures of two fluids in pipes are frequently encountered. Flow instabilities may cause the mixture to arrange itself into different geometric configurations. These geometric configurations are usually referred to as flow patterns or regimes. A little reflection will show that the orientation of the pipe makes a difference in the flow regime because of the role played by gravity and the density difference between the two fluids.

1.2 Flow patterns in gas-liquid pipe flow

When a gas-liquid mixture flows along a pipe, different flow patterns can be produced, influenced by several variables. Many flow patterns have been named in vertical, horizontal and inclined gas/liquid flow in pipes.

1.2.1 Flow patterns in horizontal systems.

Flow regimes in horizontal flow are illustrated in Figure 1.1. Here, as gravity acts perpendicular to flow direction, separation of the flow might occur. The respective flow regimes are stratified flow, where the gravitational separation is complete;

stratified-wavy flow; bubble flow, where the bubbles are dispersed in the liquid continuum; annular dispersed flow, which is similar to that in vertical flow, though there is asymmetry in the film thickness due to the action of gravity; and a variety of intermittent flows. This latter category includes plug flow, in which there are large bubbles flowing near the top of the tube; semi-slug flow, where very large waves are present on the stratified layer; and slug flow, where these waves touch the top of the tube and form a liquid slug which passes rapidly along the channel.

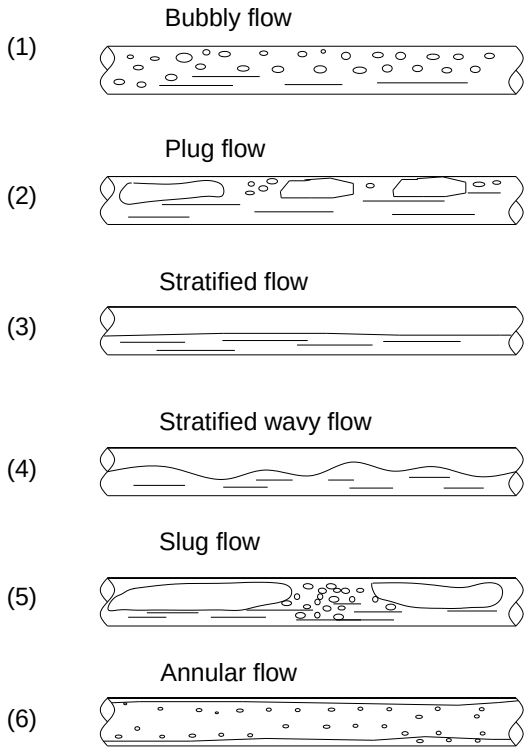

Figure 1.1 Two-phase flow patterns in horizontal pipes

It is often necessary to predict regimes, and the usual procedure is to plot the information in terms of a flow regime map. Many of these maps are plotted in terms of primary variables (superficial velocity of the phases or mass flux and quality, for instance), but there has been a great deal of work aimed at generalizing the plots, so that they can be applied to a wide range of channel geometries and physical properties of the fluids.

1.2.2 Flow patterns in vertical systems.

The major flow patterns encountered in vertical co-current flow of gas and liquid (bubbly, slug, churn, and annular) are shown schematically in figure 1.2.

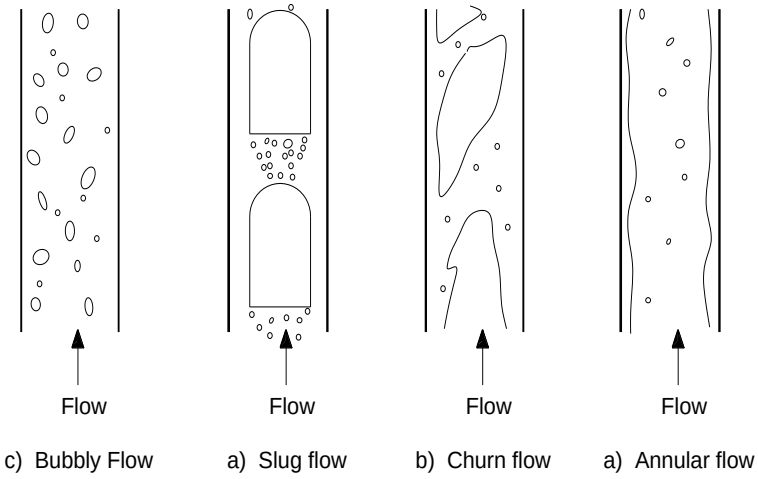

Figure 1.2 Flow patterns in vertical upward flow

At low gas flow rates, the gas phase tends to rise through the continuous liquid medium as small, discrete bubbles, giving rise to the name bubbly flow. As the gas flow rate increases, the smaller bubbles begin to coalesce and form larger bubbles. At sufficiently high gas flow rates, the agglomerated bubbles become large enough to occupy almost the entire pipe cross section. These large bubbles, known as "Taylor bubbles," separate the liquid slugs between them. The liquid slugs, which usually contain smaller entrained gas bubbles, provide the name of the flow regime. At still higher flow rates, the shear stress between the Taylor bubble and the liquid film increases, finally causing a breakdown of the liquid film and the bubbles. The resultant churning motion of the fluids gives rise to the name of this flow pattern.

The final flow pattern, annular flow, occurs at extremely high gas flow rates, which cause the entire gas phase to flow through the central portion of the tube. Some liquid is entrained in the gas core as droplets, while the rest of the liquid flows up the wall through the annulus formed by the tube wall and the gas core.

1.2.3 Flow patterns in upward inclined systems.

Flow patterns observed in upward inclined flow are quite similar to those observed in vertical upward flow, especially for near-vertical systems. They include bubbly and dispersed bubbly, slug, churn and annular flow in inclined systems, Figure 1.3.

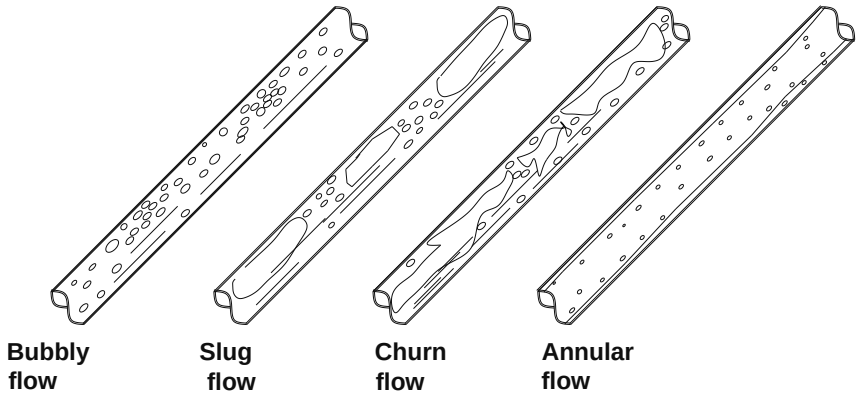

Figure 1.3 Flow patterns of co-current gas/liquid flow in inclined pipes.

For systems deviated more than 20° from vertical, churn flow is rarely observed. For near horizontal systems, the bubbly flow pattern is sometimes absent. Indeed, Taitel *et al.* (1978) contended that for systems deviated more than 50° from vertical, bubbly flow never occurs. Additionally for near-horizontal systems, stratified flow is observed.

1.2.4 Flow patterns in downward two-phase flow

Downward simultaneous flow of gas and liquid, although rare, is important in the chemical process industry and also in petroleum production. An example of two-phase down flow is the injection of wet steam in thermal recovery.

Barnea *et al.* (1982) studied the flow pattern transition for downward inclined two phase flow; horizontal to vertical. They found that increasing the inclination angle strongly affects the interface shape which varies from a smooth for zero inclination to wavy stratified at higher inclinations and to nearly axially-symmetric annular flow for inclination angles approaching the vertical.

1.3 Motivation

In the literature the majority of information on two-phase flow is for vertical and horizontal pipes. There is a moderate amount on pipes inclined a few degrees from the horizontal and data for large inclinations are much more sparse. Papers on flow patterns in steeply inclined flow have been published by Spedding and Nguyen (1976), Barnea *et al.* (1985) and Mukherjee and Brill (1985). Most of the data involved is from air-water experiments. Pressure drop data has been published by Beggs and Brill (1973) and Spedding *et al.* (1982). The last two sources also provided void fraction (1 - liquid holdup) data.

1.4 Aims of study

The study of gas-liquid flow includes the prediction of the principal variables – liquid holdup, frequency, structure velocity and pressure gradient – as a function of the inclination angle and the flow conditions. Hence, this work is aimed at addressing aspects of two-phase gas/liquid flow in inclined pipes, in particular, the case of slug flow. This involves:

- Calibration of the capacitance probes needed for measuring the liquid holdup
- Report of new data for gas liquid flow in inclined pipes
- Study of the effect of the pipe diameter on slug flow features
- Modelling the hydrodynamics of slug flow with Computational Fluid Dynamics (CFD) techniques.

1.5 Structure of the thesis

This work is divided into 7 chapters as described below and some other relevant information is provided in appendices:

Chapter 1 provides an introduction to the thesis, defining the problems, aims of the study and structure of the thesis.

Chapter 2 contains a review of published work on two-phase flows in pipelines. The flow patterns and flow pattern maps for the horizontal, vertical, and inclined pipes are described. Particular emphasis is given to models available for predicting the liquid holdup, pressure drop, and slug characteristics and the current state of research activity into the potential applications of Computational Fluid Dynamics (CFD) in gas-liquid flow.

Chapter 3 describes the experimental apparatus; the properties of fluids used and the technique for measurements of liquid holdup and pressure drop. This chapter also includes a brief description of important facility components such as the data acquisition software and instrumentation.

Chapter 4 presents the experimental results obtained in the experiments performed with a 38 mm pipe. The signal analysis that has been performed in order to process the data is explained together with the discussion of the data.

Chapter 5 focuses on experimental results obtained with 67 mm pipe. In addition, the effect of pipe diameter is studied by means of a comparison between the results obtained in both 38 mm and 67 mm pipes.

Chapter 6 is dedicated to the modelling results obtained with Computational Fluid Dynamics for the slug hydrodynamics. Comparison between the experiment and the modelling is performed in order to validate the modelling results.

Chapter 7 Brings together all the key conclusions from this work. Recommendations for further work are also provided.

Chapter 2

Literature review

In the literature, extensive studies exist on horizontal and vertically upwards gas-liquid flow. These include models and correlations for flow pattern transitions, pressure drop and liquid holdup among other parameters. Commercial pipelines, however, follow normal terrain variations and consist almost entirely of uphill and downhill inclined sections, and therefore the models and correlations developed for horizontal or vertical flow are not always applicable, Hasan and Kabir (1988). Pipe inclination adds another dimension to the already complex flow phenomena, generally observed in horizontal and vertical pipes.

This chapter aims at highlighting the most relevant aspects related to the state of the art in the field on two-phase flow in inclined pipes. These are included in the following sections: 2.1 Flow pattern identification techniques, 2.2 Flow pattern maps, 2.3 Liquid holdup, 2.4 Pressure drop, 2.5 Slug flow characteristics and 2.6 Computational Fluid Dynamics.

2.1 Flow pattern identification

The simplest way to determine the gas liquid flow pattern is to merely observe them flowing along transparent pipes. Where this is not feasible because of high gas and liquid flow rates, high-speed photography is employed. Those methods are of no use within an actual system because industrial pipelines are generally not transparent. Other techniques are briefly described below.

2.1.1 Photon attenuation Technique

Photon attenuation technique has been widely applied and is based on the absorption of X-rays or γ-rays by the liquid phase and its relationship to the void fraction. The rays can either come along a single beam as used by Jones and Zuber (1975) or from any array of multiple beams across the flow path. It was their significant work using X-ray absorption, which highlighted the usefulness of statistical analysis techniques for flow pattern determination. Typical probability density functions of the void fraction variations they used to identify flow patterns are shown in Figure 2.1.

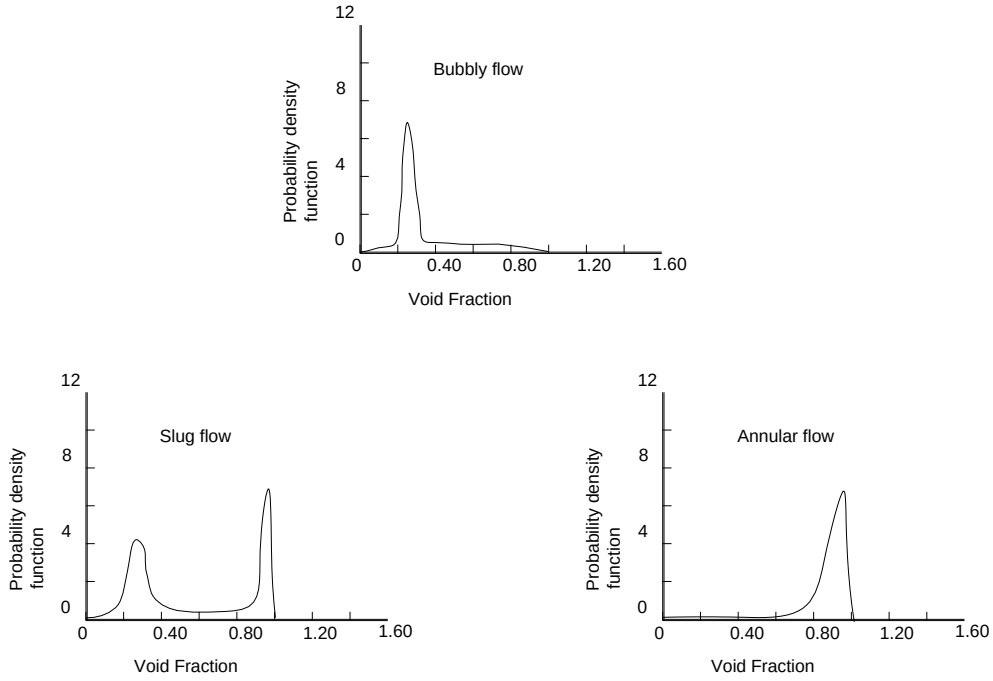

Figure 2.1 X-ray absorption Probability Density Functions of void fraction by Jones and Zuber (1975)

2.1.2 Pressure fluctuations

Hubbard and Dukler (1966) were the first researchers to analyze pressure fluctuations in an attempt to try and identify flow patterns. Using experimental data from a horizontal air-water flow facility they developed a method to determine the flow pattern from the spectral distribution of the wall pressure fluctuations. Figure 2.2 shows the three basic spectral distributions they observed.

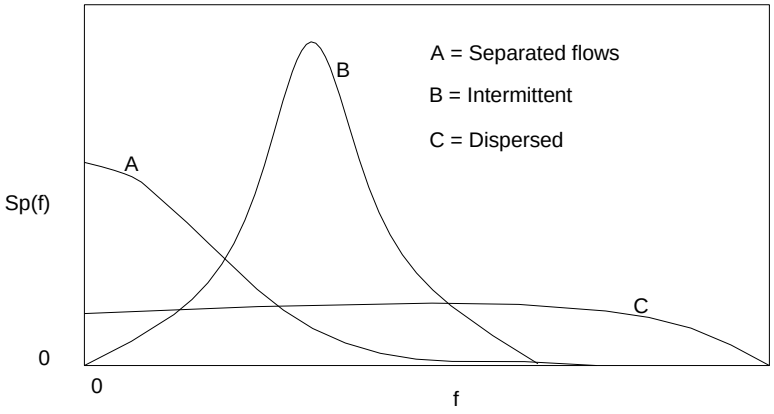

Figure 2.2 Power spectral density of wall pressure fluctuation from Hubbard and Dukler (1966)**.**

Type A distributions, which are characteristics of turbulent flows with a maximum zero frequency, correspond to stratified and low entrainment annular flows. Type B spectrum corresponds to intermittent flows, showing features typical of periodic processes. Finally, type C distributions relate to bubbly or mist flows, with a spectral characteristic of white noise. It can be noted that more complex flow patterns can be considered to be superimposition of two basic patterns.

2.1.3 Electrical tomography

The field of electrical tomography can be separated into two distinct regions based on the method by which the electrical field is produced, either conductance or capacitance. The choice will be based primarily on the electrical properties of the fluids, whether they conduct or not.

2.1.3.1 Conductance tomography

Conductance tomography consists of multiple conductance probes flush-mounted and evenly distributed around the entire pipe interior. There are essentially two methods of measurements, either using a constant current and measuring the resulting potential at the other electrodes, or applying a constant potential between two electrodes and measuring the induced current. Since there is a need for the electrodes to be in direct electrical contact with the conducting fluid, tomographic imaging of certain flow patterns, for example slug flow, can not be achieved with this flush-mounted method.

To overcome this shortfall Reinecke *et al.* (1998) proposed an extension of the conductance approach that used wire-mesh electrodes. Their arrangement, shown in Figure 2.3, consisted of three planes of 29 thin wires each with a diameter of 0.1 mm. The planes are set 3mm apart and the wires of two successive planes from an angle of 60º.

By measuring the impedance between all pairs of adjacent wires in the same plane as a projection of the conductivity distribution along the direction of the wires is obtained. For each plane, the impedance measurement is carried out with a high frequency (1000 Hz) alternating current, with the sampling of the individual electrode pairs performed by a multiplex unit. This process results in three independent projections, which are then transformed into the conductivity distribution and then further interpreted as the void fraction distribution.

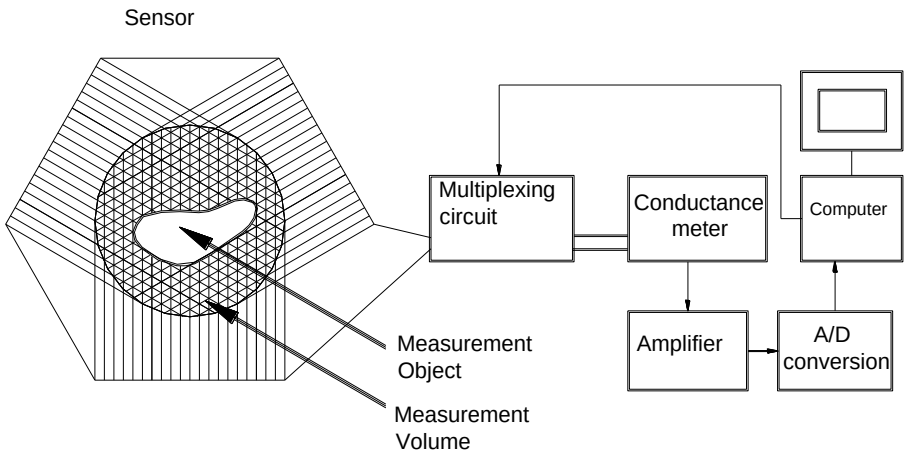

Figure 2.3 Schematic representation of the measuring chain for wire mesh tomographic measurement technique by Reinecke *et al.* (1998).

The main disadvantage of the approach of Reinecke *et al.* (1998) was, according to Prasser *et al.* (1998), the image reconstruction step, both in terms of the time overhead and the undetermined nature of the equations needed to be solved. In view of this, Prasser *et al.* (1998) presented a new wire sensor for fast tomographic imaging without the need for time consuming and potentially inaccurate image reconstruction procedures.

The sensor, shown schematically in Figure 2.4, used two electrodes planes 1.5 mm apart, one for transmitting and the other for receiving signals. Each plane consisted of sixteen 0.12 mm diameter electrode wires, producing a grid of 16x16 measurements points evenly distributed across the pipe cross-section. The grid had a free area of approximately 96 %, with a negligible pressure drop. In one measurement cycle, the transmitter electrodes are activated by a multiplex circuit in successive order.

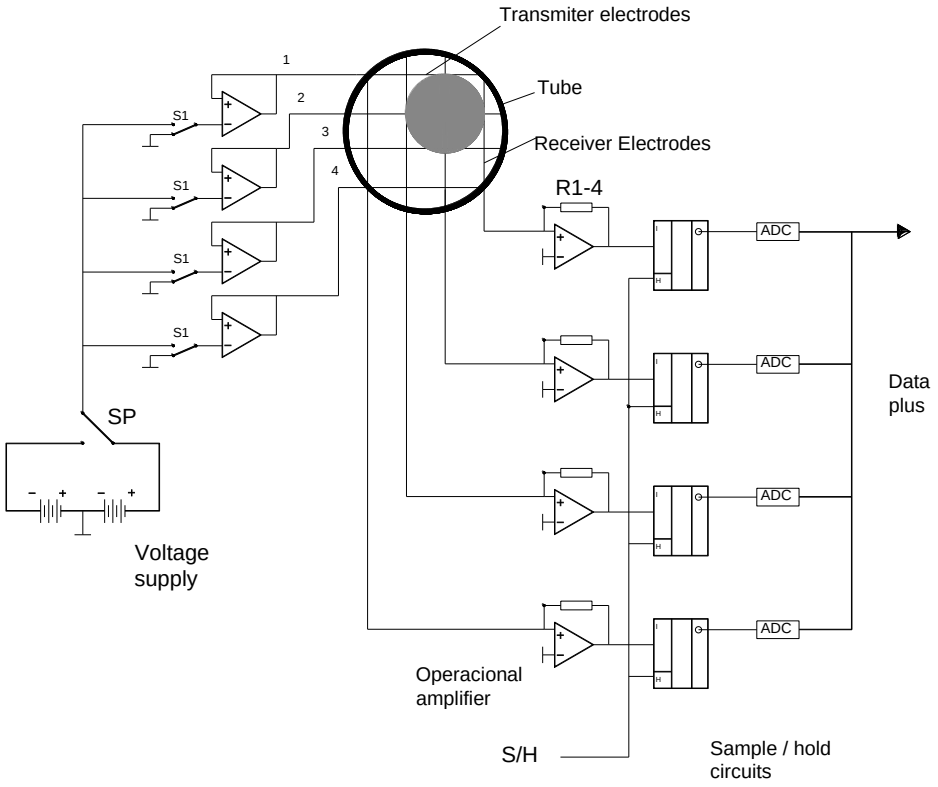

Figure 2.4 Simplified scheme of the two-plane electrode-mesh device used by Prasser *et al.* (1998).

2.1.3.2 Capacitance tomography

Electrical capacitance tomography (ECT) is a non-invasive technique since the sensing electrodes are not in contact with the fluid under observation but are located around the pipe exterior. The imaging parameter, the permittivity, is the dielectric property of each of the phases in the two-phase system. An ECT image can be reconstructed based on the permittivity distribution obtained from the measurements of the electrical capacitance taken between all possible pairs of electrodes. ECT has been used by Baker (2003) for horizontal flow.

2.2 Flow pattern maps

The following section will summarise the physical models that allow the analytical prediction of the flow patterns and the transition boundaries in steady state two-phase gas-liquid flow.

2.2.1 Flow pattern maps in horizontal

Many flow regime maps have been produced for two-phase flow in horizontal pipes. Baker (1954) gave a map based on flow in small diameter pipes using several fluids. The axes of the map involved the mass fluxes of the phase together with the fluid properties, including density and surface tension. Mandhane *et al.* (1974) studied two-phase flow in small diameter and constructed a map based on superficial gas and liquid velocities. This type of map is now the most widely used. Taitel and Dukler (1976) produced a theoretical, mechanistic flow regime map and this is widely used but with modifications to the calculation of the interfacial friction factor.

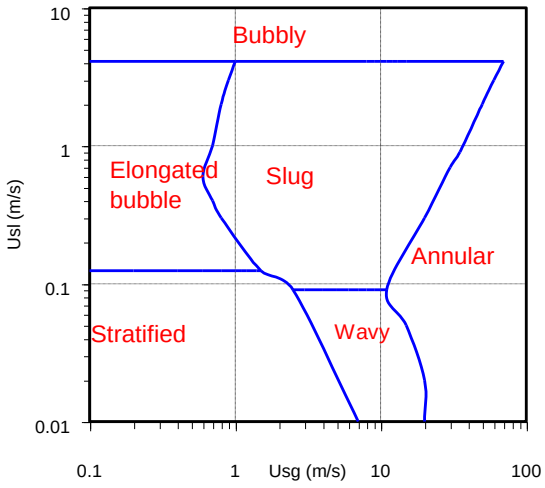

Figure 2.5 Horizontal flow pattern map of Mandhane *et al.* (1974) for horizontal tube 50 mm diameter air-water 25° C.

2.2.2 Flow pattern maps in vertical

For vertical flow the flow pattern map of Taitel *et al.* (1980) is the most popular one. But other flow patterns have been developed such as those of Bilicki and Kestin (1987), and Barnea *et al.* (1982) for vertical downward flow.

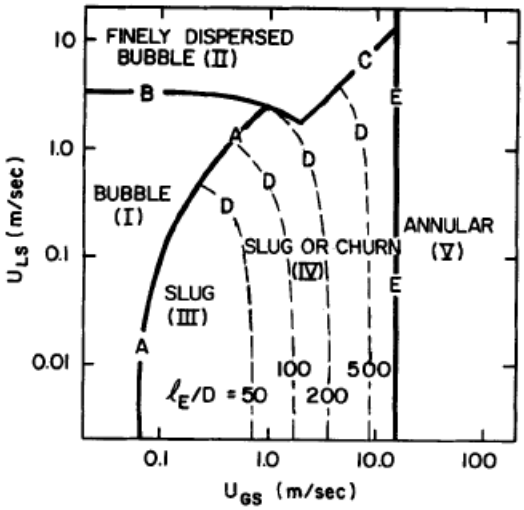

Figure 2.6 Vertical flow pattern map of Taitel *et al.* (1980) for vertical tube 50 mm diameter air-water 25° C.

2.2.3 Flow pattern maps in inclined

There are very few data sets or correlations available for flow pattern transition in inclined systems. Physical modelling of such systems is even scarcer. Gould *et al.* (1974) published flow pattern maps for horizontal and vertical flow and for up-flow at 45° inclinations. Mukherjee and Brill (1985) reported extensive data on inclined two-phase flow. Spedding and Nguyen (1976) compared the flow regime maps developed by others with air-water experimental data for conditions from vertically downward flow to vertically upward flow.

The work of Weisman and Kang (1981) is a major contribution in this area. Their basic principle is that the boundaries of flow patterns at high flow rates are usually unaffected by pipe deviation (e.g. the transitions to annular flow and dispersed bubbly flow). They claim this observation extends all the way from vertical to horizontal. Their simplified correlation for transition to annular flow, for all inclination angles, is given by

$$(\mathrm{Fr}_{SG})(\mathrm{Ku}_{SG}) = 25\left(\frac{U_{SG}}{U_{SL}}\right)^{0.625} \tag{2.1}$$

Where both the Froude number, $\mathrm{Fr}_{SG}(=U_{SG}^2/gd)$ and the Kutadelaze number, Ku_{SG}, are based on gas superficial velocity, U_{SG},

$$\mathrm{Ku}_{\mathrm{SG}} = \frac{U_{SG}}{\left[g(\rho_L - \rho_G)\sigma\right]^{0.25}} \tag{2.2}$$

Their transition to dispersed bubbly flow for all angles of inclination is given by

$$\left[\frac{\left(-dp/dz\right)_L}{g(\rho_L - \rho_G)}\right]^{0.5}\left[\frac{g(\rho_L - \rho_G)d^2}{\sigma}\right]^{0.5} \geq 9.7 \tag{2.3}$$

Where $(dp/dz)_L$, is the frictional pressure gradient of liquid flowing alone in the pipe. Predictions of Weisman-Kang correlation for the transition to dispersed bubbly flow are similar to those of Taitel *et al.* (1978) in vertical flow. Both correlations suggest a mixture velocity of about 3 m/s for air-water systems at standard conditions, for transition to dispersed bubbly flow. The Weisman-Kang correlation indicates independence of this transition to gas velocity; whereas Taitel *et al.* (1978) does not.

The stratified-wavy and separated-intermittent transitions are given respectively by

$$Fr_G^{1/2} = 0.25(U_{SG}/U_{SL})^{1.1} \tag{2.4}$$

$$\left(\frac{\sigma}{g\,d^2\,\Delta\rho}\right)^{0.20}\left(\frac{d\,G_G}{\mu_G}\right)^{0.45} = 8\left(\frac{U_{SG}}{U_{SL}}\right)^{0.16} \tag{2.5}$$

Following the Barnea *et al.* (1980) approach for horizontal and slightly inclined systems, Weisman and Kang (1981) did not distinguish churn from slug flow but lumped these two flow patterns together as intermittent flow. Their approach transition between bubbly and intermittent flow uses Froude numbers, based on U_{SG} and U_m, as the correlating parameters. Their transition expression is given by

$$\frac{U_{SG}^2}{g\,d} = 0.2\left[\frac{U_m}{g\,d}\right]^{1.56}\left(1 - 0.65\cos\theta\right)^2 \tag{2.6}$$

The last term, $(1\text{-}0.65 \cos \theta)^2$, accounts for the effect of inclination.

Figure 2.7 presents the generalized flow pattern map of Weisman and Kang (1981). The basic map, with U_{SL} and U_{SG}, as the axes is for two-phase flow in a horizontal system with particular (standard) values of fluid properties and system dimensions. The parameters ϕ_1 and ϕ_2 are used to make the map general, not only for all fluids but also for inclination angles. The expressions for ϕ_1 and ϕ_2 as reported by Weisman and Kang (1981) are reproduced in Table 2.1.

Table 2.1 Parameters for the Weisman and Kang flow pattern map.

Flow orientation	**Transition to**	ϕ_1	ϕ_2
Horizontal, vertical and inclined	Annular flow	$(\rho_{SG}/\rho_G)^{0.23}$ $(\Delta\rho/\Delta\rho_s)^{0.11}$ $(\sigma/\sigma_S)^{0.11}$ $(d/d_s)^{0.415}$	1.0
	Disperse flow	1.0	$(\rho_L/\rho_{sL})^{-0..33}$ $(d/d_s)^{0.16}$ $(\mu_{sL}/\mu_L)^{0.09}$ $(\sigma/\sigma s)^{0.24}$
Horizontal flow	Wavy-stratified	$(d_s/d)^{0.17}\ (\mu_{sG}/\mu_G)^{1.55}$ $(\rho_{sG}/\rho_G)^{1.55}\ (\Delta\rho_{sG}/\Delta\rho_G)^{0.69}$ $(\sigma_{sG}/\sigma_G)^{0.69}$	1
Horizontal and slightly inclined flow	Separated-intermittent	1	$(d/d_s)^{0.45}$
Vertical and inclined	Bubbly-Intermittent	$(d/d_S)^n$ $(1\text{-}0.65\cos\theta)$ $n=0.26e^{-0.17}$	1.0 ν_{sL}/ν_{ssL}
S denotes standard conditions, ds=1.0 in, ρ_{sg}=0.0013 kg/l, ρ_{sL}=1 kg/l, σ_s=70 dynes/cm, ν_{ssL}=1 ft/s			

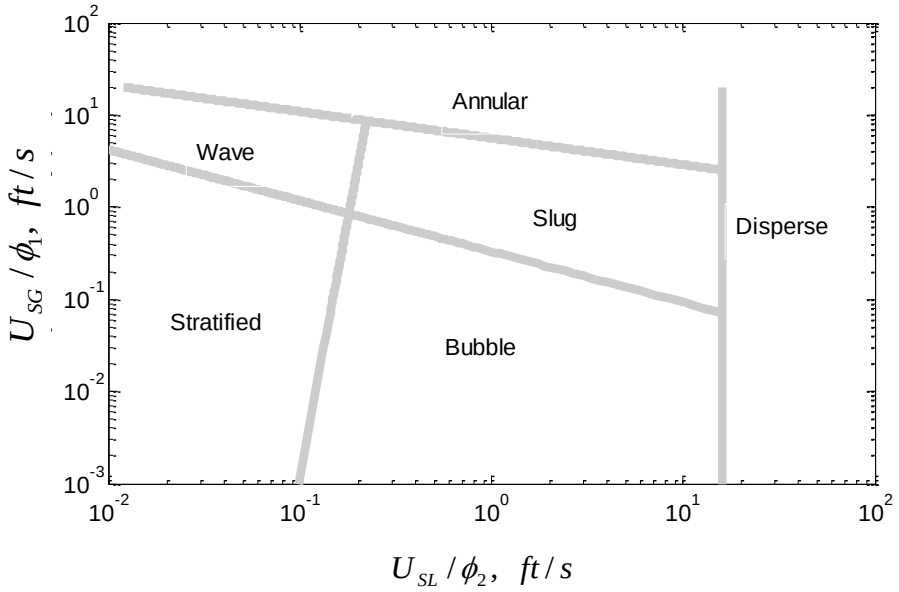

Figure 2.7 Generalized flow pattern map of Weisman and Kang (1981).

Barnea *et al.* (1985) summarised the most remarkable models for predicting flow pattern transitions in inclined gas-liquid flows. They also suggested a logical path for systematic determination of flow patterns that covers the whole range of upward inclinations from horizontal to vertical. More recently other transition criteria have been developed as presented below with data and analysis from various authors.

Transition from bubbly to slug flow

Physical analysis for the transition from bubbly to slug flow, presented by Hasan and Kabir (1988) follows an approach as for vertical systems. For vertical systems, when the void fraction exceeds *0.25*, transition from bubbly flow generally occurs. For an inclined pipe, the gas phase tends to flow along the upper wall. Thus, near the upper wall, the in-situ void fraction may exceed the value of *0.25*, as a result collisions among the bubbles increase sharply, forming Taylor bubbles, and the transition to slug flow occurs at a cross sectional average void fraction lower than *0.25*.

Assuming that in an inclined pipe the actual cross sectional area available for the gas to flow is the projection of the area in a horizontal plane and A is the cross-sectional area, the area available for the gas flow through a pipe inclined at an angle θ, to the horizontal is $A\sin\theta$, and the actual superficial velocity of the gas phase is

$$\left(U_{SG}\right)_{\theta} = \frac{Q_G}{A\sin\theta} = \frac{U_{SG}}{\sin\theta} \tag{2.7}$$

By applying the equation for holdup in vertical systems to an inclined pipe, the local volume fraction, α_G, near the upper wall is obtained

$$\alpha_G = \frac{\left[U_{SG} \big/ \sin\theta\right]}{Co\left[U_{SL} + U_{SG} \big/ \sin\theta\right] + U_{\infty}} \tag{2.8}$$

By rearranging and using $\alpha_G = 0.25$ at transition,

$$U_{SG} = \left[\frac{Co\ \alpha}{1 - Co\ \alpha} U_{SL} + \frac{Co\ \alpha}{1 - Co\ \alpha} U_{\infty}\right] \sin\theta = \left[0.43 U_{SL} + 0.357 U_{\infty}\right] \sin\theta \tag{2.9}$$

and

$$U_{\infty} = 1.53\left[\frac{g\,\sigma_L(\rho_L - \rho_G)}{\rho_L^2}\right]^{1/4} \tag{2.10}$$

The bubble rise velocity, U_{∞}, determined by the balance of the buoyancy and drag forces, might be different for an inclined pipe from that in a vertical one. The buoyancy force decreases as the pipe is deviated from vertical, which tends to reduce the bubble rise velocity. However the deviation from vertical also makes the bubble nose sharper. A sharper bubble nose causes a decrease in the drag force on it. Thus the influence of pipe inclination on the terminal rise velocity of the bubble can be negligible.

Barnea *et al.* (1985) also extended their analysis for transition in vertical systems, to inclined systems, by replacing the terminal rise velocity of the bubble with $U_{\infty}\sin\theta$. For example, they suggested that transition from bubbly flow occurs when U_{SG} is greater than $0.33U_{SL} + 0.25\sin\theta\, U_{\infty}$. .They also pointed out that preferential migration of bubbles to the upper part of a deviated pipe leads to a limited inclination angle

beyond which bubbly flow can occur. By equating buoyancy to lift forces, they proposed that when the inclination (from horizontal) is less than that given by the expression (2.11) bubbly flow can not exist.

$$\frac{\cos\theta}{\sin\theta} = \frac{3}{4}\cos 45^{\circ}\frac{U_{\infty}}{g}\left(\frac{C_L\gamma^2}{d}\right) \tag{2.11}$$

For the lift coefficient C_L, Barnea *et al.* (1985) recommended a value of *0.8*, while the distribution coefficient, γ, varies between *1.1* and *1.5*. For air-water flow through a *51 mm* internal diameter pipe at standard conditions, equation (2.11) suggests that the maximum tube inclination for bubbly flow is about 55° to 70°.

In addition to deviation, pipe diameter also imposes a restriction on the occurrence of bubbly flow. The well diameter must be large enough to satisfy the condition that the Taylor-bubble rise velocity is greater than that of the small bubbles, i.e. $U_{\infty T} > U_{\infty}$. For vertical flow, this condition results in a well diameter that must exceed the value given by equation 2.12. Barnea *et al.* (1985) suggested the same expression for deviated channels.

$$d_{\min} = 19.01\left[\frac{(\rho_L - \rho_G)\sigma_L}{\rho_L^2 g}\right]^{1/2} \tag{2.12}$$

Transition to Churn Flow: The chaotic nature of churn flow pattern makes modelling the dynamics of this flow regime very difficult. Kaya *et al.* (2001) presented an analysis that appears promising and is well supported by data. They noted that the transition to churn flow occurs when the gas volume fraction, α exceeds *0.78*. They also argued that the average α in this flow regime may be approximated, following the drift flow approach, as given by

$$\alpha = \frac{U_{SG}}{C_0 U_m + U_{\infty T\theta}} \tag{2.13}$$

With the transition α of 0.78 and C_0=*1.2* they arrived at the expression for U_{SG}, in which churn flow will occur,

$$U_{SG} = 12.19\left(1.2U_{SL} + U_{\infty T\theta}\right) \tag{2.14}$$

Transition to dispersed bubbly flow: Barnea *et al.* (1985) recommended the same criteria developed for vertical systems in inclined tubes.

$$2\left[\frac{0.4\sigma_L}{(\rho_L-\rho_G)g}\right]^{1/2}\left(\frac{\rho_L}{\sigma_L}\right)^{3/5}\left[\frac{f}{2d}\right]^{2/5}(U_{SL}+U_{SG})^{1.2} = 0.725 + 4.15\left(\frac{U_{SG}}{U_{SL}+U_{SG}}\right)^{0.5} \tag{2.15}$$

Transition to annular flow: Following the approach of Taitel *et al.* (1980), Barnea *et al.* (1985) presented an analysis that results in the expression for transition to annular flow, which is written as:

$$U_{SG} = 3.1\sin\theta^{1/4}\left(g\sigma(\rho_L-\rho_G)/\rho_G{}^2\right) \tag{2.16}$$

Equation (2.16) shows that the superficial gas velocity, needed for transition to annular flow, depends on the one-fourth power of the sine of the inclination angle.

The work of Weisman and Kang (1981) shows that, with the exception of bubbly slug flow transition, the transition criteria established for vertical systems are apparently applicable to inclined systems. However the criterion proposed by Kaya *et al.* (2001) for transition to churn flow indicates slight dependence of this transition on well deviation. The work of Barnea *et al.* (1985) also shows that the transition to annular flow is mildly affected by the channel inclination angle.

2.3 Liquid Holdup in inclined conduits

The liquid holdup is a major parameter of interest in the study of co-current pipe flow of two-phase mixtures. Since the two phases do not generally flow at the same velocity, the in-situ volume fraction will almost invariably be different from that at the inlet of the pipe. Two methods widely used in the petroleum industry for the design of

two-phase pipelines are those of Baker (1957) and Flanigan (1958). In Figure 2.8, the Baker and Flanigan correlations for H_L are shown.

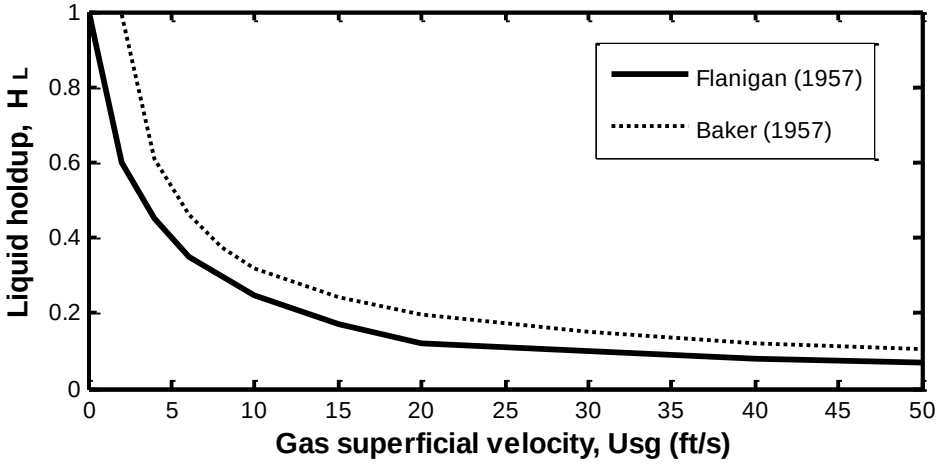

Figure 2.8 Baker (1957) and Flanigan (1958) correlations for H_L

The Baker line is defined by the relation

$$H_L = 1.61\ U_{SG}^{-0.70} \tag{2.17}$$

with U_{SG} in ft/s. The other line is based on a set of coordinates presented by Flanigan. For superficial gas velocities of less than 10 ft/s there is clearly a substantial difference in these two correlations.

Guzhov *et al.* (1967) proposed that the in situ liquid volume fraction, E_L, could be determined from knowledge of the input liquid volume fraction, C_L and the Froude number based on the mixture velocity, U_m.

$$Fr_m = \frac{U_m}{\sqrt{gd}} \tag{2.18}$$

Using data for a pipe angle of 9° to the horizontal, they obtained a series of straight lines all converging at C_L=E_L=1, Figure 2.9. All points for which $Fr_m \geq 4$ were found to lie on a single straight line.

On the basis of these results, they proposed the expression,

$$E_G = 0.81\, C_G (1 - \exp(-2.2\sqrt{Fr_m})) \tag{2.19}$$

Which they claim is applicable for pipe inclinations up to 9° from the horizontal. Equation (2.19) can be written in terms of the liquid volume fraction as

$$E_L = 1 - 0.81(1 - C_L)(1 - \exp(-2.2\sqrt{Fr_m})) \tag{2.20}$$

And for large values of Froude number reduces to

$$E_L \approx 0.19 + 0.81 C_L \tag{2.21}$$

It is evident from equation (2.20) that this correlation predicts that the smallest value of the in-situ liquid holdup expected for pipe inclinations of up to 9° is 0.19.

Greskovich (1973) suggested a simplified procedure based on the fact that straight lines were obtained by Guzhov *et al.* (1967) for a given mixture Froude number on a plot of E_L vs C_L, Figure 2.9. Since at C_L=1, all of these lines converge at E_L=1, Greskovich (1973) suggested that only the intercept corresponding to C_L=0 needed to be measured in order to establish the whole line for a given Froude number. He proposed that this could be achieved by flowing gas through an initially liquid filled pipe and measured the resulting liquid holdup when an apparent equilibrium has been obtained. Under this conditions there is no actual liquid flow and C_L=0. However one can still view the Froude number based on the gas velocity as a mixture Froude number at that point. Hence the entire line for a mixture Froude number equal to the particular Froude number based on the gas velocity can be obtained by drawing the straight line through the measured E_L at C_L=0 and the point E_L=C_L=1.

Greskovich also presents data for C_L=0 for pipe inclinations of 2°, 6° and 10°. These data show a significant inclination effect on the measured holdup which varies from

0.13 to 0.22 for Fr_m=0.4 and 0.32 to 0.41 for Fr_m=2.0. It can be noted that this is in disagreement with Guzhov et al. claim that there is little angle effect on holdup.

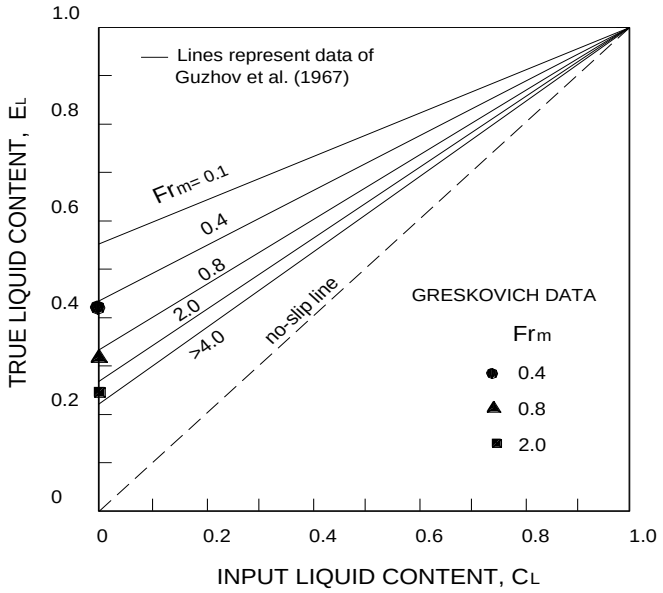

Figure 2.9 In situ liquid volume fraction correlation of Guzhov *et al.* (1967)

Gregory (1974) tested Guzhov correlation and showed that it was not reliable at low values of liquid holdup, whereas the commonly used correlations of Baker and Flanigan are subject to large errors. He recommended that the correlation of Guzhov should be used unless it predicts values less than 0.25.

Mattar and Gregory (1974) studied air-oil slug flow in an upward inclined pipe at angles of inclinations varying from 0 to 10°; they obtained data for parameters such as liquid holdup and bubble rise velocity. They proposed the following relation for liquid holdup.

$$H_L = 1 - \frac{U_{SG}}{1.3(U_{SG} + U_{SL}) + 0.7} \tag{2.22}$$

Other works on liquid holdup includes Kokal and Stanislav (1989), who focus on slightly inclined pipes and used oil-air two-phase flow with a 25 m long acrylic pipe. More recent contributions include those of Grolman and Fortuin (1997) who provided liquid holdup and pressure drop data for inclined pipes of 26 and 51 mm diameter, at inclination angles between 0.1° and 6.0°.

2.4 Pressure drop in inclined pipes

Pressure drop along a deviated pipe is associated with gravitational body force, acceleration forces and frictional shear stress. A momentum balance on a section of a two-phase flow (Figure 2.10) will produce a basic pressure gradient equation as shown below. The following equation shows the three major components of the pressure gradient.

$$-\frac{dP}{dz} = -\frac{dP_{fric}}{dz} - \frac{dP_{acc}}{dz} - \frac{dP_{grav}}{dz} \tag{2.23}$$

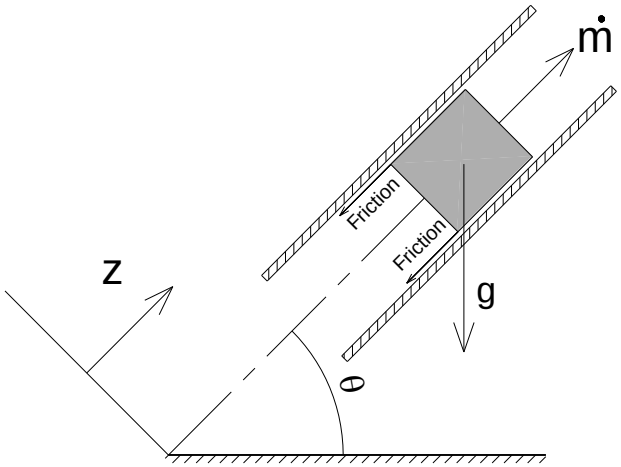

Figure 2.10 Pressure gradient diagram

The resulting two-phase flow integral momentum equation of (2.23) is shown below:

$$\int_A -\frac{dP}{dz}\,dzdA + \int_p -\tau_0\,dzdp + \int_A -\rho g\,dzdA = \int_A \frac{d}{dz}\left(m_L U_L + m_G U_G\right)dzdA \tag{2.24}$$

Mattar and Gregory (1974) proposed the following model for the pressure drop

$$\frac{\Delta P}{L} = \frac{\rho_m \frac{g}{g_c}\sin\theta + 2\frac{f\,\rho_{mE}\,U_m^{\,2}}{g_c d}}{1 - \frac{\rho_m U_m U_{SG}}{g_c P}} \tag{2.25}$$

Where

$$\rho_{mE} = H_L \rho_L + (1 - \rho_L)\rho_G \tag{2.26}$$

and H_L is calculated from equation (2.22) whereas $f = 0.0014 + \frac{0.125}{(\mathrm{Re})^{0.32}}$

In inclined two-phase flow the most extensive study has been reported by Beggs and Brill (1973). While a number of other significant works have since then been performed, most notably by Mukherjee and Brill (1985), the Beggs and Brill method remains perhaps the best known.

The Beggs and Brill (1973) correlation is based on data they gathered in 90 ft pipes with ID's of 1 and 1.5 in. These pipes were inclined at various angles between 0 and 90 degrees in both upward and downward directions. Their correlation for inclined pipes is based on its modification for horizontal systems. They divided the flow patterns observed in horizontal systems into four categories. The first is segregated flow, which include smooth and wavy stratified flow and annular flow. The intermittent flow pattern encompasses slug and plug flow. The transition flow regime includes regions between intermittent and stratified flow patterns, and the distributed flow pattern comprises bubbly and mist flow.

Beggs and Brill (1973) based their horizontal flow pattern map on the input volume fraction (C_L=U_{SL}/U_m) and the mixture Froude number (Fr_m=U_m^2/gd). They defined the four transition parameters as

$$L_1 = 316 C_L^{0.302}, \qquad L_2 = 0.0009252 C_L^{-2.4684}$$

$$L_3 = 0.1\, C_L^{-1.4516}, \qquad L_4 = 0.5 C_L^{-6.738}$$

The flow patterns are determined by the four following conditions:

Segregated $\qquad C_L < 0.01 \text{ and } Fr < L_1$

or $C_L > 0.01 \text{ and } Fr < L_2$

Transition	$C_L < 0.01$ *and* $L_2 < Fr < L_3$
Intermittent	$0.01 < C_L > 0.4$ *and* $L_3 < Fr < L_1$ or $C_L > 0.4$ *and* $L_3 < Fr < L_4$
Distributed	$C_L < 0.4$ *and* $Fr > L_1$ or $C_L > 0.4$ *and* $Fr > L_4$

The flow pattern map with the transition parameters, which are linear on log-log coordinates, is shown in Figure 2.11.

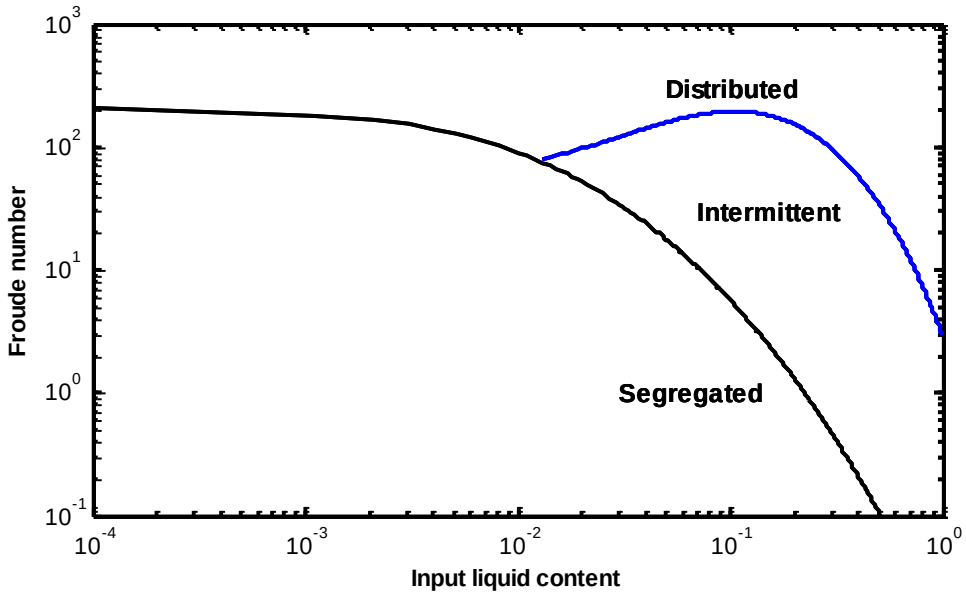

Figure 2.11 Beggs and Brill flow pattern map (1973)

They proposed the correlation for liquid holdup, H_L, for a horizontal system as

$$H_{L(0)} = a C_L^b / Fr^c \tag{2.27}$$

the following are the values of the parameters a, b, and c, which depend on specific flow patterns.

	a	b	c
Segregated	0.980	0.4846	0.0868
Intermittent	0.845	0.5351	0.0173
Distributed	1.065	.5824	.0609

When the flow regime falls in the transition zone, they suggested that H_L be estimated from a linear interpolation of H_L values calculated for the segregated and intermittent flow regimes. Thus,

$$H_{L,tran} = \left|\frac{(L_3 - Fr)}{(L_3 - L_2)}\right| H_{L,seg} + \left|\frac{(Fr - L_2)}{(L_3 - L_2)}\right| H_{L,\text{int}} \tag{2.28}$$

The frictional pressure gradient is calculated with the equation

$$\left(-\frac{dp}{dz}\right)_F = \frac{2 f_m \rho_n u_m^2}{g_c d} \tag{2.29}$$

In equation (2.29), ρ_n is the non-slip mixture density, $\rho_n = \rho_L C_L + \rho_g C_g$. The mixture friction factor, f_m, is related to the no-slip, two-phase friction factor, f_n, by

$$f_m = f_n e^s \tag{2.30}$$

Where f_n is the no-slip friction factor based on the no-slip Reynolds number, $Re_n = dU_m\rho_n/\mu_n$, and μ_n is the no-slip mixture viscosity, $\mu_n = \mu_L C_L + \mu_G C_G$. To calculate the exponent, s, needed to determine the two-phase friction factor, Beggs and Brill (1973) defined the parameter, y, in terms of C_L, and holdup as

$$y \equiv C_L / f_{L(\alpha)}^2 \tag{2.31}$$

The exponent, s, is empirically related to the parameter y, when y>1.2, and is written as

$$s = \frac{\ln y}{-0.0523 + 3.182(\ln y) - 0.8725(\ln y)^2 + 0.01853(\ln y)^4} \tag{2.32}$$

For a value of *y* between 1.0 and 1.2, *s* is given by

$$s = (\ln 2.2\, y - 1.2)\; 1 < y < 1.2 \tag{2.33}$$

Thus, frictional pressure gradient is dependent on the flow regime because y depends on $f_{L(\alpha)}$, which, in turn, depends on the flow regime, as well as the inclination angle.

For inclined multiphase systems, Beggs and Brill (1973) suggested the following calculation procedure. The flow regime that would exist if the system was horizontal is first determined using the criteria previously discussed. Holdup is then calculated with equation (2.27). Thereafter, it is multiplied by the correction factor, $F(\theta)$, to estimate the holdup for the actual inclined system. In other words,

$$H_{L(\theta)} = H_{L(0)} F(\theta) \tag{2.34}$$

$$F(\theta) = 1 + Z\left[\sin(1.8\theta) - \sin^3(1.8\theta)\right] \tag{2.35}$$

$$Z = (1 - C_L)\ln\left[d\, C_L^e\, v_{dL}^f\, Fr_g\right] \tag{2.36}$$

And $$v_{Ld} = v_{sL}\sqrt[4]{\rho_L / g\sigma} \tag{2.37}$$

Parameters d, e ,f and g depend on the flow pattern that was determined with an equivalent horizontal system. The following are the specific flow patterns with parameters values.

	d	e	f	g
Segregated uphill	0.011	-3.768	3.539	-1.614
Intermittent uphill	2.96	0.305	-0.4473	0.0978

Distributed uphill		No correction, F(θ)=1.0		
All flow regimes downhill	4.70	-0.3692	0.1244	-0.5056

Beggs and Brill (1973) did not suggest any specific method for calculating the accelerational component. Where it is significant, the accelerational gradient can be calculated with either the separated or homogeneous flow approach, and ρ_m can be estimated with the Beggs and Brill method. The total pressure gradient is given by

$$-\frac{dp}{dz} = \frac{g\sin\theta}{g_c}\left(\rho_L H_L + \rho_G(1-H_L)\right) + \frac{f_m U_m^2 \rho_n}{2 g_c d} + \frac{f_m U_m}{g_c}\frac{dU_m}{dz} \tag{2.38}$$

A few other methods have been proposed for computing flow behaviour using a flow pattern approach. Based on data from pipes inclined at 5, 10 and 15 degrees from horizontal, Singh and Griffith (1970) suggested that holdup in inclined slug flow can be represented by $H_L = U_{SG}/(0.95U_m + 1.15)$. In addition, comparison of this equation, with its counterpart in vertical systems, indicates that Singh and Griffith found the Taylor bubble rise velocity, in inclined pipes to be independent of not only pipe diameter but also of inclination angle. Beggs and Brill (1973) found holdup to be a strong function of pipe deviation.

Most of these works, however, appear to agree that the liquid holdup for intermittent flow in a tube slightly deviated from vertical is usually higher than that calculated under conditions similar to vertical flow. Indeed, the data of Beggs and Brill (1973) suggest that liquid holdup becomes a maximum at an angle of +50 degrees from the horizontal.

The Beggs and Brill (1973) correlation allows liquid holdup and pressure drop computation for all inclination angles, including in downward direction. Mukherjee and Brill (1985) also presented extensive data and a correlation for downward two-phase flow. Both correlations are quite robust. However, they are less reliable at low liquid rates because of their parametric dependence on input liquid fraction.

There are very few mechanistic models for computing holdup and pressure drop in deviated systems. Hasan and Kabir (1988), Kaya *et al.* (2001) and Gomez *et al.* (2000) have proposed comprehensive models for deviated wells.

The Hasan-Kabir model uses a flow pattern approach for vertical systems, with modifications for the system deviation from vertical orientation. Hasan and Kabir (1988) as well as Kaya *et al.* (2001) noted that for annular and dispersed bubbly flow, the flow rates are very high. Consequently, the influence of buoyancy is small and the effect of pipe inclination is negligible. Therefore, for these flow regimes, the relationships developed for vertical systems can be used without any modification.

Bubbly flow: For vertical systems, Hasan and Kabir (1988) postulated that the in-situ velocity, U_G of the gas phase, is the sum of the terminal rise velocity, U_∞, and the mixture velocity U_m, multiplied by the flow parameter C_0. Hence, $U_G = U_{SG}/\alpha = C_o U_m + U_\infty$ .The analysis should also hold for deviated pipes. Holdup is given by,

$$H_L \equiv 1-\alpha = 1-\frac{U_{SG}}{C_0 U_m + U_\infty} \tag{2.39}$$

Kaya *et al.* (2001) and Gomez *et al.* (2000) following approach of Ansari *et al.* (1994) for vertical systems, arrived at a slightly different expression.

$$H_L \equiv 1-\alpha = 1-\frac{U_{SG}}{C_0 U_m + U_\infty \sqrt{H_L \sin\theta}} \tag{2.40}$$

Therefore the procedure for estimating holdup and pressure drop in deviated wells will be similar to that for vertical systems. One however, will need values for flow parameter C_0, and the bubble rise velocity U_∞, in an inclined system.

Flow parameter and bubble rise velocity. For vertical systems, we are able to reason that the value of the flow parameter, C_0, should be 1.2 because the flow is turbulent, and the bubbles ride the central portion of the channel, where the mixture velocity is 1.2 times the cross sectional average value. The bubble concentration profile is likely

to be affected by the pipe deviation. Intuitively then, one can expect C_0, to be influenced by well deviation, which has led Gomez *et al.* (2000) to use C_0=1.15.

However, the effect of pipe inclination on C_0, appears negligible. Hasan and Kabir (1988) and Kaya *et al.* (2001) proposed a value of 1.2 for C_0 in equation 2.39 or 2.40. The bubble rise velocity may be assumed to remain unchanged with pipe inclination. Therefore, the same expression, with the identical values of parameters used in vertical pipes can be used to estimate holdup in deviated pipes. The only difference between bubbly flow in deviated tubes and that in vertical ones is the transition to slug flow.

Once holdup is estimated, the total pressure gradient may be calculated by adding the frictional and accelerational components to the static head. The contribution of these components, which are very small, may be estimated with the method applicable to vertical systems. The static head for an inclined pipe of course is $\rho_m \sin\theta$. Therefore,

$$-\frac{dp}{dz} = \frac{g\sin\theta}{g_c}\left(\rho_L H_L + \rho_G(1-H_L)\right) + \frac{f_m U_m^2 \rho_m}{2 g_c d} + \frac{f_m U_m}{g_c}\frac{d U_m}{dz} \tag{2.41}$$

Slug flow: Application of the simple drift-flux model, developed for bubbly flow, to slug flow is difficult. This difficulty stems from the difference in drift velocities between the small and the Taylor bubbles and the symmetric nature of the distribution and shape of the bubbles. One simple way to account for different drift velocities in slug flow is to use some type of an average rise velocity for all gas bubbles, large and small. Therefore for estimating in-situ liquid volume fraction during slug flow

$$H_L \equiv 1-\alpha_G = 1-\frac{U_{SG}}{C_0 U_m + \overline{U}_{\infty\theta}} \tag{2.42}$$

As in vertical flow, the average rise velocity is expressed in terms of the Taylor bubble rise velocity, small bubble rise velocity, and bubbly-slug transition velocity as

$$\overline{U}_{\infty\theta} = \overline{U}_{\infty T\alpha}\left(1 - e^{-U_t U_{SG}}\right) + U_\infty e^{-U_t U_{SG}} \tag{2.43}$$

where U_t is the superficial gas velocity for transition to intermittent flow. The flow parameter C_0 might be affected by channel inclination. However, a constant value of 1.2 makes the estimation procedure simple. Both Hasan and Kabir (1988) and Kaya *et al.* (2001) used this value for the flow parameter.

Balancing the buoyancy force against drag force, experienced by a rising bubble leads to the expression for the rise velocity of a bubble of volume V_b and projected area A_p.

$$U_b g \sin\theta\left(\rho_L - \rho_G\right) = \tfrac{1}{2} C_{D\theta} U_{\infty T\theta}^2 \rho_L A_{P\theta} \tag{2.44}$$

In equation (2.44), $C_{D\theta}$, is the drag coefficient for the bubble and $U_{\infty T\theta}$ is its rise velocity in a pipe, inclined to the horizontal by an angle, θ.

$$\frac{U_{\infty T\theta}}{U_{\infty T}} = \sqrt{\sin\theta \frac{\left(C_D A_p\right)_{90}}{C_{D\theta} A_{p\theta}}} \tag{2.45}$$

If the product of the drag coefficient and the projected area of the bubble were the same for vertical and inclined systems; that is if $\left(C_D A_p\right)_{90} / C_{D\theta} A_{p\theta} = 1$, then equation 2.45, suggests that the bubble rise velocity will gradually decrease, as the deviation of the pipe increases. However, in inclined flow, the Taylor bubble has a sharper nose, compared to that in vertical systems, with a consequent lower drag coefficient. In addition, the projected area in a deviated pipe is also smaller. The net effect is that the ratio, $\left(C_D A_p\right)_{90} / C_{D\theta} A_{p\theta}$ becomes greater that 1.0. Consequently, an increase in the terminal rise velocity, with pipe deviation occurs when the deviation is small, with a consequent increase in liquid holdup, compared to that in a vertical system.

At large deviations from vertical, the buoyancy force begins to decrease, much faster than the drag force and the bubble rise velocity begins to decrease with further deviation from the vertical. The variation in the $C_D A_{p\theta}$ product with inclination angle may be approximated by $\left(C_D A_p\right)_{90}\left(1 + \cos\theta\right)^n$.

$$U_{\infty T\theta} = U_{\infty T}\sqrt{\sin\theta\left(1+\cos\theta\right)^{n}} \tag{2.46}$$

2.5 Slug flow

The slug flow pattern is one of the most common flow patterns experienced during normal operating conditions of a two-phase pipeline. It is characterized by fast moving liquid slugs with high holdup values alternating with large gas pocket or film regions. The flow is very dynamic since the fast moving liquid slugs keep overriding slow moving liquid films in front of them. Thus a particle of liquid in the liquid film is continuously picked up by the front of the liquid slug, accelerated to a much faster velocity, then decelerated as it travels along the liquid slug body, and finally shed at the tail into the liquid film behind as the velocity approaches the film velocity once again. Hubbard (1965) and Dukler and Hubbard (1975) provided the first comprehensive slug flow model, which has served as a basis of slug flow modelling ever since.

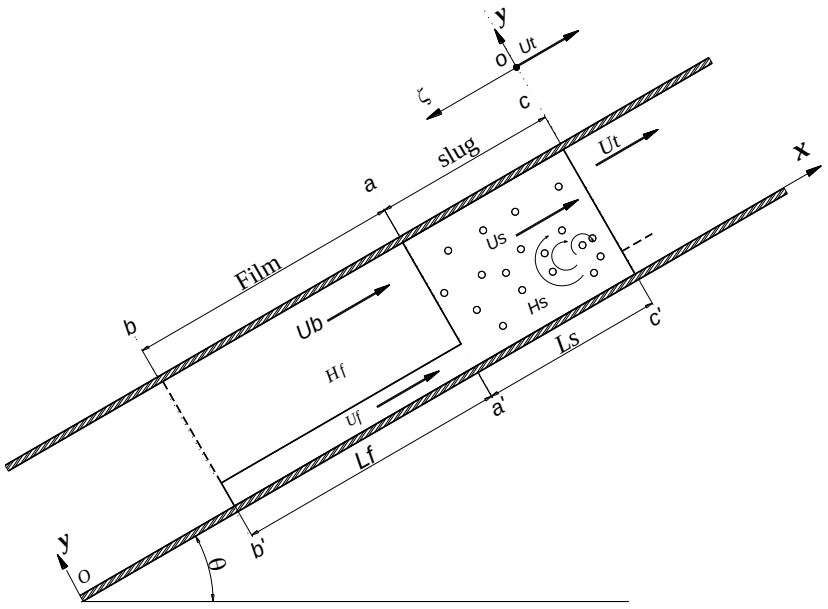

Figure 2.12 Slug unit representation

Figure 2.12 shows a simplified physical model of slug flow. The model starts from the basic concept that a slug unit is composed of a slug body of length and liquid holdup L_S and H_S respectively, and a gas pocket and liquid film zone of length L_f with liquid holdup H_f respectively. At the front of the slug body, moving at the translational velocity U_t, there exist a mixing zone where liquid is scooped up from the film in front, and accelerated to the slug velocity, U_S. There are two velocity components associated with the film zone; U_f for the liquid film velocity, and U_{GP} for the gas pocket velocity. The model assumes that the amount of liquid scooped is equal to the amount of liquid shed; therefore, the length of the slug stays constant as it travels along the tube.

In order to develop the equations for the slug, the entire liquid film and the gas pocket in the film zone are used as the control volume, as shown in Figure 2.12. Continuity and momentum equations are derived for them relative to a coordinate system moving with the translational velocity U_t.

With the fully dispersed flow assumption, the unit cell representation leads to the idealized situation in which the flow is periodic both in time and space. Even if the flow is unsteady in the frame defined by the coordinate *Ox*, there exist a particular frame $o\zeta$ moving with the cell at the velocity U_t so that the flow appears steady, the velocity of phase-k averaged over the pipe, U_k, is thus transformed by the change of frame as U_t-U_k.

2.5.1 Slug velocity

Dukler and Hubbard (1975) performed a liquid mass balance between the slug front and a point in the slug body with the fully accelerated slug velocity, U_S, which yields;

$$H_S\left(U_t - U_S\right) = H_f\left(U_t - U_f\right) \tag{2.47}$$

Equation (2.47) can be arranged in another form;

$$U_t = \left(1 + C\right)U_S \equiv C_0 U_S \tag{2.48}$$

Where,

$$C = \frac{H_f}{H_S}\left(\frac{U_t - U_f}{U_S}\right) \tag{2.49}$$

It has been reported in the literature that C_0 varies between 1.2 and 1.35. Kouba (1987) experimentally concluded that C_0 can be as high as 1.8 for some flow conditions (low superficial liquid and gas velocities). More recently, Zheng *et al.* (1994) also reported an experimentally observed value of 1.20 for C_0 for a wide range of slug flow conditions, even with inclination angles as high as 5˚. In most cases, C_0 only varies between 1.2 and 1.25. It is usually assumed a value of 1.2 for C_0, which would represent the maximum velocity for fully developed turbulent flow.

In order to calculate the liquid slug velocity mass balances are performed for both phases between the inlet and any slug unit, and showed that;

$$U_S = U_m \equiv U_{SL} + U_{SG} \tag{2.50}$$

2.5.2 Drift velocity

The first attempt to study the motion of elongated bubbles was made by Nicklin *et al.* (1962) for the vertical case; they proposed a correlation for the calculation of the translational velocity of an elongated bubble in continuous slug flow

$$U_b = C_0 U_m + U_d \tag{4.51}$$

Where U_d is the drift velocity of the bubble in a stagnant liquid and U_m is the mixture velocity defined as the sum of the liquid and gas superficial velocities, U_{SL} and U_{SG}. They based the value of the constant C_0 upon the assumption that the propagation velocity of the bubbles follows the maximum local velocity, U_{max}, in front of the nose tip and thus

$$C_0 = U_{max}/U_m \tag{4.52}$$

The value of C_0 therefore equals approximately 1.2 for fully developed turbulent flow and 2.0 for fully developed laminar flow. There is a strong indication that C_0 increases

as the Reynolds number decreases and reaches a value of about 2. The exact value of C_0 for turbulent flow and in particular for laminar flow is not conclusive. There is a spread of experimental data. For vertical flow; the accepted value for the drift velocity is given by

$$U_d^v = 0.35\sqrt{gd} \tag{2.53}$$

For horizontal flow, Zuber and Findlay (1965) suggested that the drift velocity existed due to the difference in the hydrostatic head between the liquid in the slug and the liquid in the film, causing the liquid in the slug to drain into the film. They showed that similar to vertical flows, the relationship between the drift velocity and the translational velocity U_t is given by the linear form dictated by continuity.

For horizontal flow, Benjamin (1968) derived an asymptotic solution for inertia dominated drift velocity;

$$U_d^h = 0.54\sqrt{gd} \tag{2.54}$$

Equation (2.54) has been found to correlate bubble velocity data for horizontal flows in the elongated bubble and slug flow regimes (Nicholson *et al.* (1978); Dukler and Hubbard (1975); Mattar and Gregory (1974)). Some investigators found that U_d=0 (Dukler and Hubbard (1975); Heywood and Richardson (1979); Gregory and Scott (1969)), while others did not. A few years ago it was widely believed that U_d should be equal to zero for horizontal flow. More recently however, it has been suggested that a non zero drift velocity may exist, Nicholson *et al.* (1978).

Weber (1981) exposed the drift phenomenon for horizontal flow as well as a way to calculate the drift velocity. They considered the situation where a closed horizontal tube is initially filled with liquid and one end is opened, the liquid will drain out, being driven by the hydrostatic pressure difference between the top and the bottom of the tube, Figure 2.13.

An extended vapour bubble will travel through the tube in opposite direction replacing

the liquid. The mechanism causing the draining of the liquid and hence the movement of the bubble, is identical to that causing the liquid in a horizontal surface to spread.

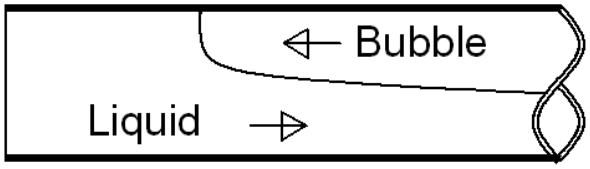

Figure 2.13 Side view of the model bubble used by Weber (1981)

Weber (1981) provided an expression for the bubble velocity, U_b, and showed that it reduces to zero for values of $E_{OD} = 12$, where E_{OD} is Eotvos number. This number in turn depends on the pipe diameter.

$$E_{OD} = \frac{\rho_L g d^2}{\sigma} \tag{2.55}$$

Zukoski (1966) studied the effect of surface tension, viscosity and tube inclination on the velocity of long bubbles. Based on his results as well as those from other researchers, he suggested that for Reynolds numbers greater than about 200, the propagation rates are substantially independent of viscous effects.

Weber (1981) suggested the following correlation for low viscosity fluids;

$$U_d = \sqrt{gd}\left[0.54 - 1.76\left(\frac{\rho g d^2}{\sigma}\right)^{(-0.56)}\right] \tag{2.56}$$

Equation (2.56) actually suggests that the drift velocity becomes negligible for small pipes (< 5mm).

Kouba (1987), following Benjamin's development, proposed the following equation for horizontal drift velocity, which accounted for gas entrainment in the liquid slug;

$$U_d = \sqrt{gd}\left[\frac{\frac{H_f}{H_S}\cos\theta_f + \frac{2}{3}\left(\frac{\sin^3\theta_f}{\pi H_s}\right) - 1}{1-\frac{2H_s}{H_f}}\right]^{0.5} \tag{2.57}$$

Where θ_f is half the angle subtended by the liquid film height measured from the bottom of the pipe, as graphically shown in Figure 2.14.

For simplicity, equation (2.53) from Benjamin's work is employed for the horizontal drift velocity.

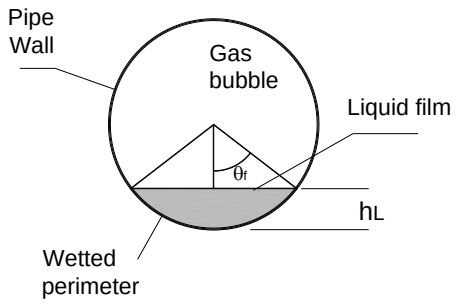

Figure 2.14 Liquid film

The drift velocity U_d depends on the inclination angle, θ, measured from the horizontal, and has a maximum for $40<\theta<60^\circ$ (Zukoski (1966); Bendiksen (1984); Hasan and Kabir (1988); Weber *et al.* (1986); Van Hout *et al.* (2002)).
For the more general upward inclined case, Bendiksen (1984) proposed as a practical suggestion, to use the following formula for the drift velocity.

$$U_d = U_d^h \cos\theta + U_d^v \sin\theta \tag{2.58}$$

Where U_d^h and U_d^v correspond to the drift velocity for the horizontal and the vertical case respectively. Hasan and Kabir (1988) proposed the relation:

$$U_d = U_d^v \sqrt{\sin\theta}\,(1+\cos\theta)^{1.2} \tag{2.59}$$

2.5.3 Slug holdup

The prediction of the liquid holdup in the slug body for two-phase gas-liquid slug flow is important for the accurate calculations of the pressure drop. Dukler and Hubbard (1975) showed that a void fraction in the slug depends on input gas liquid ratio. The effect of pipe has been investigated by Andreussi and Bendiksen (1989) and others. Fluid properties like surface tension and liquid density were included by Malnes (1983). A distinct dependency on pipe inclination was suggested by Andreussi *et al.* (1993). Brauner and Ullmann (2004) present a critical overview of the different approaches for modelling of the void fraction in slugs.

A widely used correlation for estimation of gas fraction in slugs as a function of superficial mixture flow rate was presented by Gregory *et al.* (1978),

$$H_S = \frac{1}{1+\left(U_m/8.66\right)^{1.39}} \tag{2.60}$$

Where U_m is expressed in m/s. Gregory *et al.* (1978) cautioned that the use of this correlation should be limited to cases where U_{m} is less than 10 m/s to reduce the possibility of entering the transitional zone between slug and annular flows, where the correlation would not be applicable.

Malnes (1983) included fluid properties (surface tension and liquid density), and proposed the following correlation,

$$H_S = 1-\frac{U_m}{\left[83\left(\frac{g\,\sigma_{GL}}{\rho_L}\right)^{1/4}+U_m\right]} \tag{2.61}$$

Marcano *et al.* (1996) performed experiments in a d = 77.9 mm, L = 420 m horizontal pipeline. The fluids were kerosene and air, and the operational pressure approximately 5.5 bar. Based on void fraction measurements made by capacitance sensors, a correlation was proposed for void fraction in slugs,

$$H_s = \frac{1}{\left(1.001 + 0.0179U_m + 0.0011U_m^2\right)} \tag{2.62}$$

Where U_m is the mixture velocity in [ft/s].

Gomez *et al.* (2000) used data from a number of other authors, with pressures from 1.5 to 20 bar, pipe diameters from 51 to 203 mm, and pipe inclinations in the range of 0–90◦. The data indicated a clear dependency between pipe angle, Reynolds number and slug void fraction. A correlation was suggested,

$$H_s = e^{-(0.45\theta + C\,\mathrm{Re}))} \quad 0 \le \theta_R \le \pi/2 \tag{2.63}$$

where the pipe angle θ is in [rad], the coefficient C=2.48x10^{-6}, and the Reynolds number is defined as,

$$\mathrm{Re}_l = \frac{\rho_L U_m d}{\mu_L} \tag{2.64}$$

The correlation predicted the data sets on which it was based within an error of 30%.

2.5.4 Frequency

The frequency, *f*, is in fact defined as the mean number of slugs per unit time as seen by a fixed observer; Hubbard (1965), Gregory and Scott (1969).

A very much used correlation for slug frequency prediction was developed by Gregory and Scott (1969) based on data by Hubbard (1965). Nydal (1991) compared the correlation with experimental data and found a good fit within the original data range (U_{SG} < 10 m/s and U_{SL} < 1.3 m/s).

$$f_S = 0.0226\left[\frac{U_{SL}}{gd}\left(\frac{19.75}{U_m} + U_m\right)\right]^{1.2} \tag{2.65}$$

A correlation was suggested by Greskovich and Shrier (1972). This model is on the same form as the Gregory and Scott correlation,

$$f_S = 0.0226\left[\frac{U_{SL}}{U_m}\left(\frac{2.02}{d}+\frac{U_m^2}{gd}\right)\right]^{1.2} \tag{2.66}$$

Heywood and Richardson (1979) proposed the following correlation, being almost identical to the one from Gregory and Scott, but based on a much larger amount of experimental data,

$$f_S = 0.0434\left[\lambda_L\left(\frac{2.02}{d}+\frac{U_m^2}{gd}\right)\right]^{1.02} \tag{2.67}$$

Tronconi (1990) presented a semi-mechanistic expression for the slug frequency, where the slug frequency was assumed to be half the frequency of unstable waves (slug precursors),

$$f_S = 0.305 Cw^{-1}\frac{\rho_G}{\rho_L}\frac{U_G}{h_g} \tag{2.68}$$

Where $U_G = U_{SG}/(1-H_L)$ and h_G is the height of the gas phase at the inlet, immediately upstream the point of slug initiation. C_w is the wave velocity of the waves growing to become slugs. Tronconi postulated a linear relationship between the frequency of critical waves and the slug frequency, $f_w = C_w f_S$, with $C_w = 2$.

This corresponds to observations in slug flow (by Dukler *et al.* (1985) and Kordyban (1985)), where every second slug originating from these waves was unstable and disappeared. The Tronconi correlation does not directly take into consideration any change in slug frequency with changing liquid flow rate, but indirectly through the calculations of gas flow rate and height.

Nydal (1991) argued that, at high liquid flow rates, the slug frequency should depend weakly on U_{SG}, but strongly on U_{SL}, and suggested a correlation based on the liquid

flow rate alone,

$$f_S = 0.088 \frac{\left(U_{SL} + 1.5\right)^2}{gd} \tag{2.69}$$

Jepson and Taylor (1993) published data from the 306 mm pipe diameter rig of the Harwell laboratory, and the effect of diameter was investigated by including 25.4 and 51.2 mm pipe data from Nicholson *et al.* (1978). A non-dimensional slug frequency was correlated against the superficial mixture velocity,

$$f_S = \frac{U_{SL}}{d}(7.59 * 10^{-3} U_m + 0.01) \tag{2.70}$$

Manolis *et al.* (1995) developed a new correlation based on Gregory and Scott (1969). Taking $U_{m,min}$=5 m/s and the modified Froude number

$$Fr_{\text{mod}} = \frac{U_{SL}}{gd}\left[\frac{U_{m,\min}^2 + U_m^2}{U_m}\right] \tag{2.71}$$

Where

$$f_S = 0.0037 Fr_{\text{mod}}^{1.8} \tag{2.72}$$

Zabaras (1999) suggested a modification to the Gregory and Scott correlation, where the influence of pipe inclination angle was included, equation (2.73). The data on which the modified correlation was tuned included positive pipe angles in the range of 0 to 11° relative to the horizontal.

$$f_S = 0.0226\left[\frac{U_{SL}}{gd}\left(\frac{19.75}{U_m} + U_m\right)\right]^{1.2}\left(0.836 + 2.75 \sin\theta\right) \tag{2.73}$$

2.5.5 Mean Slug length

Slug length data have been reported by several authors including: Hubbard (1965), Gregory and Scott (1969), Vermeulen and Ryan (1971), Greskovich and Shrier (1972), Heywood and Richardson (1979).

The mean length of liquid slugs have been experimentally observed to be about 12-40 pipe diameters in horizontal flow, Hubbard (1965).

Other authors have assumed that the liquid slugs have a fixed dimensionless length of 30d, Nicholson *et al.* (1978), and the method is expected to work only at high enough gas rate.

Scott *et al.* (1986) and Scott *et al.* (1987) presented an improved correlation to predict slug lengths as a function of pipe diameter for large diameter pipes. This correlation is given by;

$$\text{Ln}\,(L_S) = -26.6 + 28.5[\ln(d)+3.67]^{0.1} \qquad (2.74)$$

Scott *et al.* (1987) showed that equation (2.74) also yields valid results for pipe diameters as small as 40-50 mm. However, the correlation rapidly approaches a very low and unrealistic slug length value as the diameter decreases further. It is therefore suggested to use either equation (2.74) or the rule of thumb, $L_S = 32d$, whichever is larger, to calculate the average horizontal slug length for each specific pipeline system.

For small diameter horizontal pipes, Barnea and Taitel (1993) showed that the average slug length was 1.5 times the minimum stable slug length, whereas the maximum slug length was 3 times the minimum stable slug length. Dukler *et al.* (1985) modelled minimum stable slug lengths of about 20*d*, and the model was compared with experimental data and concluding that the actual expected slug lengths would be in the order of 1–2 times the minimum length.

In developed slug flow for horizontal and slightly inclined pipes, stable slug lengths of 15–40 pipe diameters have been reported by a series of investigators (Dukler and

Hubbard (1975), Taitel and Dukler (1977), Dukler *et al.* (1985), Nydal (1991), Barnea and Taitel (1993)). All these studies concluded with slug length being fairly insensitive to gas and liquid flow rate, and depends mainly on the pipe diameter.

In order to obtain the average film or gas pocket length, L_f, one can perform the liquid mass balance over a slug unit to yield;

$$L_U = L_S + L_f \tag{2.75}$$

If equilibrium stratified conditions are assumed for the development of the film region behavior. Thus mass balances on the liquid and gas phases can be performed between the film region and a point within the slug body. These give, respectively;

$$U_f = U_t - \frac{H_S}{H_f}(U_t - U_S) \tag{2.76}$$

$$U_b = U_t - (U_t - U_S)\left[\frac{1 - H_S}{1 - H_f}\right] \tag{2.77}$$

Dukler and Hubbard (1975) were the first investigators to describe equilibrium film behaviour by performing a momentum balance, which includes only the liquid wall shear stress and the gravity force. For horizontal flow, this would result in a zero equilibrium film velocity. The interfacial shear stress, τ_i, is another term, which contributes to the overall momentum balance, and thus should also be included in the overall momentum balance. Scott *et al.* (1987) pointed out that by including τ_i, the transfer of momentum between the liquid phase and the gas phase in the film region has been introduced into the momentum balance calculation.

Liquid film velocity, U_f and Liquid film holdup, H_f are related in the following manner:

$$U_f = U_S\left[1 - C\left(\frac{H_s - H_f}{H_f}\right)\right] = BU_s \tag{2.78}$$

In the film region the wall shear stress, τ_w, due to liquid flow is estimated by assuming pseudo parallel flow

$$\tau_w = \frac{f_f \rho_L}{2g} V_f^2 \tag{2.79}$$

The wetted perimeter, P_w,

$$P_w = \frac{\theta d}{2} \tag{2.80}$$

The length of the slug can be calculated from a material balance on the liquid. The rate of liquid flow into the pipe is W_L. Considering a plane normal to the flow at some position downstream where fully developed slug flow exists and calculating the mass of liquid crossing the plane in:

(a) The time it takes for the slug to pass, T_s, and
(b) The time it takes for the film to pass, T_f.
The sum of these two quantities is then divided by the time of passage of one slug unit, $1/f$.

$$M_s = mass\ carried\ in the\ slug = \int_0^{T_s} V_s A_{H_s} \rho_L dt = V_s A_{H_s} \rho_L T_s \tag{2.81}$$

$$\text{but } T_s = \frac{l_s}{V_t} \tag{2.82}$$

$$M_s = V_s A_{H_s} \rho_L \frac{l_s}{V_t} \tag{2.83}$$

Similarly for the film

$$M_f = \int_0^{T_f} V_f A_{H_f} \rho_L dt \tag{2.84}$$

But

$$T_f = \frac{L_f}{V_t} \tag{2.85}$$

$$M_f = \int_0^{l_f} \frac{V_f A H_f \rho_L}{V_t} d x_f \tag{2.86}$$

from equation (2.79)

$$\frac{W_L}{\rho_L A V_s} = \frac{f_s}{V_t}\left[H_s l_s + \int_0^{l_f} \left(H_s - H_f \right) d x_f \right] \tag{2.88}$$

Solving for L_S and rearranging gives

$$L_S = \frac{V_s}{V_s (H_s - H_{fe})}\left[\frac{W_L}{\rho_L A V_s} - R_{fe} + C(H_s - H_{fe}) \right] \tag{2.89}$$

Length of the film region or long bubble is

$$L_f = \left(L_u - L_s\right) = \frac{V_t}{f_s} - L_s \tag{2.90}$$

As can be seen, this model requires as input data values of the frequency, f_s, and slug holdup, H_s.

2.6 Computational Fluid Dynamics (CFD)

Although the Navier-Stokes equations meant a considerable theoretical advance in the 19th century, the analytic-mathematical solution of the full equations proved one bridge too far. The invention of the digital computer led to many changes. John von Neumann predicted already in 1946 that 'automatic computing machines' would replace the analytic solution of simplified flow equations by a 'numerical' solution of the full nonlinear flow equations for arbitrary geometries. Von Neumann's prediction did not fully come true, in the sense that both analytic-theoretical and experimental research still coexist with CFD. A new branch of research emerged, however: crucial properties of CFD methods such as consistency, stability and convergence needed mathematical study. At present much fundamental research is still to be done to increase CFD's accuracy, efficiency and robustness.

Most numerical algorithms were developed in the early 1970's. Since then new techniques have been added and new models have been developed to enhance the capability of CFD codes and packages to simulate more accurately real problems. It was in the early 1980s that commercial CFD codes came into the open market place in a big way. The use of commercial CFD software started to become accepted by major companies around the world rather than their continuing to develop in-house CFD codes. General purpose commercial codes, (Fluent, CFX, etc.) are available, as well as a series of more problem orientated models for simulating two-phase flows.

Modern CFD can handle flow around geometry of great complexity in which all details of flow significance have been faithfully represented. Fluid flow associated with other phenomena, such as chemical reactions, turbulence, multiphase, or free surface problems and radioactive heat transfer can all be simulated by the commercial CFD packages now available, with a suite of built-in models describing these processes.

CFD is often used to understand fundamental processes involving bubble dynamics. In the study of bubble dynamics, the understanding of the behaviour of a bubble rising through a liquid is an important problem. Lun *et al.* (1996) performed modelling of two-phase flow using a commercially available CFD package. They highlight the importance of adequate grid density. The motion, the shape and the size of the bubbles as well as the motion of the liquid are dynamically modelled, employing the Volume of Fluid (VOF) technique. Later Cook and Behnia (2001) presented a numerical investigation of the drift of bubbles in stagnant liquid using Volume of fluid (VOF), they showed that this technique is able to predict interface of bubbles, rising in a quiescent liquid, remarkably well. They compared the bubble interface shape against data obtained with the use of a parallel wire conductance probe. More recently Frank (2005) performed numerical simulations of slug flow in horizontal pipe using the Multi-fluid model.

Chapter 3

Experimental Arrangement

As it is known, for two-phase flow problems, experimental data of the laboratory provide the main source of information about specific flows. In this work, two-phase flow experiments were carried out on an inclinable rig in the Chemical Engineering laboratory of the School of Chemical, Environmental and Mining Engineering (SChEME). Having introduced the overall objectives of this study in Chapter 1 and the literature review in Chapter 2, this chapter presents an outline of the experimental arrangements and equipment used to investigate the two-phase flow behavior in inclined pipes. It describes in detail the methodology and procedures undertaken to acquire the experimental data. An overview of the experimental facility is given in Section 3.1, followed by Section 3.2 that gives further information on important facility components such as details of the data acquisition software and instrumentation. Section 3.3 describes the experimental methodology and Section 3.4 summarizes the experimental uncertainty of the measurements.

3.1 Overview of the flow facility

Figure 3.1 presents a schematic diagram of the experimental facility used which had been employed earlier for annular flow studies by Azzopardi *et al.* (1997), Geraci *et al.* (2007a) and Geraci *et al.* (2007b). Figure 3.2 is the actual picture of the rig. The experimental facility consists of an inclinable 6 m long rigid steel frame. The test pipe is mounted on this frame and could be rotated between vertical to horizontal in 5° increments meaning the effect of different inclinations could be monitored.

Two pipe diameters were studied, namely 38 mm and 67mm. This rig used an air/water mixture. The experiments were performed at room temperature (20° C). The properties of the two fluids used in the experiments are as shown in Table 3.1. Water feed is pumped into the facility from the water tank, situated just below the rig, by a centrifugal pump. A recycle loop was installed to allow part of the liquid to be returned to the main water storage tank. This arrangement aided flow stability and allowed better control of the liquid feed flow rate than could be otherwise achieved by means of simple feed systems.

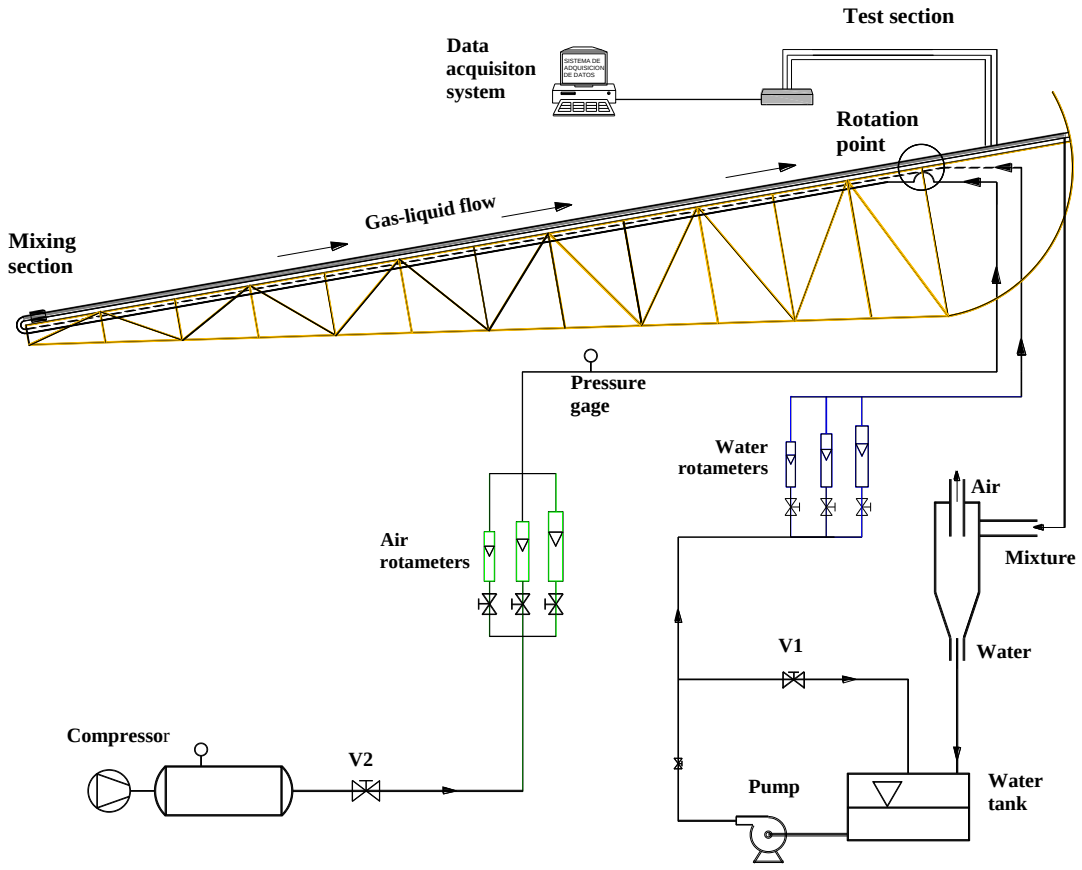

Figure 3.1 Experimental arrangement

Table 3.1 Properties of the Fluids

Fluid	Permittivity Fm^{-1}	Density (kg/m^3)	Viscosity (kg/ms)	Surface tension (N/m)
Air	$8.9x10^{-12}$	1.224	0.000018	0.072
Water	$7.1x10^{-10}$	1000	0.001	

Figure 3.2 Inclinable rig

Air from the laboratory 6 bar_a compressed air main was used as the gas phase. It is fed into the facility through a 0.022 m internal diameter stainless steel pipe. A pressure regulating valve sets the maximum air inlet pressure and a pressure relief valve, set at 100% of the required feed pressure protects the facility against overpressure. Both the airflow rate and gage pressure are measured prior to entering the mixing section using a set of rotameters that covered a wide range of flow rates as well a pressure gage meter respectively. Inlet volumetric flow rates of water are determined prior to entering the mixing section with a set of rotameters that cover the range from 0-0.73 m/s of superficial velocities. The two separate phases are then mixed at the gas liquid mixing section. From the mixing section, the two-phase mixture flows along the inclined pipe before reaching the test section where the capacitance sensors are located. The pipe outlet is connected to the separator tank open to the atmosphere.

Two capacitance sensors separated by a distance of 0.45 m and placed directly on the outside wall of the pipe, provided a pair of time series of liquid holdup. The first capacitance probe was located at 5 m from the inlet; this gives a flow development length of approximately 150 pipe diameters to the first capacitance sensor and a total of approximately 170 pipe diameters to the second sensor.

Table 3.2 Location of instrumentation on the test section of the rig

	DP cell tapping 1	Cap 1	Cap 2	DP cell tapping 2
Location from the mixing section (m)	4.75	4.90	5.35	5.50

Capacitance probes were developed looking forward to use nonconductive liquids in a later stage of the research programme. To measure the pressure drop a differential pressure transducer (0-70 kPa ABB Deltapi K series DP cell) was installed and connected to pressure tappings in the pipe separated 0.765 m. The signals were recorded through a computer using Labview 7 software (National Instruments), and were taken at a sampling frequency of 200 Hz over 180 seconds for each run.

It is worth mentioning that in order to get the best results; a calculation of the distance between the two capacitance probes was performed based on the flow conditions under operation. In addition, for the 67 mm diameter pipe, a previous calculation was done to make sure the frame of the rig had the capabilities to support the weight.

3.2 Flow facility components

3.2.1 Gas-liquid mixing section

The mixing of the gas and liquid phases must be done in such a way as to try and minimize the flow instability, thus providing maximum time for the two-phase flow to develop. This was achieved by using a purpose built mixing unit.

The mixing unit itself is made from Polyvinyl chloride (PVC) pipe as shown in Figure 3.3. The water is introduced from one side of the mixer. Air is fed from the rear of the mixing section directly into the two-phase stream through a porous wall section, thus creating a more even circumferential mixing effect.

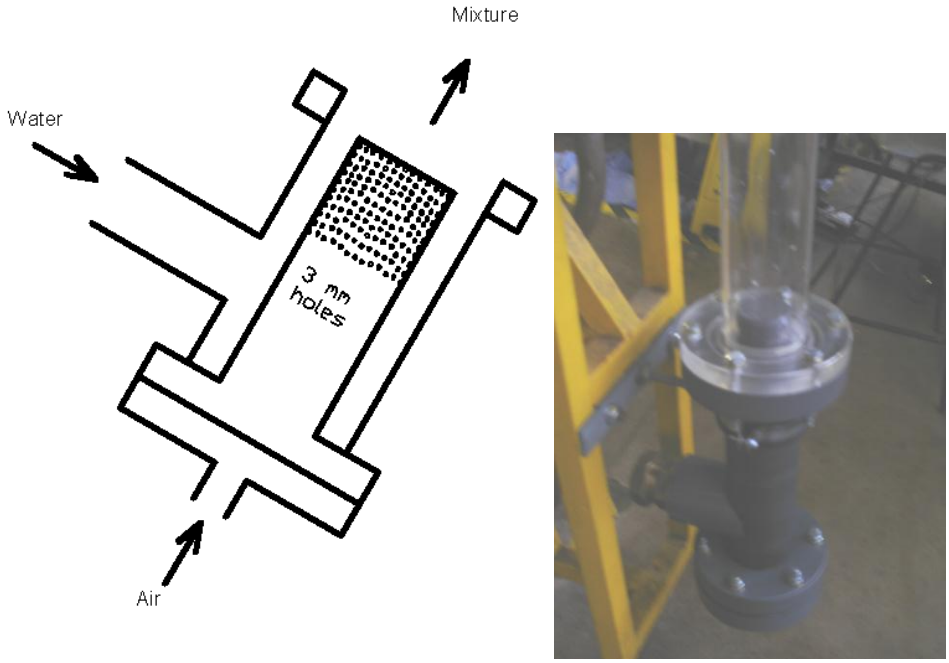

Figure 3.3 Gas-liquid mixing section

3.2.2 Gas-liquid separation tank

At this phase separation tank, the gas and liquid are gravity separated. The two-phase mixture is fed into the top of the tank through a flow distributor system, to prevent jetting. The air stream exits the top of the tank and the return of the water to the water reservoir tank is achieved by gravity.

3.2.3 Flow measurement section

The sections of flow measurement for both air and water are similar. The flow meter element was a rotameter of the type (Variable Area Meters). The two air rotameters together cover the range 10-1000 l/min. A picture of the flow measurement section is presented in Figure 3.4.

Figure 3.4 Flow rotameters

3.2.4 Data acquisition

Data acquisition involves gathering information using a combination of PC-based measurement hardware and software to provide a flexible, user-defined measurement system. Software transforms the PC and the DAQ hardware into a complete data acquisition, analysis, and presentation tool. Driver software is the layer of software that allows easy communication to the hardware.

Voltages were recorded through a computer using "LABVIEW 7" software of National Instruments. Because LabVIEW has the flexibility of a programming language combined with built-in tools designed specifically for test, measurement, and control, an application was created and data were taken every 0.005 seconds over 180 seconds for each run.

A schematic diagram of the arrangement used for the data collection is shown in Figure 3.5. The signal from the 2 probes and DP cell could be obtained simultaneously and, after filtering by the unit, this was fed to a PC equipped with a multi-channel DAQ card. The signal was driven to this DAQ card by a terminal block. Before calibration, the gains were adjusted to obtain optimal operation in the expected range

of heights of the liquid. Data acquisition was carried on using a block diagram assembled in LABVIEW.

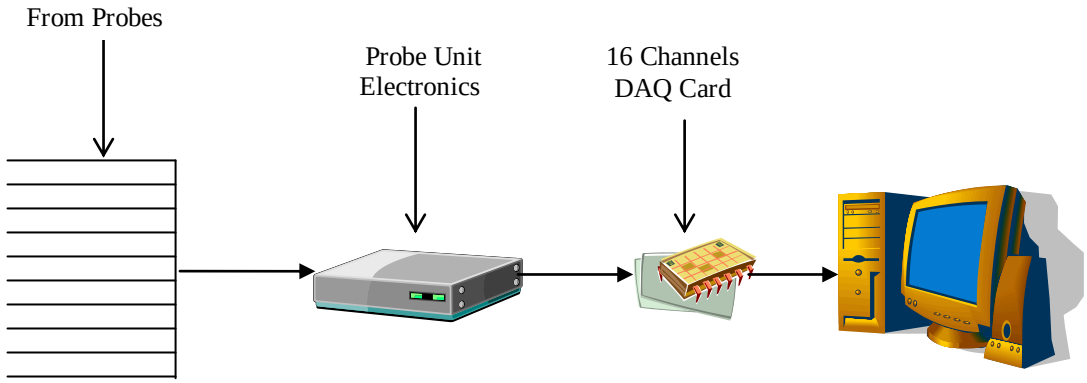

Figure 3.5 Sketch of the arrangement for data collection

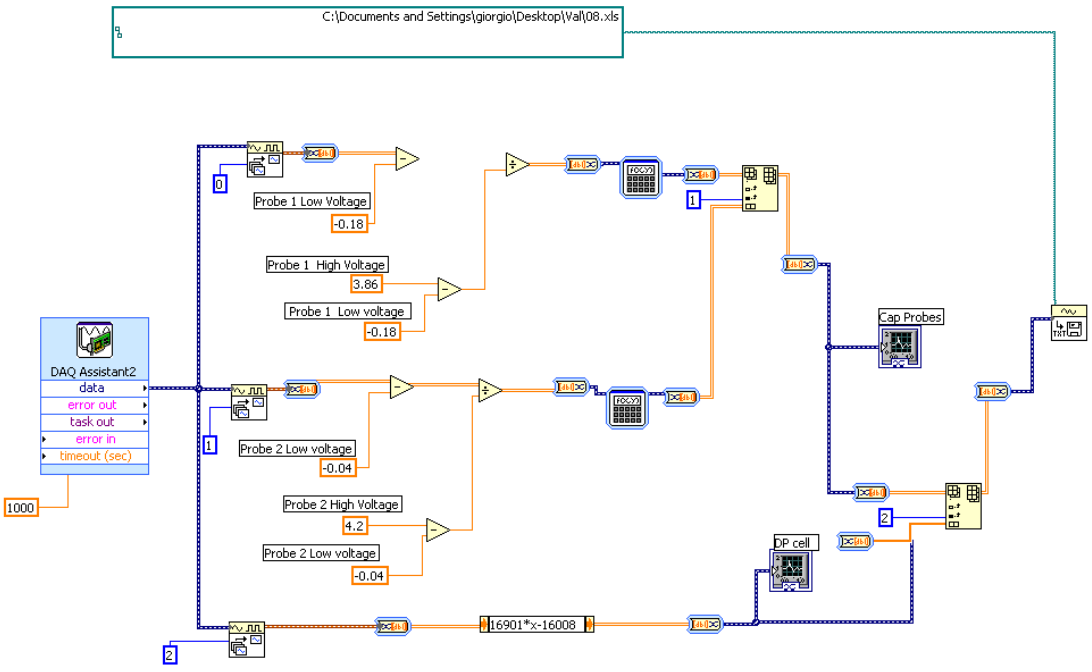

Figure 3.6 Block diagram of the Laview program for data acquisition

3.2.5 Pressure sensors

In order to measure the pressure drop, a differential pressure transducer (DP cell) was installed after a careful selection. In selecting the DP cell, both the range and sensitivity were taken into account. A capacitor was added in parallel with the DP cell in order to improve the sensitivity of the DP cell. Having selected the DP cell to be used, it was calibrated by using the arrangement shown in the Figure 3.7. This calibration from the sensor to the computer file gives the relationship between the output voltage of the DP cell and the differential pressure. The calibration curve is fairly linear as given in the specifications and demonstrated in Figure 3.8. The associated equations were programmed then into the data acquisition software.

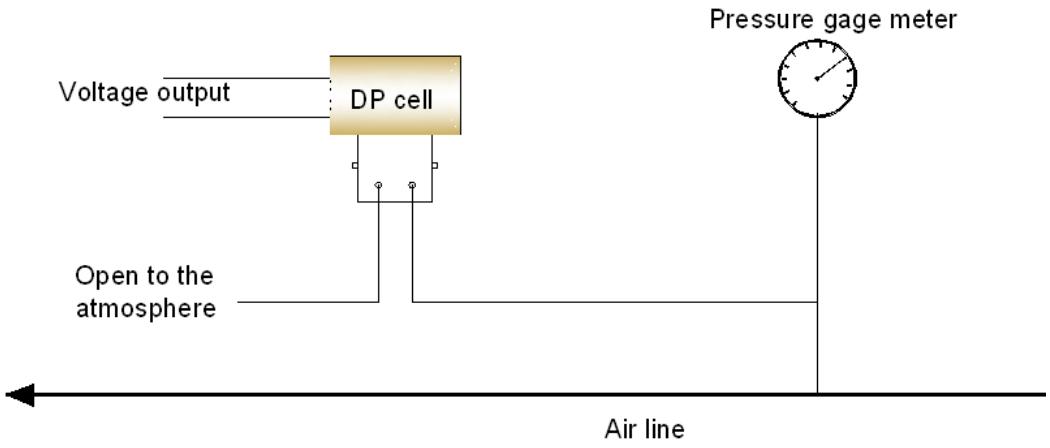

Figure 3.7 Arrangements for DP cell calibration

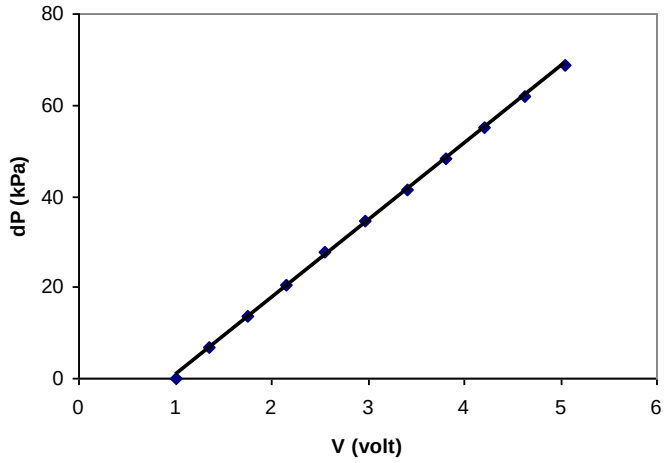

Figure 3.8 DP cell calibration

A purging system (shown schematically in Figure 3.9) was used in order to have a continuous liquid line from the pressure tapings to the DP cell. The purge was operated before every run by opening and closing the valve from the liquid line.

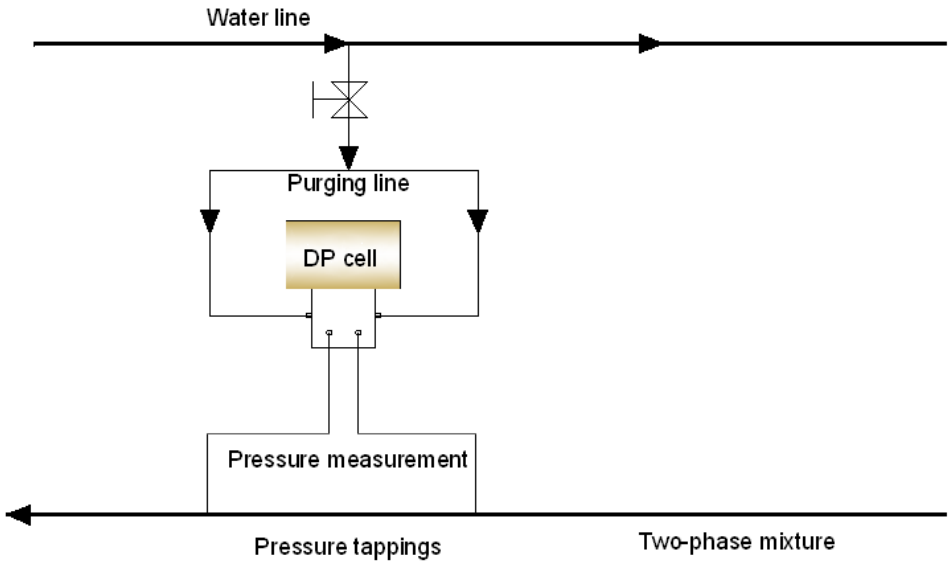

Figure 3.9 DP cell purging arrangement

3.2.6 High speed video system

A high-speed video camera was used in order to visualise the flow patterns. The KODAK HS 4540 camera has a maximum resolution of 256 x 256 pixels, and an upper frame recording speed of 45000 frames per second (fps). A schematic diagram of the experimental setup and the camera configuration is shown in Figure 4.10. The images were carried out at a location of about L/d=150, where L is the length of the pipe from the pipe inlet to the measurement zone and d is the pipe inner diameter. The test section was enclosed in a cubic Plexiglas box filled with water. This was done to reduce the pipe optical curvature. The camera was run at 256x256 pixels using a recording rate that ranged from 125 to 750 frames/s depending on the flow conditions. Various third-party lenses were used. This technique allowed capturing the image sequence of the flow.

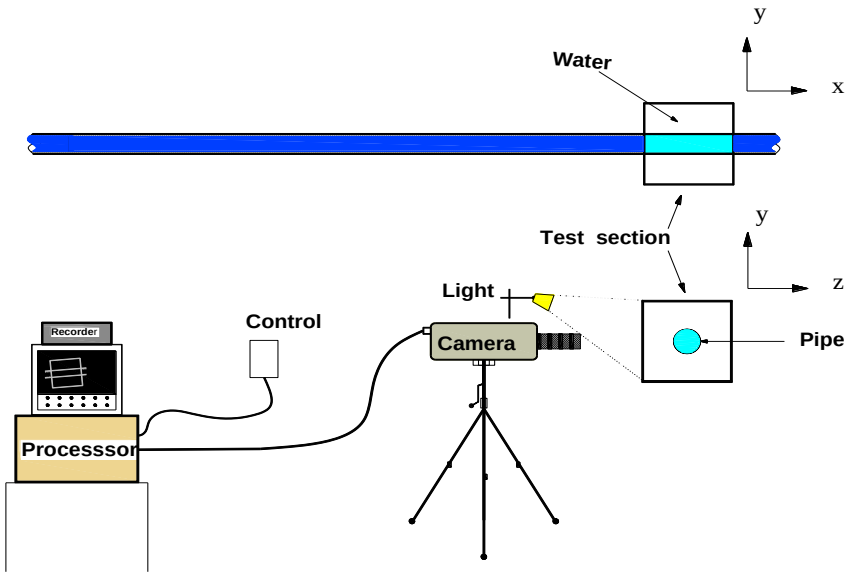

Figure 3.10 High speed video camera KODAK HS 4540

3.2.7 Capacitance probes for Liquid holdup measurement

3.2.7.1 General considerations

In order to be able to determine the liquid holdup, it was necessary to use a special liquid holdup measurement unit that fits the characteristics of this experimental work; the main factors to take into account are the fluid and the flow pattern. The fluids are air-water and the flow pattern is slug flow, however, we look forward to use nonconductive liquids in a later stage.

Capacitance sensors require the use of capacitance plates or rings to measure the dielectric constant of the two-phase mixture. This approach would prohibit the use of pipe or fluid that will conduct electricity. Thus in principle, capacitance sensors can not incorporate steel pipe and water as the liquid phase. For this reason, they are unsuitable for use in field operation. However they can be used in laboratory multiphase flow experiments where PVC, acrylic, or glass pipe is also used, and where the liquid phase can be a hydrocarbon mixture, such as kerosene. In the present work acrylic pipe has been used. Therefore a capacitance sensor for liquid holdup measurements was used. It consists of such a typical arrangement by construction of etched copper plates that produce a capacitor with change in the dielectric permittivity being sensed; in this case the dielectric material consists of the acrylic wall pipe and

air-water mixture. There was a need for further processing to be performed on the output to gather a realistic value as explained below. A review of capacitance-sensor techniques has been carried out by Huang *et al.* (1988).

3.2.7.2 Principle of operation

A capacitor consists of two conductors (plates) that are electrically isolated from one another by a nonconductor (dielectric). When the two conductors are at different potentials (voltages), the system is capable of storing an electric charge. The storage capability of a capacitor is measured in farads (F). It is known that the capacitance of a parallel-plate capacitor varies linearly with the dielectric constant of the medium between the plates, this relationship is described by:

$$C = \alpha K \tag{3.1}$$

Where

C= Capacitance of the capacitor in appropriate units

α= Constant of proportionality determined by the geometry of the device

K= Dielectric constant for the medium between the plates

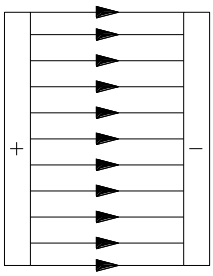

Figure 3.11 Capacitor

If we have a compound medium formed say by sandwiching layers of different materials together, the effective dielectric constant is known to be the linearly weighted average of the dielectric constants of the pure components. Thus for the case of a two-phase mixture occupying the space between the plates such that the entire cross section of the space occupied by the two-phase mixture is "seen" by the plates we can write

$$K_{tp} = \alpha_L K_L + (1 - \alpha_L) K_G \tag{3.2}$$

where

K_{tp}= Effective dielectric constant of the two-phase mixture

K_L, K_G = Dielectric constant of the pure liquid and pure gas respectively.

α_L = in-situ volume fraction of the liquid phase

This relationship may be rearrange to give

$$K_{tp} = (K_L - K_G)\alpha_L + K_G \tag{3.3}$$

$$= \beta_1 \alpha_L + \beta_2 \tag{3.4}$$

Where

$$\beta_1 = (K_L - K_G)$$

$$\beta_2 = K_G$$

Then

$$C = cK_{tp}$$

$$= c\beta_1 \alpha_L + c\beta_2$$

i.e. the capacitance is a linear function of the in-situ volume fraction

3.2.7.3 Electrode System

The first to attempt to use capacitance sensors was made by Gregory and Mattar (1973). They evaluated several designs and concluded that the use of two helical capacitance plates, 180 ° out of phase, worked best. They also recommended specific dimensions and angles for the electrodes, depending on the pipe diameter. However Kouba (1986), Kouba (1987) and Kouba *et al.* (1990) developed a different design in which the electrodes were three equally spaced rings. The centre ring was the positive

electrode, and the outer rings were ground-referenced. They showed that measurements with this design were as accurate as those with the helical sensors, and that the overall length of the sensor was much shorter, especially for larger diameter pipe. Later Butler *et al.* (1995) developed a ratio-arm bridge capacitance transducer.

In the present work, the two electrodes of the capacitor are mounted on the outer side of pipe walls. The variations in the percentage of phases in two-phase flow cause changes of the equivalent permittivity of the dielectric between the electrodes.

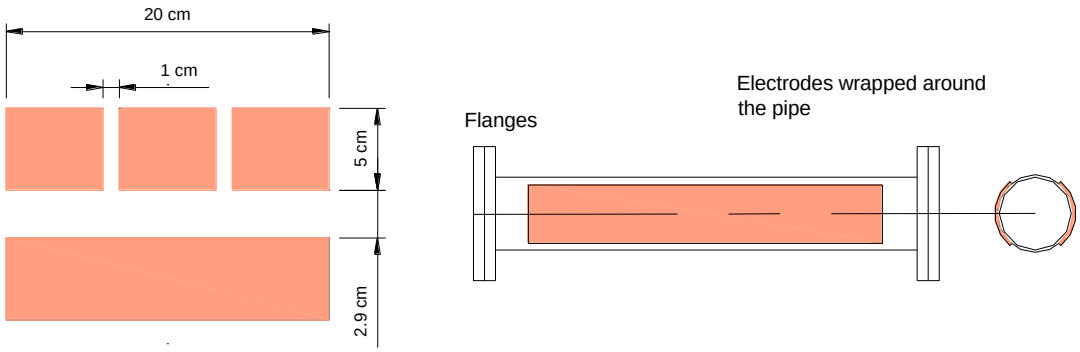

Figure 3.12 Electrode configuration of the capacitor sensor

The instantaneous liquid holdup measurement is averaged over pipe section occupied by the sensor. Also since the measurement sensitivity of a capacitance sensor is proportional to the electrode area. Sensitivity can be increased by increasing the probe length or by decreasing the size of the gap between the electrodes. However, as the electrode size decreases, the signal to noise ratio (SNR) of the system decreases. Thus the noise level of the data acquisition system limits the electrode size.

In order to optimise the sensor performance a number of parameters should be carefully selected. The most important parameters are the wall thickness of the insulating pipe and the dimensions of the electrodes. In this case, the dimension of the electrodes was the parameter to modify since it is more practical to specify a longer or shorter probe than to decrease the distance from the pipe wall (thickness). The length

chosen is based on the flow pattern in order to get a signal as big as possible without losing details of the flow pattern.

Several electrodes sizes were tried (including without guard electrodes) and the final electrode configuration of the primary sensor is shown in Figure 3.12. Two sensing electrodes are mounted flush to form a capacitor. The electrode length along the flow direction is 60 mm. The two pairs of electrodes in both sides of the sensing electrodes work as guard electrodes, they keep the electric field between the plates uniform (Figure 3.13) so that the phase distribution does not affect the capacitance.

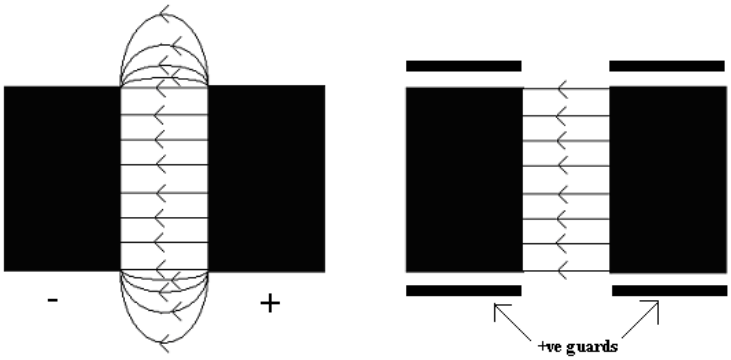

Figure 3.13 Guard electrodes

3.2.7.4 Electronics and Housings

The system used in the probe consists of a number of electronic circuits which serve to energise and then sense and record electrical currents in electrodes embedded in the wall of the pipe. This is performed in four main stages: 1) rectifying and filtering the incoming power, 2) generating the radio frequency signal, 3) measuring the changes in the frequency, and 4) recording the signal.

In general the electronics necessary to process the capacitance sensor signal poses difficulties. The difference in capacitance between a pipe full of air vs. one full of water is relatively small. As a result, such things as changes in humidity can cause significant measurement errors.

A practical capacitance sensor always needs an earthed screen to shield the electrode plates from external electrical fields, Figure 3.14 (a). This results in a three-terminal

sensor consisting of the electrode capacitance C_x, and the stray capacitances between the electrodes (including the leads to the measuring circuit) and the shielding screen, C_{S1} and C_{S2}. The values of C_{S1} and C_{S2} usually range from a few tens to several hundred pF. Other strays may arise from the parasitic capacitances C_{p1} and C_{p2} of the capacitance measuring electronics connected to the sensor. The value of these strays usually ranges from a fraction to a few tens of pF. The equivalent circuit of a practical capacitance sensor taking all the strays into account is shown in Figure 3.14 *(b)*.

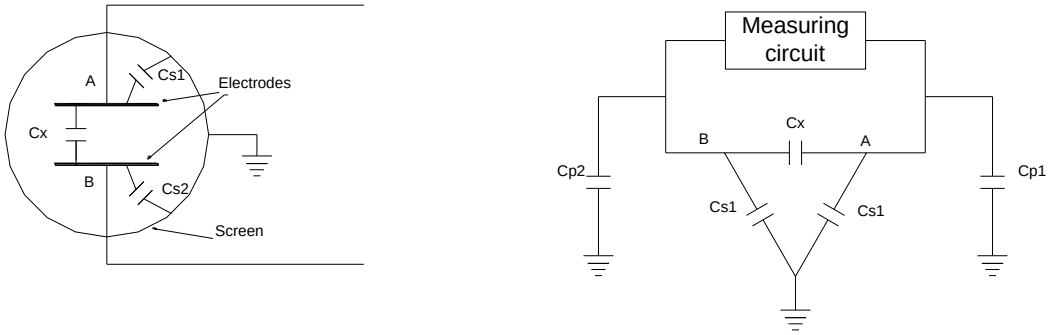

(a) (b)

Figure 3.14 Capacitor sensors. (a) Sensor structure. (b) Equivalent circuit**.**

Figure 3.15 shows the capacitance probe. We can also see the shield that was used in order to isolate the probe from external electromagnetic fields that can affect the measurements.

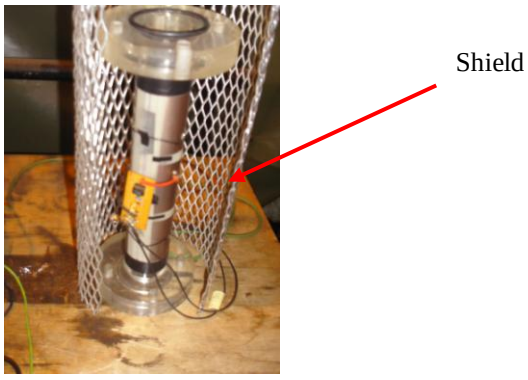

Figure 3.15 Capacitance probe. The overall screen is used to protect the sensor from the interferences of external electromagnetic fields.

The capacitance measuring circuit is based on the RC (resistive-capacitive) oscillation method, in which an RC oscillator converts dc power to ac power at a predetermined frequency ranging from several hundred kHz to a few hundred MHz. The oscillation

frequency of the *RC* oscillator depends on the unknown capacitance *Cx*. The frequency is measured by using a frequency-to-voltage converter (FVC) to obtain an analogue output, and then used to determine the unknown capacitance. Figure 3.16 shows the diagram of the RC oscillator based transducer used. It can be seen that the two main components are the oscillator and the (FVC).

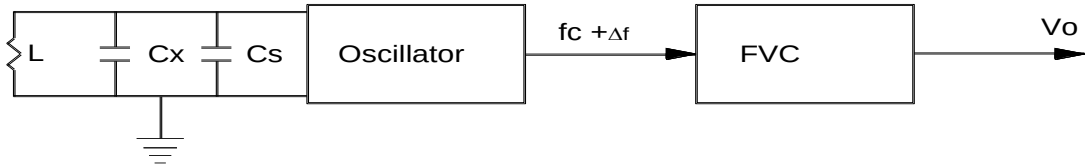

Figure 3.16 The diagram of the RC oscillator based transducer

The change in the oscillation frequency can be expressed as

$$\Delta f = -\frac{f_0}{2(C_x + C_S)} \Delta C_x \tag{3.5}$$

Where *Cs* is the overall energy stray capacitance in parallel with *Cx*. and f_0 is the standing oscillation frequency.

A phase-locked loops (PLLs) type FVC was used. A FVC is a circuit which responds to the frequency of its input and delivers an output voltage which is linearly proportional to that input frequency. Figure 3.17 shows the frequency-voltage conversion section of the circuit of the void fraction detection unit. The circuitry is provided with potentiometer adjustments for setting sensitivity and time delays.

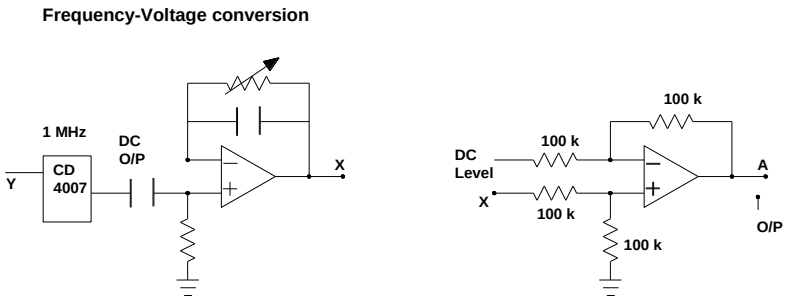

Figure 3.17 Frequency-voltage conversion section of the RC oscillator transducer

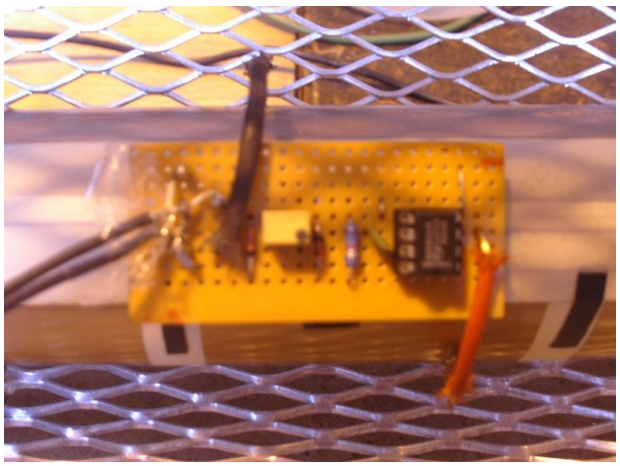

Figure 3.18 RC Oscillator on the pipe.

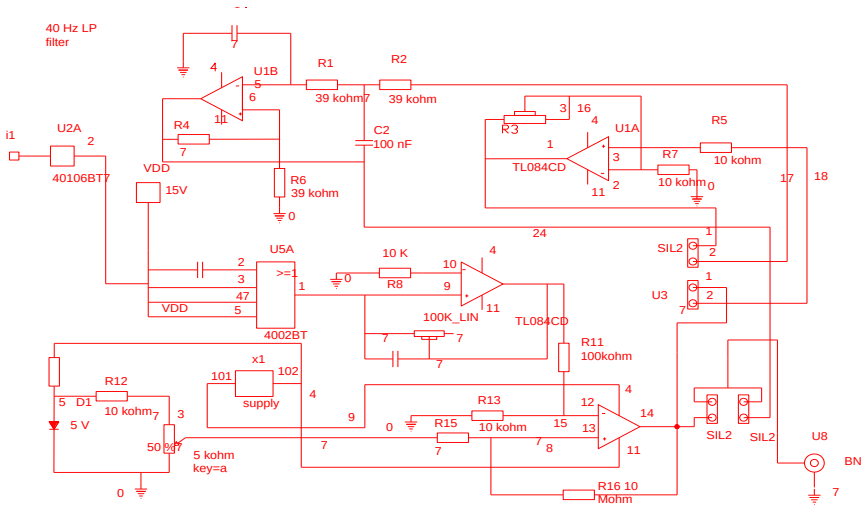

Figure 3.19 Layout of the electronic circuit of the capacitance probe

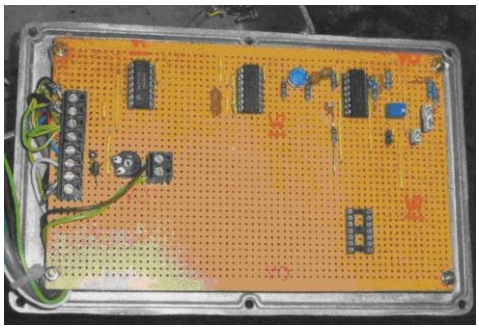

Board layout of the signal conditioning unit

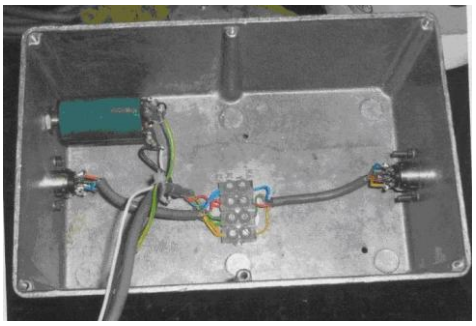

Offset control pot and daisy chain connection of supplies (0V, +5V, ±15V,-5V)

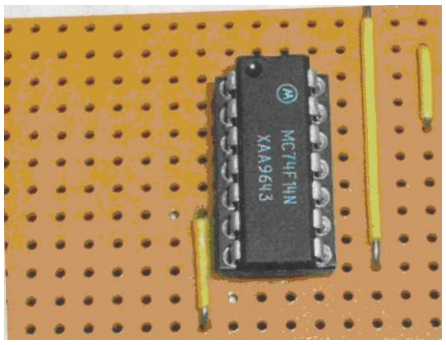

SCHMITT Hex inverter conditions the arrival signal to sharper square waves

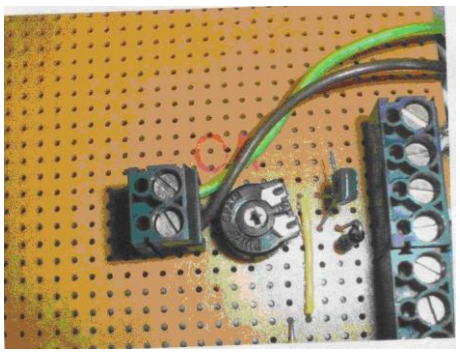

Voltage offset to coordinate displacement to run 0-+ve O/P

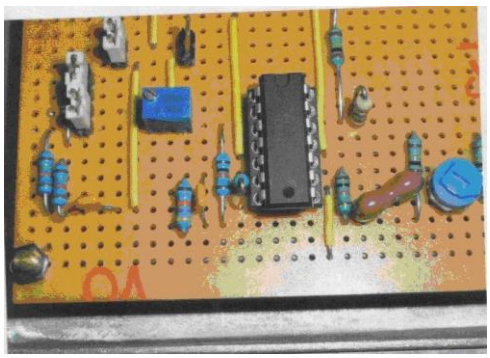

Amplifier section with adjustable gain and filter

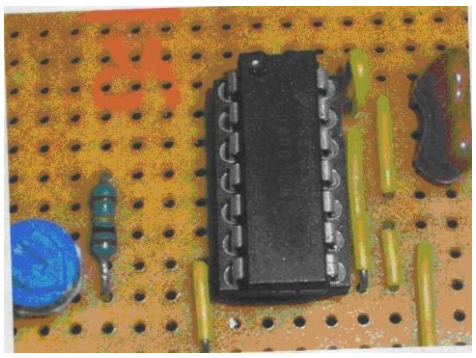

CD4007
Complimentary pair with inverter used to convert frequency to voltage

Figure 3.20 Components of the electronic circuit of the capacitance probe

3.2.7.5 Construction of the capacitance probe

The capacitance sensor was built using Printed Circuit Board (PCB) technology. In order to manufacture the plates the following points are performed:

1) Art work produced via software programme such as power point or AutoCAD.

2) Photocopy from black & white print to overhead print transparency film. At least 4 films needed.

3) The 4 film prints are bound together using double-sided tape. Locate on UV machine glass plate using clear single sided tape. Position as near centre as possible for UV influence to be as equal as possible over whole area of foil.

4) This section to be subdued lighting as the foil laminate has a photosensitive etch resistant layer along with a 35 μ copper layer and finally a 50 μ polyester base layer. With the mask from 3) above introduce, a piece of photo resistive foil cut to size and place with photosensitive film facing down over mask and use location card as necessary to set foil in relation to mask.

5) Close lid of UV and set timer to ensure reaction to photo resistive film (3min).

6) Ensure tank of developer is on and up to temperature. Then introduce foil into tank net holder. When after a short while an examination of foil shows the stripping of photo resistance material that was affected by the UV light source to unveil the copper cladding. When the copper cladding gives a clear outline of the inverse of the mask then take out of the tank.

7) Wash in tray of clean water.

8) With etching tank up to temperature place foil in net holder. Keep examining the foil for the removal of all exposed copper. When complete, remove from tank.

9) Wash in another tray of clean water.

10) Dry off foil on glass plate. Then swill with methanol and using tissue wipe off surplus photo-resistive material.

11) Wash with clean water and dry off.

Chemical info. Caustic Soda NaOH 0.3 % to 5 l tank developer temp 20-25 °C

Ferric Chloride $FeCl_3$ 2kg to 5 l tank and Etching temp 45-50 °C.

3.2.7.6 Calibration

A good calibration is required in order to get good results. Due to the fact that separated flow (slug, stratified, wavy) is expected, the calibration was performed with stratified flow in a horizontal pipe. Phase distribution or flow pattern effect was coped by making sure the electrodes covered the circumference around the pipe as much as possible. The electrode configuration is with the electrodes on the west and east sides of the cross sectional area of the pipe as shown in Figure 3.21.

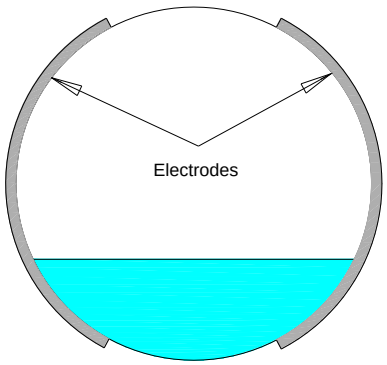

Figure 3.21 Electrodes configuration on the pipe

The corresponding calibration curve for such an arrangement is illustrated in Figure 3.22.

Dynamic tests were performed with the probes mounted on the inclinable rig with air flow in still water. For these test average values of both real and measured liquid holdup were compared, Figure 3.23. The real liquid holdup is known from the difference in the height of the liquid level in the pipe with and without air flow, taking advantage of the transparent section of the pipe. This demonstrated that this calibration could be applied for all inclinations. In this way the capabilities of the probe are extended. A typical set of signals obtained is shown in Figure 3.24.

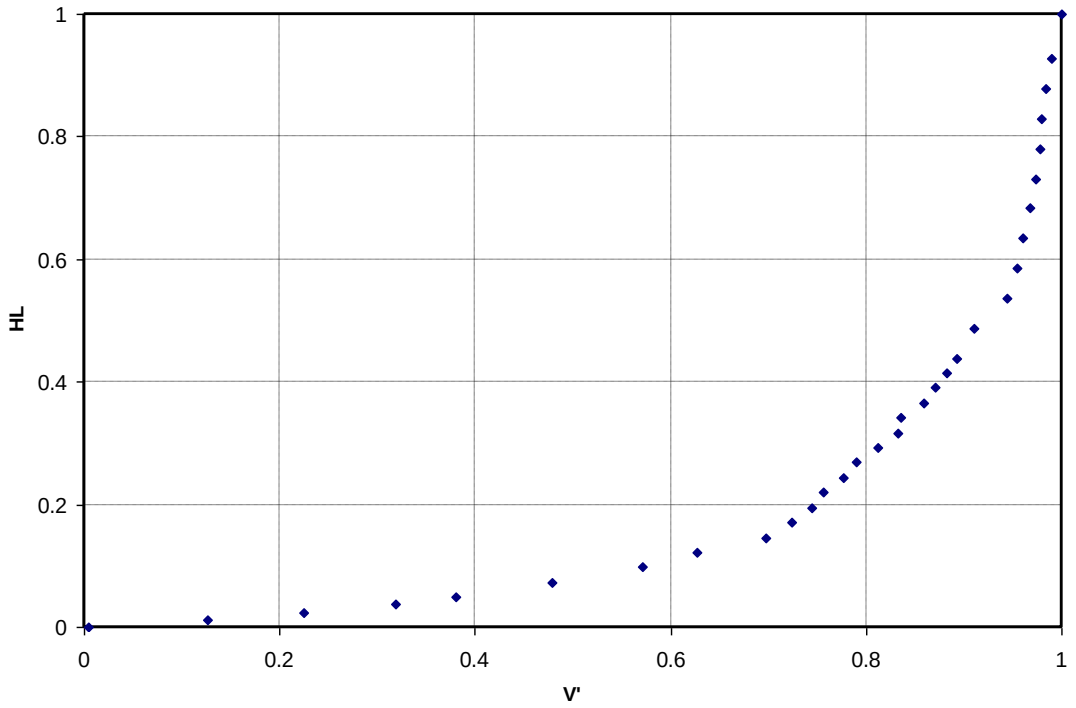

Figure 3.22 Calibration curve of the capacitance probe, liquid holdup, H_L vs. dimensionless voltage, v'

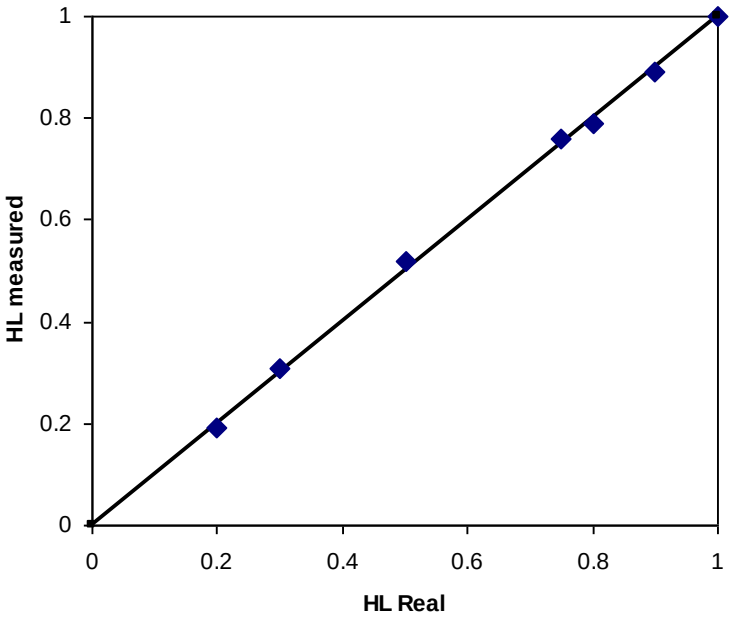

Figure 3.23 Comparison of measured and actual liquid holdup using air flow in still water

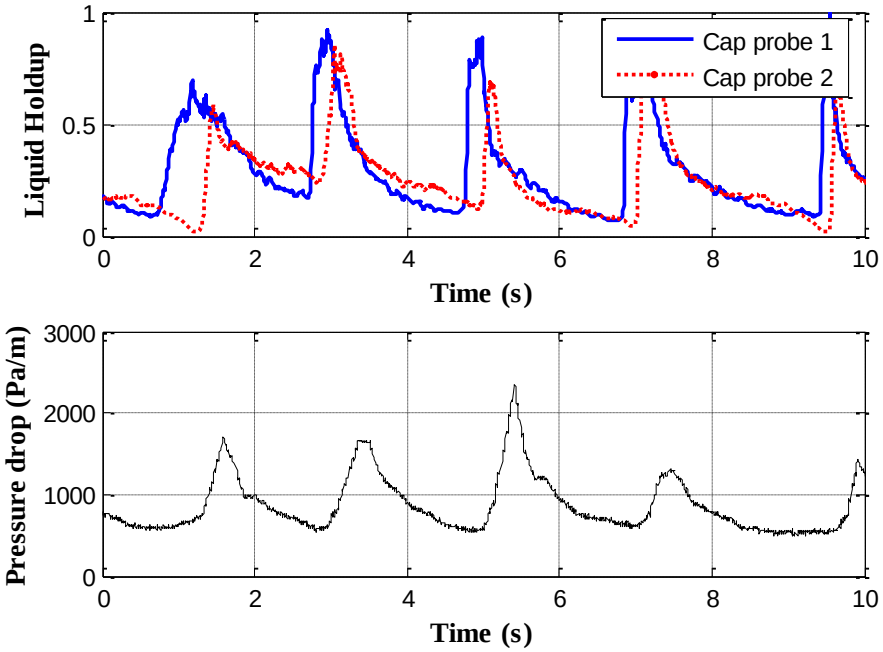

Figure 3.24 Typical set of signals obtained with the data acquisition, horizontal flow.

3.2.7.7 Effect of temperature:

In order to observe how the temperature variations could affect the calibration of the void fraction meter, a temperature control system was constructed and utilised, Figure

3.25. This control system consists of basically a chamber enclosing an environment where the temperature is kept constant by the action of an auto tune-temperature controller, CAL 2300, which reads the temperature from a thermocouple and depending on the value of this signal with respect to a set point, takes an action that can be either: to switch on and off a fan or a bulb. Then a relationship is obtained between the signal in the oscilloscope (voltage) and the void fraction for a fixed temperature. Later in some way the signal can be adjusted by subtracting a value due to increase by temperature.

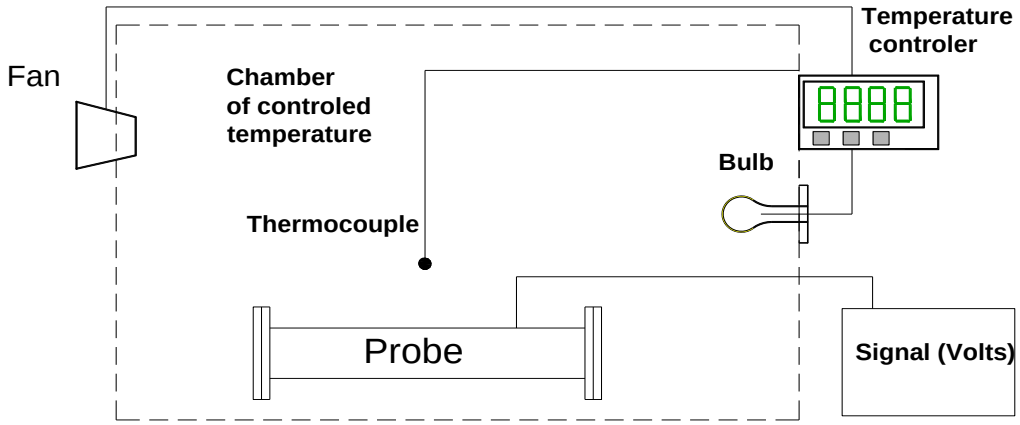

Figure 3.25 Effect of the temperature on the capacitance probe

The response of the capacitance probe to the changes in the fluid temperature can be observed in Figure 3.26. Even though the fluid temperature increases during the running of the experiments, only adjustments are performed on the voltage for the pipe empty and full of water respectively, without measuring the temperature.

The capacitance sensor used gives a volume averaged liquid holdup at each point in time, giving an estimate of the actual liquid holdup profile changing with time.

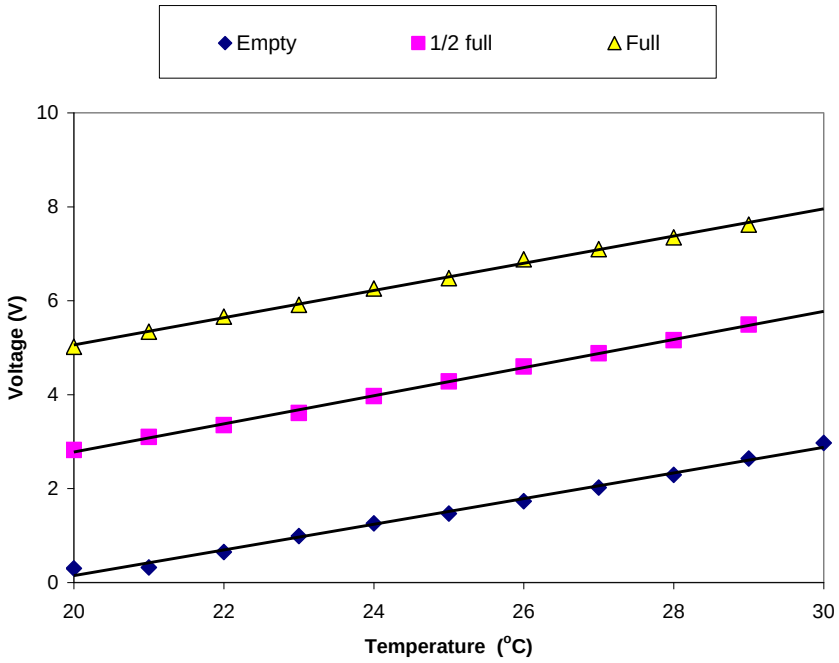

Figure 3.26 Effect of change in the fluid temperature on the response of the probe

In order to get the actual gas superficial velocity in the pipe, the gas superficial velocity was corrected using the equation.

$$U_{SG} = \frac{\dot{m}}{\rho_P A_P} \tag{3.5}$$

Where

$$\dot{m} = \sqrt{\rho_R \rho_A} Q \tag{3.6}$$

ρ_P = gas density at pipe pressure = 1.2 P_P

A_P = Pipe area

Q = indicated flow at the rotameter

ρ_R = gas density at reference (1.2)

ρ_A = gas density at rotameter =1.2 P_A

P_P = Pipe pressure

P_A = Pressure at the rotameter

3.3 Methodology during an experimental run

In order to provide data on gas-liquid two-phase flows behaviour in inclined pipes an experimental programme was carefully designed. In doing so, the exploration of the factors affecting the evolution of slug flow was undertaken. First it is necessary to determine the experimental conditions to be studied and then to proceed to establish the corresponding gas and liquid flow rates. Once a particular inlet flow condition has been set, the condition is maintained until the experiment is performed and the data is recorded. Once the full series of experiments is completed, the analysis of the corresponding results is made with the purpose of determining if they behave in an acceptable way, if not, the runs are repeated and we look for causes of error. The same procedure is repeated until having tested the entire matrix of inlet flow conditions.

3.4 Uncertainty of experimental measurements

Uncertainty of a measured value is an interval around that value such that any repetition of the measurement will produce a new result that lies within this interval. This uncertainty interval is assigned following established principles of uncertainty estimation. Due to the fact that only one sample experiment was performed for each run, a reasonable estimate of the measurement uncertainty due to random errors is based on the least count approach. Table 3.3 presents estimated error in each of the measurements carried out in the experiments presented in this work. Appendix C provides the details of the calculation, including propagation error in calculated variables.

Table 3.3 Uncertainty of the experimental measurements

Measurement	**Uncertainty ±**
Superficial liquid velocity	0.06 ms^{-1}
Superficial gas velocity	0.01 ms^{-1}
Liquid holdup	15% of the reading
Pressure drop	0.025% of full scale

Chapter 4

Gas-Liquid Flow in 38 mm Pipe

In this chapter the results of the experiments carried out in a 38 mm pipe will be presented. The experimental arrangement was described in Chapter 3. In the experiments performed, measurements of liquid holdup were taken at two locations downstream of the mixing section for horizontal and different inclinations for a wide range of flow rates. The pressure drop was also taken by means of a differential pressure transducer. This permitted the effects of flow rates and of pipe inclination to be studied. Time series analysis was performed on the holdup time traces and average and distribution of the flow characteristics are reported, e.g. slug frequency, bubble propagation velocity, liquid holdup in the liquid slug body and slug length. Also the results comparisons with models and correlations are reported. Both analysis and new data on gas-liquid flow parameters are reported for the inclined pipe considered. Visual observations were performed in order to identify the flow patterns.

This chapter is divided into the following sections each of which will provide details about the results presented as well as some discussion: 4.1 Test matrix, 4.2 Visualisation of the flow patterns, 4.3 Flow pattern maps, 4.4 Liquid holdup, 4.5 Frequency, 4.6 Pressure drop, 4.7 Structure velocity, 4.8 Estimation of characteristic parameters of slug flow from the PDF plot and finally 4.9 The effect of increasing the liquid flow rate.

4.1 Test matrix

A total of 960 experiments were carried out for several inclination angles within the range of -5° to 90° (with respect to the horizontal) and most of them with the same inlet flow conditions.

The experiments were divided into two campaigns; low and high liquid flow rate. For very high superficial velocities the flow pattern can be considered independent of the inclination angle as it has been shown by Weisman and Kang (1981). For lower mixture velocities however the flow pattern is more sensitive to the inclination angle and therefore the effect of pipe inclination needs to be taken into consideration, since modelling flow pattern transitions and pressure drop in deviated wells often requires holdup and pressure drop estimates for multiphase fluid. Therefore in order to observe the changes of the flow parameters with pipe deviation, a selected range of superficial velocities are considered in this study.

In the methodology used, the effect of the inclination angle was systematically investigated by conducting a series of air-water experiments for different inclination ranging from 5° downward to 90° upward. The data from the visual observations, plus the data obtained from time series analysis will allow obtaining a picture of the behaviour of multiphase flow in deviated pipes. Table A.1 in appendix A summarises the test conditions examined in this work.

Each point in the matrix of inlet flow conditions is determined by the values of both gas and liquid superficial velocity. The experimentation process involves the methodology to follow in order to perform any run defined within the matrix of tests of inlet flow conditions and inclination angles.

4.2 Visualization of flow patterns

The first and simplest approach to study two-phase flow behaviour in deviated pipes is to visualise the flow. Flow patterns play very important roles in two-phase flow. Each regime has certain hydrodynamic characteristics, occurrence in nature and many applications in industries. In this work, the designation of the flow pattern has been based largely on individual interpretation of visual observation, carried out through the transparent pipe section of the rig, by means of a high speed video system as well as the naked eye. Also techniques of Probability Density Function (PDF), lag plot and cross correlation have been used to characterise the flow pattern as can be seen in the following sections.

Regarding the high speed video system, in order to diminish deformation of the pictures due to the refraction by the cylindrical pipe wall, the recordings were performed with a squared sided, 0.2x0.2x0.2 m^3 acrylic resin box filled with water mounted around the pipe, and it has been found that front lighting gave the best results. The observations in the current work are illustrated in Figures 4.1 to 4.5 by a set of photographs that show mainly the effect of inclination angle on the flow pattern.

Stratified flow was only observed when the pipe was horizontal or inclined downwards (Figure 4.1a and Figure 4.4a). For relatively low gas superficial velocities the dominant flow pattern is intermittent (Figure 4.1b-4.1g), intermittent flow includes both slug and churn. Inclined slug flow is observed to have back flow in the liquid film part of the slug unit. It appears as if most of the liquid is at some time flowing backward.

For upward inclined flow and the conditions of the test matrix of Appendix A, as the inclination angle increases with respect to the horizontal, the flow pattern gradually changes from stratified to slug and then to churn flow as shown in Figure 4.1, with the transition form stratified to slug flow occurring at very small inclinations (less than 5°) whereas the transition from slug to churn flow occurs at an inclination angle of about 60°.

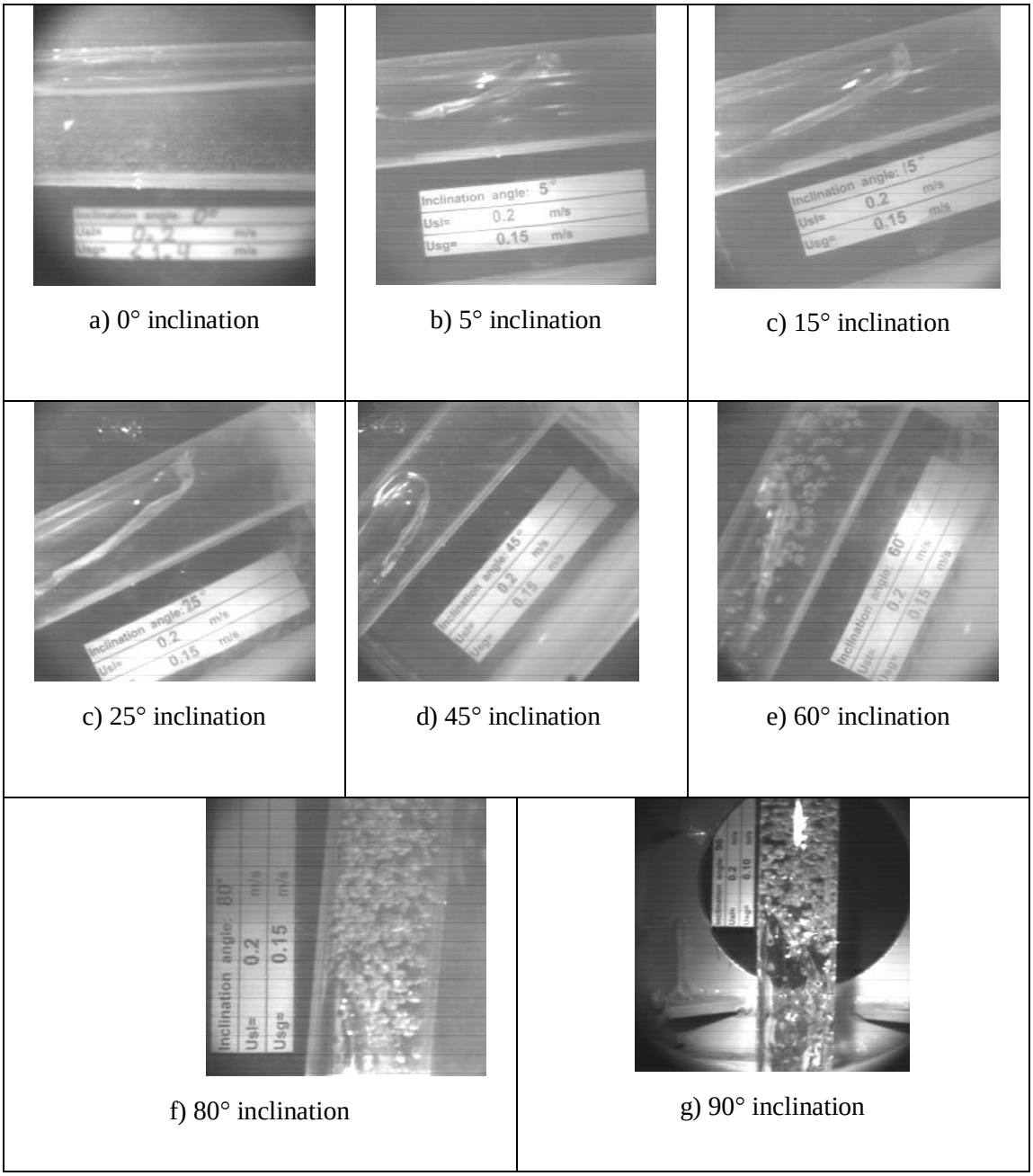

a) 0° inclination

b) 5° inclination

c) 15° inclination

c) 25° inclination

d) 45° inclination

e) 60° inclination

f) 80° inclination

g) 90° inclination

Figure 4.1 Visualization of flow patterns in deviated pipes; liquid superficial velocity = 0.2 m/s, gas superficial velocity = 0.15 m/s.

As the pipe orientation comes close to the vertical, the bubbly flow pattern appears at low liquid and gas rates because of high local concentrations of bubbles, that move from the top of the pipe (in inclined) to the centre (Figure 4.2). The changes observed in the flow pattern with inclination angle and can be related with the change of the liquid holdup with inclination and also in others parameters such as the pressure drop and the frequency.

Also, for inclined upward flow at low gas superficial velocities, small discrete gas bubbles flow through the upper part of the pipe cross section. The concentration of bubbles tends to increase with the liquid superficial velocity, and the mixing section of the slug becomes more turbulent which in turn provokes air entrainment into the liquid slug. As the gas superficial velocity is increased, the gas bubbles tend to occupy an increasing cross section of the pipe. Figure 4.1e to 4.1g depicts such a difference in the flow pattern at different pipe inclinations

One distinction between flow patterns in vertical and inclined systems can be obtained from the examination of the pictures in Figure 4.2. Because of the buoyancy force, more of the gas phase tends to flow along the upper wall of the pipe than the lower wall. The gas segregation that occurs is particularly characteristic for flow patterns in which phase velocities are not too high, as with bubbly and slug flow. In this two flow regimes, gravity effects dominate and bubbles tend to flow in the upper portion of the pipe.

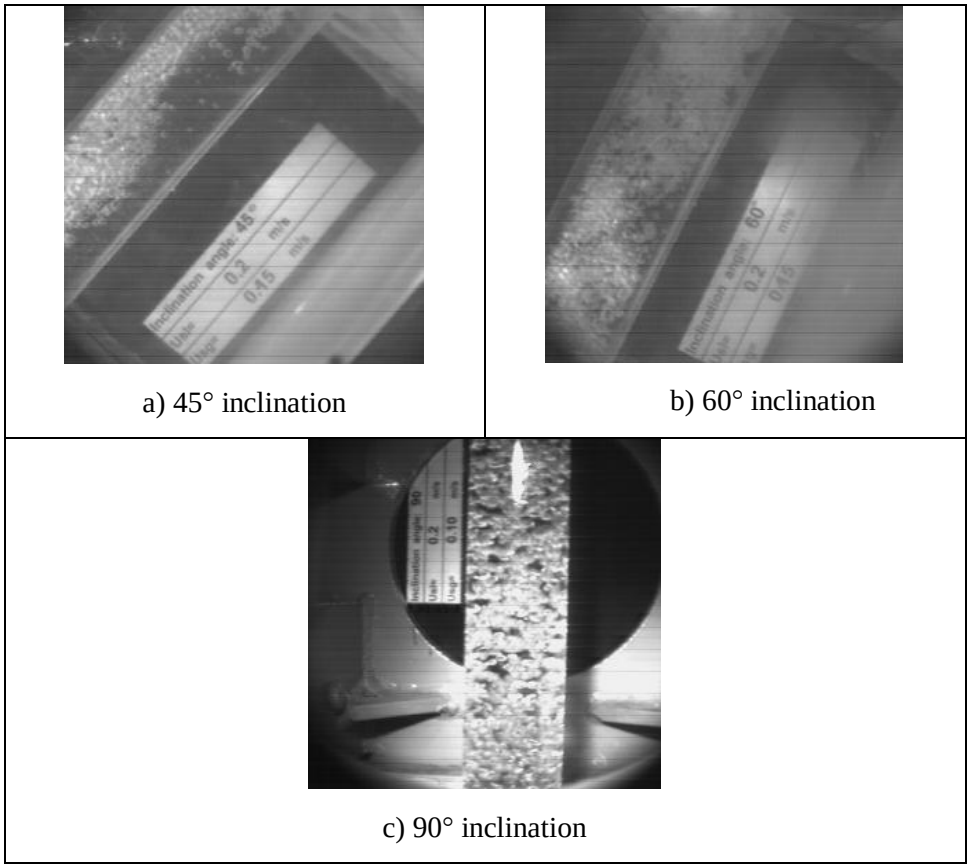

Figure 4.2 Visualization of flow patterns in deviated pipes; liquid superficial velocity = 0.2 m/s, gas superficial velocity = 0.45 m/s.

Another distinction between vertical and inclined flow is the influence of pipe inclination on the shape of large bubbles (see Figure 4.3). The increased radial pressure on the bubbles tends to make them sharper than their counterparts in vertical systems, Hasan and Kabir (1988). This observation is particularly true of Taylor bubbles in slug flow. In vertical flow, the Taylor bubbles have been observed to have a symmetrical hemispherical top (Figure 4.3b). In inclined flow, the top of the Taylor bubble is shaped more like an ellipsoid than a hemisphere and no longer symmetrical about the bubble axis (Figure 4.3 a).

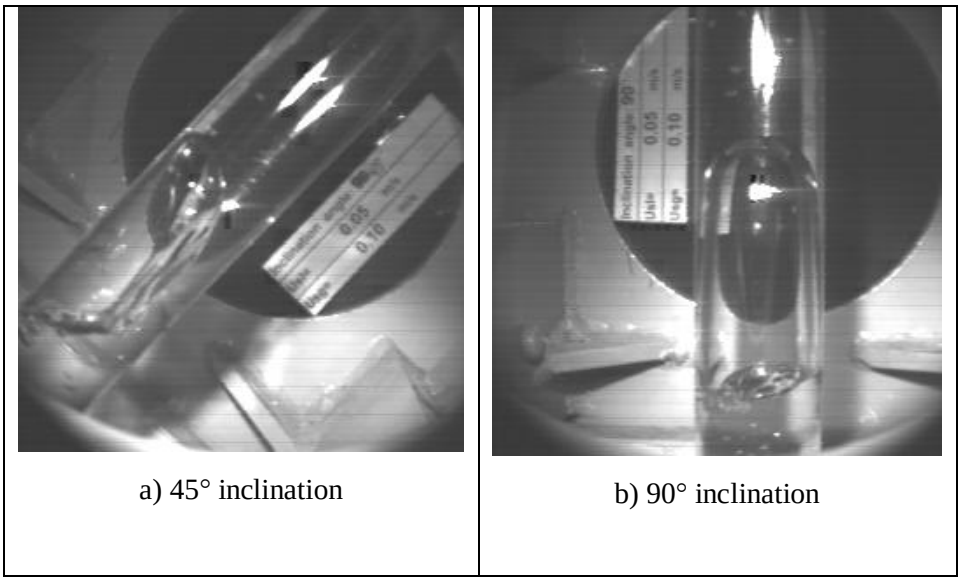

a) 45° inclination

b) 90° inclination

Figure 4.3 Visualization of flow patterns in deviated pipes; liquid superficial velocity = 0.05 m/s, gas superficial velocity = 0.10 m/s.

By increasing the gas superficial velocity, highly aerated slugs or waves with back flow and roll-waves that sometimes look like static are observed (Figure 4.4). This appears to be almost independent of the angle of inclination. In addition, a very thin film is seen to form at the top of the pipe. For such flows, strong fluid shear force counteracts gravity, and much of the gas tends to flow through the central portion of the pipe, as in vertical flow.

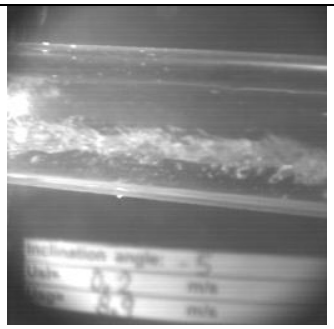

a) -5° inclination

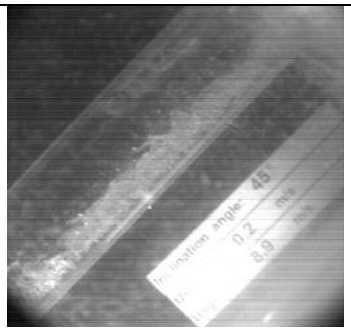

b) 45° inclination

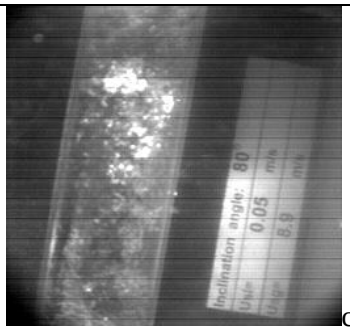

c) 80° inclination

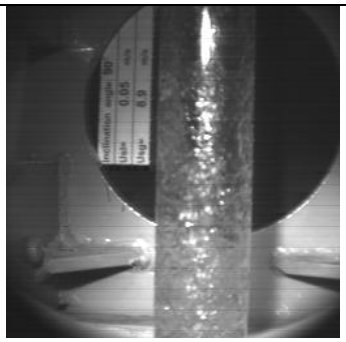

d) 90° Inclination

Figure 4.4 Visualization of flow patterns in deviated pipes; liquid superficial velocity = 0.2 m/s, gas superficial velocity = 8.9 m/s.

Experimental detection of flow patterns and transition boundaries has to be based on the prerequisites knowledge of expectant flow patterns. Industrially there is a requirement not only to understand the possible flow patterns but also to predict which flow regime exist within a given pipe line. Since different flow mechanisms are dominant in different flow patterns, correct identification of the different flow patterns is the basis for prediction of liquid holdup and pressure drop. A revision of flow patterns identification techniques was made in Chapter 2.

Following the suggestions of Jones and Zuber (1975) and Costigan and Whalley (1997) Probability Density Functions (PDF) of the time series of the liquid holdup were examined to identify flow patterns. The PDFs of holdup provides a more objective method by which flow patterns two-phase flow may be defined, Heywood and Richardson (1979).

The first step in the time series analysis performed, consisted of plotting the time series, this allows detecting the essential components of the series. An example of a typical time trace of liquid holdup obtained with the capacitance probes is shown in Figure 4.5. The variation of the liquid holdup in the time series shows the unsteady character of the flow.

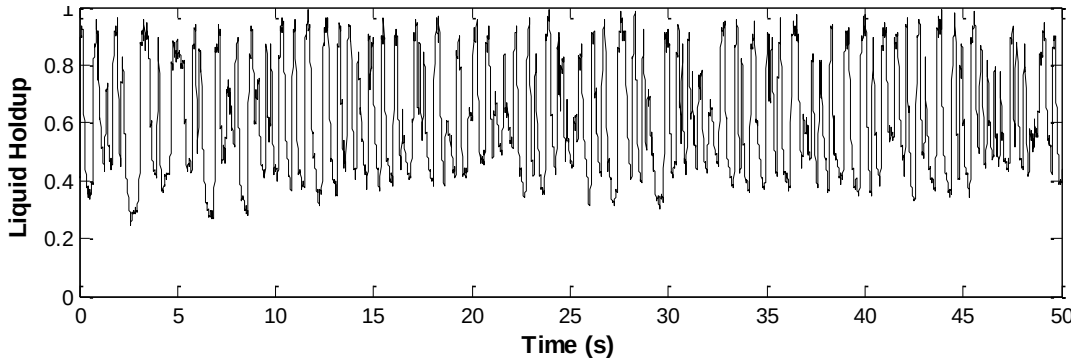

Figure 4.5 Typical time trace of the liquid holdup for 45° inclination angle, Usl=0.73 m/s Usg=0.9 m/s.

The time trace of holdup can provide lots of information, however the corresponding time series analysis has to be performed. In this section, the adopted procedure is based on the statistical analysis of the liquid holdup records. Simultaneous analysis of multiple time series from each of the experiments requires some degree of automation, due to the large amount of data involved. For one data point, two holdup and one pressure drop sensor time traces were analysed, each containing up to 36000 samples. An analysis tool kit was implemented in Matlab. The main motivation for generating a tool kit was to ensure equal treatment of all data points, and to interactively be able to evaluate and modify the automatic calculations.

The rate of data acquisition was selected based on the lag plot of the data (Figure 4.6b). A lag is a fixed time displacement. For a lag plot on a single time series, the lag plot consists of:

- Horizontal axis = $H_L(i)$
- Vertical axis = $H_L(i+1)$

Where H_L(i) is the liquid holdup at point *i*. *i*=1, 2, 3,… A lag plot checks whether a data set or time series is random or not. Random data should not exhibit any identifiable structure in the lag plot. This sample lag plot exhibits a linear pattern. This shows that the data are strongly non-random.

The corresponding autocorrelation plot (Figure 4.6a) of the data shows that there is a high degree of autocorrelation between adjacent and near-adjacent observations (i.e., there is time dependence in the data) and therefore time series is non-random. It can be observed that in general the holdup is a non-random variable.

Autocorrelation plots are formed by

- Vertical axis: Autocorrelation coefficient
- Horizontal axis: Time lag *h* (*h* = 1, 2, 3, ...)

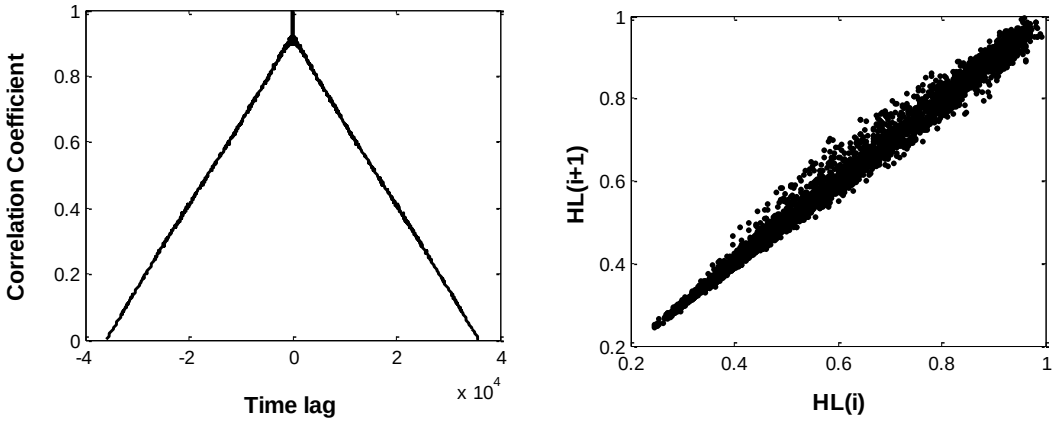

a) **b)**

Figure 4.6 Typical autocorrelation plot (a) and the corresponding lag plot (b) for the time series of figure 4.5.

Autocorrelation was also a useful tool for finding repeating patterns in a signal, such as determining the presence of periodic structures in the signal which have been buried under noise, or identifying the fundamental frequency of a signal which does not actually contain that frequency component, but implies it with many harmonic frequencies.

In Figure 4.7, several time series plots for different inclination angles are put together in order to observe the effect of inclination on the time series, this is done for several liquid superficial velocities as well. For these conditions, the major differences are clearly seen at inclination angles close to horizontal.

Since the cross sectional area-average holdup distribution along the pipe length was recorded by rapid scanning of the pipe at one point, a Probability Density Function $p(H_L)$ may be estimated from the holdup time trace.

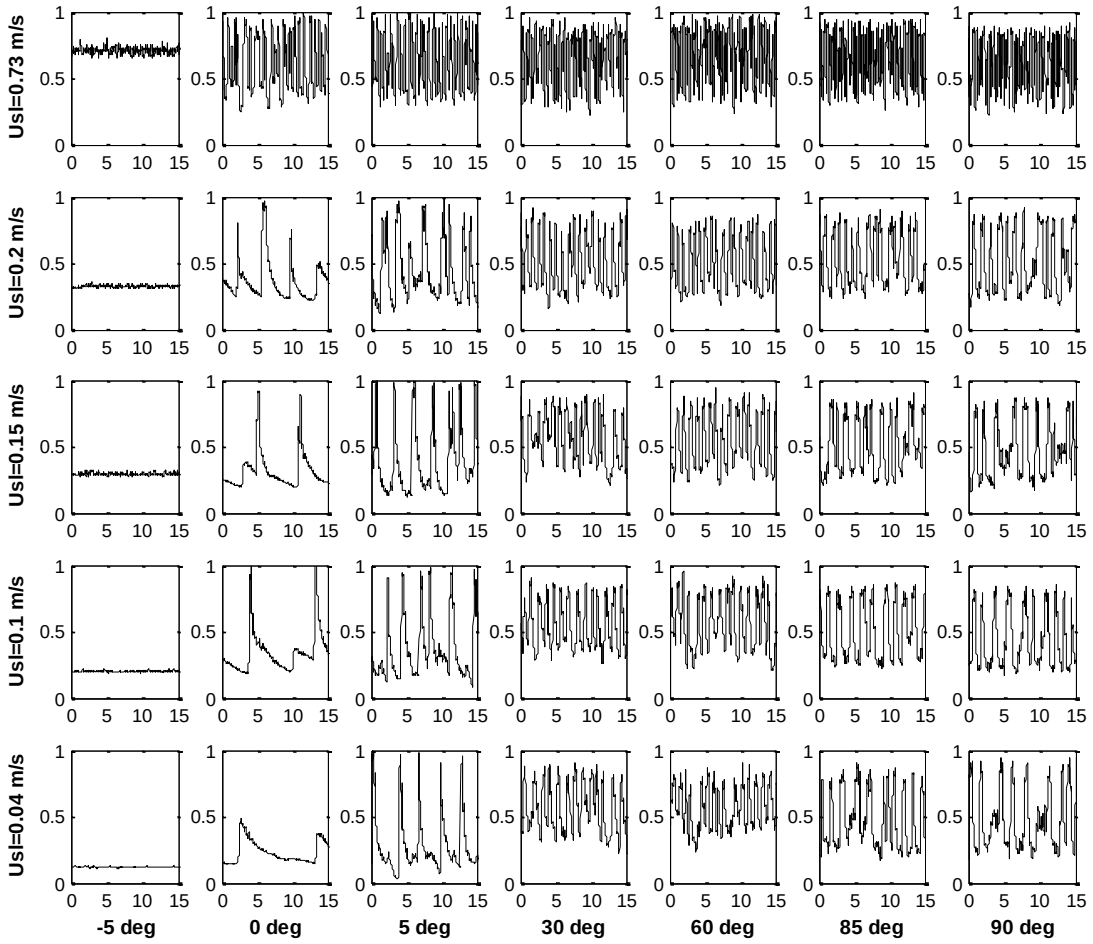

Figure 4.7 Time series U_{SG}=0.9 m/s. x-axis, time (s); y-axis, Liquid holdup.

The Probability Density Function is defined as the derivative

$$p(H_L) = \frac{dP(H_L)}{d\,H_L} \tag{4.1}$$

Where the quantity $dP(H_L) = p(H_L)\, d\, H_L$ represents the probability that the holdup lies between the values H_L and $H_L + d\, H_L$

If the holdup trace has its holdup scale broken into equal increments of $\Delta H_{L\,j}$, and the time scale broken into equal increments of Δt_j and during the total time interval T, the holdup is seen to lie in the interval for a total of *n* times, then

$$\frac{n_i / N}{\Delta H_L} = \frac{1}{\Delta H_L} \sum_{j=1}^{n_i} \frac{\Delta t_j}{T} \tag{4.2}$$

Since the ratio $\sum \frac{\Delta t_j}{T}$ is the estimated probability that the holdup lies within the given interval $\Delta H_{L\,j}$, it is seen that

$$\lim_{\Delta H_{L\,j} \to 0} \left[\frac{1}{T \Delta H_{L\,j}} \sum_{j=1}^{ni} \Delta t_j \right] \to p(H_L) \tag{4.3}$$

where p(H_L) represents the PDF of the particular holdup trace examined and will have particular form according to the nature passing through the probe during the sample time. If the sample is made large, then $p(H_L)$ will approximate closely to the true PDF, i.e.

$$\lim_{T \to \infty} \left[p_1(H_L) \right] \to p(H_L) \tag{4.4}$$

Alternatively if several holdup traces (M) are obtained for constant flow conditions, an average PDF may be defined by

$$\overline{p(H_L)} = \frac{1}{M} \sum_{m=1}^{M} p_m(H_L) \tag{4.5}$$

For the PDFs shown in the next sections, a number of segments of 100 was used. Figure 4.8 shows the PDF for the time series of Figure 4.7. It shows the effect of both inclination angle and liquid superficial velocity on the histogram.

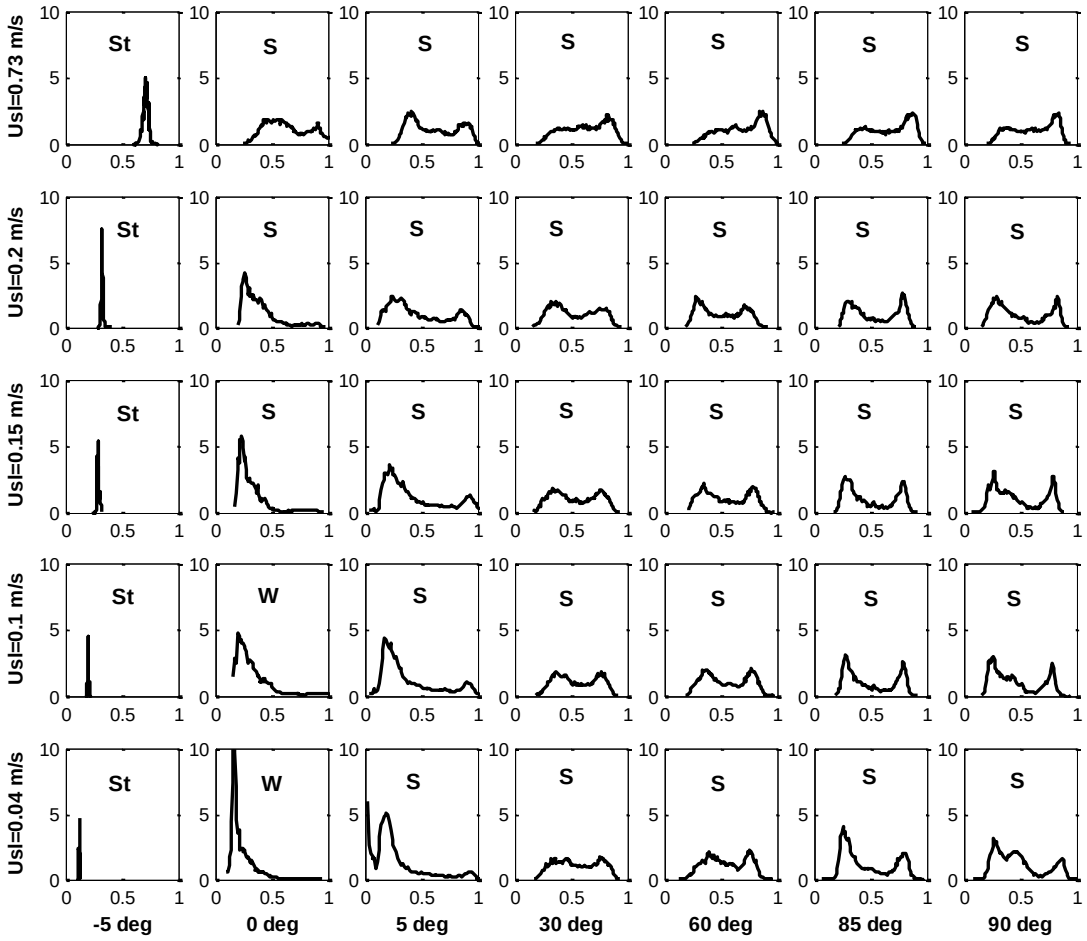

Figure 4.8 Probability Density Function U_{SG}=0.9 m/s. x-axis, liquid holdup; y-axis, PDF (%). St=Stratified flow, S=Slug flow, W=Wavy flow.

As it is known, the concept of PDF for the time series of liquid holdup has been used by Jones and Zuber (1975) as well as Costigan and Whalley (1997) in developing a more objective method by which flow regimes in vertical two-phase flow may be defined. In the stratified, bubbly, annular and slug flow regimes the PDFs will have the following forms:

- Dispersed bubble flow: single peaked PDF occurring at high liquid holdup.
- Annular flow and stratified flow: single peaked PDF occurring at low liquid holdup.

- Slug flow: twin-peaked PDF, one peak characteristic of dispersed bubble flow and the other characteristic of annular flow.

As we can see, the comparison between the visual observations presented in Figure 4.1 and the PDFs presented in Figure 4.8 shows good agreements since the shape of the PDF graphs indicates that intermittent flow is apparent as was observed. This also agrees with other works, including Kokal and Stanislav (1989), who have found that for the case of inclined upward flow, since uphill flow must overcome the force of gravity, for a wide range of gas and liquid flow rates, intermittent flow will dominate in the pipe, while stratified flow dominates in downward inclined pipes.

In Figure 4.9, two more sets of PDFs are presented for the range of inclinations from -5 degrees to 90 degrees, they correspond to a U_{SG}=1.5 and U_{SG}=2.9 m/s respectively. As we can observe, for U_{SG}=1.5 m/s the double peak shape of the PDFs shows that slug flow is present for the liquid superficial velocities and inclinations from horizontal to vertical. However for the case of 2.93 m/s, slugs can only be observed for the case of U_{SL}=0.73 m/s and the slugs that used to exist at lower U_{SG}, now change into waves.

By means of the PDF it is not easy to distinguish between wavy and churn flow, and in order to differentiate we have observed that slug-churn transition might occur at an inclination angle around 60°. Therefore we name churn flow to these PDFs with one peak at an inclination angle greater than 60°.

For plots of PDFs corresponding to the higher gas superficial velocities used in this work, the shape of the PDF indicated that intermittent wavy or churn will be present in the pipe. Based on this analysis presented so far for flow pattern identification in the following section the data will be plotted on the corresponding flow pattern map, which will summarize the occurrence of flow patterns for the conditions under investigation.

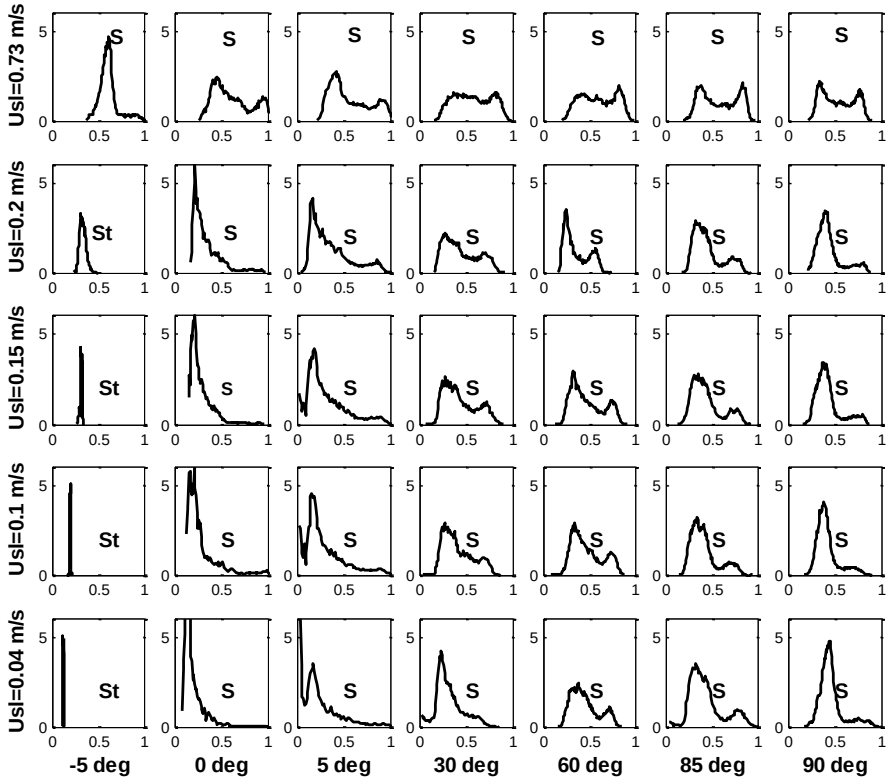

a)

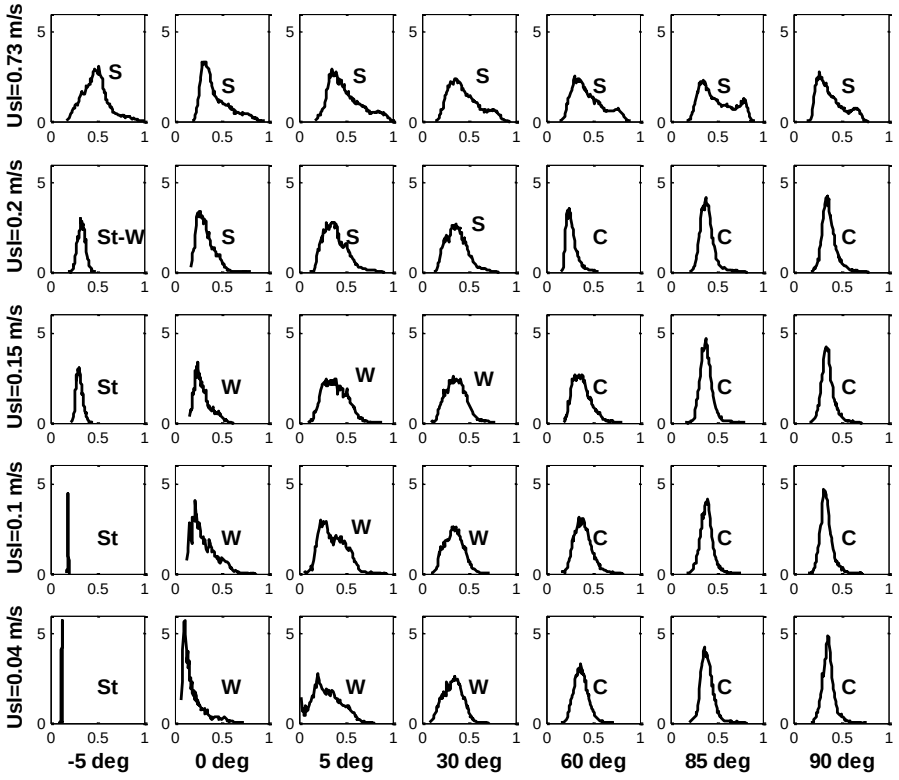

b)

Figure 4.9 Probability Density Function a)U_{SG}=1.47 m/s and b)U_{SG}=2.93 m/s. x-axis, liquid holdup; y-axis, PDF (%).St=Stratified flow, S=Slug flow, W=Wavy flow, C=churn flow.

4.3 Flow pattern map

When a gas-liquid mixture flows along a deviated pipe, the mixture can arrange itself in different geometric distributions of the phases, influenced by several variables such as inlet flow rates, fluid properties, pipe geometry and orientation of the flow. These geometric configurations are usually referred to as flow patterns or regimes. The most common way of identifying which flow pattern occurs for a given set of flow rates is to use a flow pattern map.

The present section reports new data on flow pattern transitions for gas-liquid flow in inclined pipes. The study of the conditions at which flow pattern transitions occur in inclined pipes has been made qualitatively characterizing the flow pattern seen during co-current gas-liquid flow in the inclined rig as described in Chapter 3.

Before getting any further, it is important to specify briefly but as precisely as possible the features of the flow used to characterise the flow pattern designated, and for the present work, the following criteria apply:

Stratified flow (St): The liquid phase flows at the bottom of the pipe with the gas at the top. Depending on the interface, it can be either smooth or stratified wavy.

Intermittent flow (I): This flow pattern is characterised by a non-uniformly distributed axially liquid hold-up. Plugs or slugs of liquid which fill the pipe are separated by gas zones which contain liquid layer flowing along the bottom of the pipe. The liquid may be aerated by small bubbles which are concentrated toward the front of the liquid slug and the top of the pipe. The intermittent flow pattern is usually subdivided into slug (*S*) and elongated bubble (*EB*) flow patterns, but the distinction between them has not been clearly defined. Following Barnea *et al.* (1980), in this work, the elongated bubble pattern is considered the limit case of slug flow when the liquid slug is free of entrained slug bubbles.

Annular flow (A): The liquid flows as a film around the pipe wall. A liquid film surrounds a core of high velocity gas which may contain entrained liquid droplets. For non-vertical flow, due to the gravity force, the film at the bottom is normally thicker

than at the top depending on the flow rates of liquid and gas. At the lowest gas rates at which transition to annular flow from slug flow is observed, most of the liquid flows at the bottom of the pipe.

A study of the different flow pattern maps available in the literature was made in Chapter 2, where the equations that describe the boundaries between the flow patterns are given. These are plotted below for different inclination angles together with the data gathered in the present work. First we present the flow pattern map of Taitel and Dukler (1976).

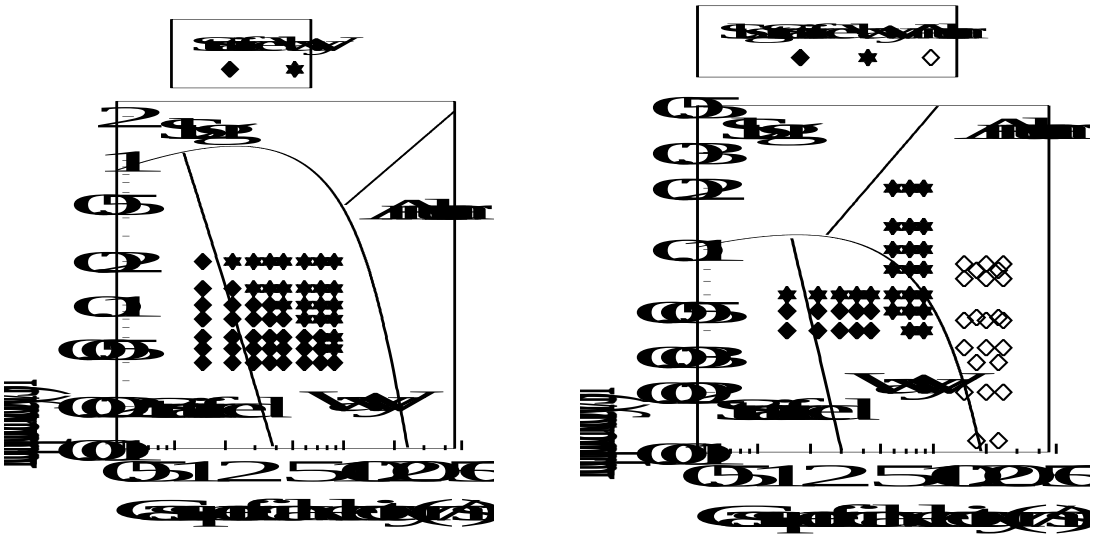

-5° Inclination **0° Inclination**

Figure 4.10 Flow pattern maps for horizontal and 5° downward inclination. Taitel and Dukler (1976)

The flow regime map at -5° downward inclination is shown in Figure 4.10. Here, the transition from stratified to slug flow becomes much more dependent upon the superficial gas velocity. At a superficial gas velocity of 1.5 m/s, only stratified flow was observed at all superficial liquid velocities studied. However, for horizontal flow, as we can see in Figure 4.10 slug flow is observed for these conditions. It occurs at lower liquid superficial velocities and gas velocities as well, substituting the wavy

flow and stratified flow in some cases. These changes, as was illustrated in the previous section are observed at low gas superficial velocities. Data for annular flow shown in Figure 4.10 are from Geraci (2005).

For the same conditions presented in the flow pattern maps of Figure 4.10, from 1° upwards, Taitel and Dukler (1976) flow pattern map predicted that slug flow would be present. Indeed when a pipe is only slightly inclined to the horizontal, the flow pattern behaviour is very similar to that seen in a horizontal line. The major change observed is that stratified flow disappears at very low angles of inclination. The region formerly occupied by stratified flow is now occupied by plug flow. Wavy flow is still observed, but the wavy flow region now begins at a higher gas flow rate. The region formerly occupied by the wavy flow is generally occupied by broken slug flow (highly aerated slug flow).

Because the experiments were performed at steeper inclination angles, where the Taitel and Dukler (1976) flow pattern map for horizontal and slightly inclined pipe does not apply, next we will plot the data of flow regimes observed in the experiments on both the Weisman and Kang flow pattern map and Barnea *et al.* (1980) flow pattern map. These flow pattern maps extend in the whole range of inclinations.

Four uphill flow regimes have been observed; these are bubble, slug, churn, and annular flow. Each of these occurs in progression with increasing gas rate for a given liquid rate.

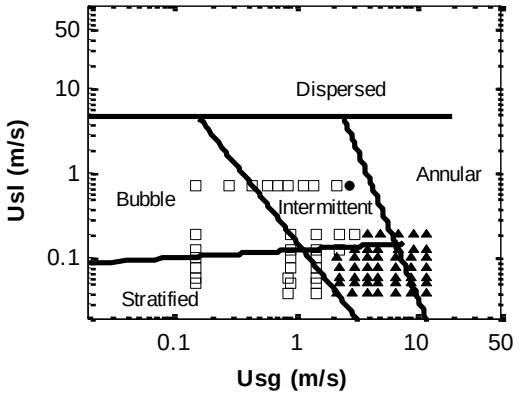

0 degrees inclination

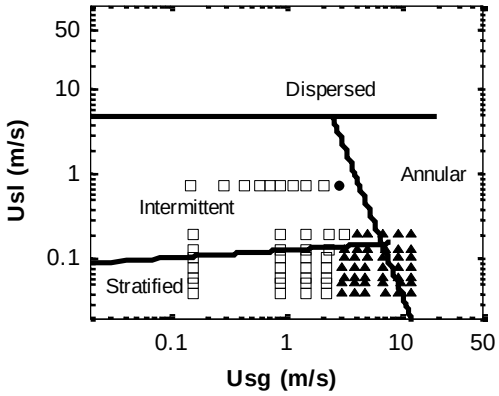

5 degrees inclination

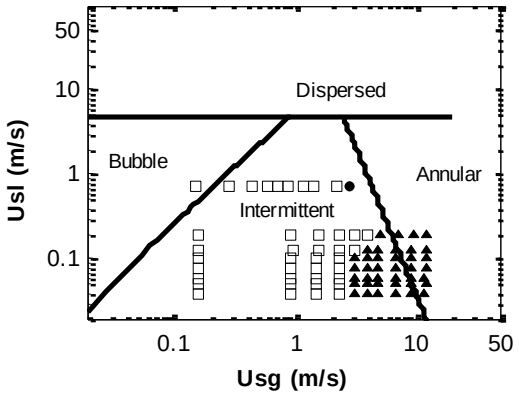

10 degrees inclination

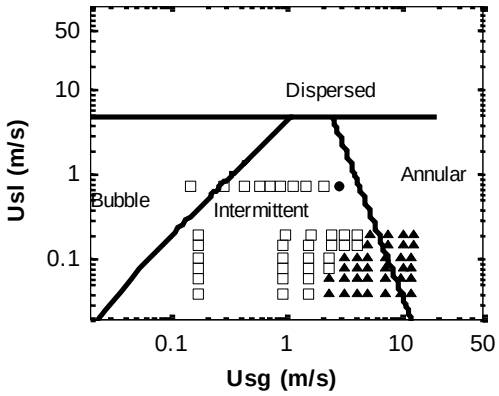

30 degrees inclination

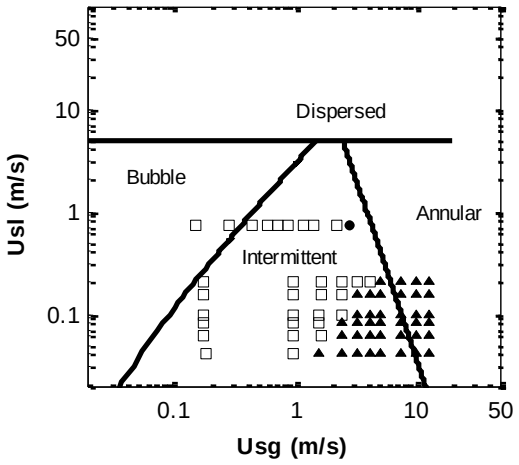

45 degrees inclination

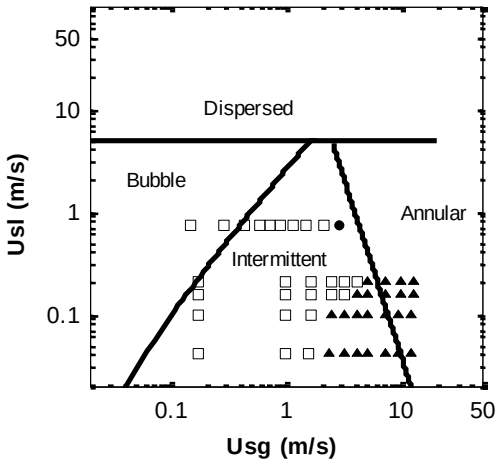

50 degrees inclination

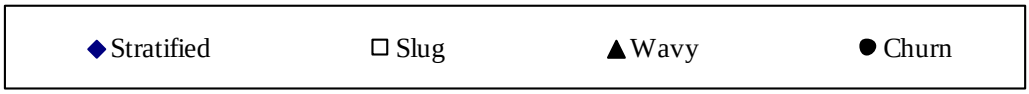

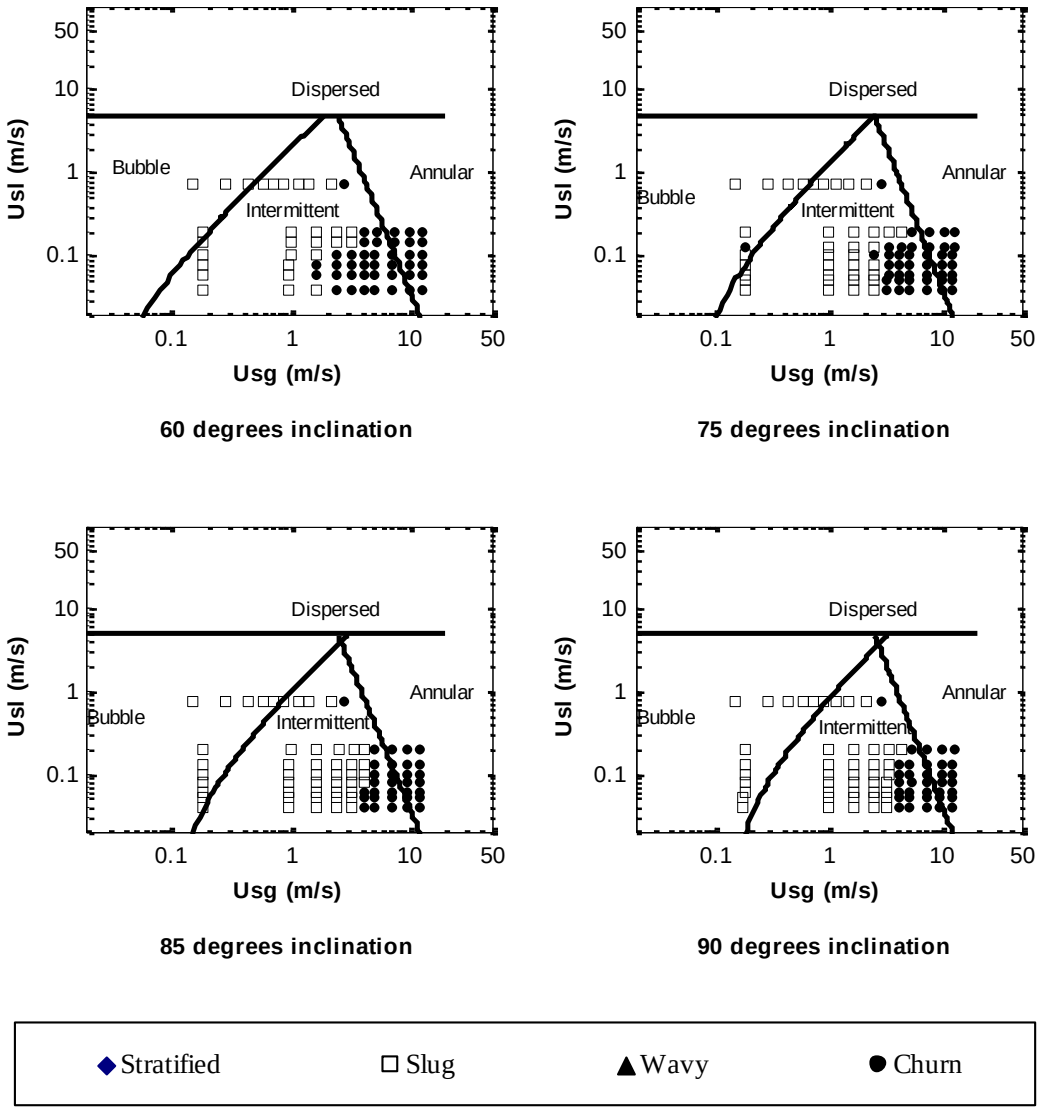

Figure 4.11 Flow pattern maps for different inclination angles. Weisman and Kang (1981). Note for 45, 75 and 85° flow pattern maps the data at U_{SL}=0.73 actually correspond to 40, 70 an 80° respectively

The flow pattern map of Figure 4.11 is showing the behaviour in a 38 mm pipe inclined upward. It is observed, as it was also observed by Weisman and Kang (1981) that at high gas superficial velocities the flow pattern appears not to be influenced by the angle of inclination.

The Weisman and Kang (1981) flow pattern map does not differentiate between slug an churn flow. Indeed, the flow patterns slug and churn are often described together as intermittent flow, since they behave similar, but more importantly because they are difficult to distinguish. There is a history of uncertainty over the correct location of the slug to churn flow boundary and this uncertainty persists to date. However, more detail analysis of the flow characteristics, obtained with the time series analysis can be considered to identify flow pattern boundaries, for example structure velocity behaviour and frequency.

Unlike Weisman and Kang (1981), in the next flow pattern, there is a boundary that separates slug flow from churn flow, this was proposed by Brauner and Barnea (1986) by taking into consideration a relationship between the mixture velocity and void fraction at the dispersed bubble flow boundary.

Barnea (1987) summarized the more relevant models for prediction of flow patterns and suggested a logical path for flow pattern determination for the whole range of pipe inclinations. The main purpose is to construct a completely general method that allows the prediction of the flow pattern, once the flow rates, the conduit geometry, the inclination angle and the fluid properties are specified.

Figure 5.12 shows the flow regime map for different inclination angles, the curve corresponding to the model of Brauner and Barnea (1986) for slug-churn transition seems to make its appearance for upwards inclination angles from 30° upwards. However this curve does not agree quite well with the flow pattern found for this work, having its closes agreement for the case of vertical flow.

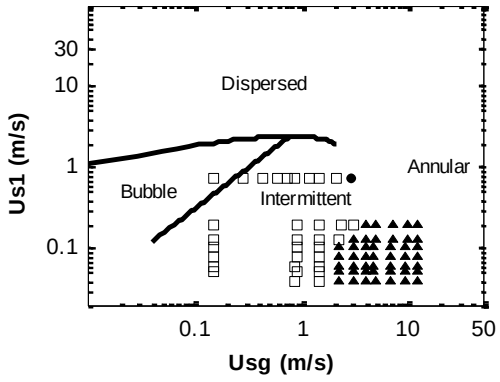

0 degrees inclination

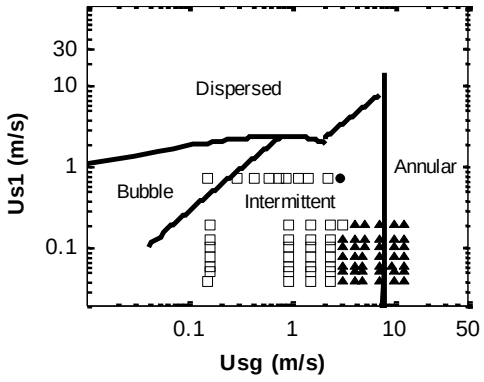

5 degrees inclination

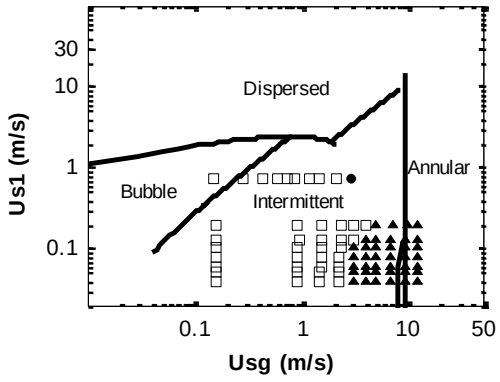

10 degrees inclination

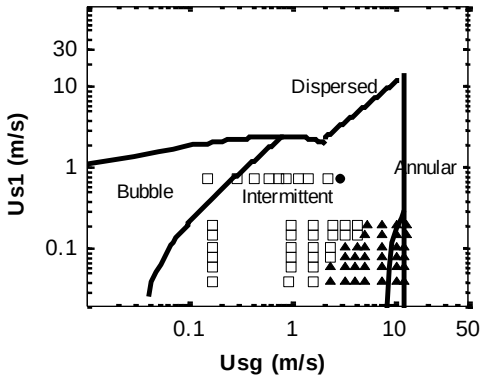

30 degrees inclination

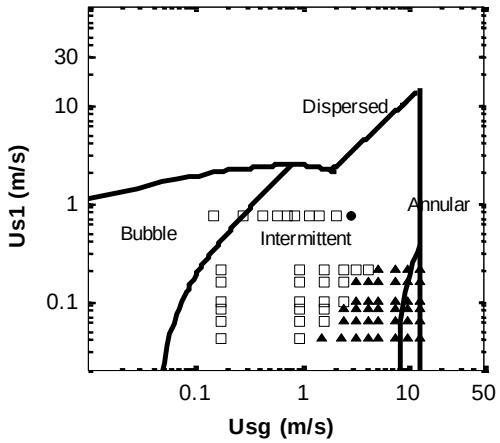

45 degrees inclination

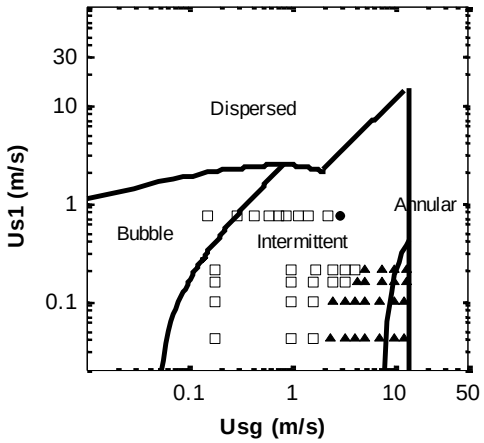

50 degrees inclination

◆ Stratified □ Slug ▲ Wavy ● Churn

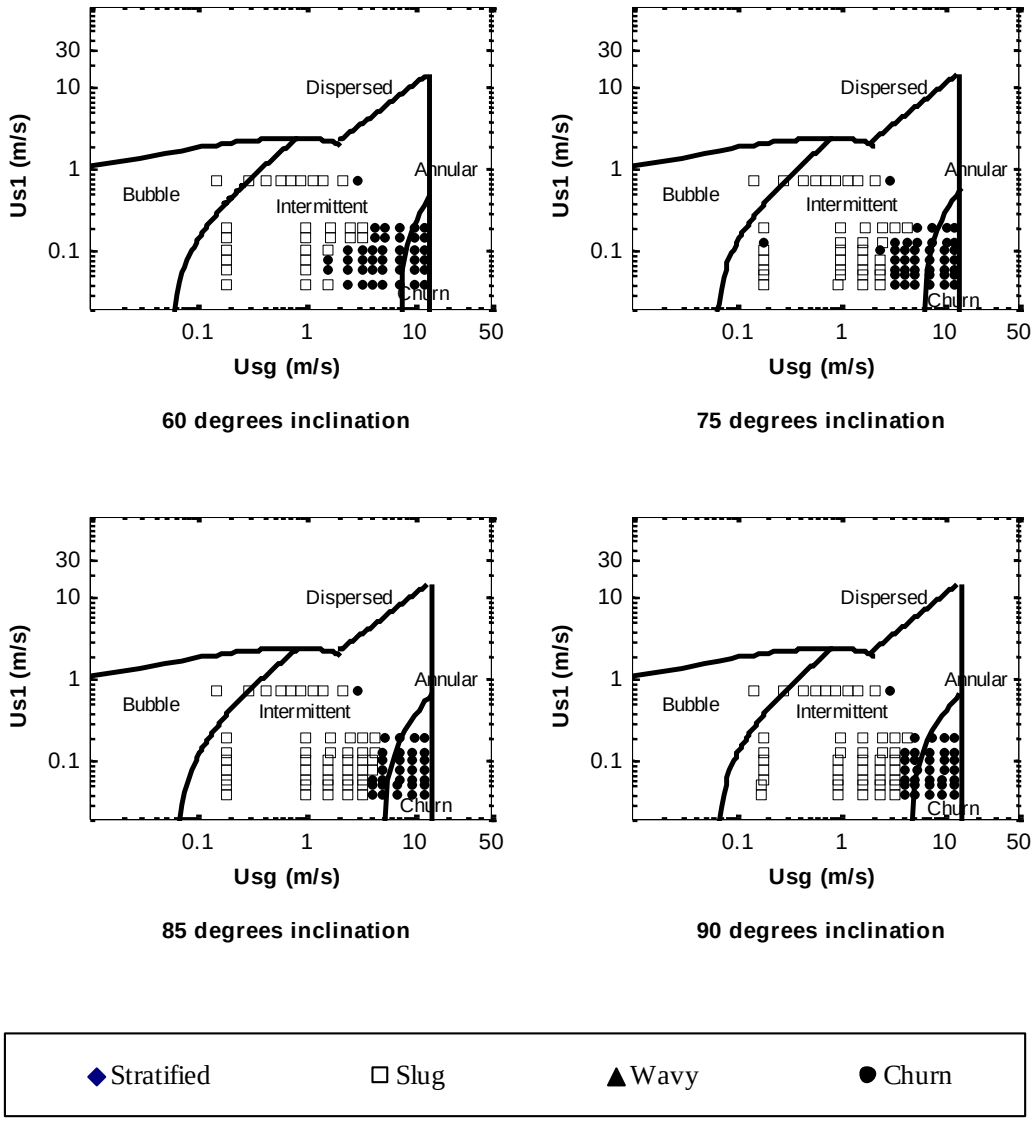

Figure 4.12 Flow pattern maps for different inclination angles. Barnea (1987). Note for 45, 75 and 85° flow pattern maps the data at U_{SL}=0.73 actually correspond to 40, 70 an 80° respectively

The models for flow pattern boundaries considered in this section try to represent the true physics of the flow behaviour observed in experiments. However, they simplify the description of the physical phenomena so that a mathematical simulation is possible. In order to see how well these flow patterns predict, a comparison is made and it is presented in the form of a table, see Table 4.1.

Table 4.1 Comparison of flow regime maps

Flow regime	Number of points	Taitel and Duckler Correct (%)	Weisman Correct (%)	Barnea Correct (%)
stratified	44	45	50	NA
Slug (horizontal)	22	36	45	NA
Slug	366	NA	39.6	49
Wavy (horizontal)	22	50	NA	NA
Wavy	318	NA	NA	NA
churn	151	NA	NA	37.7

From Table 4.1 it is clear that predictions of the flow patterns tested do not have a good agreement with the results obtained in the present work. However there is still the necessity to improve such predictions for slug-churn transition, which depends on both flow rate and inclination angle.

In addition to the PDF of the liquid holdup, the Coefficients of skewness and kurtosis associated with the *N* samples of liquid holdup data were also obtained, since these parameters have been successfully used by Hasanein et al. (1997) among others to determine the flow pattern in small pipes. The results are presented in appendix D for the sake of completeness.

4.4 Liquid holdup

The next section of this chapter will focus on analysis and interpretation of the liquid holdup results. Liquid holdup plays a large role in inclined pipes. An accurate prediction of the liquid holdup within a transport pipeline is an important factor within many two-phase flow calculations and is often the starting point for many predictive models. The liquid holdup was measured with the capacitance probes in form of a time series, as described in Chapter 3. The probes were conditioned on a daily basis to account for drift, in order to normalize the signals (0–1). The sensors were only used for stratified, wavy, elongated bubble and slug/churn flow detection. These are the dominant flow patterns.

In practice sometimes we are interested in knowing the mean value of the time varying liquid holdup. Therefore from the liquid holdup time series (Figure 4.7), using α_k, as the instantaneous volumetric fraction of the phase-*k* (*k* is either air or water) existing over the pipe cross section of either of the capacitance probes, we can obtain the average phase volume fractions over the whole time series,

$$\langle \alpha_k \rangle_T = \frac{1}{T}\int_T \alpha_k dt = \frac{1}{N}\sum_{n=1}^{n=N} \alpha_k \tag{4.6}$$

Where $\langle\ \rangle_V$ stands for the average over the entire time series period (T) and N is the number of data points in the time series. In the same way other quantities presented in the following sections will be averaged.

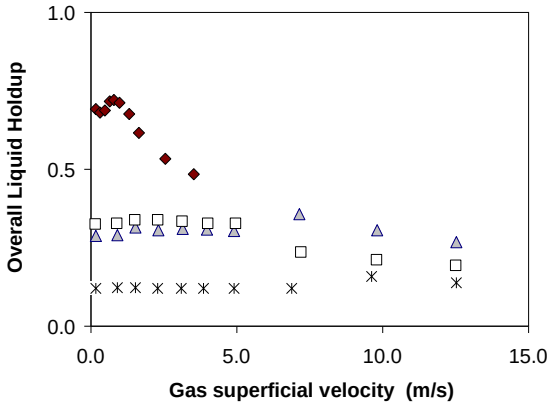

-5 ° Inclination

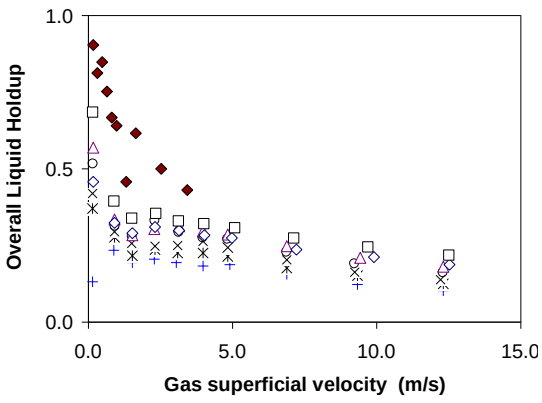

0 ° Inclination

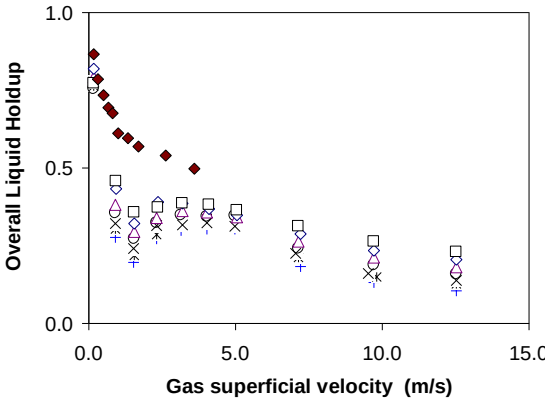

5° Inclination

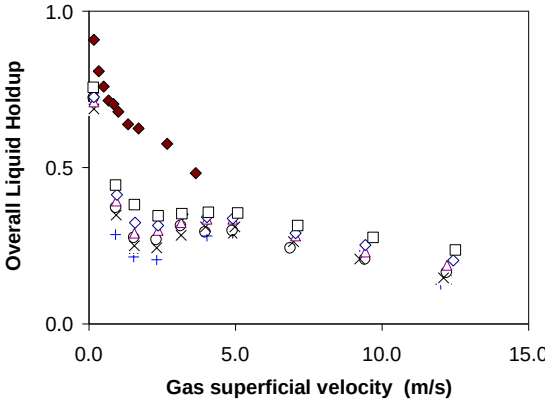

10 ° Inclination

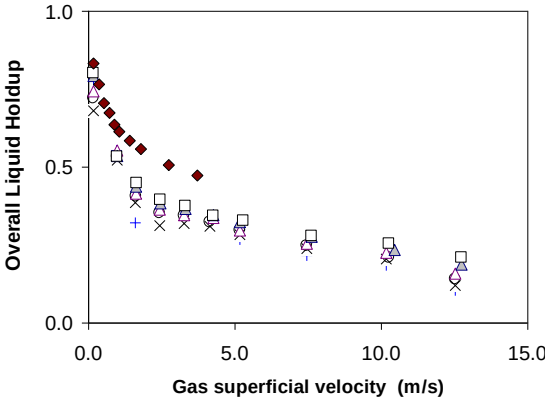

30° Inclination

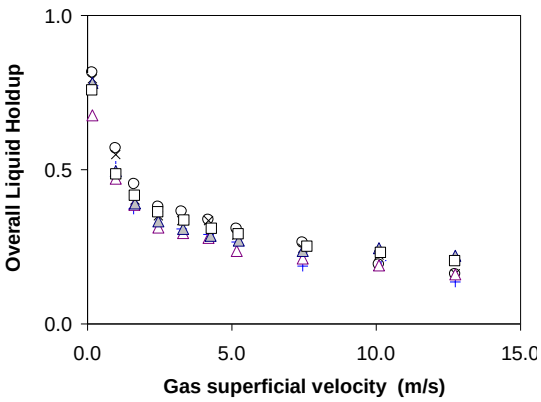

45 ° Inclination

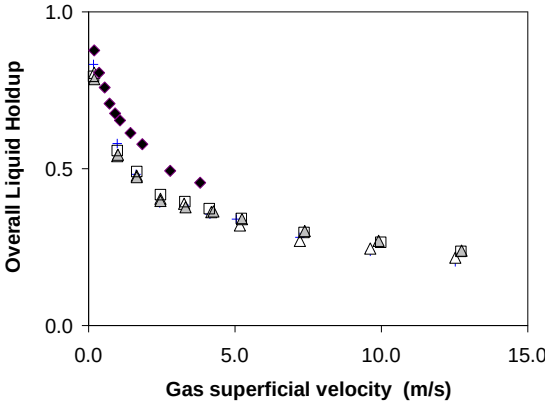

50° Inclination

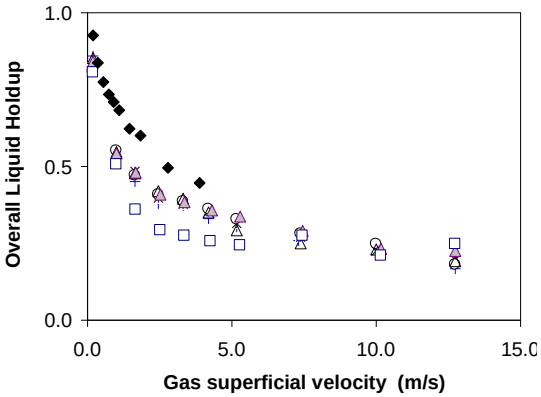

60 ° Inclination

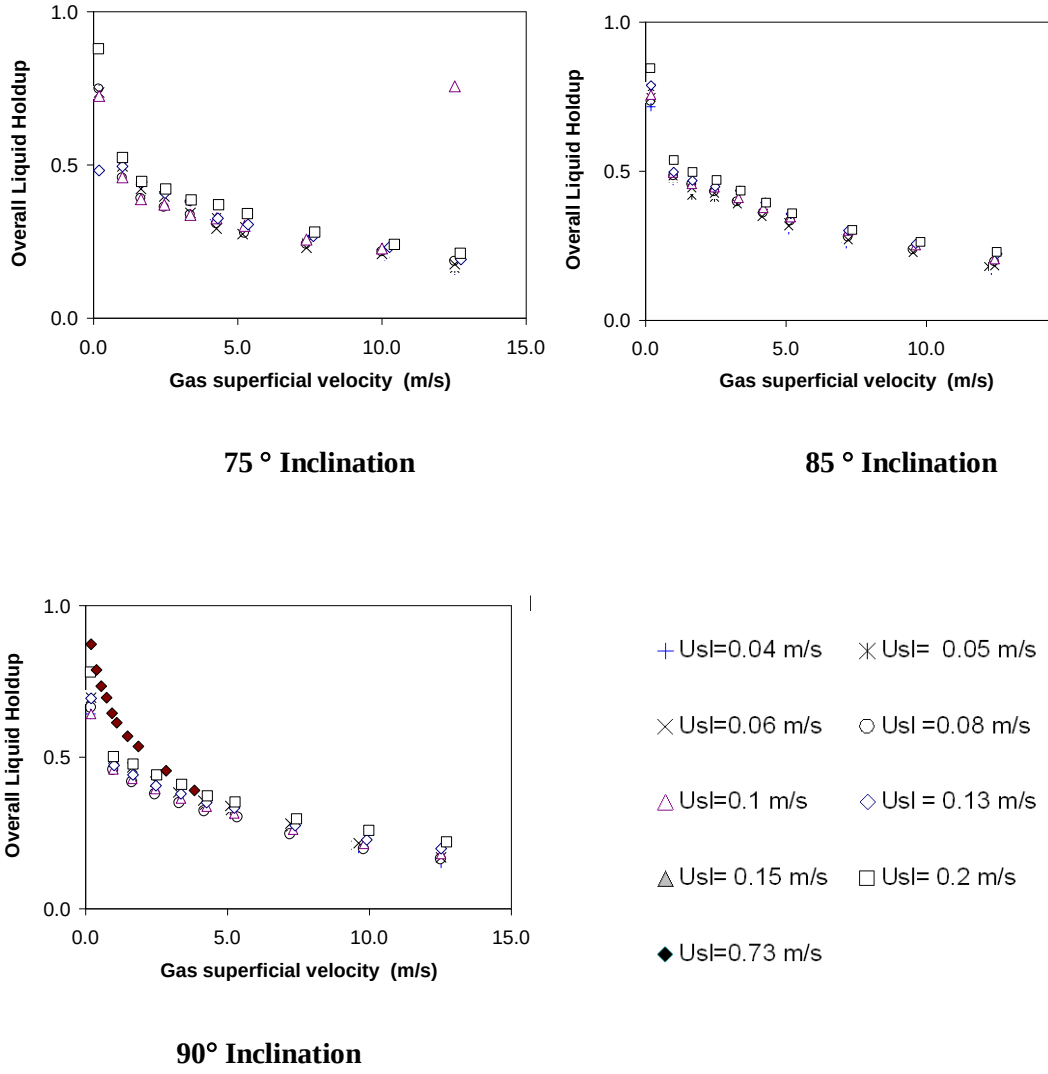

Figure 4.13 Liquid holdup for different inclination angles

The average values of liquid holdup for different inclination angles and gas superficial velocities were plotted above in Figure 4.13. We can observe that in general, for a constant liquid superficial velocity, the average liquid holdup decreases when the gas velocity is increased. Indeed Baker (1957) and Flanigan (1958) both develop correlations for calculation of liquid holdup in pipes based on the the gas superficial velocity. However this tendency is slightly affected by the inclination angle and the usual tendency of the liquid holdup with inclination angle is affected by the gas superficial velocity. The main effect is observed in how fast the liquid holdup decreases.

For downwards stratified flow, the liquid holdup becomes independent of the gas superficial velocity over the range of gas flow rate employed but is a function of the liquid flow rate. In uphill flow, the pipe inclination has just a slight effect on the liquid holdup. The liquid holdup increased slightly for the higher inclination angles.

The dependence of time averaged liquid holdup on the angle of inclination can be explained as follows: for downhill flows, the liquid moves faster due to gravity, resulting in lower liquid holdups, whilst for uphill flows this effect is reversed and the liquid moves slower resulting in intermittent flow and higher holdups.

From Figure 4.14, another interesting thing that can be seen is the fact that liquid holdup also changes with the flow pattern, this effect is stronger for the cases of 5, 10 and 15 degrees of pipe inclination, there is a decrease and increase in the mean liquid holdup when the gas superficial velocity is around the range of 1.5 - 4 m/s. This behaviour occurs for all of the liquid superficial velocity.

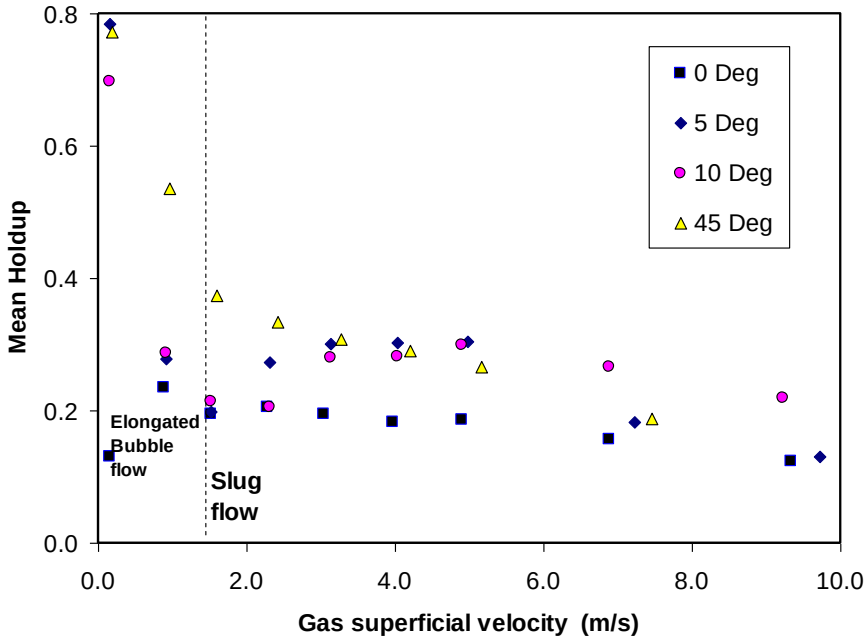

Figure 4.14 Effect of flow pattern on liquid holdup, U_{SL}=0.04m/s.

For a fixed liquid flow rate, when the gas flow rate is as low as possible, the gas travels along the pipe in the form of elongated bubbles whereas the liquid tends to stay in the pipe, as a result the liquid holdup is high, however it decreases very quickly

until certain value where further increase in the gas flow rate will result a change of flow pattern, and slug which in spite of the fact that they displace liquid out of the pipe, provoke a considerable back flow of the liquid in the pipe because of the shedding process at the tail of the liquid slug and therefore the liquid holdup increases slowly until a value where increasing the gas flow rate a bit more results in a situation where the gas flow rate is capable of overcoming the back flow and the liquid holdup will decrease again but slowly.

A few correlations for calculating liquid holdup were found in the literature and now we take them into consideration to compare with the data obtained in the present work, first we compare Guzhov *et al.* (1967) correlation, which was developed for small inclination angles (<10°) . The comparison is illustrated in Figure 4.15 by considering three different inclination angles, namely 0, 5 and 10°.

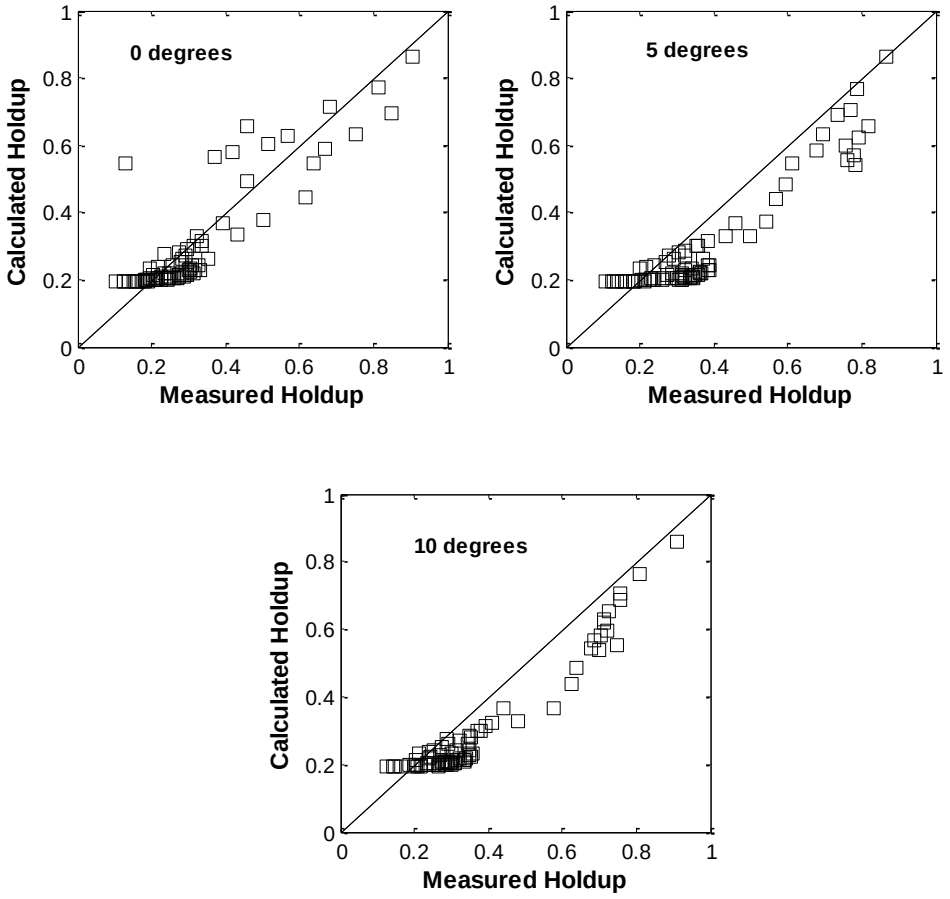

Figure 4.15 Comparison of measured overall liquid holdup and predicted by Guzhov *et al.* (1967) correlation.

We can observe that Guzhov *et al.* (1967) correlation is not reliable at low values of liquid holdup; it seems to fail to predict values of holdup less than 0.2. Indeed, Gregory (1974) suggested that this correlation should not be used for cases where the predictions of holdup are less than 0.25. In addition, this correlation is independent of inclination angle from 0 to 9 degrees, which can justify the disagreement with the present data, since it has been observed that it is at this angles that the holdup presents the biggest changes, particularly at low gas superficial velocities.

In order to determine the quality of the predictions the absolute error for each data point was calculated as

$$\varepsilon = \frac{\alpha_{pred} - \alpha_{meas}}{\alpha_{pred}} x100 \tag{4.7}$$

The mean absolute error and the standard deviation of the absolute error were then used to compare the correlations,

$$\bar{\varepsilon} = \frac{1}{n}\sum_{i=1}^{n} \varepsilon_i \tag{4.8}$$

$$S = \sqrt{\frac{\sum_{i=1}^{n} (\varepsilon_i - \bar{\varepsilon})^2}{n-1}} \tag{4.9}$$

The same procedure is applied whenever a model or correlation is compared in the following sections.

Greskovich (1973) suggested a simplified procedure to calculate the liquid holdup in inclined pipes based on the fact that straight lines can be obtained by Guzhov *et al.* (1967) correlation for a given mixture Froude number on a plot of in-situ liquid holdup vs input liquid holdup (E_L vs C_L.), see Chapter 2. Since at C_L=1, all of these lines converge at E_L=1, Greskovich (1973) suggested that only the intercept corresponding to C_L=0 needed to be measured on order to establish the whole line for a given Froude number. In order to see this behaviour in the present data, in Figure 4.16 we plot the actual liquid holdup as a function of the input liquid holdup.

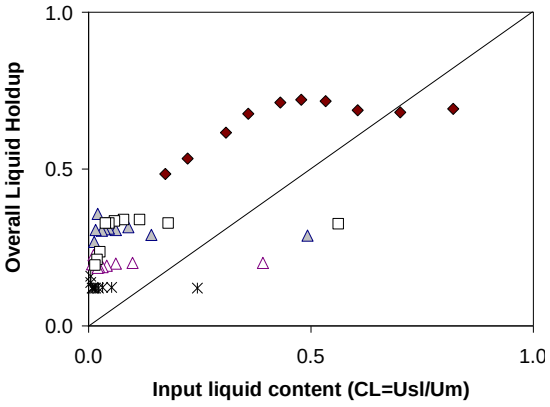

-5 ° Inclination

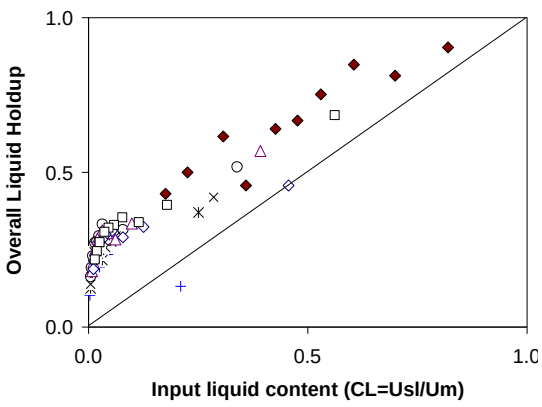

0 ° Inclination

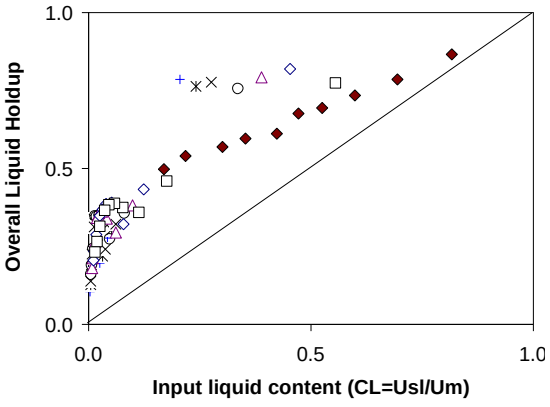

5° Inclination

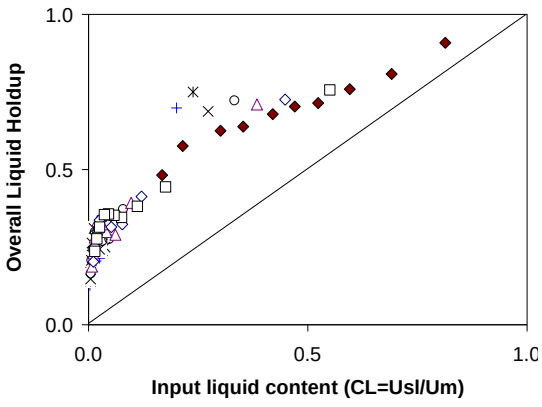

10 ° Inclination

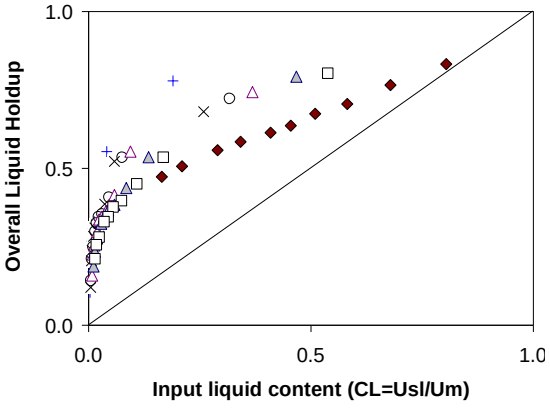

30° Inclination

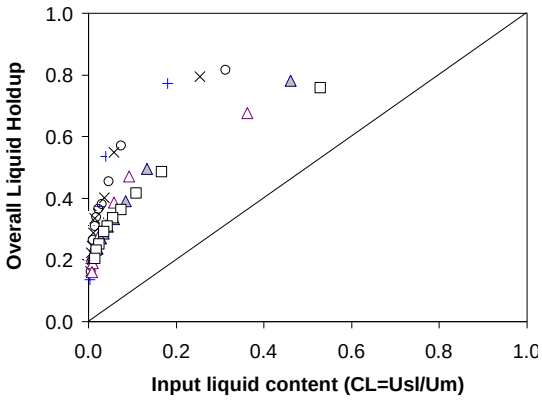

45 ° Inclination

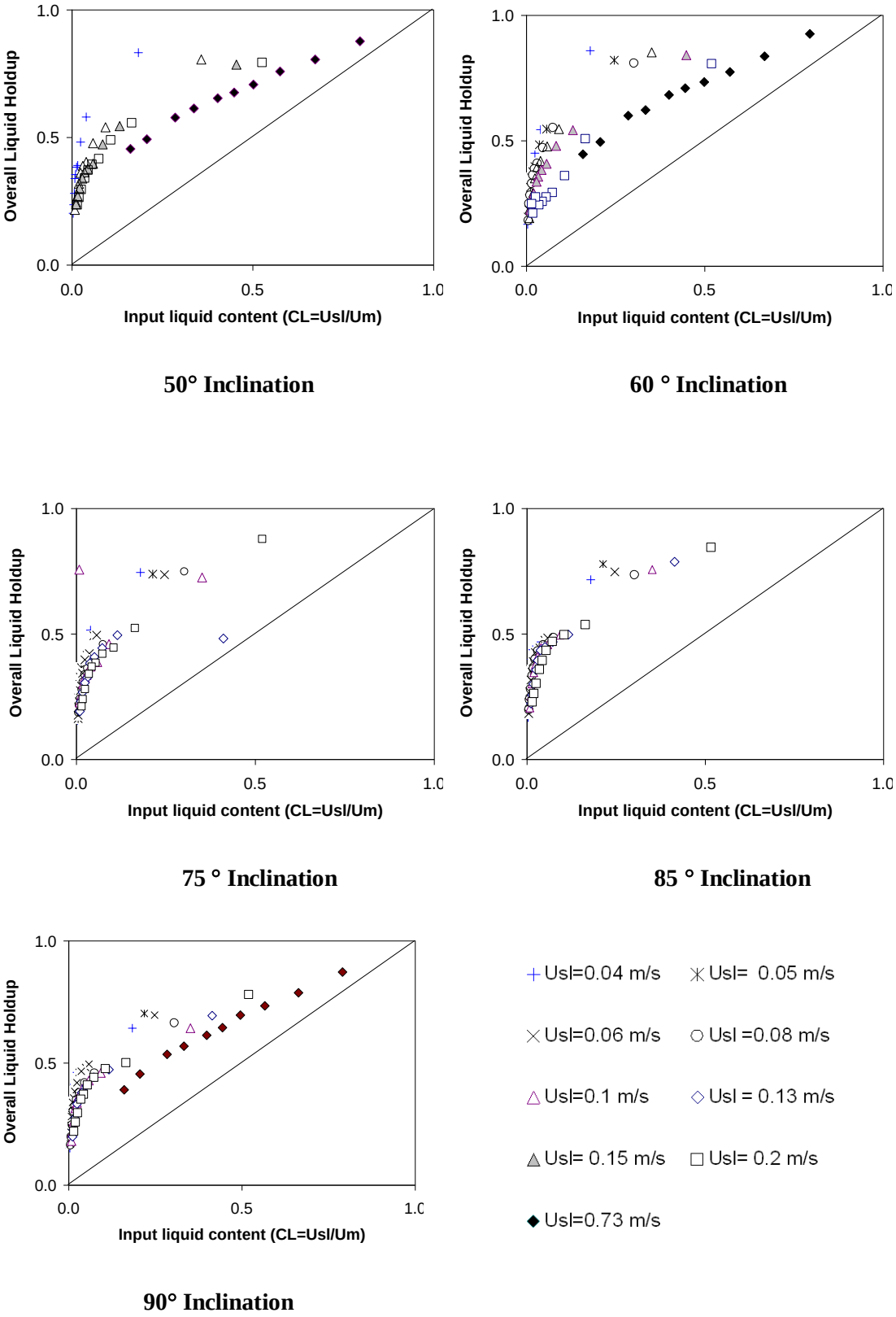

Figure 4.16 Mean in-situ liquid holdups plotted as function of the input liquid holdup for different inclination angles

In Figure 4.16, the linear tendency can be observed specially for the case of U_{SL}=0.73 m/s, for which higher values of both in-situ liquid holdup and input liquid holdup are obtained. It can be seen that the in-situ liquid holdup is bigger than the input liquid holdup, particularly for the low values of input liquid holdup, since the liquid tends to accumulate in the pipe when it is inclined upwards and not surprisingly for when input liquid holdup tends to 1, the in-situ liquid holdup follows the same behaviour.

Another model for liquid holdup was proposed by the Mattar and Gregory (1974) model. They developed their model especially for slug flow at inclination angles less than 10°. Figure 4.17 shows the comparison between the model and the present work. It is worth noting that they develop the model based on parameters they found with air-oil slug flow, which justify the disagreement observed.

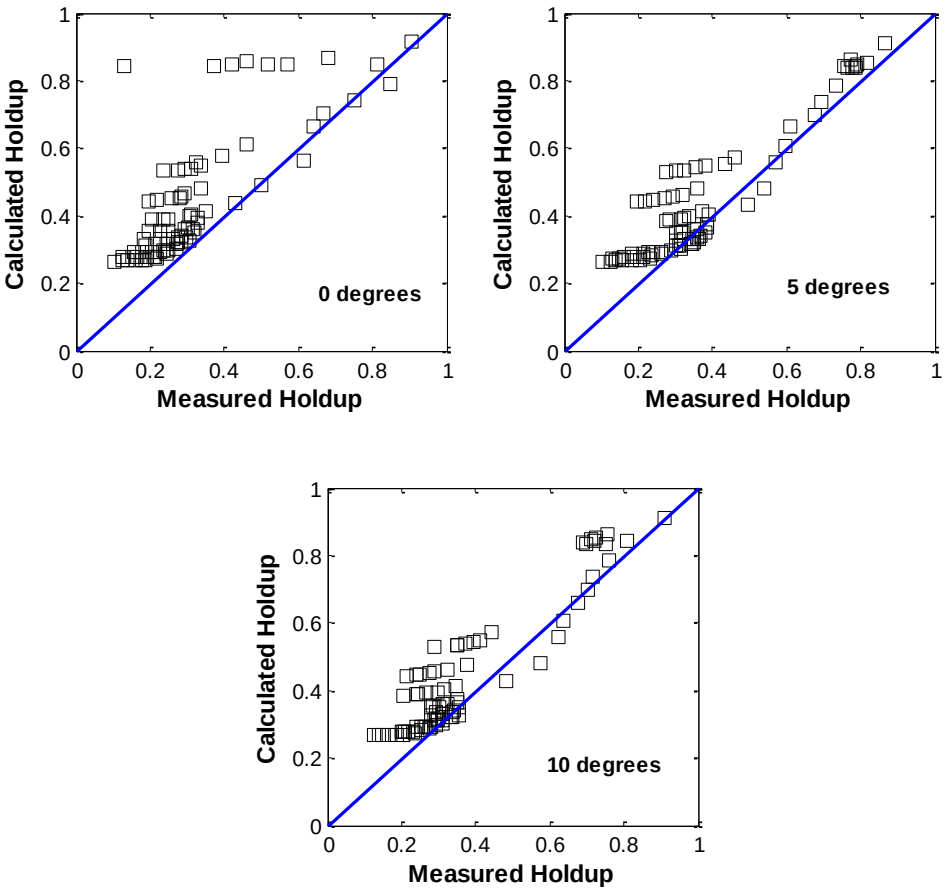

Figure 4.17 Comparison of measured overall liquid holdup and predicted by Mattar and Gregory (1974) model.

As we can see the correlations compared so far fail to predict the liquid holdup measured in most of the experiments of this work. However this can be justified, by the fact that in not all the experiments, slug flow was observed. Next comparison is with Beggs and Brill (1973) correlation for liquid holdup and pressure drop, since it is the most complete work for prediction of liquid holdup and pressure drop in inclined pipes.

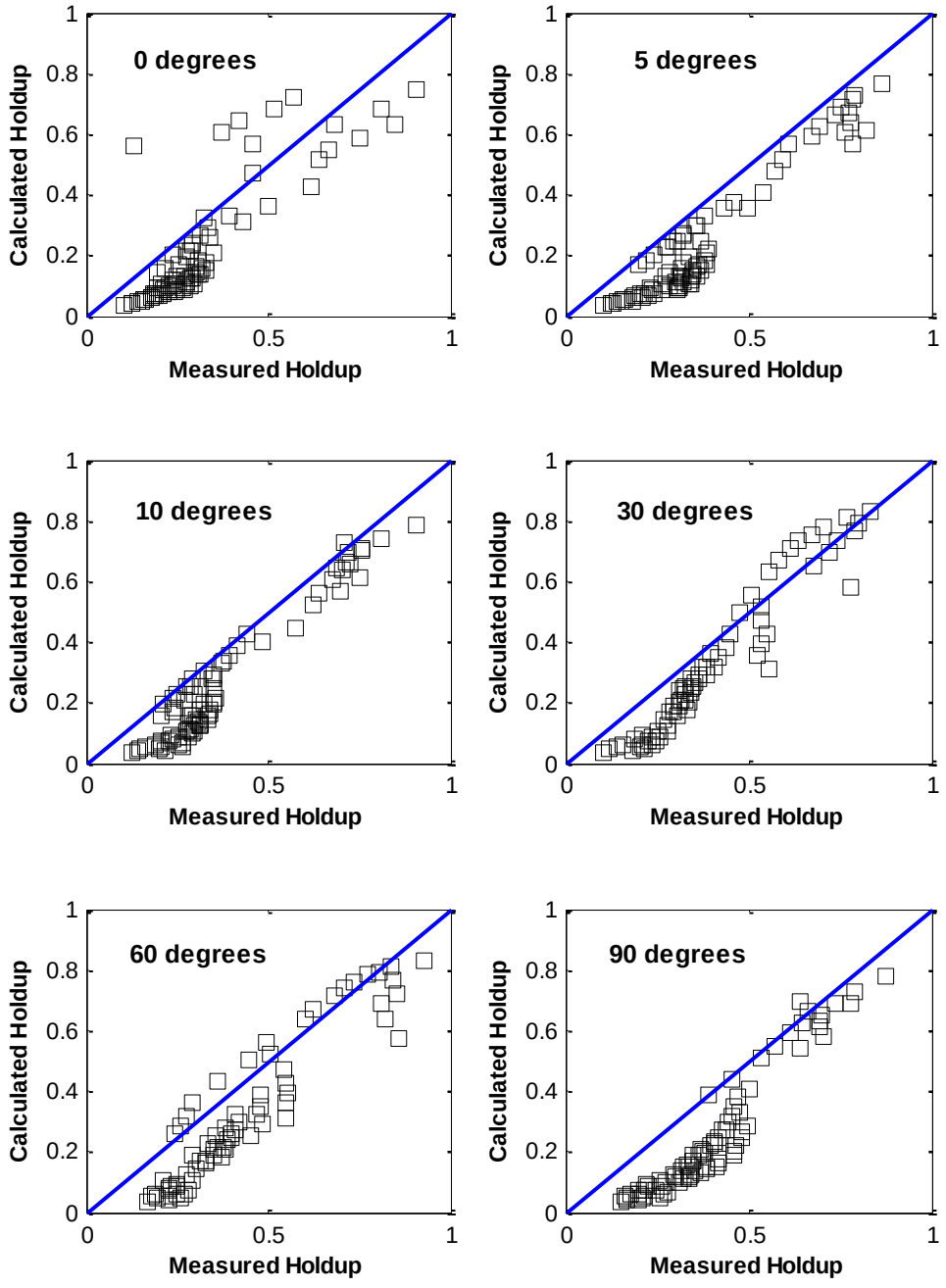

Figure 4.18 Comparison of measured overall liquid holdup and predicted by Beggs and Brill (1973) correlation.

It was observed that for low values of liquid holdup, the correlation under predicts. Over-prediction was observed only at intermedium values of H_L, Figure 4.18. Among the correlations tested, the Beggs and Brill (1973) has performed better in comparison to the present data, it might be due to the fact that it was developed from data taken with the same pipe diameter (38 mm).

In Table 4.2, a comparison is reported between the correlations tested. This is in order to summarise the graphs presented above and also to quantify the error obtained with the different correlations.

Table 4.2 Comparison of Liquid holdup correlations

Correlation	Inclination	Number of points	Mean error (%)	Standard Deviation
Guzhov *et al.* (1967)	0°	80	1.46	42.63
	5°	80	-15.96	23.82
	10°	80	-17.47	16.89
Mattar and Gregory (1974)	0°	80	54.1	66.4
	5°	80	26.9	36
	10°	80	25.5	28.9
Beggs and Brill (1973)	0°	80	-35.7	50.5
	5°	80	-43.48	23.3
	10°	80	-37.3	25.6
	30°	70	-29.9	26.5
	45°	60	-33.3	25.7
	50°	50	-30.3	28.7
	60°	70	-32.8	29.1
	75°	70	-41.3	24.8
	90°	80	-45.4	24.4

4.5 Frequency

It has been shown that intermittent flow exists as the dominant flow pattern in upward inclined flow. Intermittent flow is characterised by the variation of the liquid holdup with time, mainly in the form of periodic structures. To characterise these structures, analysis of the fluctuations in liquid holdup the time series was carried out, and the frequency was calculated. When analysing the frequency, it was found that it is a very complex parameter and therefore care must be taken when performing the calculations. Also interpretation of the result is important to verify the values, since the frequency is a very fundamental parameter of intermittent flow and it is used together with the translational velocity for the calculation of slug length.

In order to determine the frequency of periodic structures (slugs) the methodology of Power Spectral Density (PSD) was applied. In addition the number of slugs visible on the liquid holdup time traces were counted. The latter was carried out using different discrimination levels.

Regarding the counting method, following the criterion used by most researchers (e.g. Nydal (1991)) we used a critical value of 0.7 for the liquid holdup in the slug in order to be considered slug flow pattern. From Figure 4.19 it can be seen that using different values for the threshold will result in a different number of slugs, which in turn gives a different frequency.

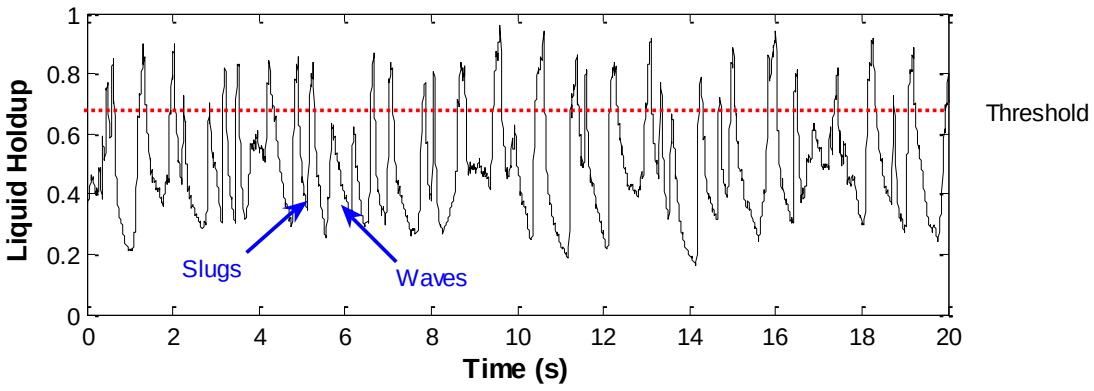

Figure 4.19 Threshold for the liquid holdup level used to determine the number of slugs in the time series

A very important feature of the liquid holdup signal is its average power. The holdup signal's instantaneous power is defined as the square of the signal. The average power is the average of instantaneous powers over their time interval. For a periodic signal, the natural time interval is clearly its period and the average power is the mean square value of the signal.

The Power Spectral Density, PSD, is a measure of how the power in a signal changes over frequency and therefore, it describes how the power (or variance) of a time series is distributed with frequency. Mathematically, it is defined as the Fourier Transform of the autocorrelation sequence of the time series. The Discrete Fourier Transform (DFT), sometimes called the Finite Fourier Transform, is a Fourier transform widely employed in signal processing and related fields to analyze the frequencies contained in a sampled signal, solve partial differential equations, and to perform other operations such as convolutions. The DFT can be computed efficiently in practice using a Fast Fourier Transform (FFT) algorithm.

In terms of signal processing, the transform takes a time series representation of a signal function and maps it into a frequency spectrum. That is, it takes a function in the time domain into the frequency domain; with decomposition of a function into harmonics of different frequencies.

A representation of a signal in the frequency domain is the frequency spectrum. This is the projection of the function onto a range of sinusoidal basis functions. It can be found from the result of a Fourier-related transform. A frequency spectrum contains both amplitude and phase information and describes how much of the "energy" of the function or signal lies in any given frequency band, without regard for the phase.

In order to use the PSD technique to determine the frequency we will follow the sugestions of Hubbard (1965), see Chapter 2. Figure 4.20 illustrates an example of the time series and corresponding PSD plot that will be used from now on.

The spectral plot is formed by:

- Vertical axis: Smoothed variance (power)
- Horizontal axis: Frequency (cycles per second)

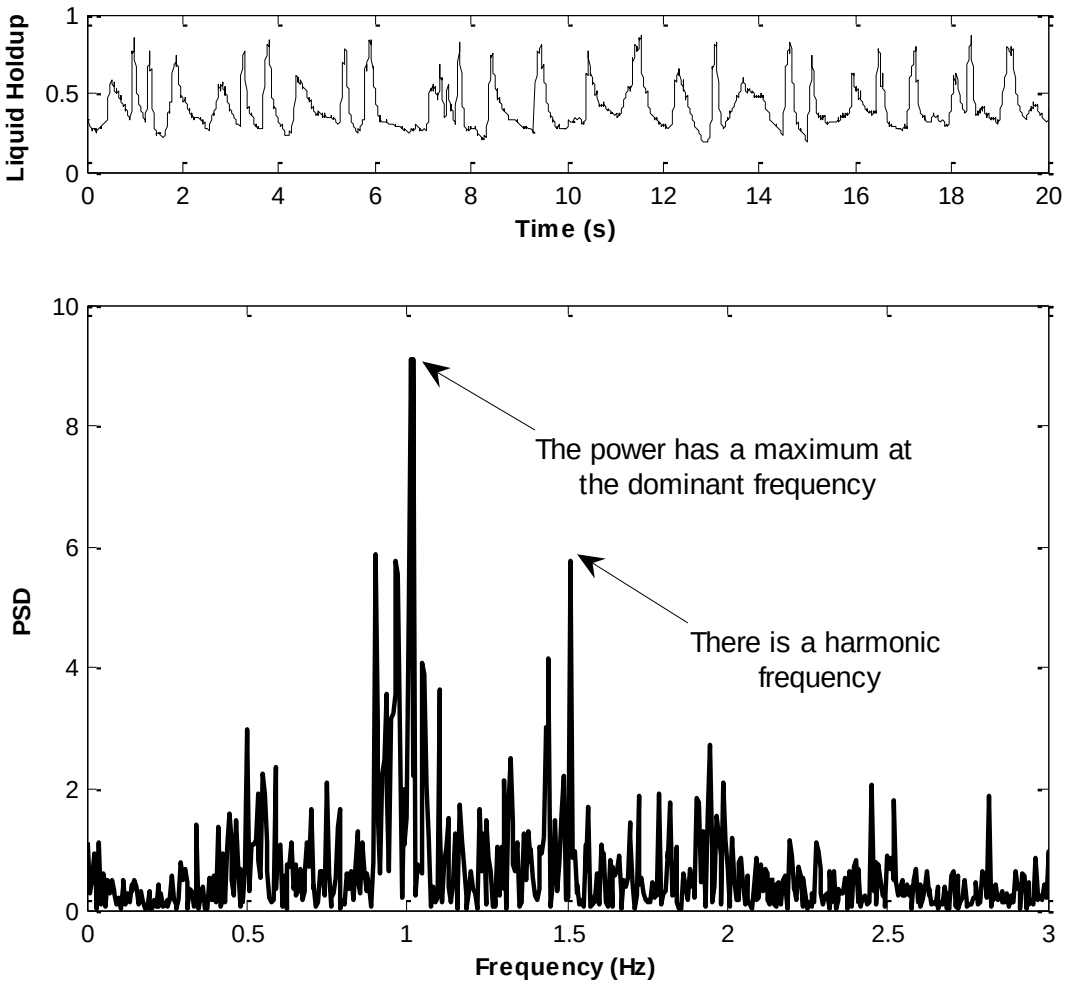

Figure 4.20 Example of PSD (at the bottom) obtained from the corresponding time series (at the top) for 40° inclination, U_{SG}=0.9 m/s and U_{SL}=0.7m/s.

From the analysis of the whole set of experiments, the main frequency tendencies were obtained. A parametric analysis makes it easier to understand the complex behaviour of the frequency, due to the number of variables involved.

First of all it was found that for a particular inclination angle, the frequency increases with the liquid flow rate as it has been reported in the literature for horizontal flow, Manolis *et al.* (1995). This behaviour is illustrated clearly in Figures 4.21 and 4.22,

which contain a set of PSD plots for different inclination angles and liquid superficial velocities. The gas superficial velocity is kept constant. In Figure 4.21 The PSDs corresponds to the same conditions as the set of timeseries and PDFs previuosly presented in Figure 4.8.

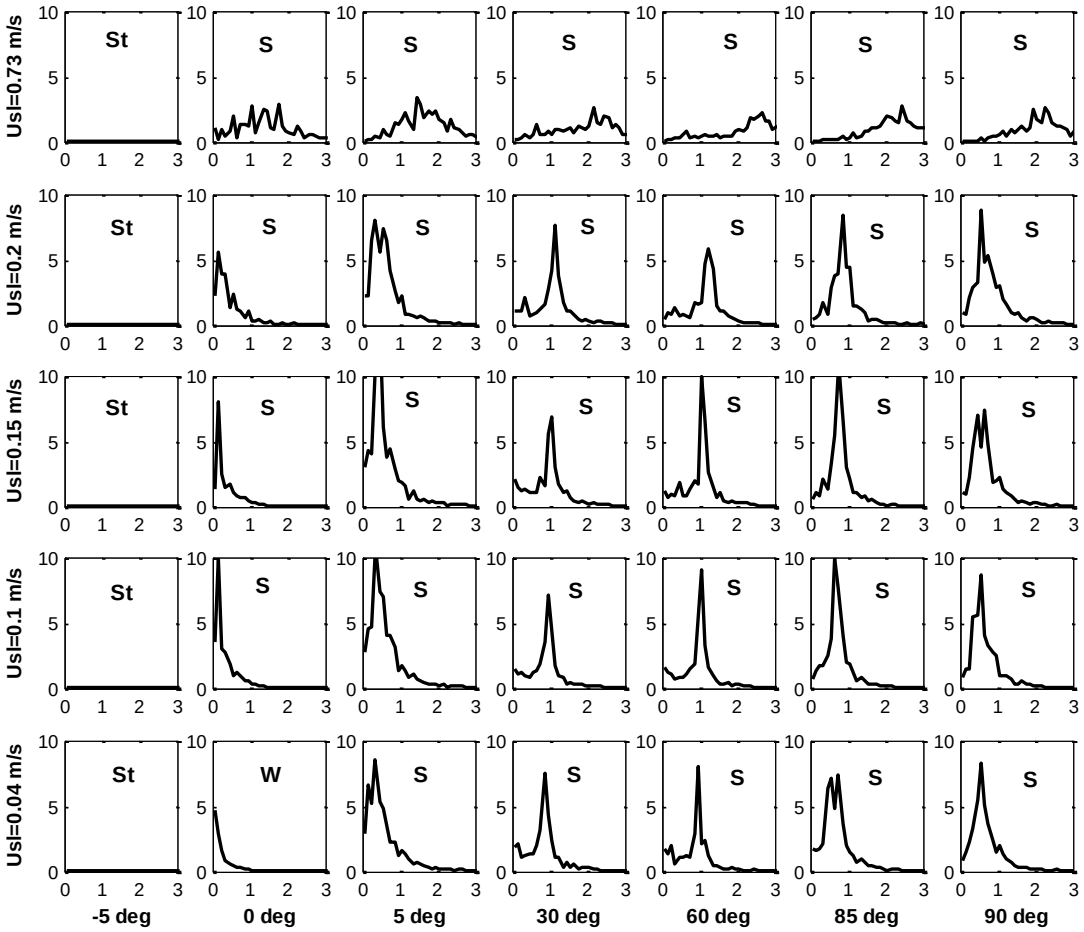

Figure 4.21 PSD graphs for Usg=0.9 m/s and different inclination angles and superficial velocities. x-axis, frequency (Hz); y-axis, PSD. St=Stratified flow, S=Slug flow, W=Wavy flow, C=churn flow.

In Figure 4.21 we can observe that for downwards inclination of 5° the shape of the PSD graph is flat, which indicates that the flow pattern is stratified flow.As we move to horizontal, a peak appears in the plots, which gives an indication of the intermittent flow.

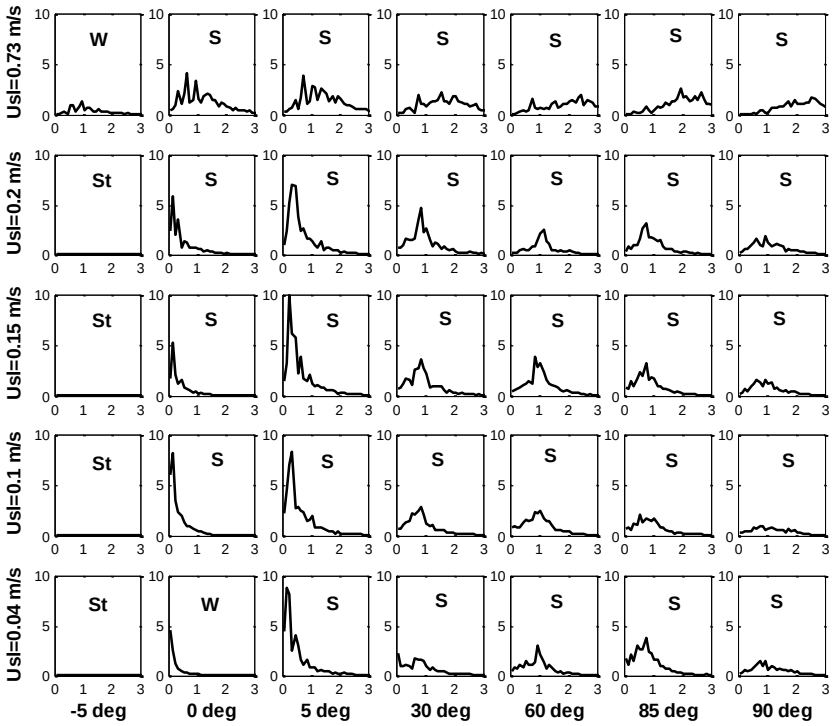

a) U_{SG}=1.5 m/s

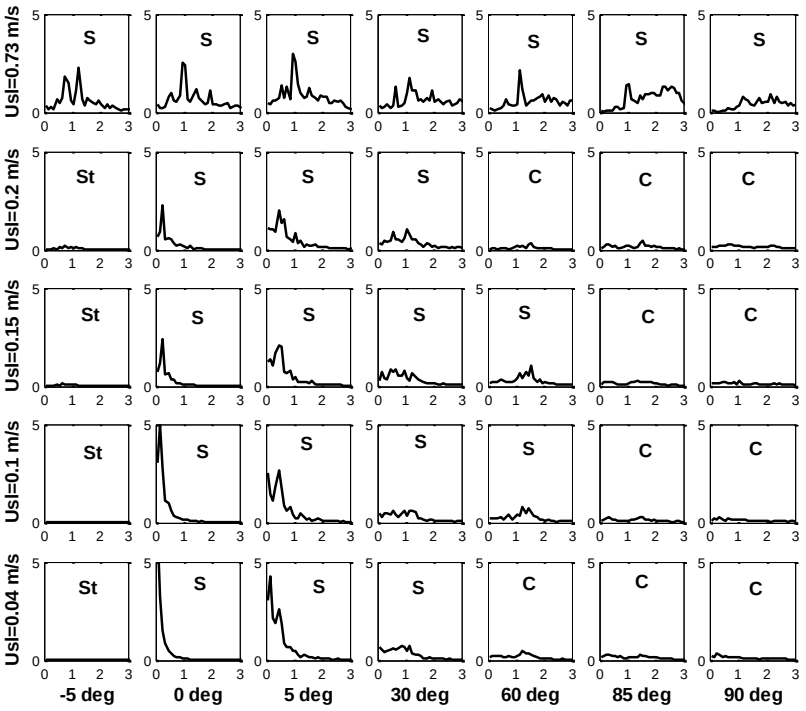

b) U_{SG}=2.9 m/s

Figure 4.22 PSD graphs for different inclination angles and liquid superficial velocities. x-axis, frequency (Hz); y-axis, PSD. St=Stratified flow, S=Slug flow, W=Wavy flow, C=churn flow.

The inttermittent flow for the conditions of Figure 4.21 extends until the vertical pipe. However for different values of gas superficial velocities, the behaviour changes as ilustrated in figure 4.22 by means of the PSDs for U_{SG}=1.5 and U_{SG}=2.9 m/s. Figure 4.22 contains 2 sets of PSD plots. In all cases, the Power in the PSD plots decreases when the the gas flow rate increased. These PSD plots together are helpful to illustrate how the flow pattern is changing for U_{SG}= 1.5 m/s and U_{SG}= 2.93 m/s (by the shape of the PSDs).

In addition, Figures 4.21 and 4.22 show the effect of liquid flow rate on the frequency. It was observed from the experiments that the frequency of slugging increases with the increase in liquid superficial velocity. This is expected, as the time required to rebuild the level of the film to form the next slug would reduce with an increase in the liquid input.

After anlysing the whole set of experiments, the frequencies were obtained and next in Figure 4.23 we present the corresponding values for the frequency for all the experiments.

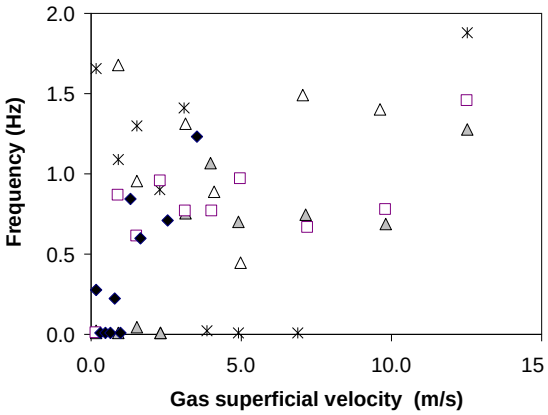

-5 ° Inclination

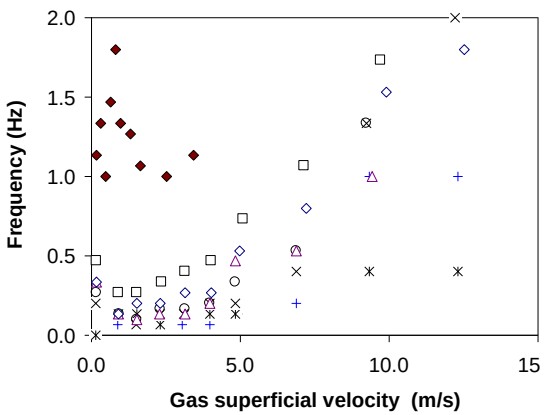

0 ° Inclination

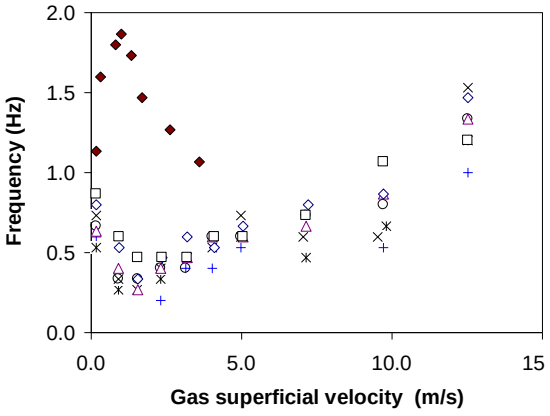

5° Inclination

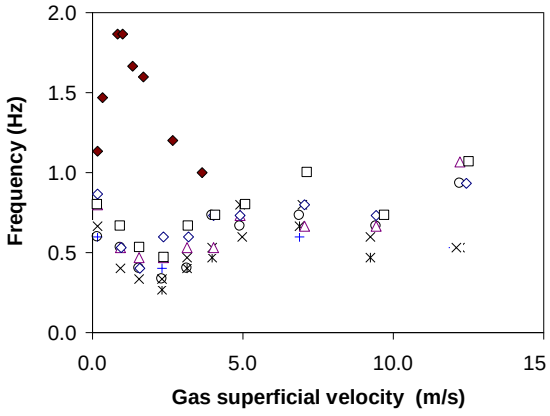

10 ° Inclination

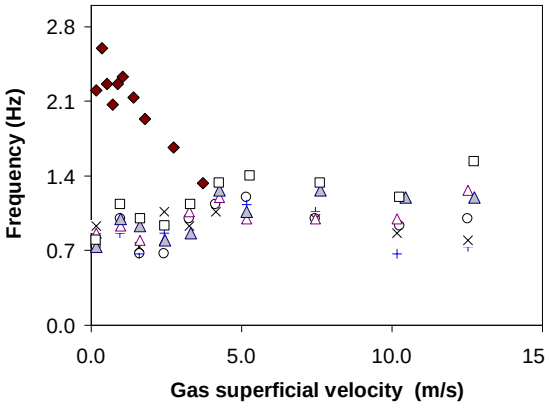

30° Inclination

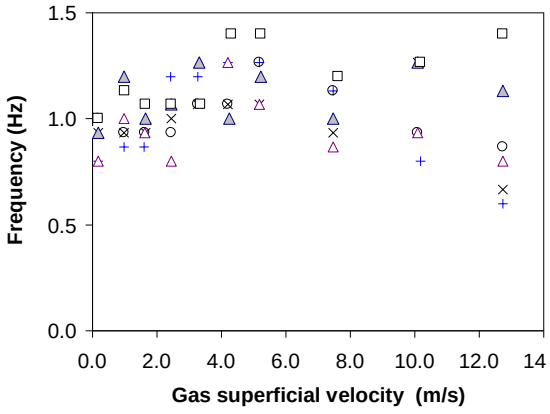

45 ° Inclination

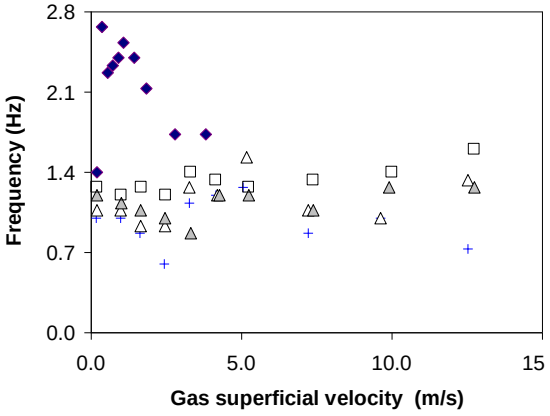

50° Inclination

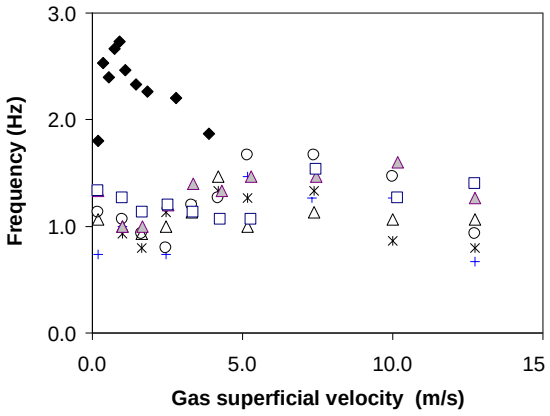

60 ° Inclination

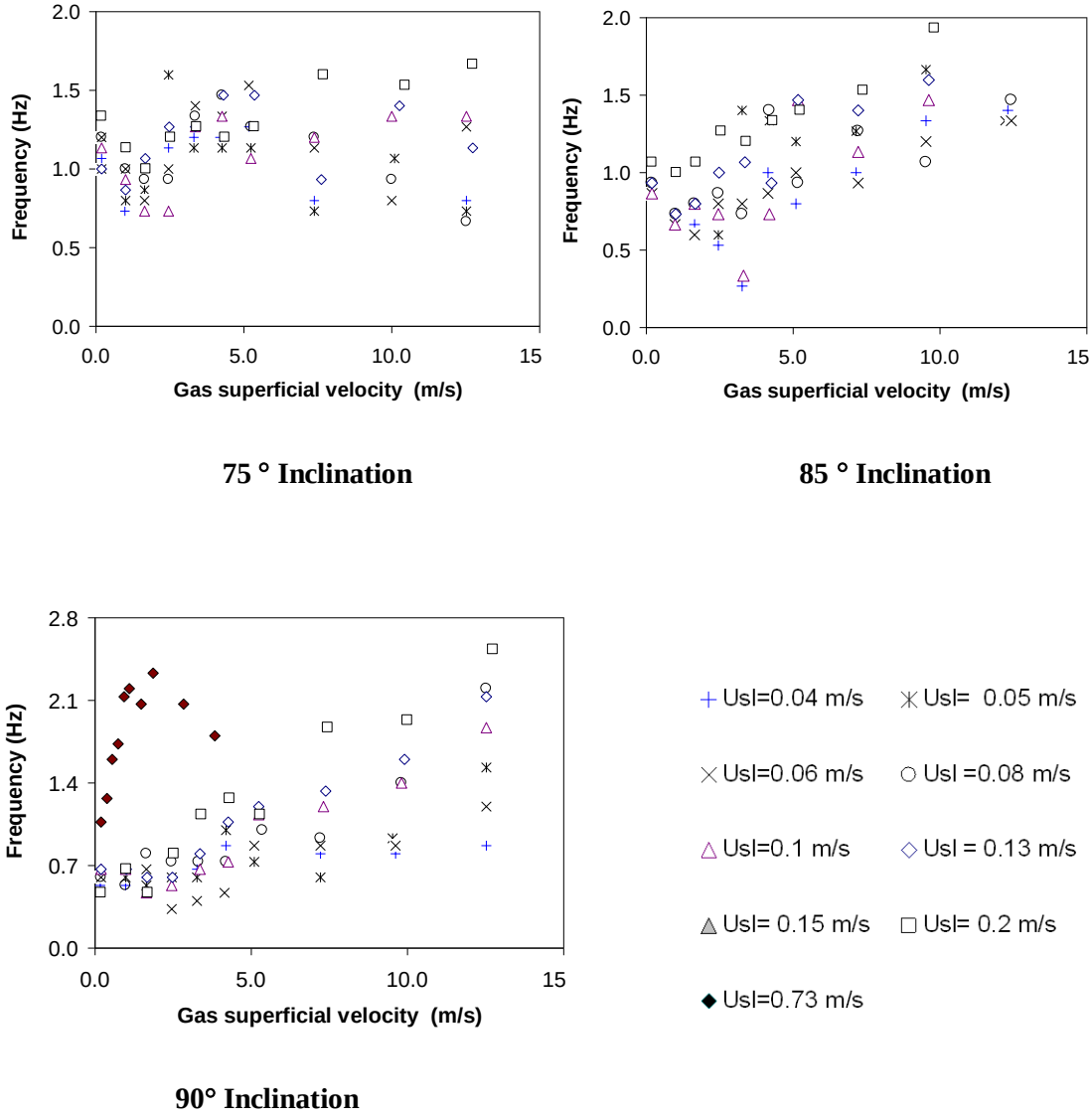

Figure 4.23 Frequencies for different inclination angles.

In Figure 4.23 we can observe the effect of the gas flow rate on the frequency. It is interesting to see that for a given liquid superficial velocity, the slugging frequency in general first tends to decrease and then increase.

When the frequency is ploted as a function of the inclination angle, the results indicate that unlike the liquid hold up, the frequency is strongly affected by the inclination angle. At low gas superficial velocities, the frequency depends on the inclination angle

in such a way that it tends to have a maximum at about 50 degrees. For small inclination angles the liquid tends to go back due to gravity and forth due to mixture velocity and at these velocities the oscillation is more affected by the mixture velocity than by gravity.

For high mixture velocities, the more deviated from horizontal, the higher the frequency. This dependence can be seen in the graph below.

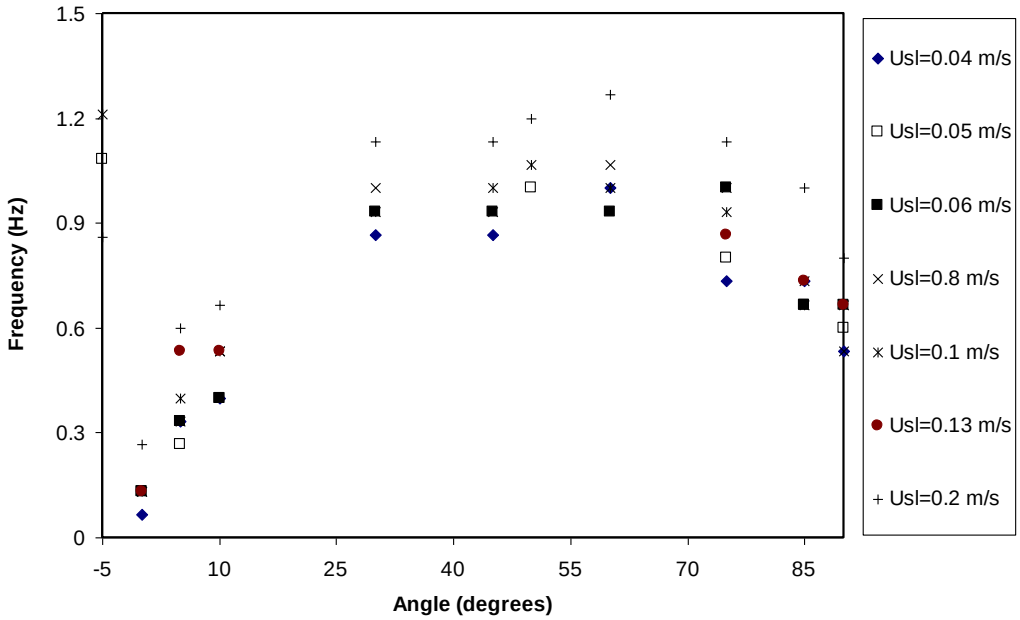

Figure 4.24 Effect of inclination angle on the frequency for U_{SG}=0.9 m/s.

The frequency behaviour also seems to depend on the flow pattern. It was found that not all of the intermittent structures are slug flow but waves or churn flow, therefore the behaviour is more complex to be predicted properly with the PSD, since they are characterised by many peaks in the PSD plot, also the power is very low, which in turn gives uncertainty in the frequency.

One interesting observation about the effect of the gas superficial velocity on the frequency can be made when we plot the time series and PSDs for a particular

inclination angle and keeping the liquid flow rate constant at the same time, as in Figure 4.25.

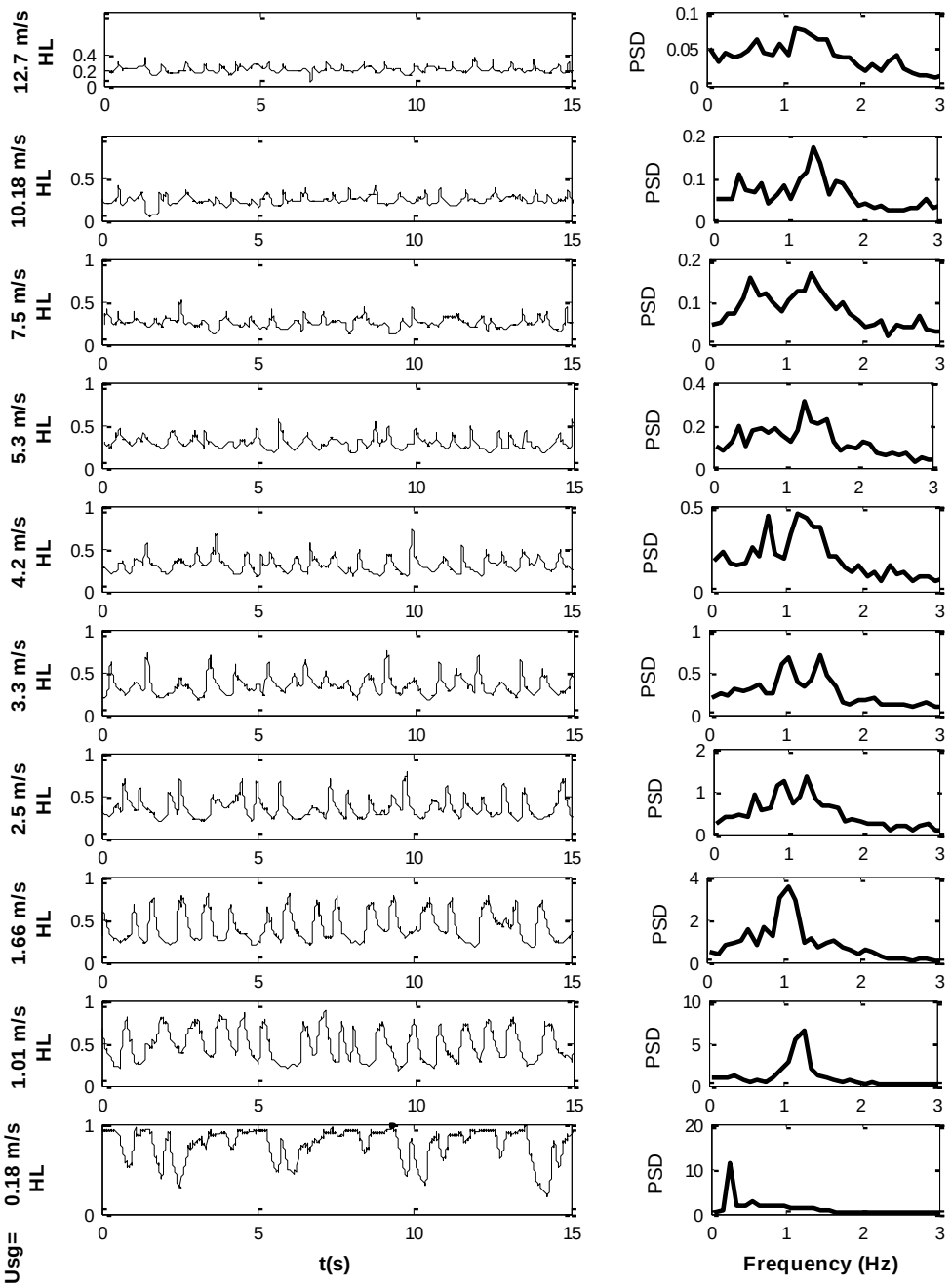

Figure 4.25 Time series (left column) and corresponding PSDs plots (right column) for constant liquid superficial velocity U_{SL}= 0.2 m/s at 50° inclination**.**

For these conditions a transition from slug to wavy flow occurs when the gas superficial velocity is increased. Therefore two peaks on the PSD graphs begin to

appear, and the reason is because there exist slugs and waves for the same condition, however, when the gas superficial velocity is increased, the flow pattern changes from slug to wavy flow. The wavy frequency is high, whereas the slug frequency tends to be lower. When the gas superficial velocity is increased further and the wave flow dominates, the peak corresponding to the slugs decreases both in the Power and frequency, whereas the peak corresponding to the waves increases in the frequency but decreases in power.

Figure 4.25 also illustrated the difficulty in using PSD of holdup time traces for frequency calculation. In these cases, counting was required in addition to the Power Spectral Density method.

In order to examine the prediction of slug frequency measured in the present study with respect to different physical models and correlations, the following models were examined for the horizontal case. The comparison is shown in the Figure 4.26. It can be observed that the Gregory and Scott (1969) and Greskovich and Shrier (1972) models gave identical results.

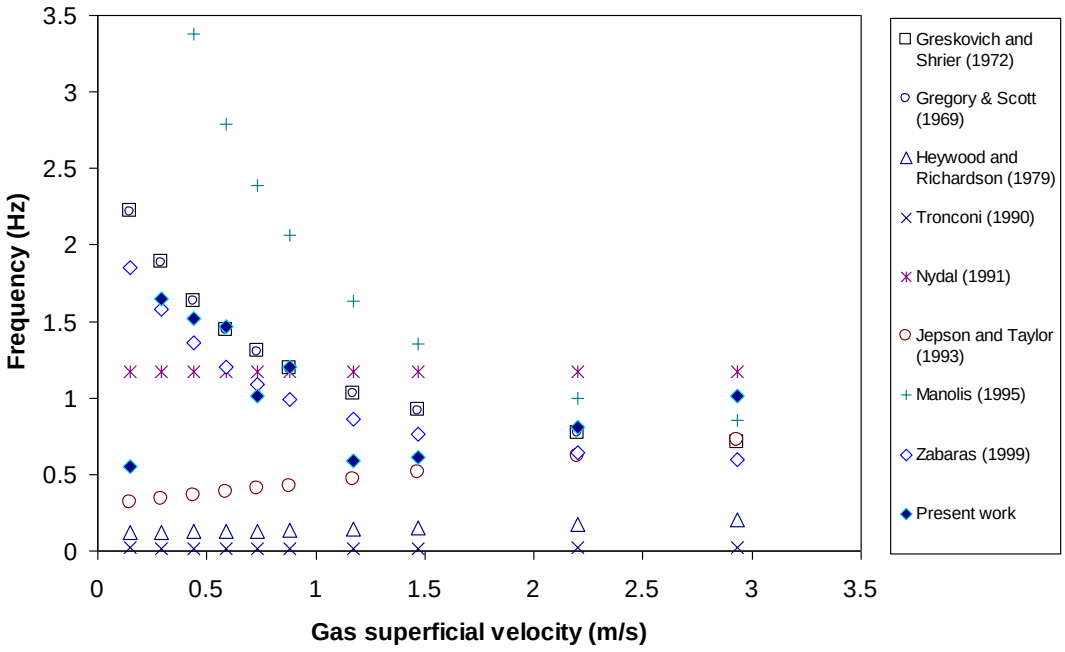

Figure 4.26 Comparison of frequency correlations. Horizontal flow and U_{SL}=0.73 m/s.

Most of the correlations found in literature (see chapter 2) correlate slug frequency towards one or few parameters and extrapolation to other flow systems should be done with care. In fact, only Zabaras (1999) take into account the inclination angle and only small inclinations with respect to the horizontal are considered. Since it has been shown that pipe deviation has a strong effect on the slug frequency it is expected that no good agreement will be with frequency at different inclination angles, as can be seen in Figure 4.27 below.

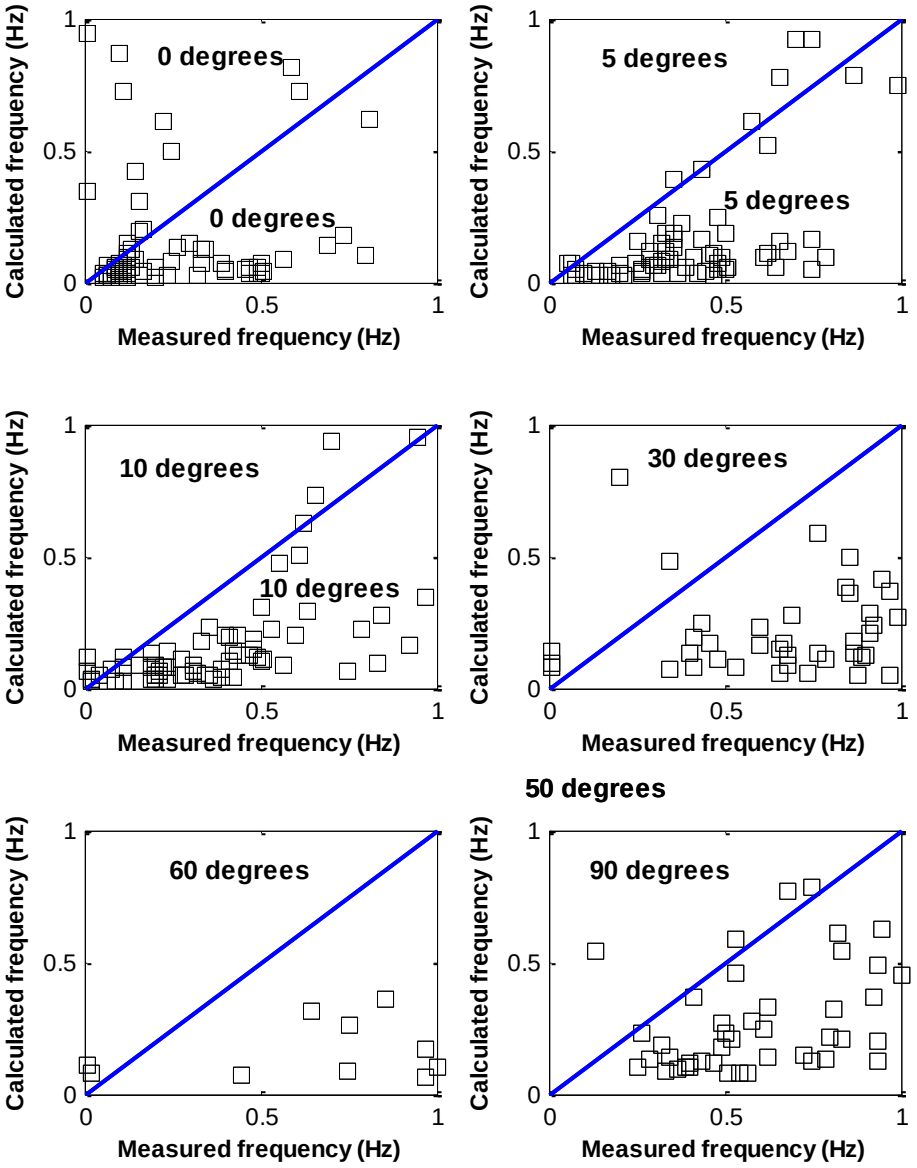

Figure 4.27 Comparison of frequency with Zabaras (1999) correlation.

Table 4.3 Comparison of frequency correlations

Correlation	Inclination	Number of points	Mean error (%)	Standard Deviation
Gregory and Scott (1969)	0°	80	35	0.74
Greskovich and Shrier (1972)	0°	80	53	2.5
Heywood and Richardson (1979)	0°	80	39	3.5
Tronconi (1990)	0°	80	154	1.4
Nydal (1991)	0°	80	84	4.6
Manolis *et al.* (1995)	0°	80	51	1.5
Zabaras (1999)	0°	80	272	1.64
	5°	80	40	0.87
	10°	80	1.9	1.77
	30°	70	60	3.04
	45°	60	300	9.10
	50°	50	72	3.41
	60°	70	269	1.05
	75°	70	168	8.25
	90°	80	8.2	1.56

It is seen in Figure 4.27 that the slug frequencies in the current study are predicted within *±300%*. None of the slug frequency correlations work very well for very low frequencies in inclined pipes; however the comparison might be subjective since it depends on different factors such as the flow conditions.

For that reason, using these frequency correlations for further estimate of other parameters such as slug length may deviate the result one or several orders of magnitude.

When we deal with the analysis of oscillating, unsteady fluid flow dynamics problems, a dimensionless value useful is the Strouhal Number. It represents a measure of the ratio of inertial forces due to the unsteadiness of the flow or local acceleration to the inertial forces due to changes in velocity from one point to another in the flow field.

The Strouhal Number can be expressed as:

$$St = \omega \, l / U \tag{4.10}$$

where

St = Strouhal Number

ω = oscillation frequency

l = characteristic length (for example hydraulic diameter)

U = flow velocity

In Figure 4.28, the Strouhal number based on the gas superficial velocity is plot as a function of the input liquid holdup.

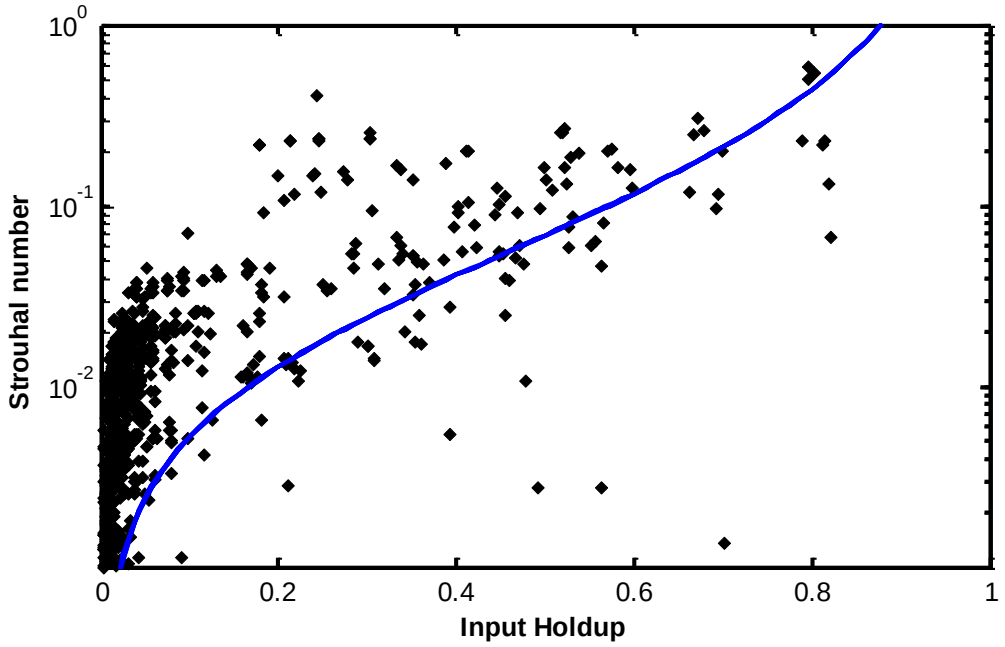

Figure 4.28 Strouhal number as a function of the input liquid holdup for different inclination angles**.**

Azzopardi (1997) proposed that the pipe diameter and the superficial gas velocity should be used in the Strouhal number. These plots are shown in Figure 4.29.

$$St = \frac{fd}{U_{SL}} \tag{4.11}$$

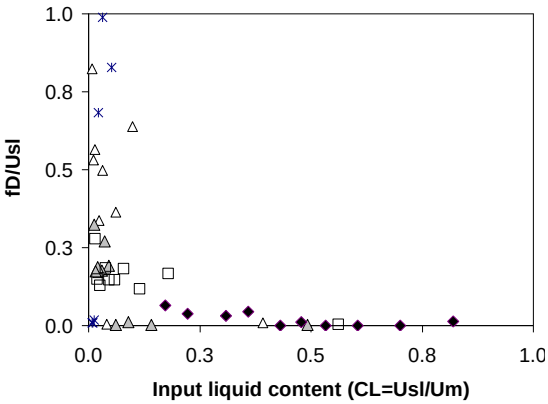

-5 ° Inclination

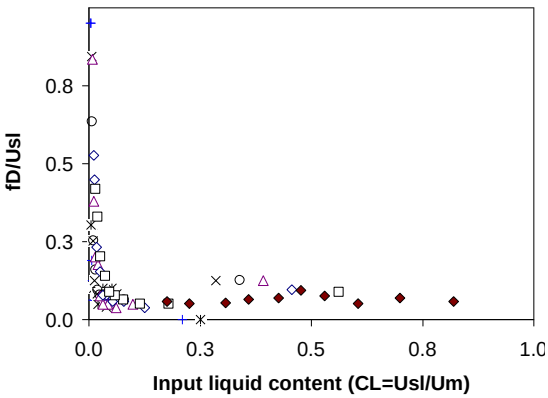

0 ° Inclination

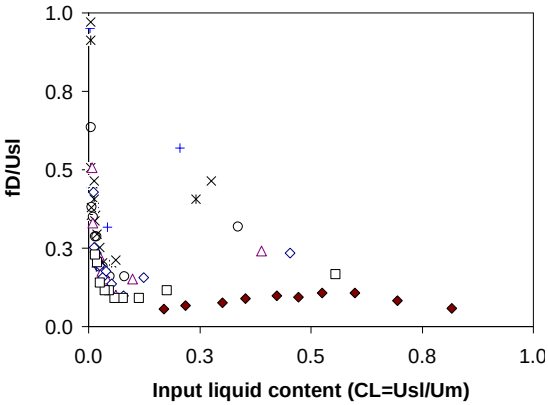

5° Inclination

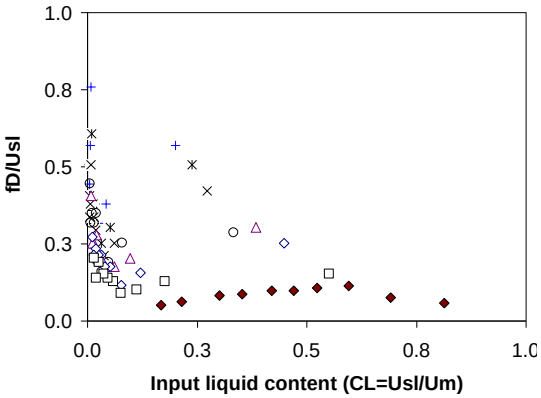

10 ° Inclination

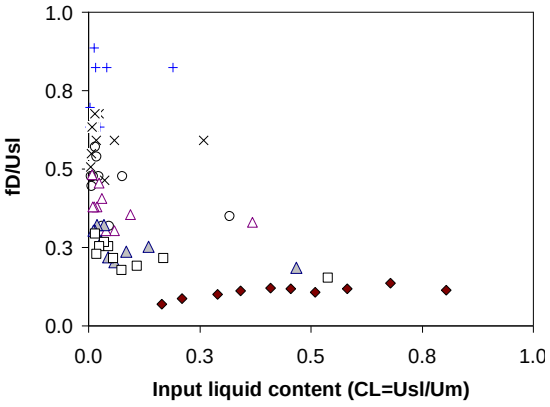

30° Inclination

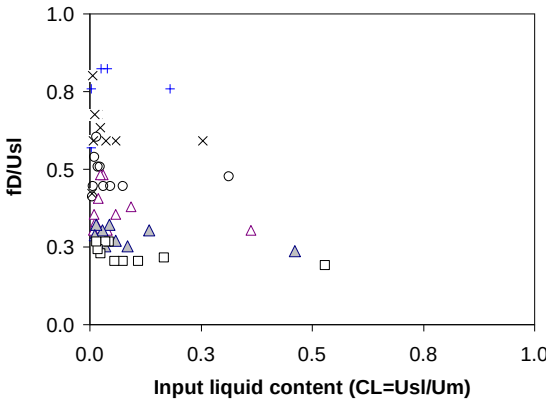

45 ° Inclination

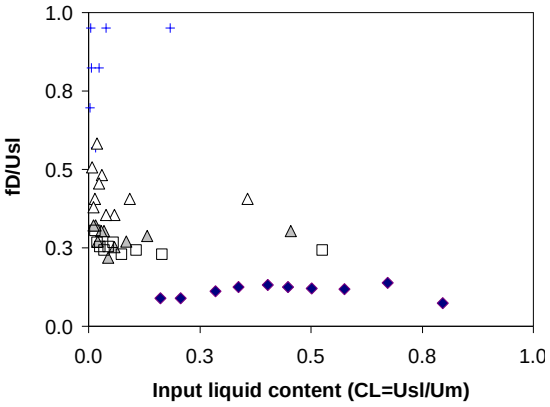

50° Inclination

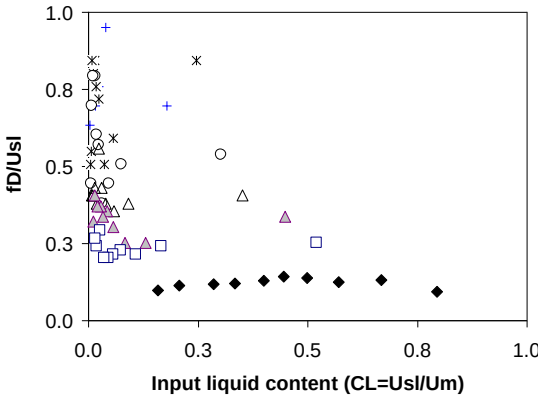

60 ° Inclination

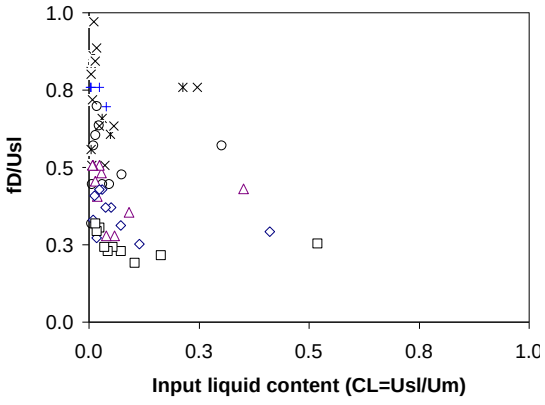

75 ° Inclination

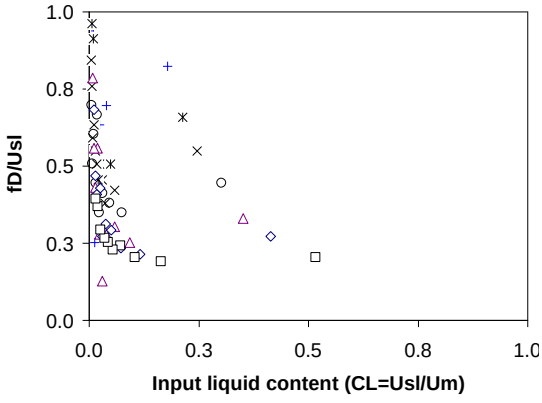

85 ° Inclination

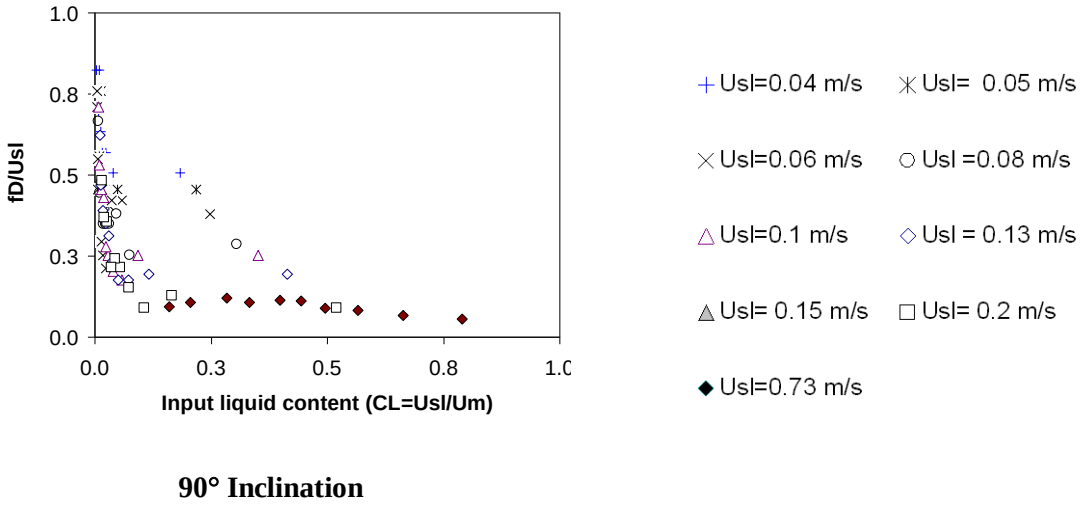

Figure 4.29 Strouhal number as a function of the input liquid holdup for different inclination angles.

Azzopardi (1997) found that such a plot shows that many of the data lie on a straight line and, therefore, are well correlated by the two dimensionless group employed. However, it is only the air/water data that lie on one line. Data for other fluid systems lie above or below the main curve. The deviation is systematic and depends on the liquid/gas density ratio. In an attempt to reconcile that data Azzopardi (1997) tried an alternative correlation method.

The original Strouhal number was replaced by one using the superficial liquid velocity instead of that for the gas and this was plotted against the Lockhart-Martinelli parameter. The Lockhart-Martinelli parameter is defined as the square root of the pressure drops for the liquid part of the flow flowing alone in the pipe divided by that for the gas and it is approximately equal to the ratio of liquid and gas superficial velocities times the square root of the liquid to gas density ratio.

$$X = \sqrt{\frac{\rho_L}{\rho_G}} \frac{U_{SL}}{U_{SG}} \tag{4.12}$$

Figure 4.30 illustrates the correlation between a liquid based Strouhal number and the Lockhart-Martinelli parameter, X. The linear relationship of these two parameters illustrates a good correlation.

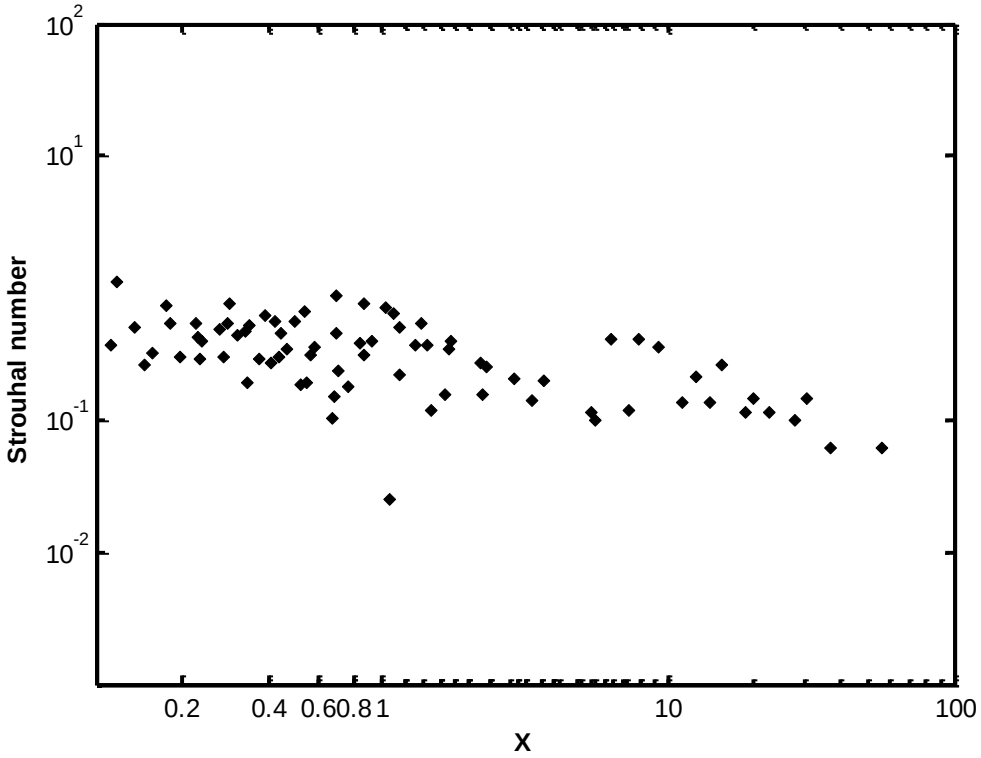

Figure 4.30 Strouhal number as a function of the Lockhart-Martinelli parameter.

4.6 Pressure drop

Pressure drop is an important parameter in pipeline design. The pressure loss in a system is an essential variable for the determination of the pumping energy for a given flow. In this work, pressure drop has been obtained in the form of a time series by using the differential pressure transducer as described in Chapter 3.

A typical time series of pressure drop for slug flow is shown below. The unsteady character of the flow is indeed clearly visible in variation of the pressure drop in the time series recorded by the differential pressure transducer (DP cell). It can be observed that the occurrence of slugs causes the measured pressure drop to fluctuate rapidly and widely.

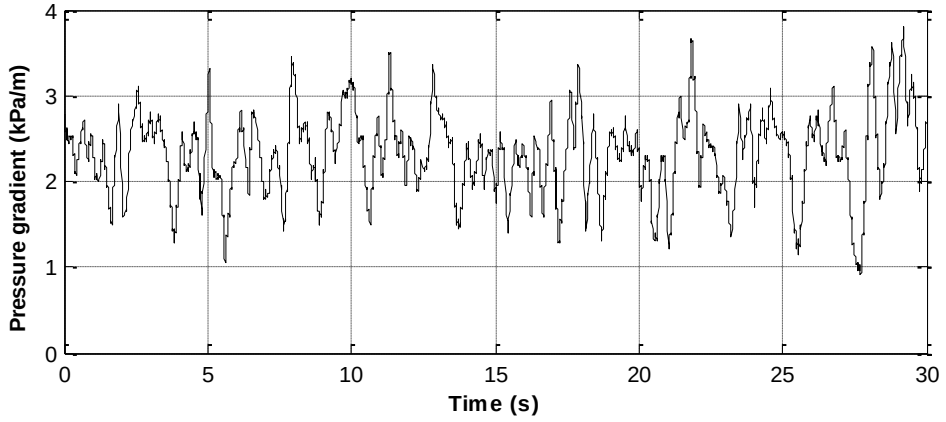

Figure 4.31 Example of pressure drop time series obtained with the DP cell.

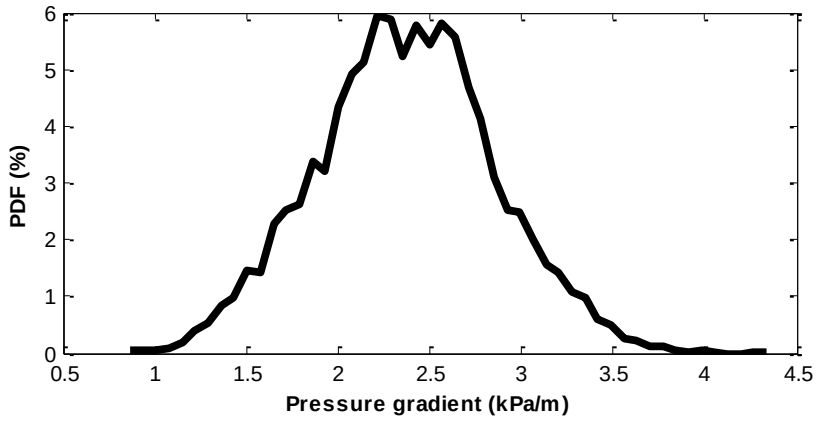

Figure 4.32 Typical pressure drop PDF

After analysis of the the whole set of experiments, the pressure drop tendency found was as can be seen in Figure 4.33. For downward flow and constant liquid flow rate, the pressure drop increased with the gas superficial velocity, this also happens for horizontal flow. This is explained by the fact that in this case the main contribution to the pressure loss comes from friction losses. For upward inclined flow, the main contributor is the hydrostatic head, which depends directly on the mixture density, which in turn is a function of the in-situ liquid volume fraction or holdup. This fact is proved by the experimental results, which show that pressure drop and liquid holdup have a similar behaviour (Figure 4.13 and 4.33).

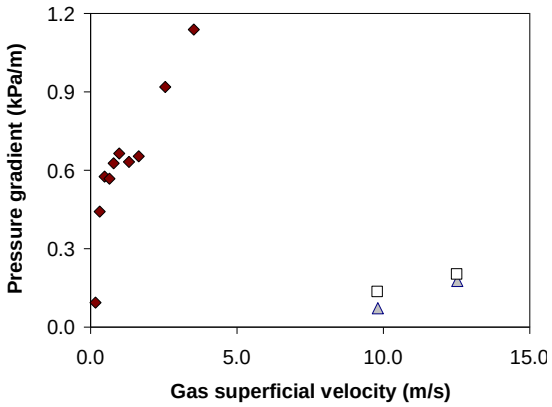

-5 ° Inclination

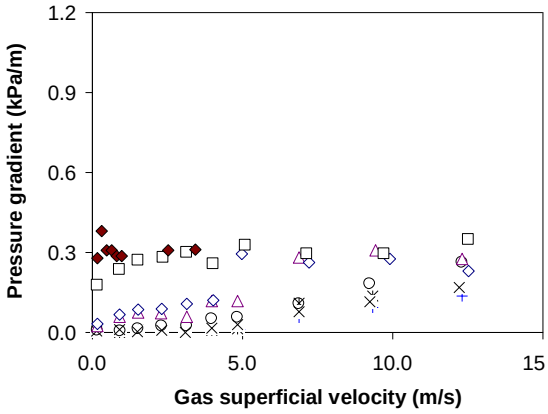

0 ° Inclination

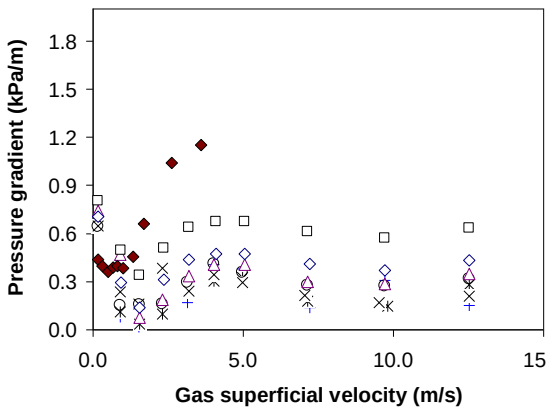

5° Inclination

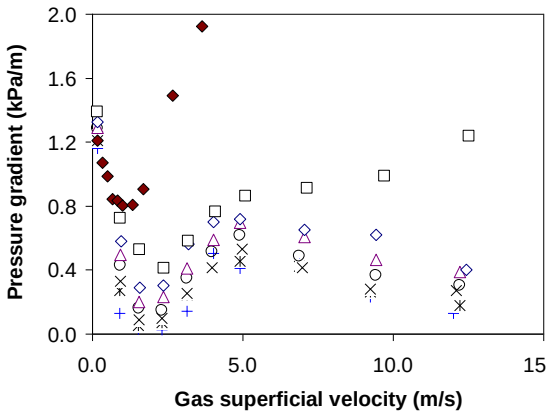

10 ° Inclination

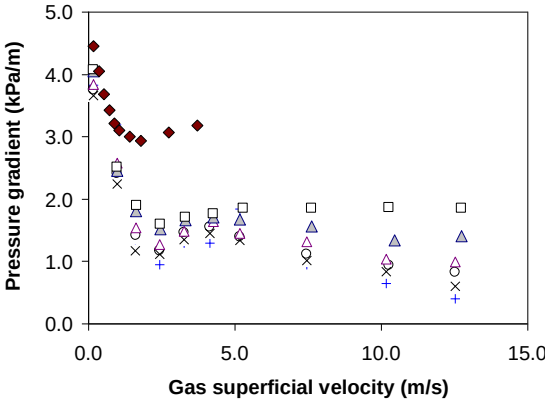

30° Inclination

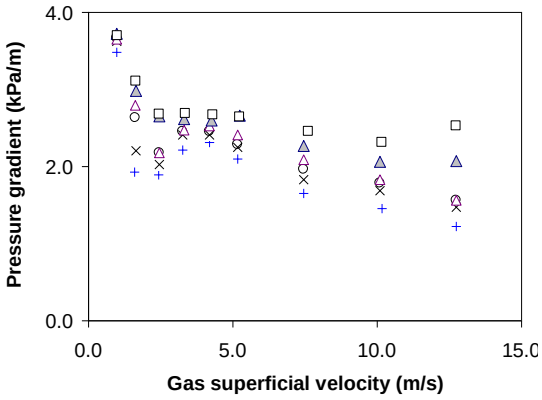

45 ° Inclination

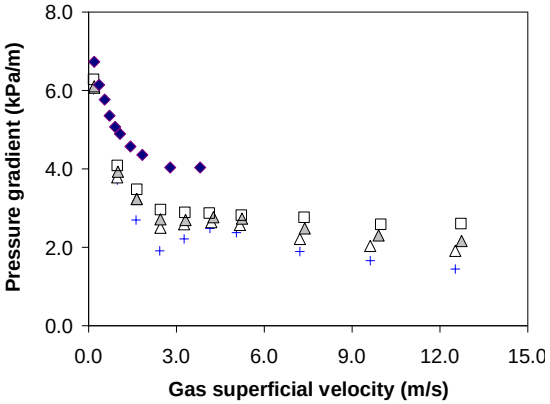

50° Inclination

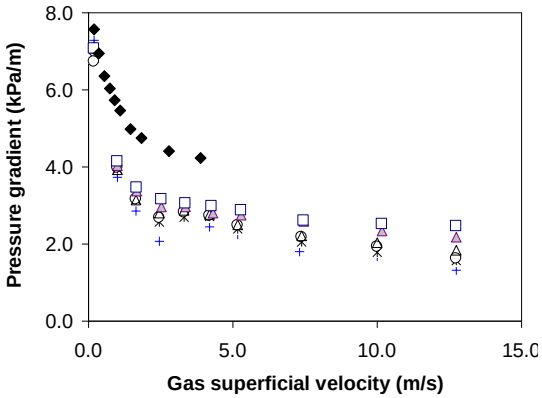

60 ° Inclination

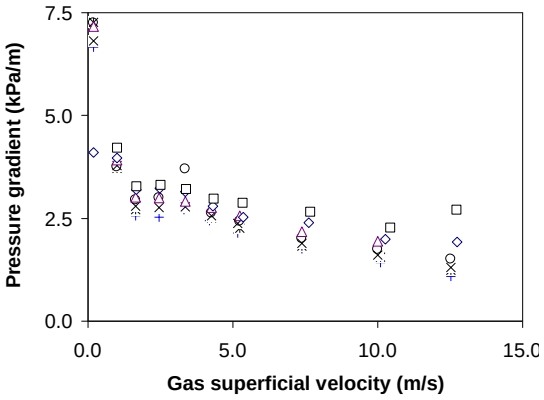

75 ° Inclination

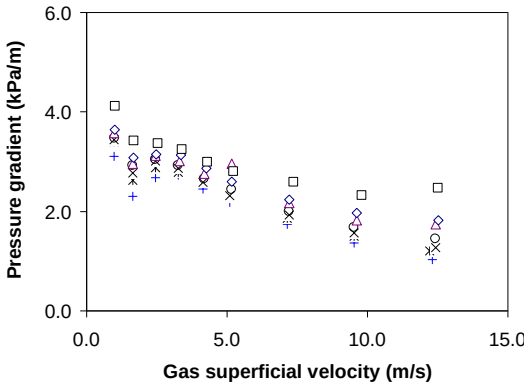

85 ° Inclination

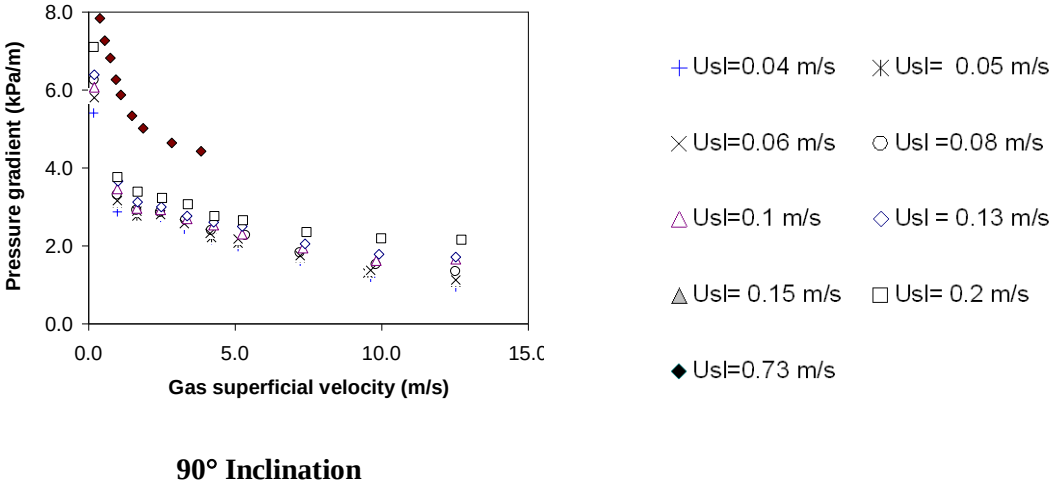

Figure 4.33 Pressure drop for different inclination angles and superficial velocities.

In order to better visualise the effect of the pipe inclination angle on the pressure drop, a 3D graph is presented below in Figure 4.34. In this graph we can clearly observe that for a constant liquid flow rate, the maximum pressure drop will occur for the 90° inclination when the gas superficial velocity is a minimum. It can also be observed that the pressure drop increases with the liquid flow rate.

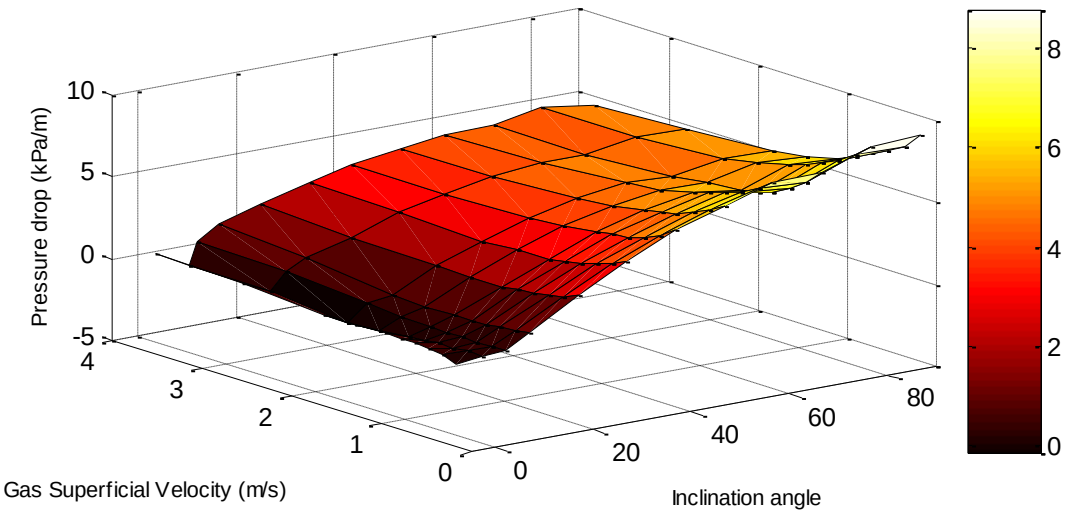

Figure 4.34 Effect of Inclination angle and superficial velocity on pressure drop, liquid superficial velocity = 0.7 m/s.

In the literature, a large number of investigations have been reported on the determination of pressure drop characteristics of two-phase flow in horizontal and vertical conduits and comparatively little has been reported on two-phase pressure drop in inclined pipes (see Chapter 2). Most models proposed today are applicable, if not actually derived for, a specific flow pattern or regime.

When correlations describing pressure drop in two-phase flow has been developed two main approaches have been used; conservation of momentum or conservation of energy. For single phase flow these two approaches lead to identical results. However, in two-phase flow the approach has an influence on the distribution of the pressure losses among the different terms in the total pressure drop. Theoretically, the total pressure drop is of course the same for both approaches. It is therefore important to remember from which approach different correlations are developed. In the present work, only the most recommended friction pressure drop correlations will be presented.

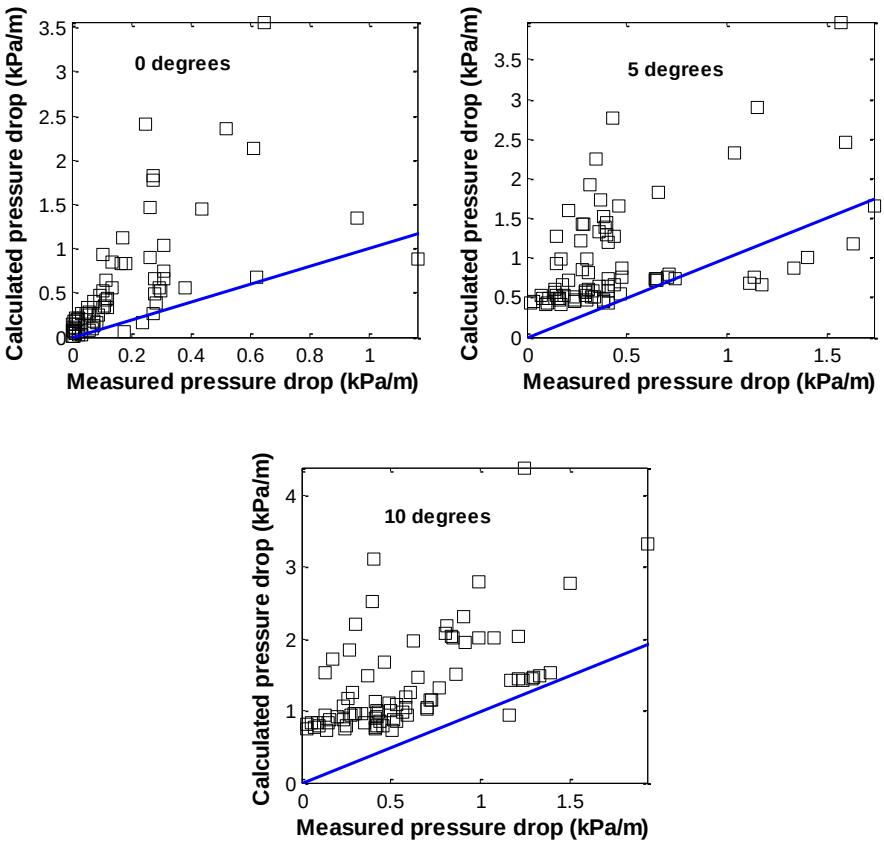

Figure 4.35 Comparison of measured overall pressure drop and predicted by Mattar and Gregory (1974) correlation

The most widely employed empirical correlation method appears to be the Beggs and Brill (1973) correlation. The results from comparison with the current experimental data set are plotted in Figure 4.36. When the measured pressure drop is compared with the predictions of the correlation of Beggs and Brill (1973), it is observed that in general the correlation under predicts, the correlation performs almost the same for all inclination angles. A relatively wide scatter with comparison with experimental data was observed. The discrepancies may in part be caused by the results from the predictions of holdup in stratified flow using the stratified flow model

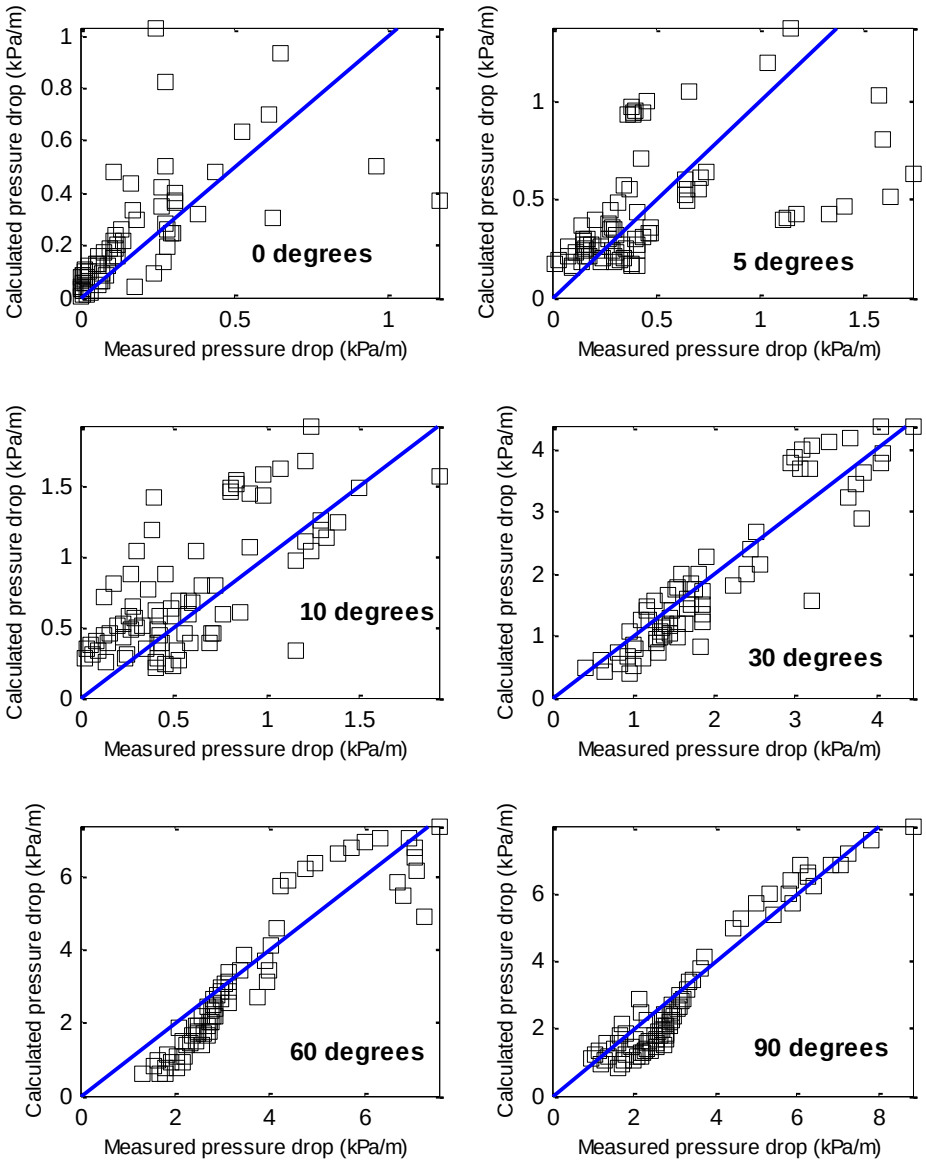

Figure 4.36 Comparison of measured overall pressure drop and predicted by Beggs and Brill (1973) correlation

However, the correlation is less reliable at low liquid rates because of their parametric dependence on input liquid fraction.

Table 4.4 Comparison of Pressure drop correlations

Correlation	Inclination	Number of points	Mean error (%)	Standard Deviation
Mattar and Gregory (1974)	0°	80	287	16.88
	5°	80	225	3.28
	10°	80	294	4.45
Beggs and Brill (1973)	0°	80	74	8.5
	5°	80	37	1.2
	10°	80	88	1.8
	30°	70	9	0.2
	45°	60	-28	0.2
	50°	50	-18	0.2
	60°	70	-19	0.2
	75°	70	78.4	2.3
	85°	70	58.7	6.2
	90°	80	-14	0.2

In additions, PDF and PSD techniques can be applied to the pressure drop time series as it was done to the liquid holdup, we obtained the following behaviour as can be seen below.

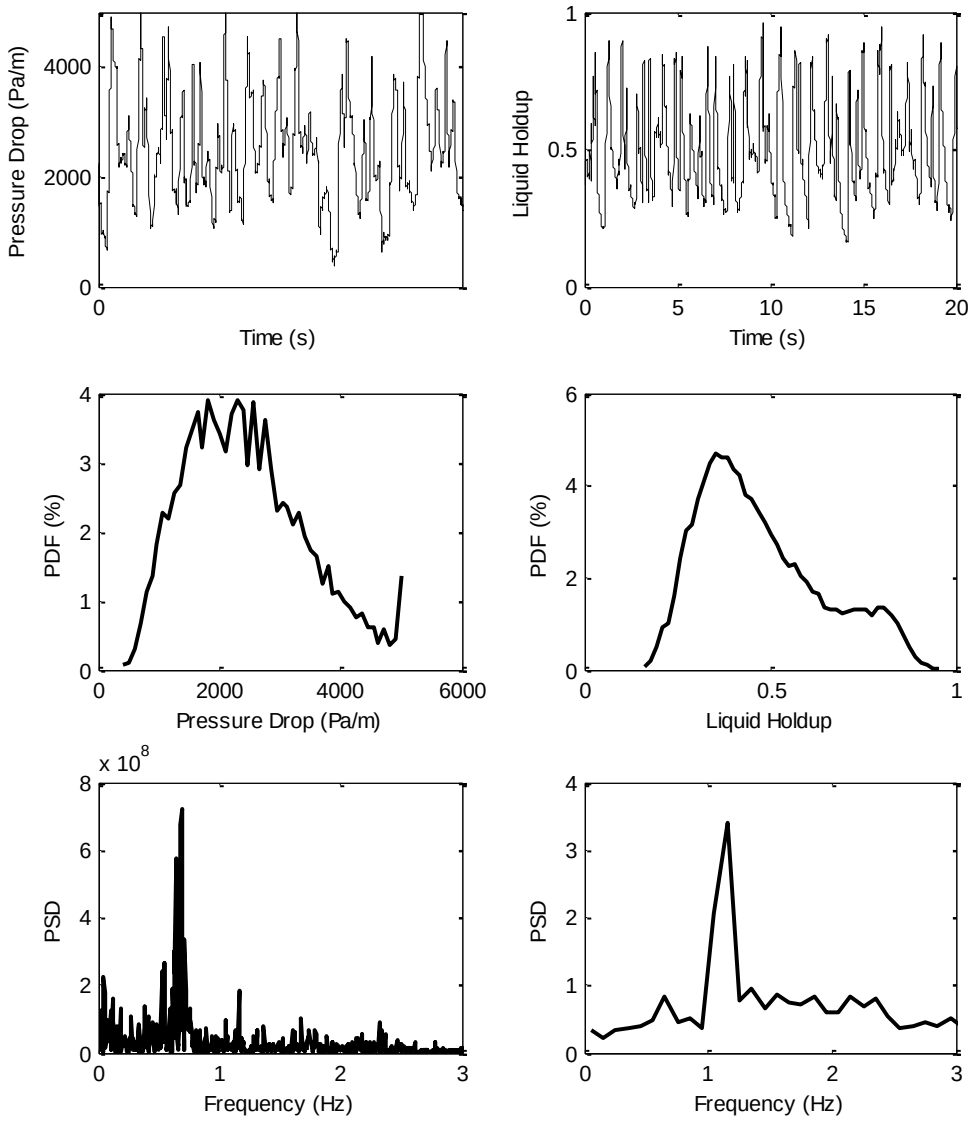

Figure 4.37 Comparison of time series, PDF and frequencies obtained from pressure drop and liquid holdup respectively**.**

It can be seen that the frequency of slugs obtained by using the pressure drop time series is lower than that obtained by using the liquid holdup. The difference is thought to be because the separation distance between the pressure tapings (0.75 m) could be longer or shorter than the slug or bubble length. Therefore, some fluctuations are not detected by DP cell, whereas the capacitance probes can detect the high transient behaviour of the flow. For further analysis, the capacitance probe signals were used. However, the averaged pressure drop (obtained as in equation 4.6) is not affected by the distance between the pressure taps.

The result of correlating the average values of the liquid holdup and pressure drop signals is shown in Figure 4.38, which means there is a high dependence between them because the gravitational pressure drop is the major contribution to the total pressure drop.

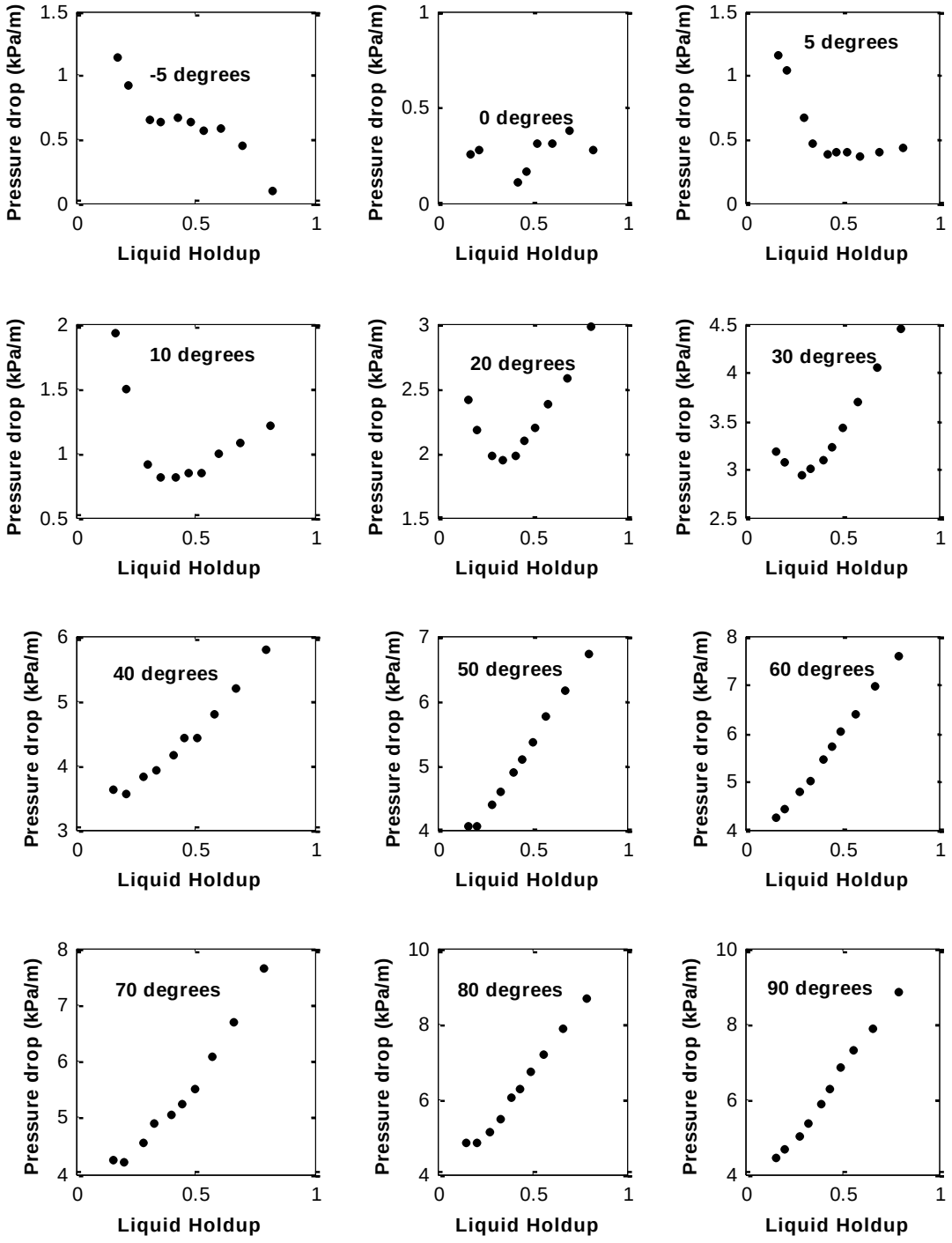

Figure 4.38 Pressure drop as a function of the liquid holdup for U_{SL}=0.73 m/s.

4.7 Translational velocity

Cross-correlation of the holdup time series produced by the two capacitance probes allows the translational velocity of periodical structures such as slugs to be determined. A plot of time series for the two capacitance probes is shown below in Figure 4.39.

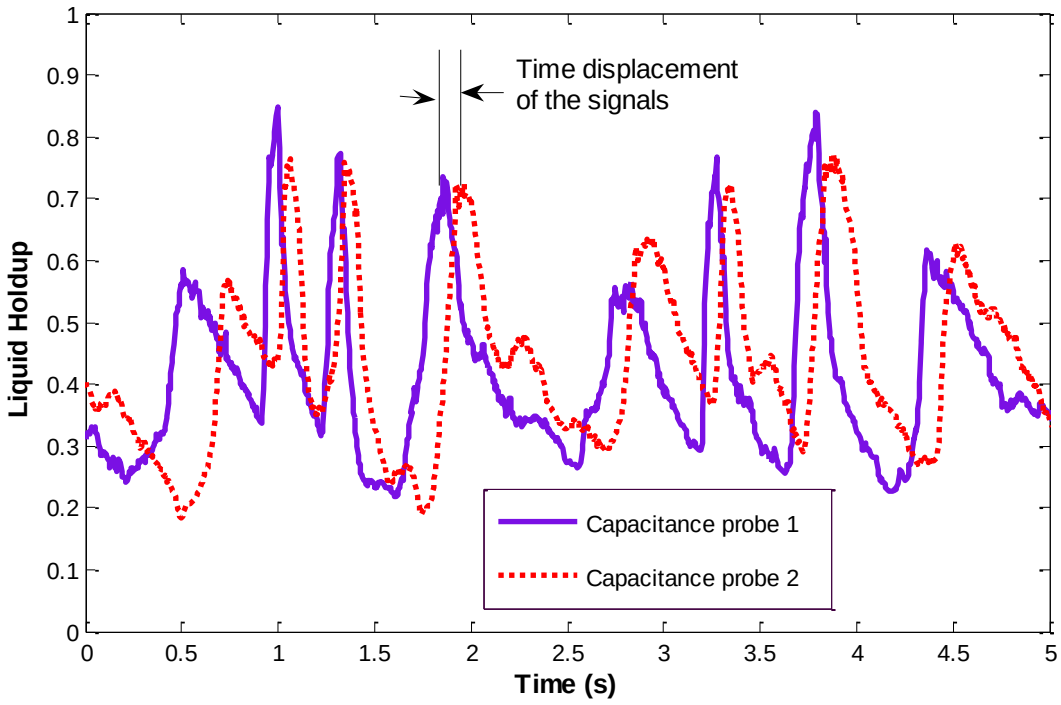

Figure 4.39 Liquid holdup signals from the two capacitance probes. 50° inclination angle, U_{SL}=0.7 m/s and U_{SG}=1.5 m/s

The character of the each signal is distinguished by only two variables, the amplitude of the fluctuations and their frequency. In the general theory of harmonic analysis, an expression of considerable importance and interest is, in the case of periodic functions,

$$\frac{1}{T_1}\int_{-\frac{\pi}{2}}^{\frac{\pi}{2}} g_1(t) \bullet g_2(t+\tau)dt \qquad (4.13)$$

Where g_1(t) and g_2(t) are periodic functions having the same fundamental frequency and τ is a continuous time of displacement in the range (-∞,∞), independent of t. This integral involves three important operations:

1. The periodic function, $g_2(t)$, is given a displacement τ.
2. The displaced function is multiplied by the other periodic function, $g_1(t)$, of the same fundamental frequency.

3. The product is averaged by integration over the complete period.

These steps are repeated for every value of τ in the interval $(-\infty,\infty)$ so that a function is generated. This combination of the three operations, displacement, multiplication and integration is called correlation.

The cross correlation is a measure of the similarity between any two different signals and also it is a function of the relative time between the signals, is sometimes called the sliding dot product. Figure 4.40 shows the cross correlation plot corresponding to the pair of liquid holdup signals in Figure 4.39. This is a typical cross correlation plot that resulted for the rest of the experiments performed.

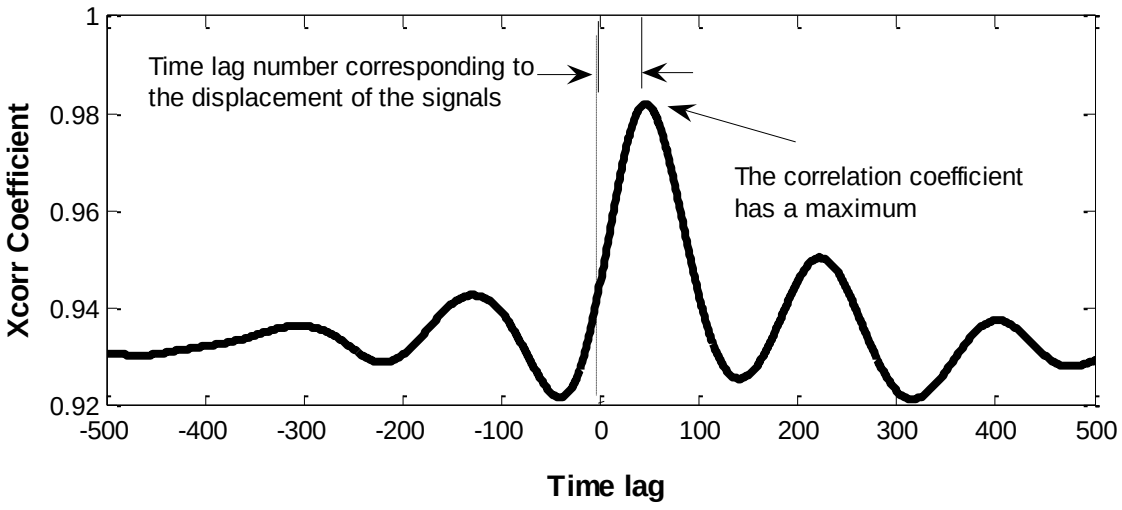

Figure 4.40 Cross correlation Coefficient for the two liquid holdup signals of figure 4.39**.**

Correlation is computed into what is known as the correlation coefficient, which ranges between -1 and +1. Perfect positive correlation (a correlation coefficient of +1) implies that as one signal moves, either up or down, the other signal will move in lockstep, in the same direction. Alternatively, perfect negative correlation means that

if one signal moves in either direction the signal that is perfectly negatively correlated will move by an equal amount in the opposite direction. If the correlation is 0, the movements of the signals is said to have no correlation, it is completely random. If one signal moves up or down there is as good a chance that the other will move either up or down, the way in which they move is totally random.

By following the procedure explained above, the structure velocity was calculated for all the experiments and the results are presented below in Figure 4.41, each subplot corresponds to a particular inclination angle.

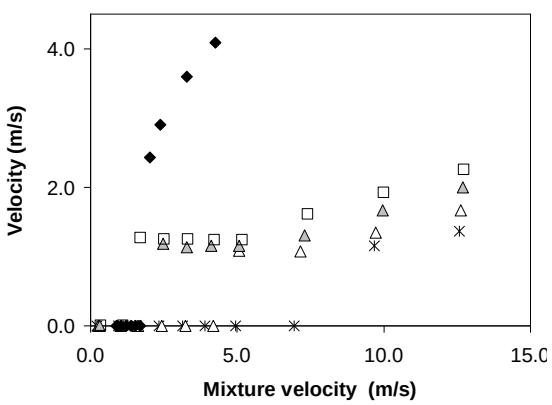

-5 ° Inclination

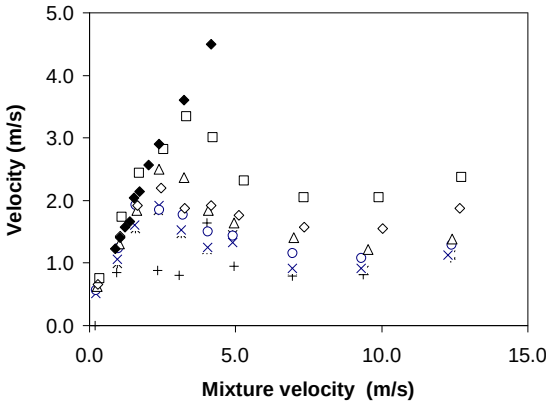

0 ° Inclination

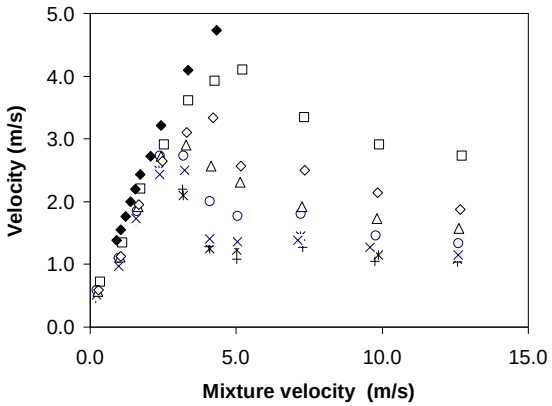

5° Inclination

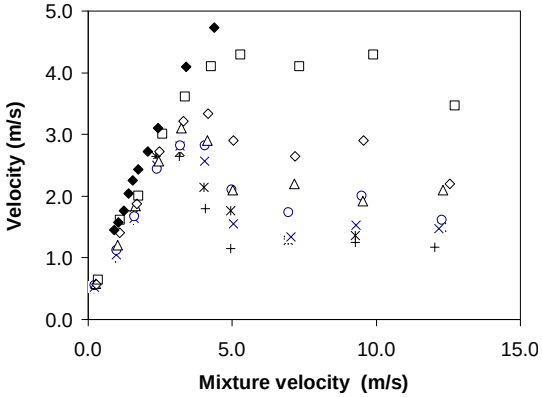

10 ° Inclination

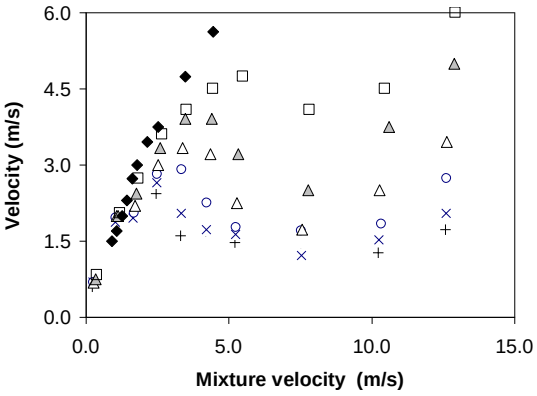

30° Inclination

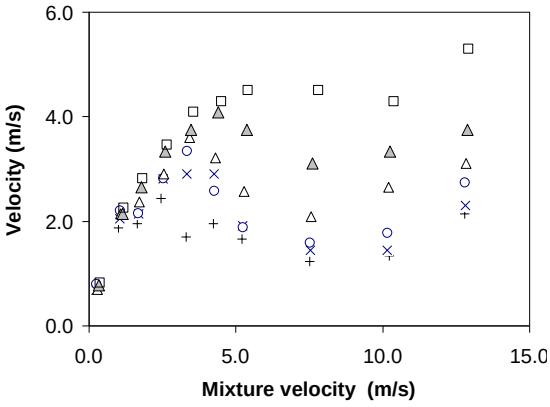

45 ° Inclination

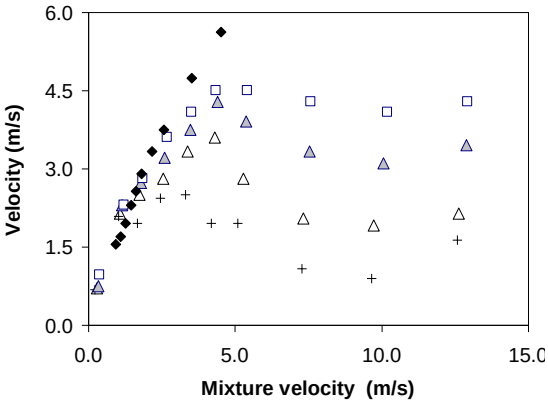

50° Inclination

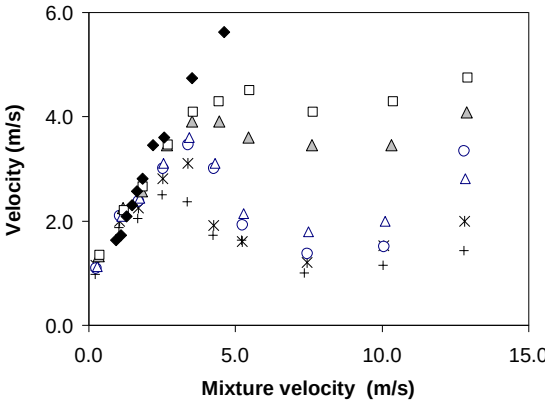

60 ° Inclination

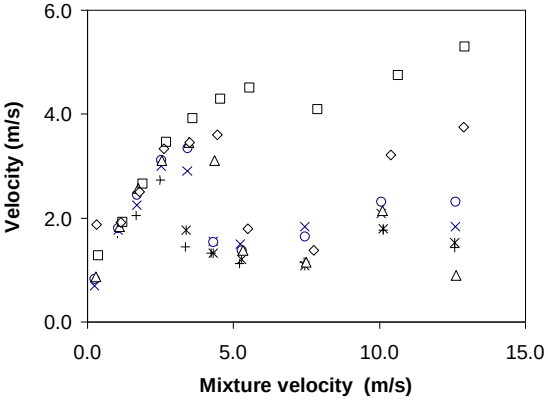

75 ° Inclination

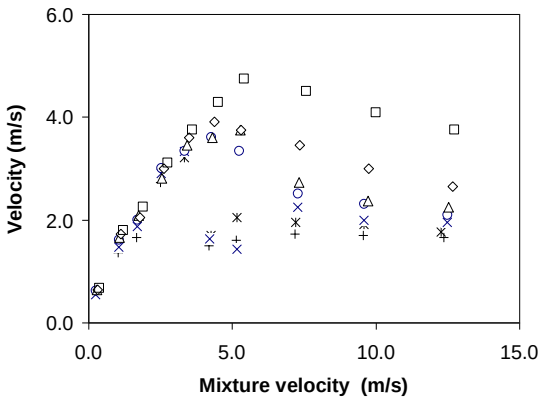

85 ° Inclination

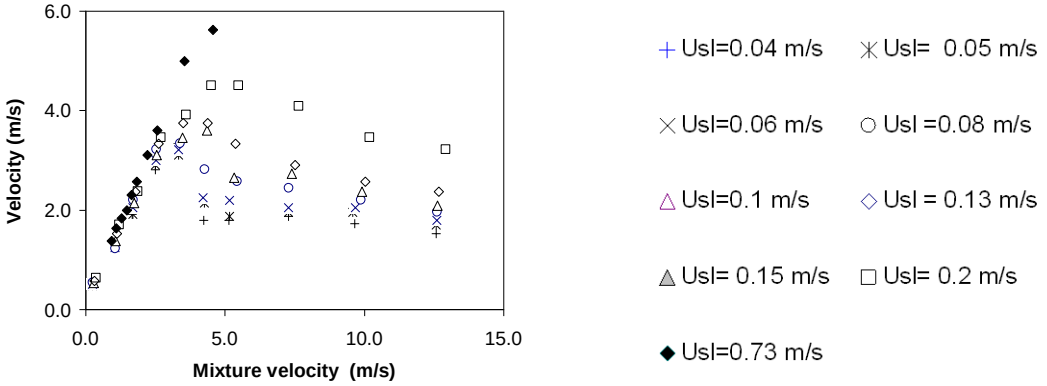

90° Inclination

Figure 4.41 Structure velocities as a function of the mixture velocity for different inclination angles

By choosing, from the data shown in Figure 4.41, those for which the structure velocity is directly proportional to the mixture velocity, a correlating equation can be determined linking these two values. The subset of data is shown in Figure 4.42 for the horizontal case as a typical example. Both observation and PDF have shown that these conditions correspond to slug flow regime.

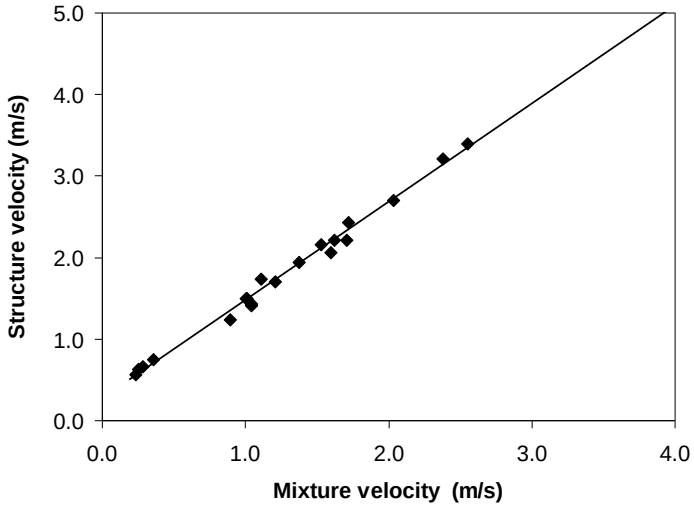

Figure 4.42 Structure velocities as a function of the mixture velocity, U_m, for the data corresponding to slug flow pattern.

The correlating line for the case of the graph has the relationship $Ub = 1.205\ U_m + 0.2439$ with a regression coefficient of 0.946.

In fact, the velocity of individual bubbles of gas, U_b, in the intermittent regime of gas-liquid flow has often been correlated as a linear function of the mixture velocity, U_m, the total volumetric flow divided by the cross section area.

$$U_b = C_0 U_m + U_d \tag{4.14}$$

Therefore in slug flow the expected linear dependence of the structure velocity on the mixture velocity has been found. However trends in other flow patterns are more complex and the data do not follow equation (4.14) but it is considered that the conditions when deviation occurs from this equation can provide a more objective method for identifying flow pattern boundaries.

For the case of wavy and churn flow the structure velocity decreases and increases again as a function of the mixture velocity. Another distinction can be made between the elongated bubbles that flow at low velocities and slug flow at high velocities. In fact Cook and Behnia (2001) have made a distinction between intermittent sub-regimes based on the behaviour of the properties of the flow.

In Figure 4.42, the non-zero intercept of the line with the *y* axis indicates that there is a drift velocity component of bubbles. For the horizontal case during two-phase flow this is a concept which might not be obvious. For example, Wallis (1969), Dukler and Hubbard (1975) as well as Bonnecaze *et al.* (1971) claimed that the drift velocity is zero for the horizontal case since the buoyancy force does not act in the flow direction. Nicholson *et al.* (1978), Bendiksen (1984), and others showed that a drift velocity exists also for the horizontal case and, in fact in the present work it has been found that it may even exceed its value in the vertical case. This behaviour was also found by Weber (1981).

In order to observe the changes in the drift velocity with the inclination angle, let us plot the drift velocity as a function of the pipe deviation angle, Figure 4.43. In this graph we can observe that the drift velocity increases as the pipe is inclined upwards from the horizontal position. The drift velocity the decreases again toward the vertical

position such that the maximum drift velocity occurs at an intermediate angle of inclination around 40° to 60° from the horizontal.

Bonnecaze *et al.* (1971) were the first to give a qualitative explanation for this particular behaviour, arguing that the gravitational potential that drives the liquid velocity along the curved surface at the bubble nose increases and then decreases as the angle of inclination changes from the vertical position towards the horizontal position.

For the inclined case there is no proposed model and one relies primarily on experimental data. The inclined case, as well as the vertical and the horizontal cases, were studied by Zukoski (1966), Singh and Griffith (1970), Bonnecaze *et al.* (1971), Bendiksen (1984), and Hasan and Kabir (1988). All report a particular behaviour that the drift velocity increases as the inclination angle is declined from the vertical position. The drift velocity the decreases again toward the horizontal position such that the maximum drift velocity occurs at an intermediate angle of inclination around 40° to 60° from the horizontal.

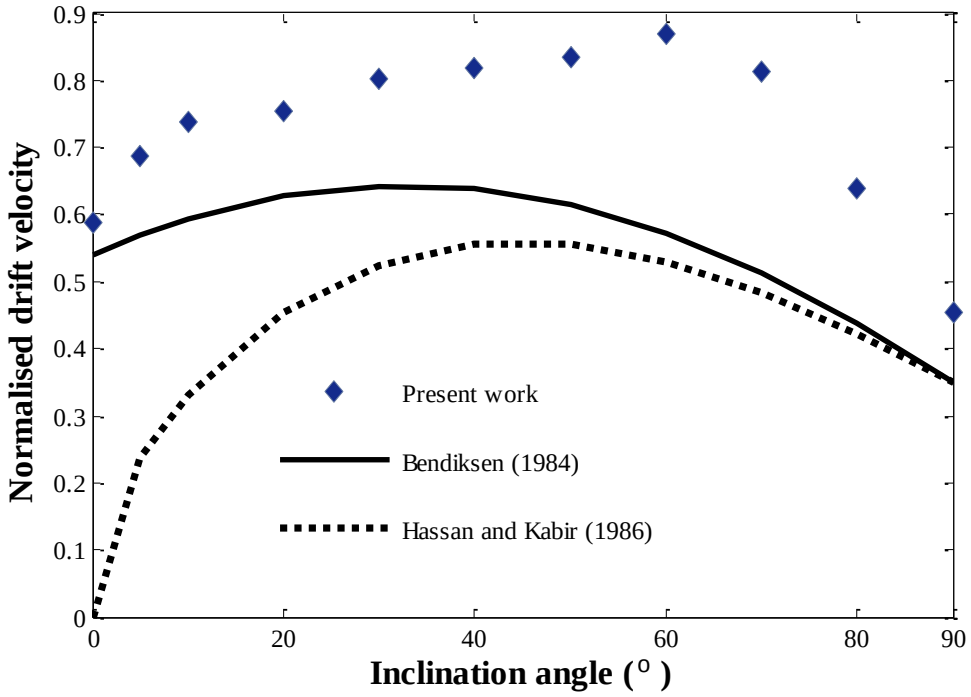

Figure 4.43 Normalized drift velocity, $U_d / \sqrt{gd}$, as a function of the inclination angle.

It can be observed that the drift velocities found are higher than the values predicted by Bendiksen (1984) and Hasan and Kabir (1988).This may be due to the different liquid velocity profile that exists in the aerated slug that was generally obtained for the conditions under investigation compared with the liquid velocity profile in the singe bubble flow. Due to the fact that drift velocity for continuous slug flow was obtained by extrapolation, the results obtained are higher than those predicted by theory for single Taylor bubble.

As can be seen, the Bendiksen (1984) correlation which is a weighted interpolation between the horizontal and vertical cases correlates better with the present data. Hasan and Kabir (1988) is valid only for data taken in sharply inclined flow and goes to zero, which means that assumes no drift velocity for horizontal flow.

The constant C_0 in equation (4.14) represents a contribution of the mixture velocity to the translational velocity of the elongated bubble. Nicklin *et al.* (1962), gave C_0 a value of 1.2 that comes from the fact that the ratio of the maximum to the average flow velocity in turbulent flow is equal to approximately 1.2 and based on the assumption that the propagation velocity of the bubbles is equal to the maximum local liquid velocity in front of the nose tip. Figure 4.44 shows that the constant C_0 is nearly constant at about 1.2 to 1.3, which is in agreement with values in literature for turbulent flow. In fact the Reynolds number for most of the experiments performed was higher than 3000.

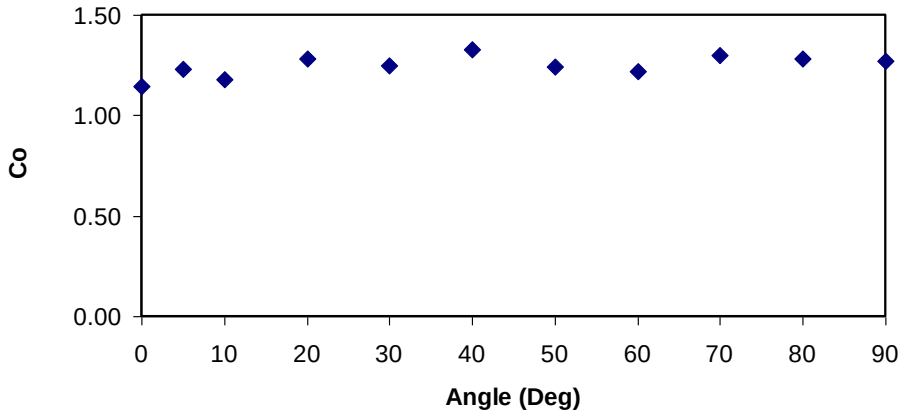

Figure 4.44 The constant C_0 as a function of the inclination angle.

Hasan and Kabir (1988) proposed the relationship (2.59), which they claim to correlate well experimental data in the range 90°>θ>30° however, it has been observed that this model under-predicts the drift velocity for the whole range of pipe inclinations, specially for inclinations near the horizontal, this can be expected immediately since the equation only considers the vertical drift velocity. Structure velocity and frequency are parameters directly proportional, with the proportionality factor being the structure length. Figure 4.45 shows this proportionality factor is not constant. Further discussion for slug length will be presented in the following section.

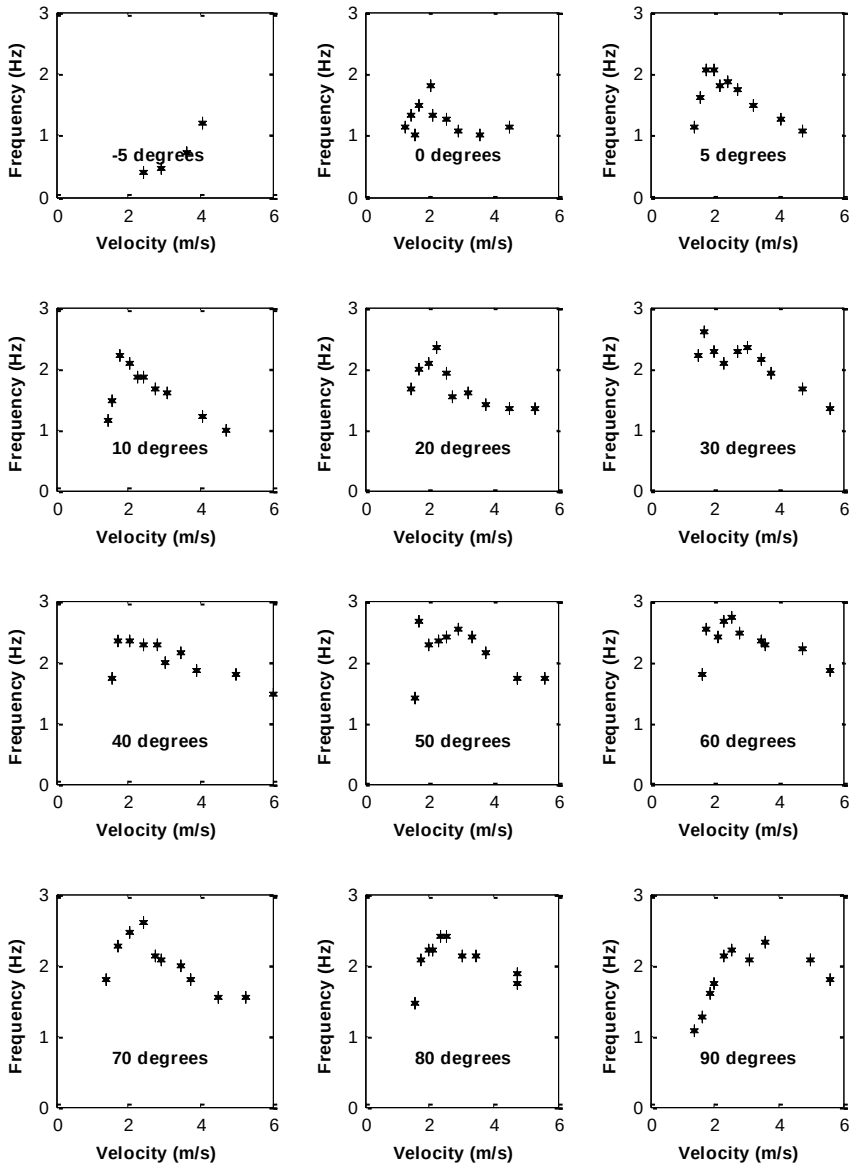

Figure 4.45 Structure velocity vs frequency for U_{SL}=0.73 m/s and different inclination angles**.**

4.8 Estimation of slug flow characteristics from PDF

Having identified and plotted the main parameters we move to analyse the flow behaviour in more detail. The dominant flow pattern that is of great interest to this research is the slug flow. It is the purpose of this section to provide information about slug characteristics. In most cases, a successful recognition of slug flow has been obtained by monitoring the liquid phase fraction in the pipe with the capacitance probe and plotting the PDF. Whenever the shape of the PDF presents a double peak, then slug flow has been identified.

The values of holdup at which the maxima in a PDF occur correspond to the most probable values of liquid film (bubble) and slug holdup in the slug flow regime. If $p_b(H)$ and $p_s(H)$ are these two maxima in the PDF respectively, then

$$H\big|_{pb(H)} = H_b \tag{4.15}$$

And

$$H\big|_{ps(H)} = H_s \tag{4.16}$$

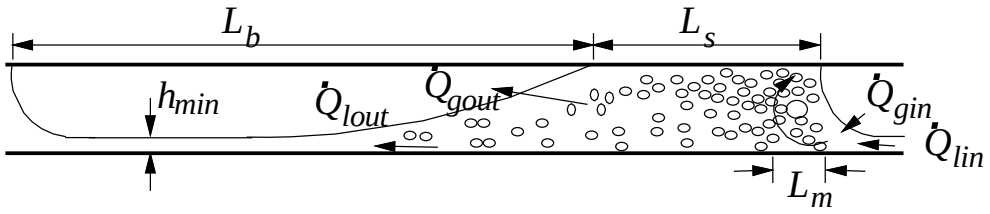

Figure 4.46 Slug unit diagram that shows the slug flow parameters.

The ratio of the liquid residence time (t_S) to the gas bubble residence (t_b) time may be approximated by

$$\frac{t_S}{t_b} = \frac{p_S(H_S)}{p_b(H_b)} \tag{4.17}$$

The above expression is exact in the ideal case where the system noise is constant and the liquid holdup is either exactly α_s or α_b for the duration of the holdup trace.

Also, if the gas bubble is assumed to move with the same translational velocity as the liquid slug, it follows from previous equation that the ratio of the average liquid slug length to the average gas bubble length is

$$\frac{L_S}{L_b} = \frac{p_S(H_S)}{p_b(H_b)} \tag{4.18}$$

Based on the equations (4.15) to (4.19), in this section, the parameters of slug flow determined experimentally from the PDF include:

- Slug void fraction.
- Liquid film holdup
- Slug length.

4.8.1 Liquid holdup in the slug body

It has been shown in Figure 4.38 that for inclined and vertical flows hydrostatic pressure drop is quite significant. Since it is a function of the liquid holdup in the slug body, evaluation of slug void fraction is important. Slug holdup is considered one of the primary variables in slug flow modelling, as the solution of the averaged momentum and balance equations requires an independent method to predict the liquid holdup averaged over the volume of the slug, R_S. The characteristic lengths, pressure drops and velocities to be computed thus are functions of the average voids.

Figure 4.47 presents the results for liquid holdup in the liquid slug body for different inclination angles. It appears to decrease with the gas superficial velocity and slightly with pipe inclination.

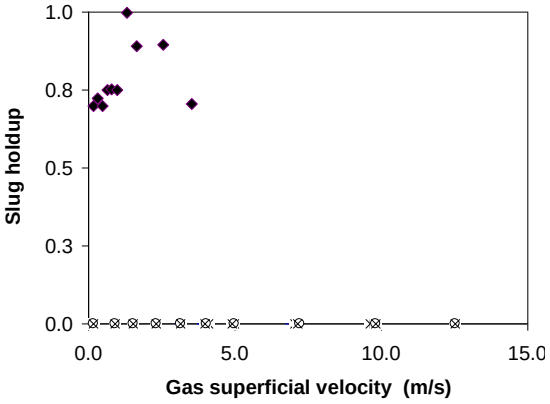

-5 ° Inclination

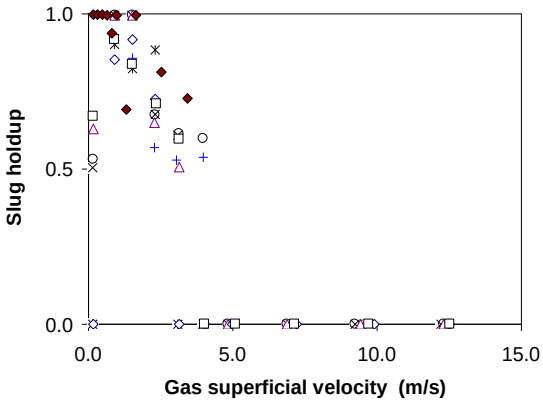

0 ° Inclination

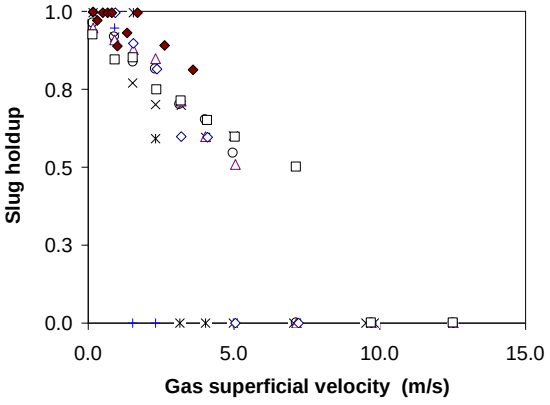

5° Inclination

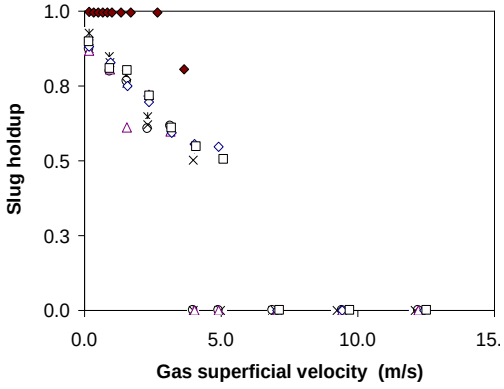

10 ° Inclination

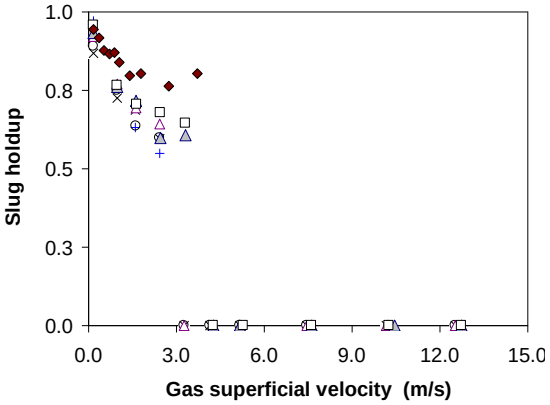

30° Inclination

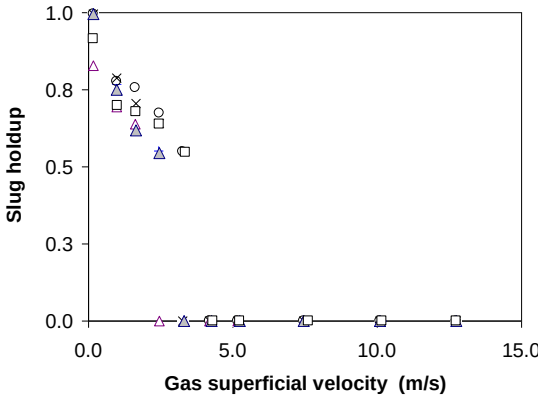

45 ° Inclination

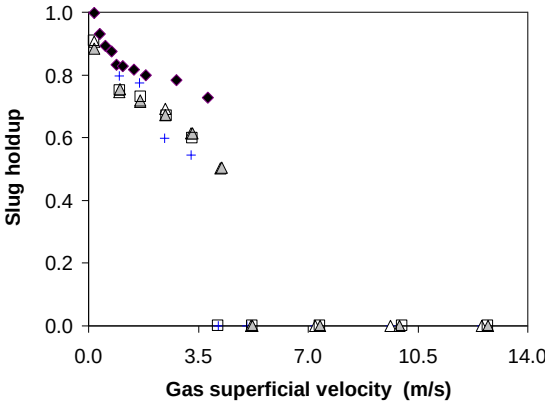

50° Inclination

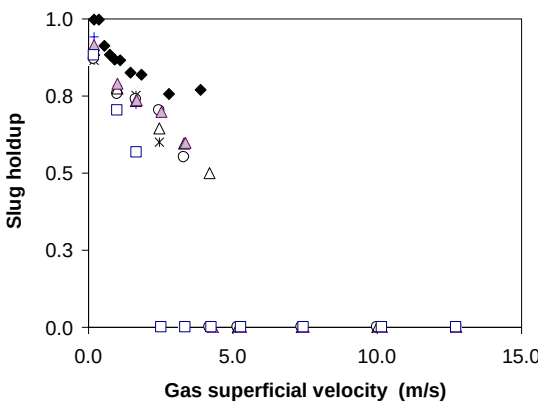

60 ° Inclination

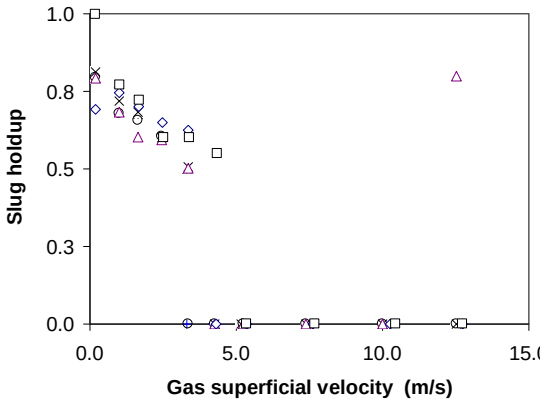

75 ° Inclination

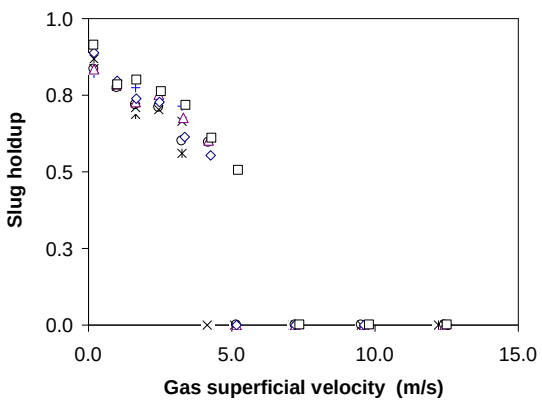

85 ° Inclination

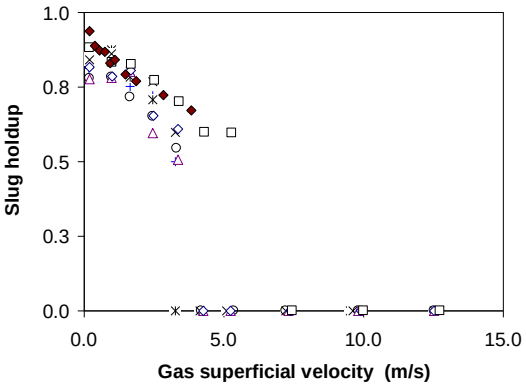

90° Inclination

Figure 4.47 Void fraction in the slug for different inclination angles

In Figure 4.48 a comparison is presented for slug void fraction between the data of the present work and some data of Nydal (1991). The conditions are not exactly the same however the most similar conditions were chosen to compare. It can be observed that the agreement is good.

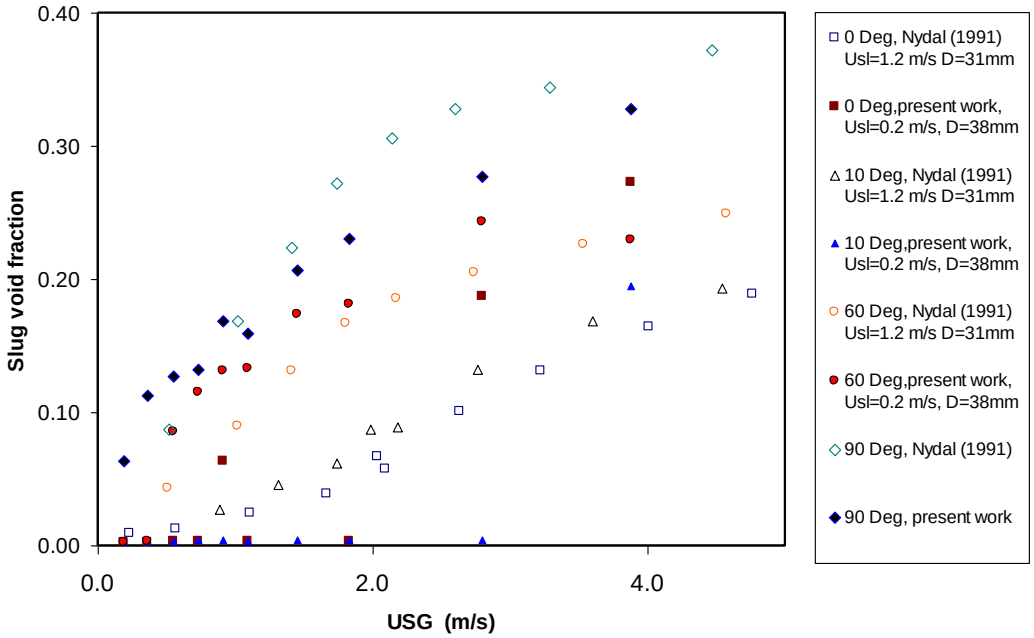

Figure 4.48 Comparison of void fraction in the slug data.

A number of models for void fraction within the slug body are presented in the literature review of Chapter 2 (Gregory *et al.* (1978), Malnes (1983), Ferschneider (1982), Marcano et al. (1996)), Nydal (1991) and have been compared with the current data set in this section. However, there appears to be no universal model for void fraction in slugs in the literature. Most of them are correlations based on curve fit of average void fraction experimental data, and the applicability to other flow conditions might questionable.

In Figure 4.49 a comparison is presented for slug void fraction between the data of the present work and the models found in literature. It is observed that the Gregory et al correlation gives the closest agreement.

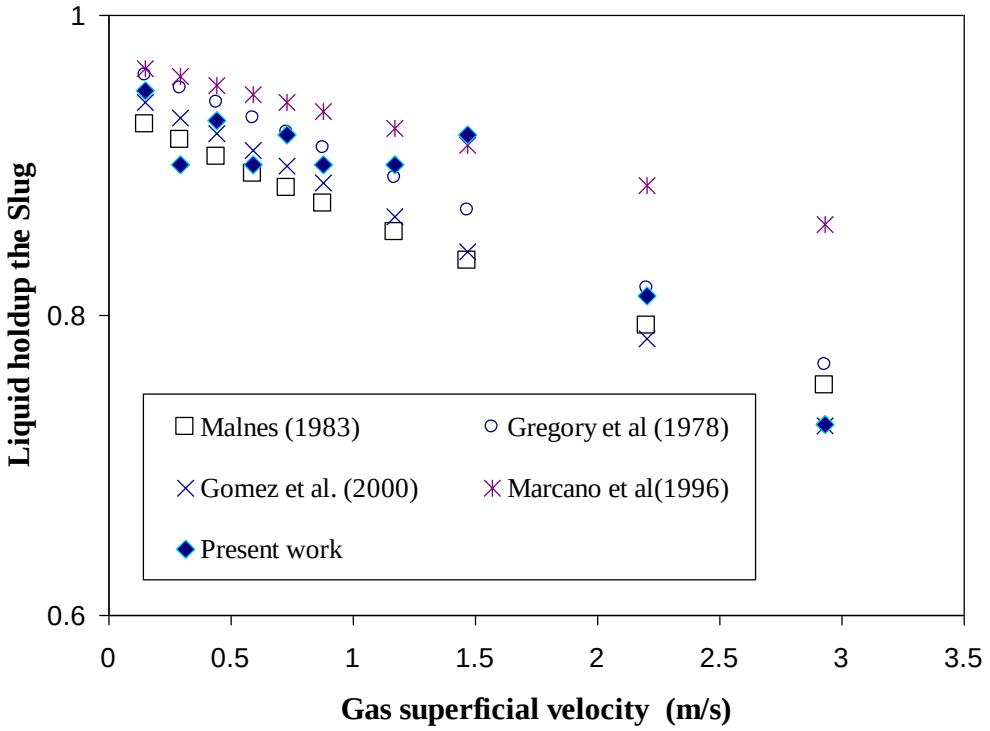

Figure 4.49 Comparison of correlations for liquid holdup in the slug. Horizontal flow and liquid superficial velocity of 0.7 m/s.

Regarding the holdup in the liquid film part, an interesting observation is made when we focus on the dependence of the liquid holdup in the slug body with respect to the holdup in the liquid film. This dependence is plotted in Figure 4.50. In general it can be observed that for high values of holdup in the slug body, there exists a high holdup in the bubble section as well since low values of holdup in the liquid film with high values of holdup in the slug would provoke that the liquid slug transfer liquid to the film and therefore slug disapear.

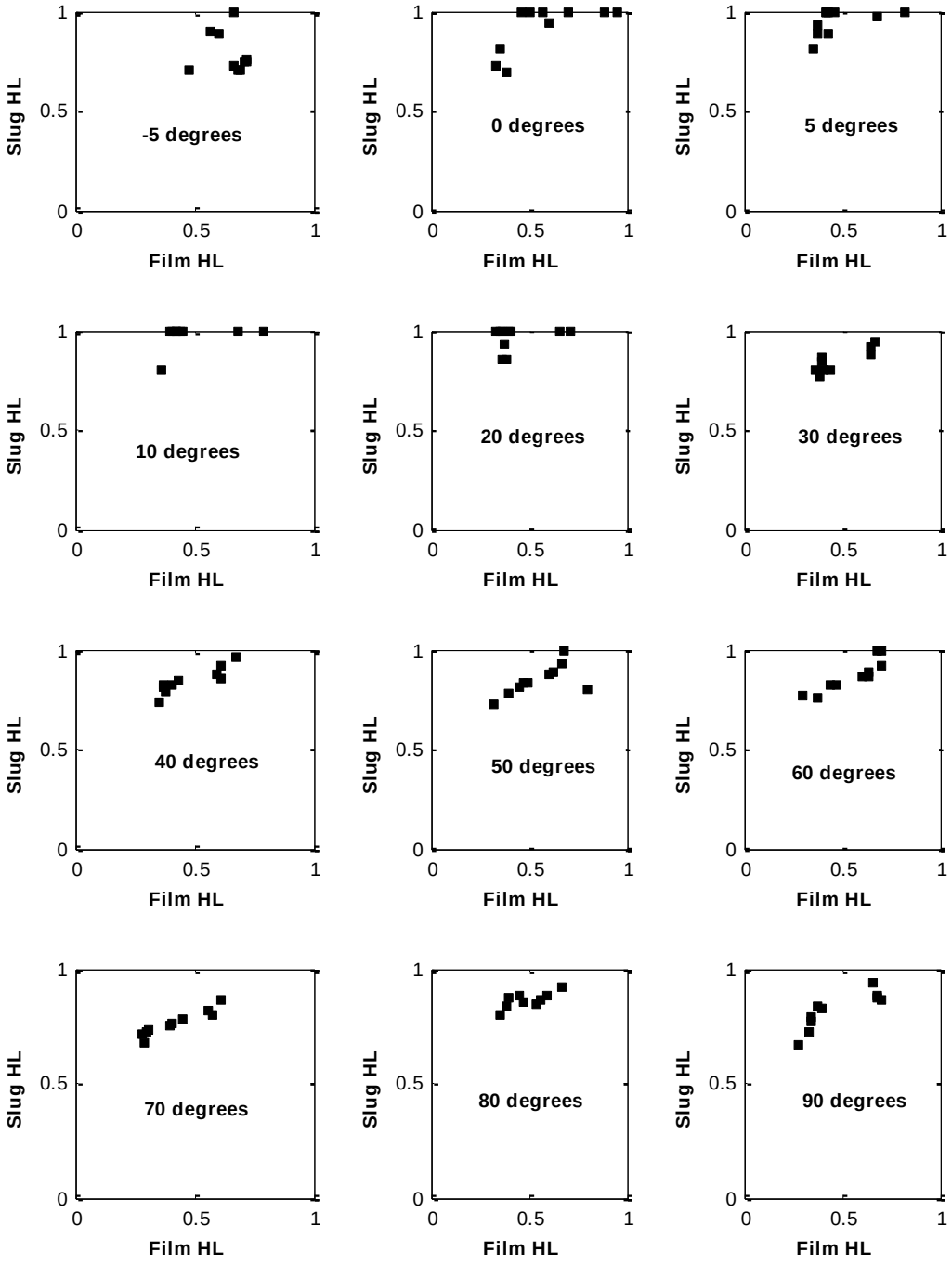

Figure 4.50 Liquid holdup in the slug compared with the liquid holdup in the liquid film for U_{SL}=0.7 m/s.

4.8.2 Slug length

Another primary variable in slug flow modelling is the slug length, L_S. Frequency and slug length are two quantities that are strongly interrelated. First in Figure 4.51, we present the behaviour of the ratio ls/lf as a function of the gas superficial velocity for

different angles of inclination, calculated from equation (4.21). It is observed that ls/lf decreases as it is expected. It seems to tend to zero as U_{SG} gets bigger.

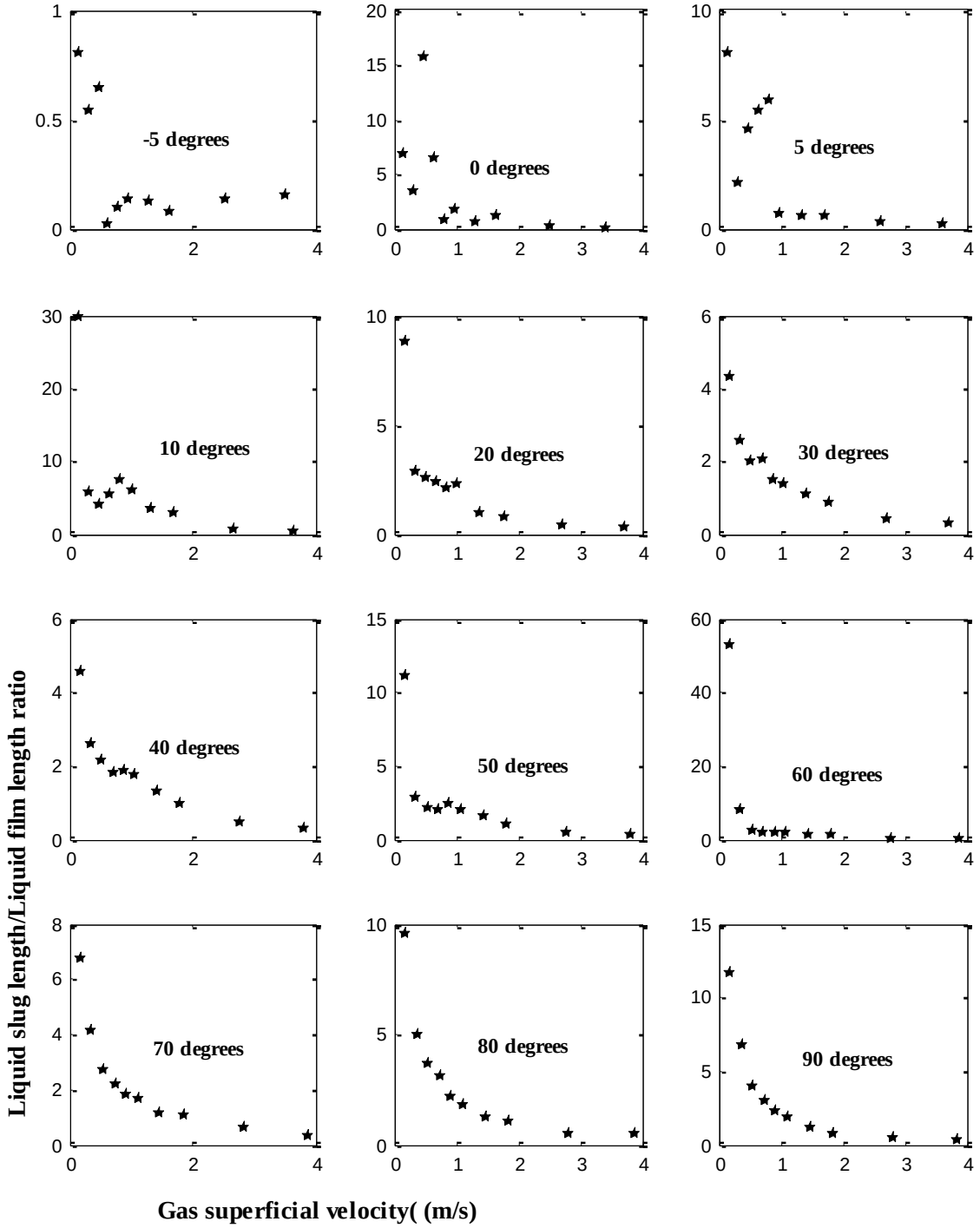

Figure 4.51 ls/lf ratio as a function of the gas superficial velocity for different inclination angles. U_{SL}=0.73 m/s.

The slug unit length, which is in turn the sum of slug and film lengths

$$L_u = L_s + L_b \tag{4.19}$$

is determined by multiplying the residence time of the slug unit in the distance between the capacitance probes by the structure velocity. The length of a slug unit is

$$L_u = \frac{U_b}{f_s} \tag{4.20}$$

In Figure 4.52 it can be observed that the length of the slug unit in general increase with the gas superficial velocity. For convenience, a dimensionless length is introduced, which is defined as the ratio of liquid slug length over test pipe diameter. And it appears to be shorter when pipe inclination is increased.

By combining the values obtained with equation (4.19) and (4.20), the slug and bubble lengths are can be determined as well. They are given by:

$$L_f = \frac{L_u}{L_s / L_f + 1} \tag{4.21}$$

$$L_s = L_u - L_f \tag{4.22}$$

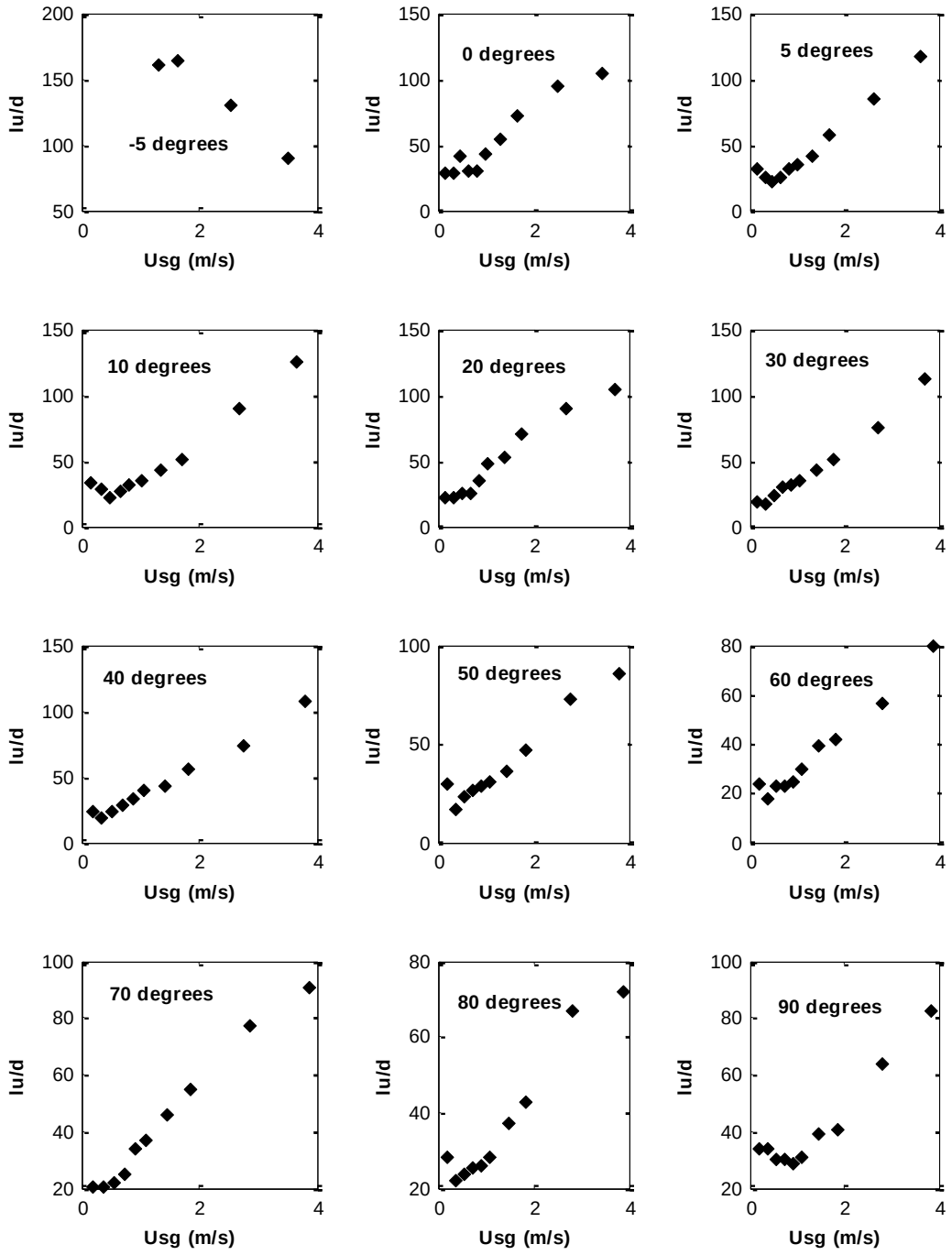

Figure 4.52 Slug unit length as a function of the gas superficial velocity for U_{SL}=0.7 m/s and different inclination angles.

The dimensionless liquid slug length exhibits an unclear function of the slug unit length and other variables, however average liquid slug lengths were in the order of 10 to 30 pipe diameters, and relatively independent of flow conditions.

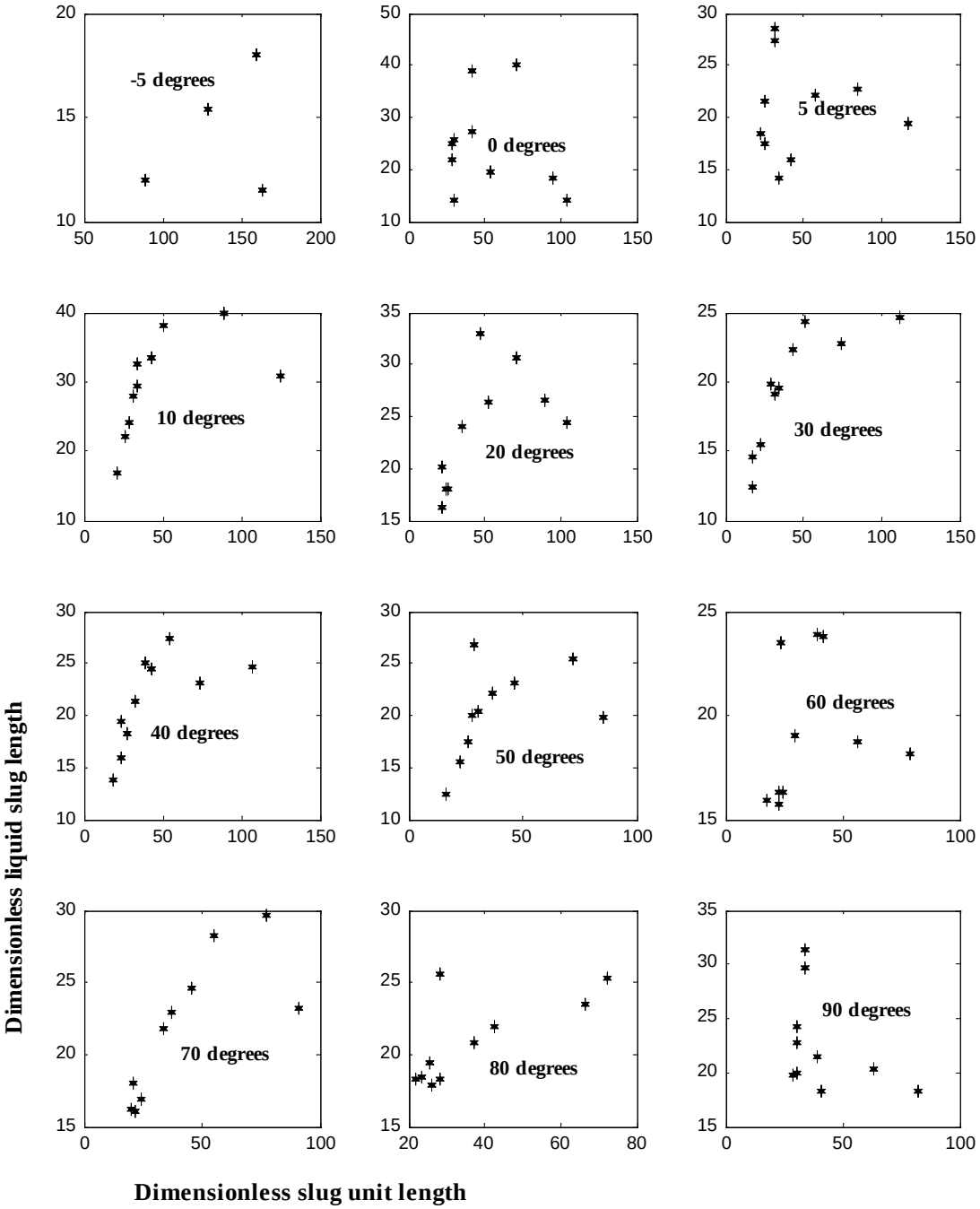

Figure 4.53 Slug length as a function of the total slug unit length for U_{SL}=0.73 m/s and different inclination angles.

On the other hand, the liquid film length follows a nearly linear relationship with the total slug unit length, which means that the liquid film is the main component of the

slug unit since they appear to have nearly the same length specially for small pipe inclinations where it becomes bigger.

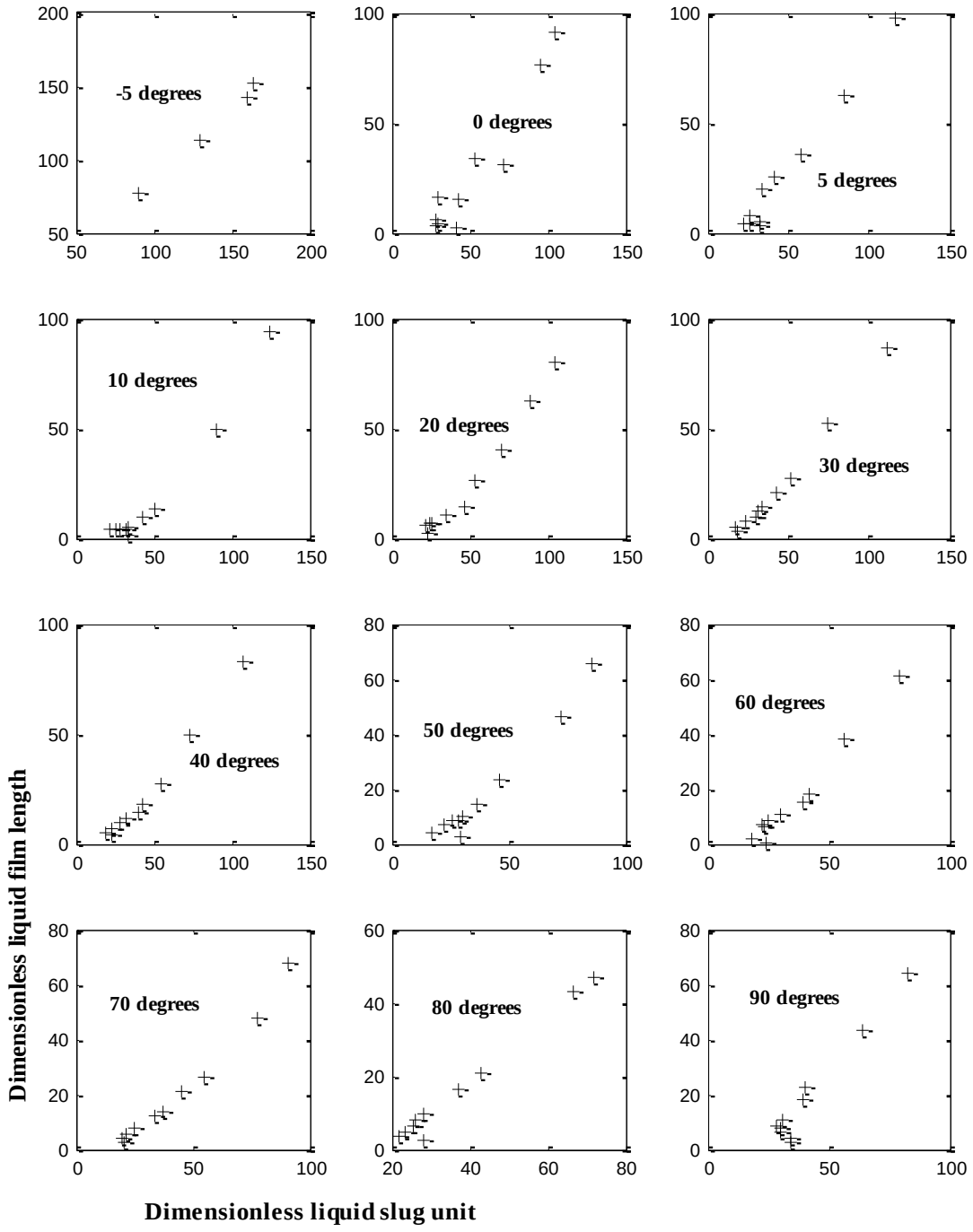

Figure 4.54 Liquid film length as a function of the total slug unit length for U_{SL}=0.73 m/s and different inclination angles**.**

From Figure 4.55, it can be observed that in general the slug length tends to decrease as the frequency increases.

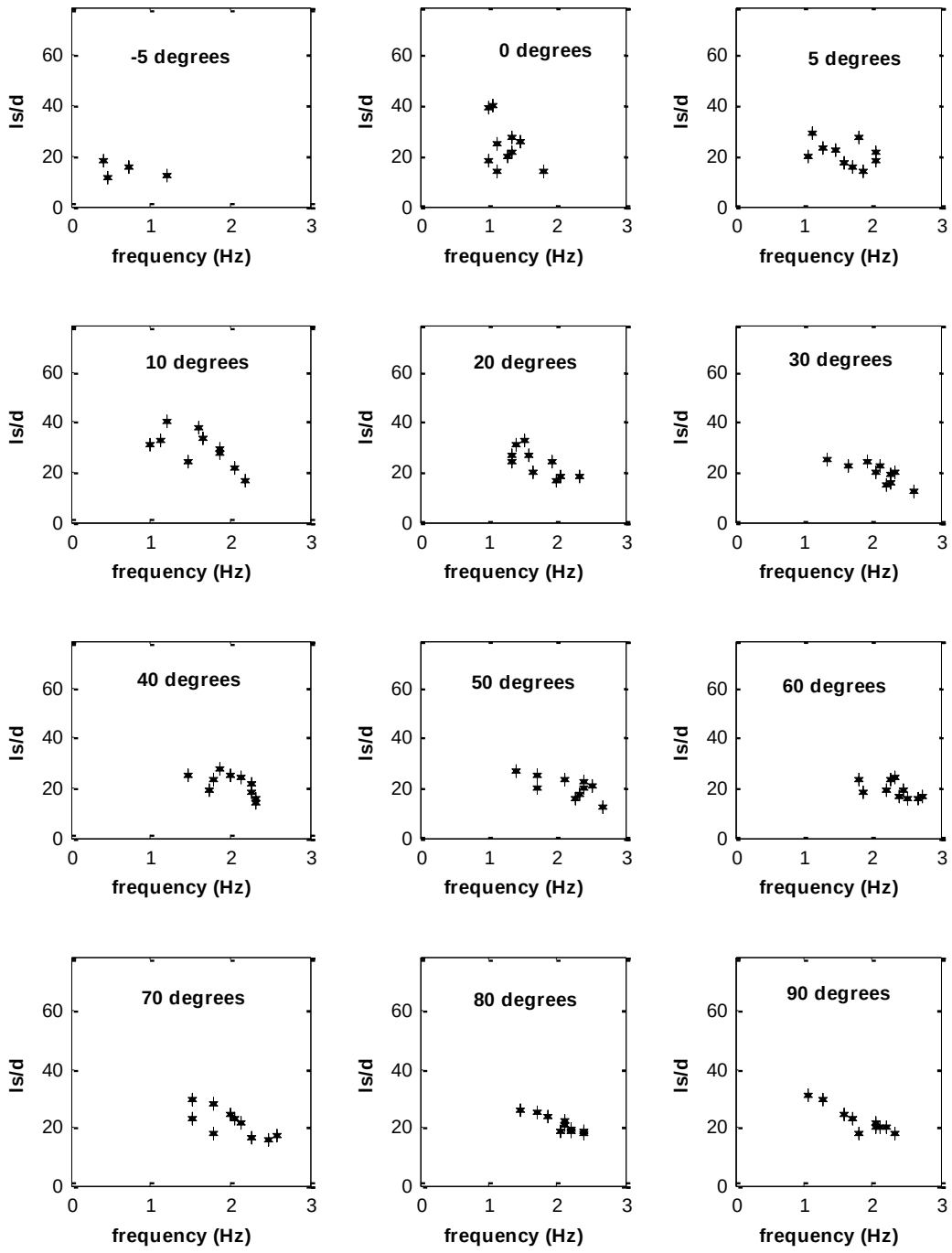

Figure 4.55 Liquid slug length as a function of the frequency for U_{SL}=0.73 m/s and different inclination angles.

4.9 Effect of Liquid flow rate

In the first campaign of experiments, high aerated slugs and churn flow were observed due to the low liquid flow rate used. It was then motivating to see what changes in the flow regime and flow parameters could be observed by increasing the liquid flow rate. The liquid flow rate was increased by using a bigger pump, that could deliver 50 l/min for this system, which in turn gives a liquid superficial velocity of 0.73 m/s, and another set of experiments was performed. In Figure 4.56, a typical example of the effect of liquid flow rate is illustrated by means of the time series, PDF and PSD.

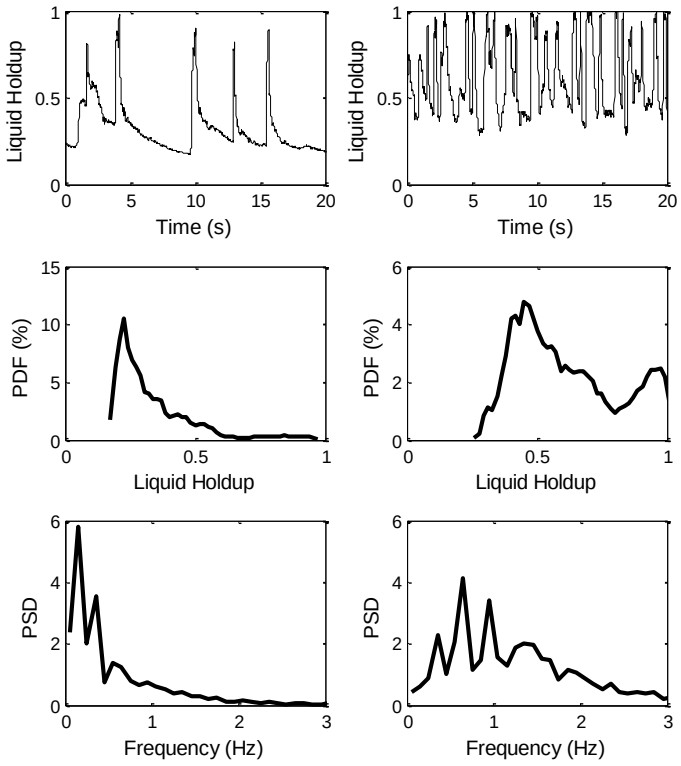

Figure 4.56 Effect of increasing the liquid flow rate at U_{SG}=2.9 m/s in horizontal. Column the left corresponds to U_{SL}=0.2 m/s. Column on the right corresponds to U_{SL}=0.7m/s.

What can be observed in Figure 4.56 is that the flow pattern changes from waves to slug flow, the liquid holdup and frequency were significantly increased for some cases like in this example; this can be seen directly from the comparison of the two cases in terms of the time series and also from the PDF and PSDs graphs.

Dukler and Hubbard (1975) have shown that the length of a stable liquid slug is only a function of the pipe diameter and is generally in the range of 12 to 30 pipe diameters, which is in agreement with the present work. Therefore, based on this assumption, the addition of extra liquid, by increasing the liquid superficial velocity, cannot be transferred into the slug body because of this known finite length. Also, the gas-pocket region and the associated stratified liquid layer must remain constant at the equilibrium level, otherwise decay or formation of slugs would happen. Thus, in order to accommodate this new material slugs are formed more frequently. This has the effect of increasing the overall liquid holdup in the pipe as well as the pressure drop.

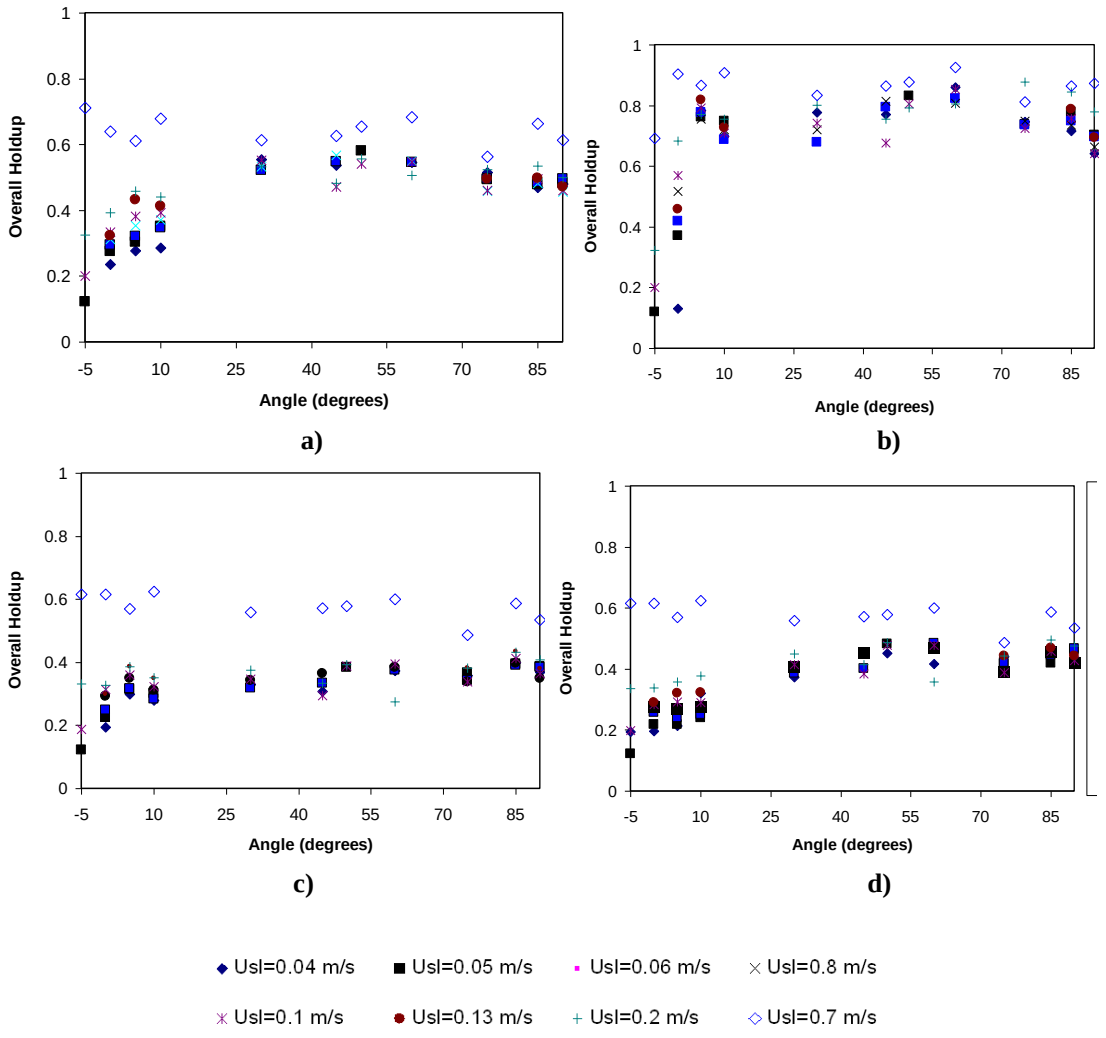

Figure 4.57 Liquid holdup as a function of the inclination angle. a)U_{SG}=0.15 m/s, b) U_{SG}=0.9 m/s, c) U_{SG}=1.5 m/s, d) U_{SG}=2.9 m/s.

For steep inclinations, the liquid holdup does not change as much as for low inclination angles. However, as mentioned before, the frequency is significantly affected by the change in the liquid flow rate. In Figure 4.58, values of frequency are plotted as function of the pipe inclination angle, the biggest increase is found for the case of Usg= 0.9 m/s, it can also be seen that frequency reaches its maximum value at a pipe inclination angle of about 60° .

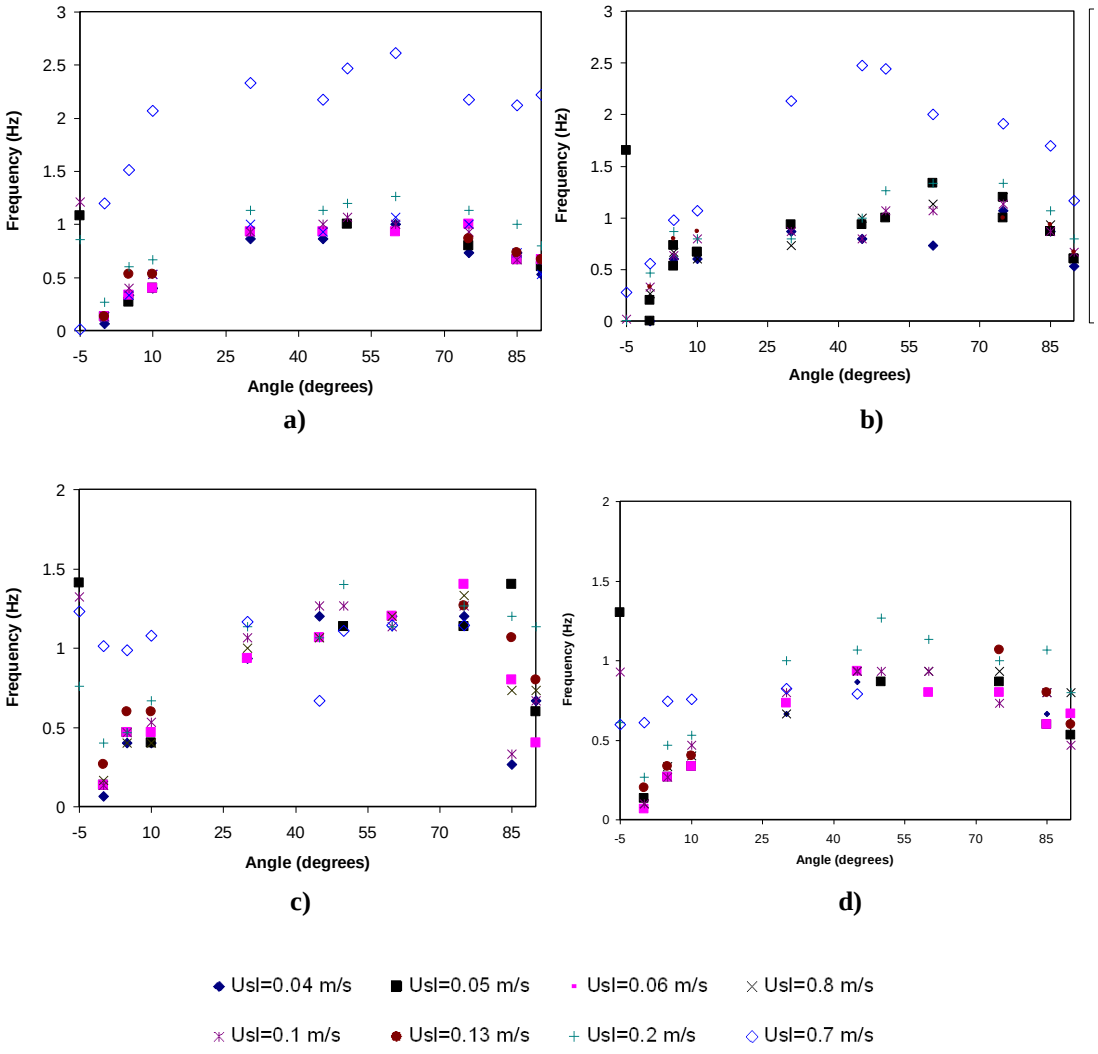

Figure 4.58 Frequency as a function of the inclination angle. a)U_{SG}=0.15 m/s, b) U_{SG}=0.9 m/s, c) U_{SG}=1.5 m/s, d) U_{SG}=2.9 m/s.

Regarding the pressure drop, the data are plotted in the Figure 4.59 below. These results indicate that the pressure drop is proportional to the liquid holup as it has been stated previously (section 4.6). The biggest effect of increasing the liquid flow rate is

observed at higher values of gas superficial velocity and so does it happen for the liquid holdup plotted in Figure 4.57 above.

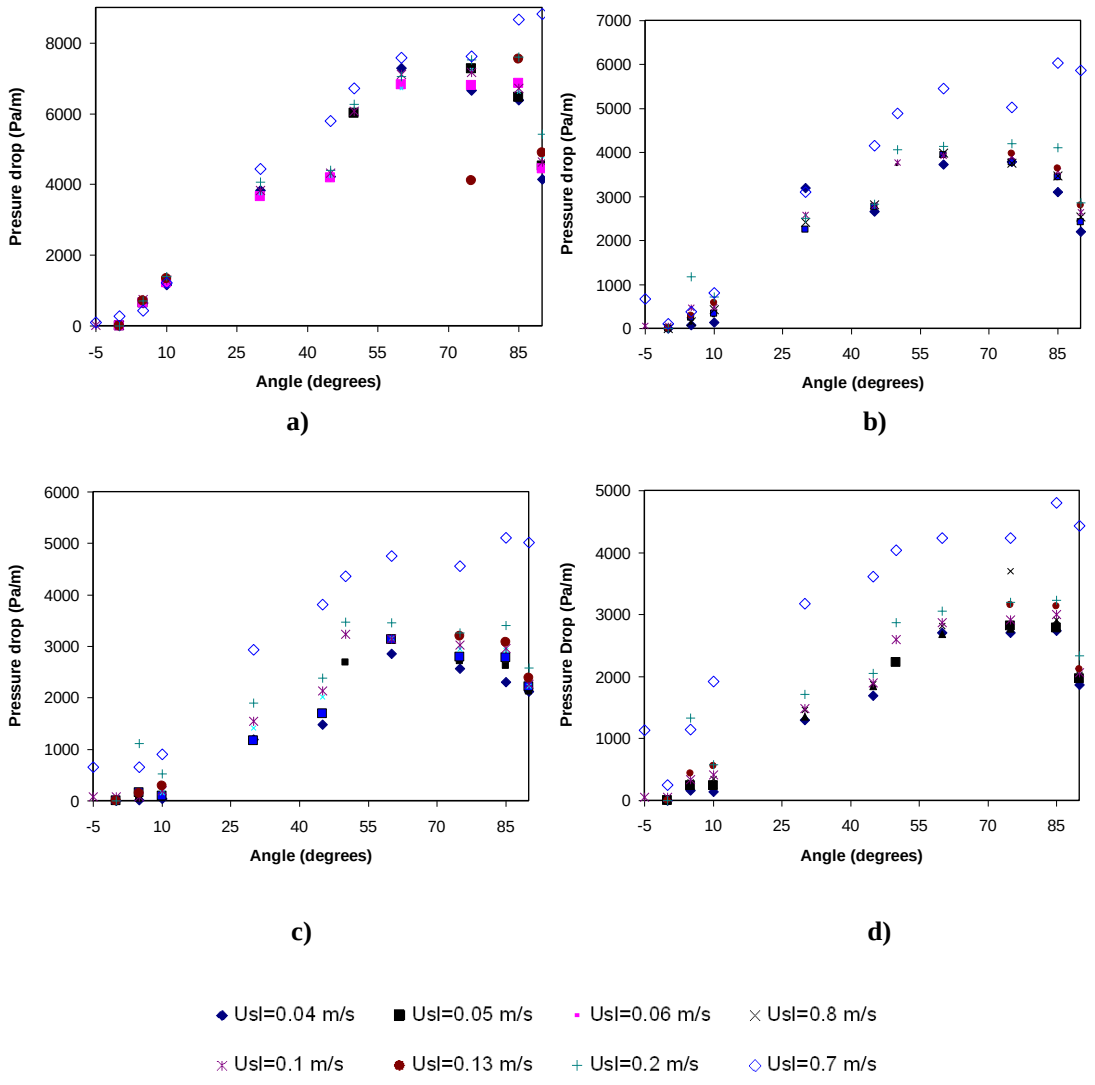

Figure 4.59 Pressure drop a function of the inclination angle. a)U_{SG}=0.15 m/s, b) U_{SG}=0.9 m/s, c) U_{SG}=1.5 m/s, d) U_{SG}=2.9 m/s.

It is worth noting that the slugs travel faster than the waves as can be seen in the Figure 4.60 where the time it takes for the slugs to travel from one probe to the other is shorter than for the waves.

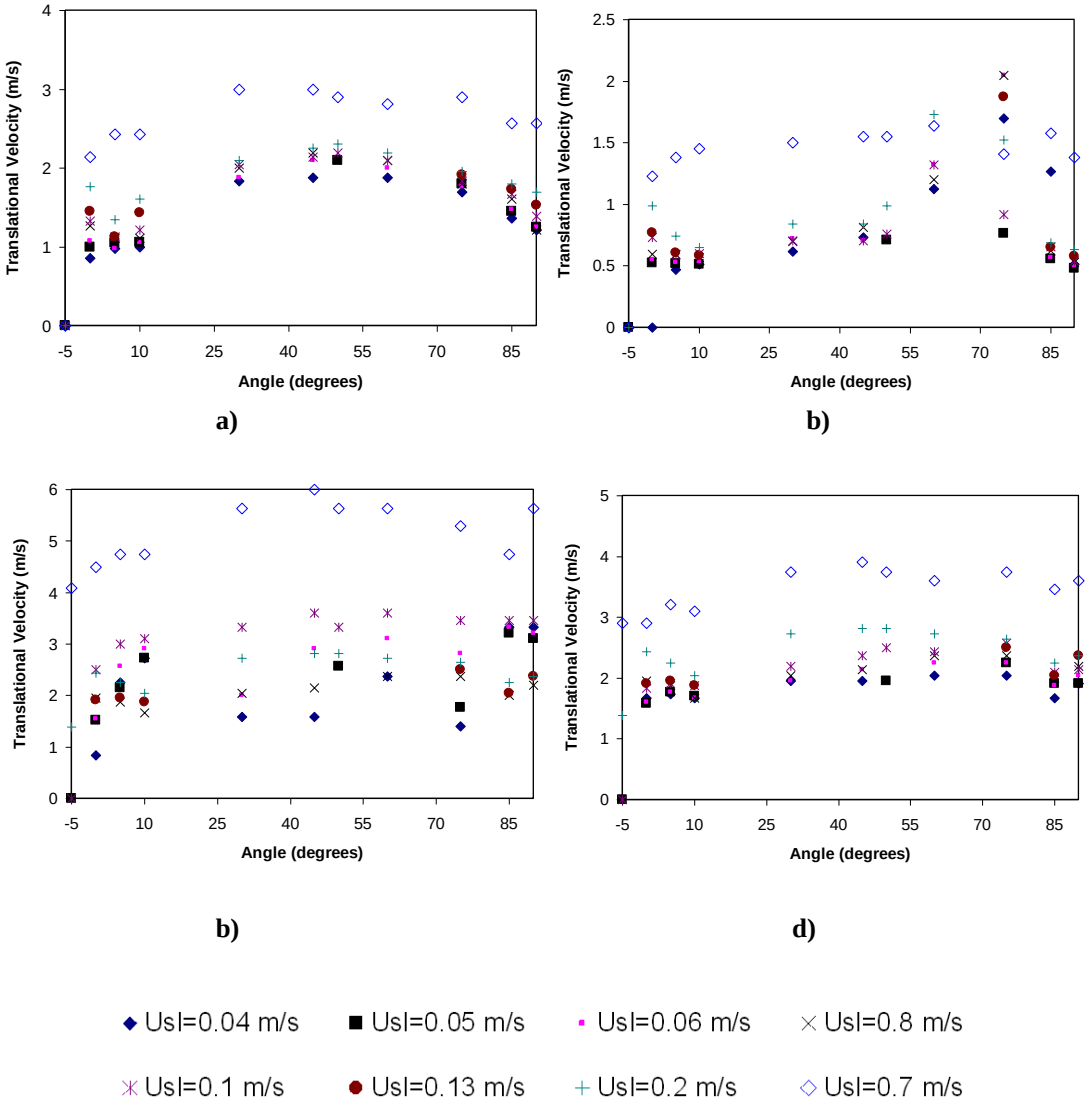

Figure 4.60 Structure velocity as a function of the inclination angle. a)U_{SG}=0.15 m/s, b) U_{SG}=0.9 m/s, c) U_{SG}=1.5 m/s, d) U_{SG}=2.9 m/s.

4.10 Flow development between the two probes

In this section we will take a look at the flow development from one probe to another. First a comparison of the average values of liquid holdup are plotted for both probes and then the PDF are presented for a typical pair of signals. It can be seen that both probes provide a fairly similar average liquid holdup; this is a good indication of the development of the flow.

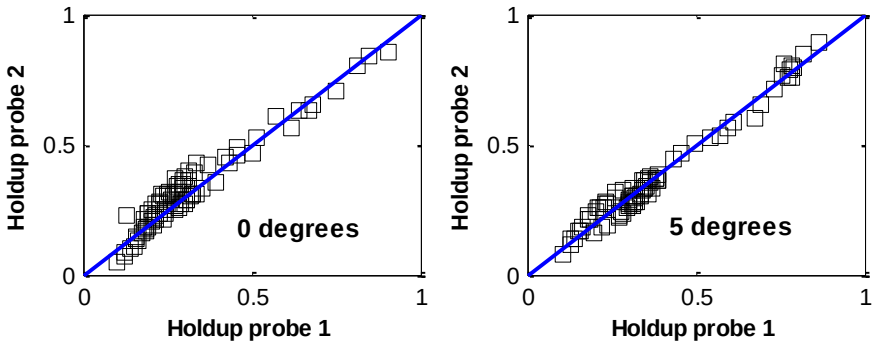

Figure 4.61 Comparison of the average liquid holdup between the two capacitance probes**.**

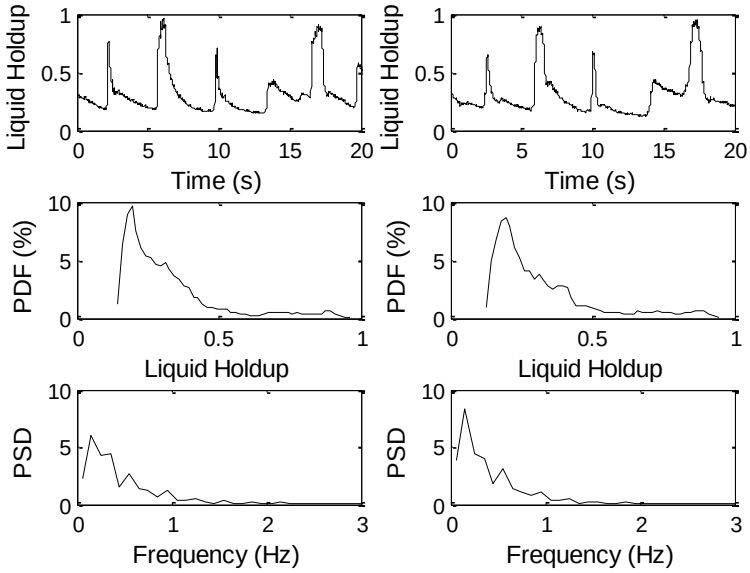

Probe 1 **Probe 2**

Figure 4.62 Typical comparison of the time series, PDF and PSD for liquid holdup between the two capacitance probes.

4.11 Summary

In this chapter experimental data obtained with a 38 mm diamer pipe have been presented. In these experiments the inclination angle has been varied for a wide range of flow conditions. In the first stage, visualisation of the flow patterns was carried out and flow patterns were identified on the flow pattern map. The experimental data include liquid holdup, frequency, pressure drop, structure velocity, estimation of characteristic parameters of slug flow from the PDF plot and finally the effect of

increasing the liquid flow rate was studied. In this section a summary of the key findings will be made.

- It has been shown that intermittent flow exists as the dominant flow pattern in upward inclined flow.

- For a constant liquid superficial velocity, the average liquid holdup decreases when the gas velocity is increased. For downwards, stratified flow is the main flow pattern observed and the liquid holdup becomes independent of the gas superficial velocity over the range of gas flow rate employed, as the phases flow with little interaction, but holdup is a function of the liquid flow rate.

- In uphill flow, the pipe inclination has just a slight effect on the liquid holdup. The liquid holdup increased slightly for the higher inclination angles.

- Unlike the liquid hold up, the frequency is strongly affected by the inclination angle. At low gas superficial velocities, the frequency depends on the inclination angle in such a way that it tends to have a maximum at about 50 degrees. For high mixture velocities, the more deviated from horizontal, the higher the frequency.

- In slug flow the expected linear dependence of the structure velocity on the mixture velocity has been found.

- The liquid holdup in the liquid slug body appears to decrease with the gas superficial velocity and slightly with pipe inclination.

- Average slug lengths were in the order of 10 to 30 pipe diameters, and relatively independent of flow conditions. The slug length tends to decrease as the frequency increases and also with the inclination angle.

- The frequency is significantly affected by the change in the liquid flow rate.

Chapter 5

Gas-Liquid Flow in 67 mm Pipe

Experimental data obtained in a 38 mm pipe were presented in Chapter 4 as well as in Hernández-Pérez and Azzopardi (2006), covering a wide range of flow rates and inclination angles. However it is a well known fact that two-phase mixtures may exist in a variety of sizes of pipe work throughout a wide range of industrial applications, such as in chemical, power, oil/gas production and oil refining plants. As reported by several authors, including Singh and Griffith (1970), Andreussi and Bendiksen (1989), Jepson and Taylor (1993), Shemer *et al.* (2004) and more recently Kaji *et al.* (2007), among others, different pipe diameters might have different effect on the flow behaviour, since flow instabilities resulting from pressure and/or temperature fluctuations may cause the mixture to arrange itself into different and unpredictable flow regimes. It is therefore important to study the flow behaviour in more than one pipe diameter.

In this chapter the effect of pipe diameter on inclined gas-liquid flow is studied by using the data of the measurements carried out in a 67 mm pipe along with 38 mm pipe data. Additional data from other references have been used where appropriate to compare, clarify and expand the knowledge of the complex behaviour of the flow. The experimental arrangement was described in Chapter 3 and the experiments were performed at ambient conditions of pressure and temperature in an analogous way as those presented in Chapter 4, similar processing for the data was performed as well.

Therefore, this chapter will focus on discussing the most relevant results that were found, mostly in the form of a comparison with respect to 38 mm results of Chapter 4 so that the effect of pipe diameter can also be observed. The following aspects of the flow behaviour will be covered: liquid holdup, pressure drop, structure velocity, frequency, flow pattern map, estimation of characteristic parameters of slug flow from the PDF plot (holdup in the liquid slug body and slug length), since it remains unclear how these parameters are affected by the pipe diameter and finally a summary will be drawn. A total of 160 experiments were carried out for several inclination angles within the range of -5° to 90° (with respect to the horizontal) and most of them with the same inlet flow conditions as those in 38 mm pipe. The full test matrix is given in appendix A.

5.1 Liquid holdup

Liquid holdup is a critical unknown parameter involved in predicting pressure loss and heat transfer in a multiphase system. In this section, the effect of the pipe diameter on the liquid holdup is analysed. In doing so we compare the liquid holdup obtained with both pipe diameters, namely 38 mm and 67 mm. In addition the correlations of Beggs and Brill (1973), Mattar and Gregory (1974) and Hasan and Kabir (1988) are plotted along with the experimental data. The main feature of these correlations is that they aim to deal with inclined flow. The liquid holdup is directly obtained as raw data with the capacitance probes in the form of time series. A direct visual comparison between the time series of the 38mm and 67 mm pipes (Figure 5.1) presumes that they are quite similar. However, time series analysis used in the following sections reveals that differences in the respective parameters might exist.

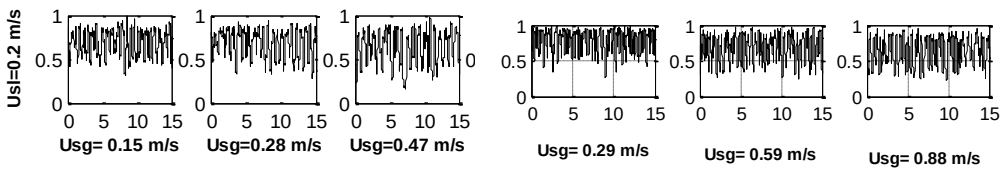

Figure 5.1 Effect of pipe diameter on time series obtained from the liquid holdup. 90° inclination; x-axis, time (s); y-axis, Liquid holdup

Analysis of the data from the time series, involving the average holdup, Probability density function, and Power Spectral Density (PSD), is performed and comparisons are made. A typical example of these comparisons is shown in Figure 5.2. For this case, a fraction of the time series has been plotted. The average liquid holdup is fairly similar, the liquid slug looks more aerated for the bigger pipe diameter and the fluctuation amplitude is wider for the smaller pipe diameter. The reason for that difference could be that for this case, slug flow is obtained for 38 mm pipe but not for 67 mm, which can be deduced from the PDF plot shown in the same figure.

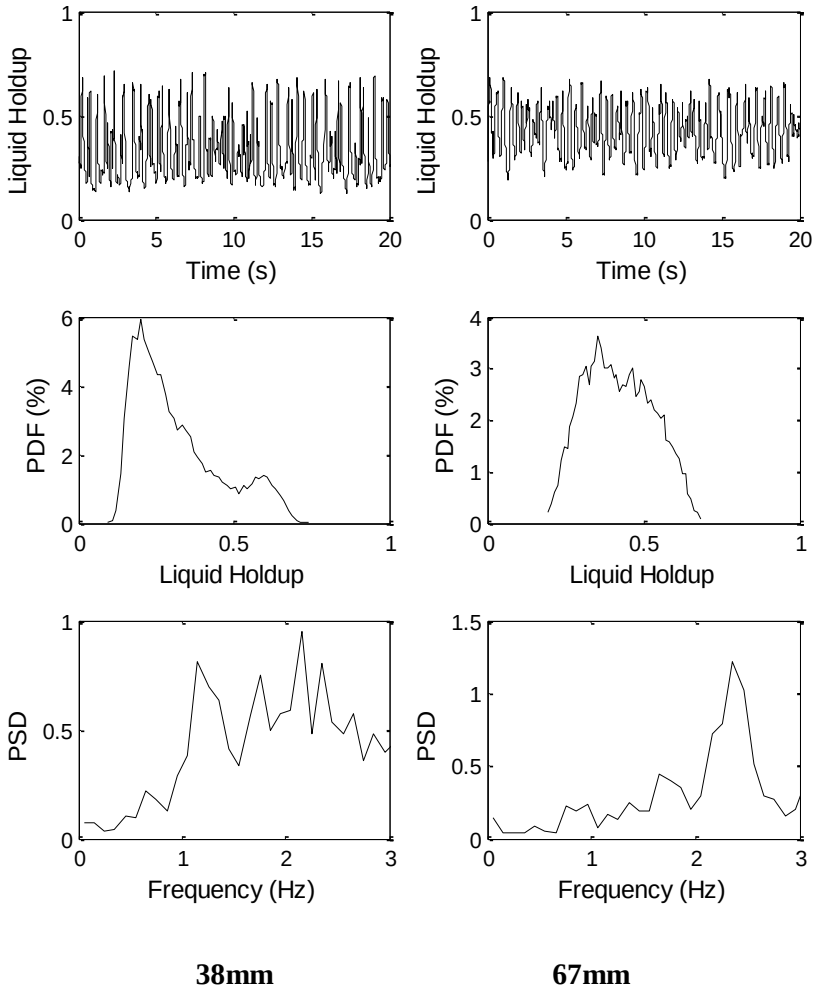

Figure 5.2 Effect of pipe diameter on time series, Probability Density Function and Power Spectral Density obtained from the liquid holdup for 90° inclination and superficial velocities (m/s): liquid=0.7 m/s and gas=2.9 m/s

The holdup average values for different inclination angles and gas superficial velocities are plotted below in Figures 5.3 and 5.4. For the U_{SL}=0.2 m/s, no effect of the pipe diameter is identified over the range of gas flow rate employed. This happens for all inclination angles shown in this figure.

A comparison with the correlation of Beggs and Brill (1973) using both pipe diameters shows that in general it under predicts the data and also it suggests that the effect of pipe diameter is from minimal to non existent, in spite of the fact that their holdup correlation is based on the Froude number ($Fr_m=U_m^2/gd$) and they have used 38 mm pipe in their study. The two curves obtained with this correlation corresponding to 38 mm and 67 mm overlap and they are indistinguishable from each other in both Figure 5.3 and Figure 5.4.

On the other hand, Mattar and Gregory (1974) did not consider the pipe diameter at all in their model for liquid holdup, although it is originally developed for low inclination angles from the horizontal, this is a very simple model that gives good predictions for a wide range of inclinations as can be observed in Figures 5.3 and 5.4. In fact the Mattar and Gregory (1974) model is just a version of the drift flux model (Zuber and Findlay (1965) and Wallis (1969)) with the values of C_0=1.3 and U_d=0.7. This semi-empirical model seems to have some physical basis though.

Further modifications to the drift flux model have been made by other authors most notably by Hasan and Kabir (1988) proposing different values for the drift velocity for different inclination angles based on a balance of the forces experienced by a rising bubble and using a flow pattern approach. However they do not improve the liquid holdup prediction when testing with the data from this work as can be seen in Figures 5.3 and 5.4.

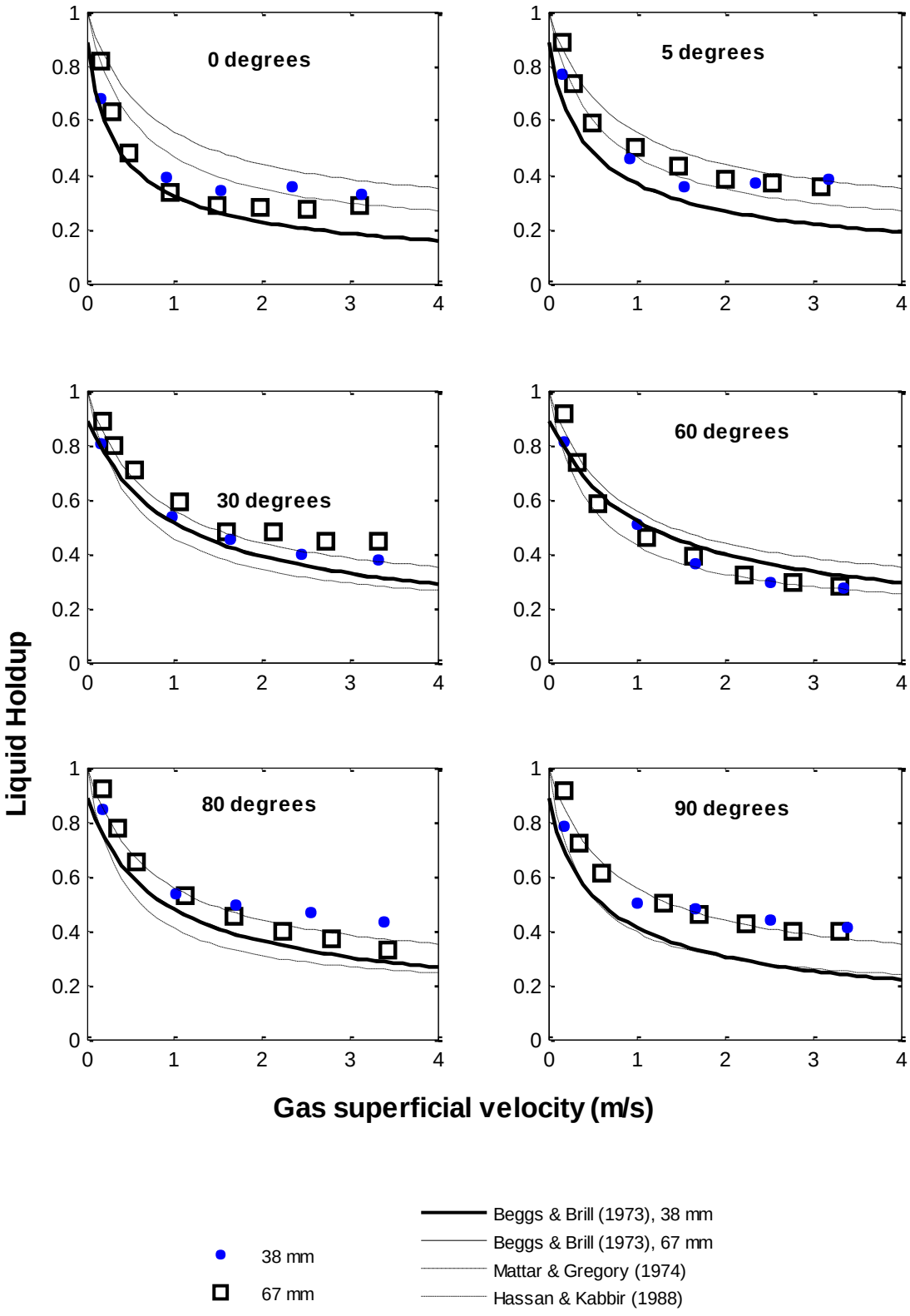

Figure 5.3 Liquid holdup results for U_{SL}=0.2 m/s and several inclination angles

When the liquid superficial velocity is increased up to 0.7 m/s (Figure 5.4), and for the range of gas superficial velocity taken, the experimental results show that the liquid holdup is slightly greater for the bigger pipe diameter, particularly for the inclinations close to vertical. The most physically based explanation is that the liquid holdup depends on the flow pattern, since for different flow patterns the two phases will arrange and travel at different velocities; it is obvious that the liquid holdups will be different.

When two phases flow through the same pipe, the gas usually flows faster than the liquid. In addition, as the diameter increases, it takes longer to form a Taylor bubble that is big enough to block the pipe, therefore the liquid is not forced by the gas to travel as fast as the mixture velocity, it tends to accumulate in the pipe and reduces the cross-sectional area available for the gas to flow, as a result the liquid holdup is bigger.

The finding that the liquid holdup is slightly higher for the bigger diameter pipe is in agreement with Singh and Griffith (1970) who found that the for a fixed flow condition and inclination angle, the gravitational pressure gradient increases as the pipe diameter increases, which implies an increase in the liquid holdup, see Section 5.2 for pressure gradient.

The increase in the pipe diameter increases the liquid holdup but it seems to depend on the flow conditions and since the liquid holdup is a very fundamental parameter in describing multiphase flow, it is expected that a change in the liquid holdup will be reflected on other parameters such as the pressure drop and the slug frequency which will be discussed in the following sections.

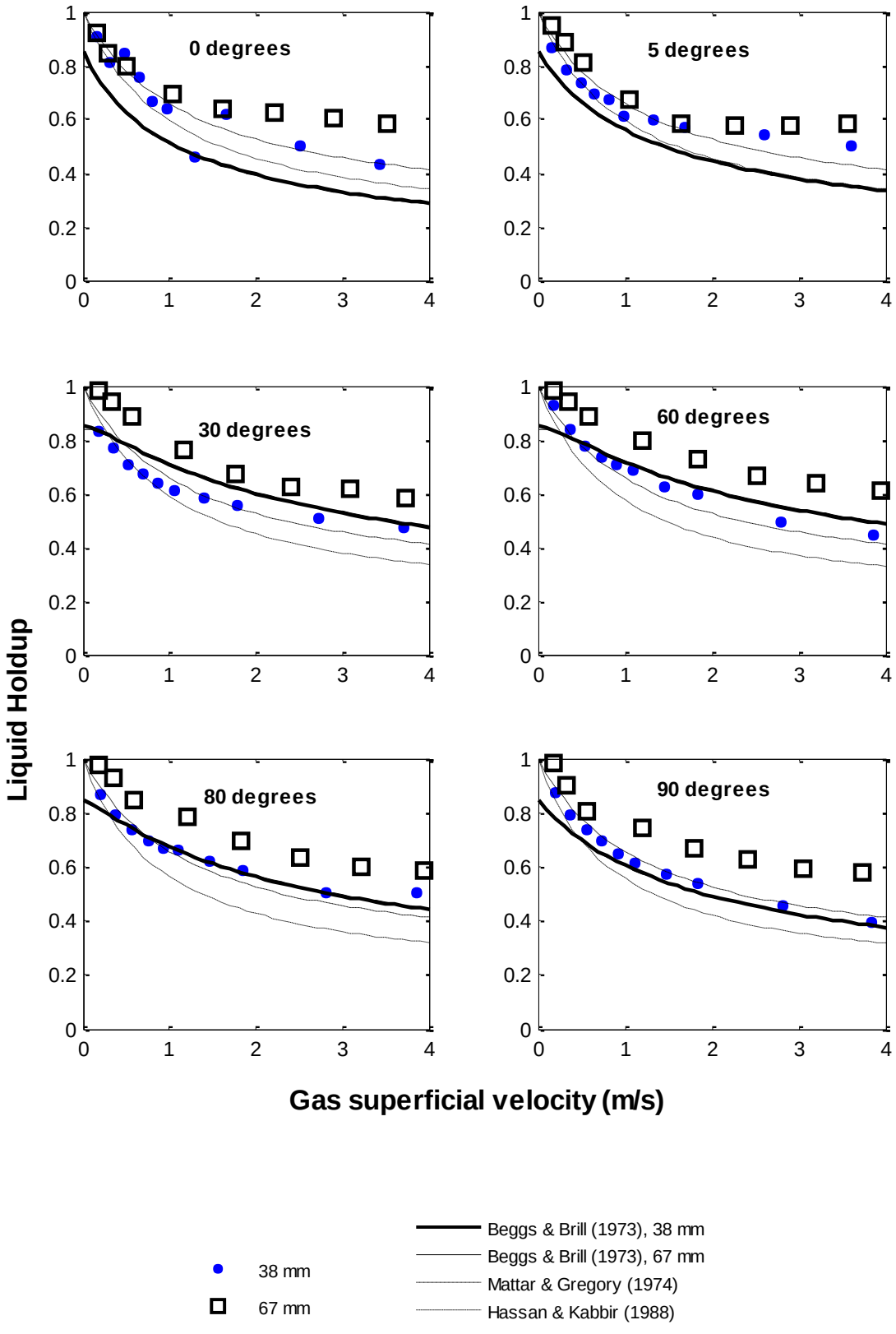

Figure 5.4 Liquid holdup results, U_{SL}=0.7 m/s and several inclination angles

5.2 Pressure gradient

The diversity of techniques used by different authors to present the two-phase flow pressure drop (Baker (1957), Griffith and Wallis (1961), Bonnecaze *et al.* (1971), Grescovich and Shrier (1971), Chen and Speding (1981), Jepson and Taylor (1993)) indicates, among other things, that pressure drop in two-phase flow can depend on a significant number of variables where the conduit diameter is of no less importance.

In this work, time series of pressure gradient were obtained directly with the DP cell (see Chapter 3). In general, it has been found that the time series for pressure drop in the two pipes are similar. For the particular situation illustrated in Figure 5.5, it can be observed that the fluctuations in the pressure gradient are comparable but the average value is higher for the 67 mm pipe.

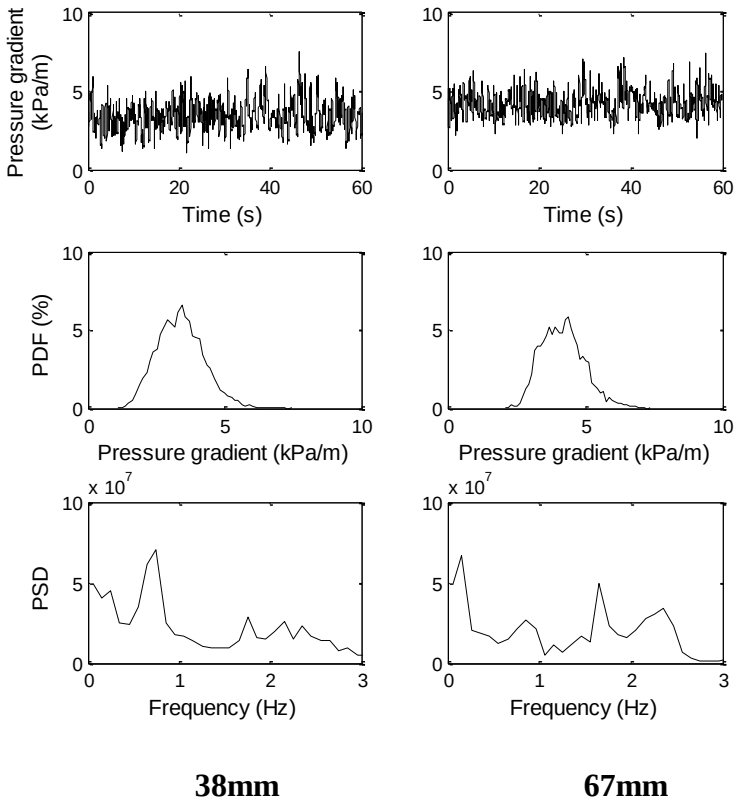

Figure 5.5 Comparison of time series, Probability density Function and Power Spectral Density obtained from the pressure gradient for 38 and 67 mm diameter pipes respectively. 90° inclination and superficial velocities (m/s); liquid=0.7 and gas=2.9

Due to the separation distance between the two pressure tapings (which means that the pressure gradient is averaged over this distance) fluctuations produced by the liquid slugs are not clearly observed, the shape of the PDF consists of one single peak and the PSD frequency does not match the frequency value from the liquid holdup (see also Figure 4.37 where a comparison was made).

Average pressure gradient is shown in Figures 5.6 and 5.7. As it is expected, a similar behaviour to that observed in the liquid holdup occurs with the pressure drop, since the hydrostatic pressure is the main contribution to the pressure drop even though frictional component of the total pressure drop might decrease with the bigger diameter. This observation is consistent for all the measurements in all inclination angles particularly for big inclinations (>30°) as shown below.

The major difference between the two pressure gradients between the two pipe diameters seems to occur for 0.7 m/s liquid superficial velocity around a value of 1.5 m/s for the gas superficial velocity. This value of gas superficial velocity where the maximum difference of pressure gradient between the two pipes takes place is different from the corresponding one for liquid holdup difference; for the holdup the difference is kept constant for all conditions whereas in the pressure gradient, we can observe that further increase in the gas flow rate will make the pressure gradient for the two pipes equal. This implies that the frictional component increases.

There has been little work reported in which two-phase pressure drop is treated as a topic unique in itself, Spedding *et al.* (1982) is perhaps one of the most extensive. Most models found today are applicable, if not actually derived for, a specific flow pattern or regime, for instance Hasan and Kabir (1988).

The effect of pipe diameter on pressure drop has been studied by Singh and Griffith (1970), they investigated slug flow in small inclination angles from the horizontal and interestingly found that an optimum pipe size existed, for constant flow rate of the fluid at which the total pressure drop was a minimum. They pointed that the same feature was apparent in the vertical upward flow data of Govier *et al.* (1957) and Govier and Short (1958).

In Figure 5.6, a comparison is made between some of the data of Singh and Griffith (1970) and the present work for an inclination angle of 5 ° and the flow conditions specified, which differ slightly. However, the agreement is good. Furthermore, this comparison clearly illustrates the effect of pipe diameter on the pressure gradient over a wider range. Figure 5.6 also suggest that an optimum pipe diameter is about 35 mm for this flow condition and inclination angle.

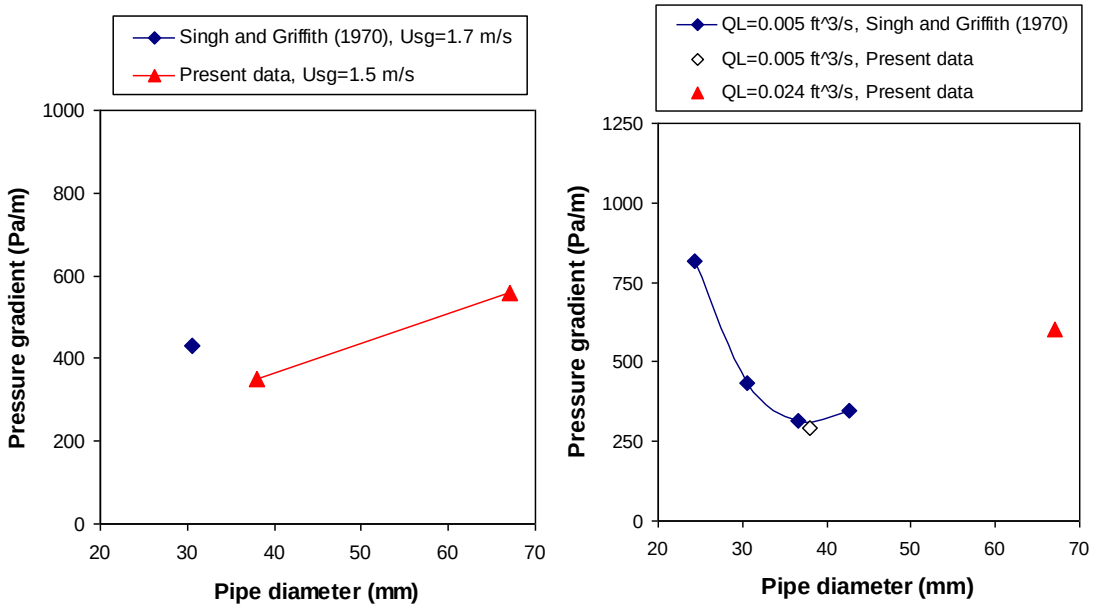

a) **b)**

Figure 5.6 Pressure gradient behaviour as a function of the pipe diameter at 5 degrees inclination: a) U_{SL}=0.2 m/s and b) Q_G≈0.04 ft^3/s

The basic reason for this effect is that, for given flow conditions, the relative contribution to the total pressure drop due to elevation increases with pipe size, while the frictional pressure drop contribution does the contrary. The pressure loss of a fluid flowing through a pipe is inversely proportional to the fifth power of the pipe diameter, Baker (1954). The accumulated liquid in the pipe has a similar effect to that reducing the pipe diameter.

Further comparisons of the present work is performed against the correlation of Beggs and Brill (1973) and Mattar and Gregory (1974) in Figures 5.7 and 5.8, it can be deduced that the first one performs better for some conditions. However it is not clear under which conditions this correlation will give the best predictions.

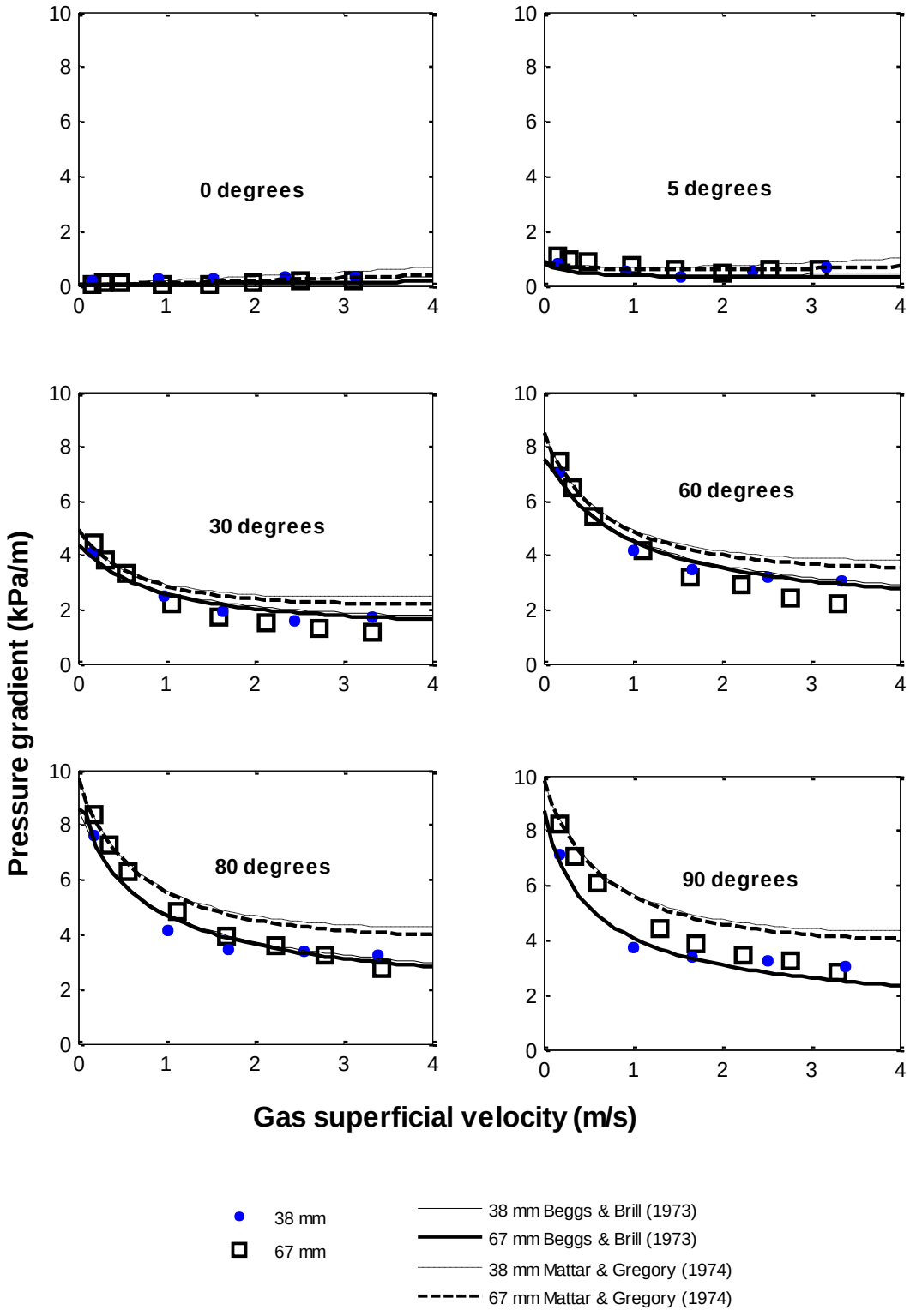

Figure 5.7 Pressure gradient, U_{SL}=0.2 m/s and several inclination angles

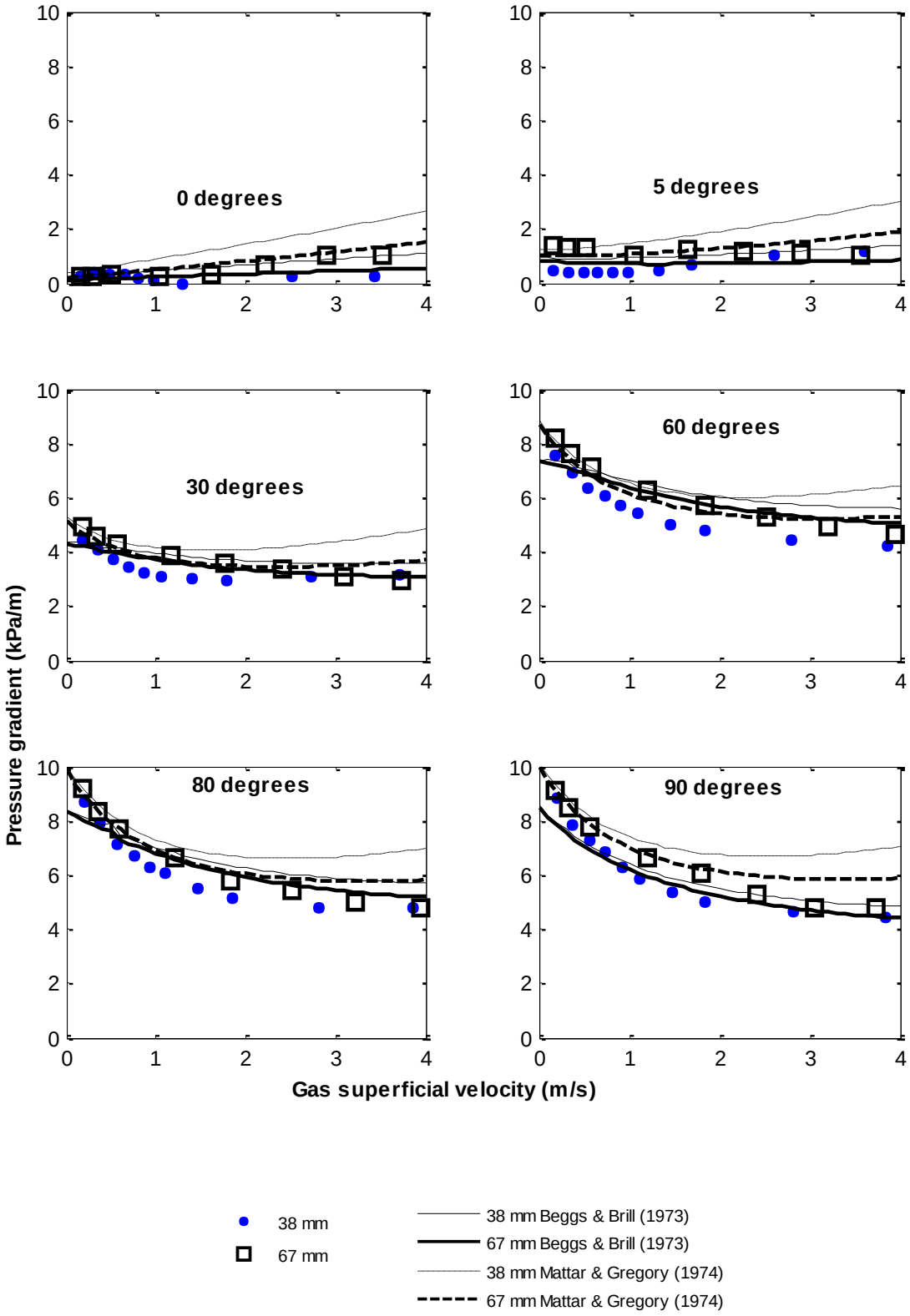

Figure 5.8 Pressure gradient, U_{SL}=0.7 m/s and different inclination angles

5.3 Structure velocity

By following the procedure explained in Section 4.6, the structure velocity was calculated for all the experiments and the results are presented below in Figures 5.9 and 5.10.

It has been found that increasing the pipe diameter results in an increase of the translational velocity. Even though it is what is expected due to the fact that the equations for the calculation of the drift velocity, such as Bendiksen (1984) and Weber (1981), suggest that this parameter increases with the pipe diameter, the difference is quite big compared to what the equations suggest. Indeed, we plotted the Bendiksen (1984) correlation (equation (2.59)) along with the data and the difference can be seen. In this equation, the value of 1.2 for the parameter C_0, makes the estimation of the velocity simple. Both Hasan and Kabir (1988) and Kaya *et al.* (2001) have used this value, however, the data supporting a constant value of 1.2 for all inclinations are limited. In the present work, the value of 1.2 has been found to be right but not necessarily for the drift velocity.

In this work, the drift velocity has been found to be higher than the predictions of Bendiksen (1984) and Hasan and Kabir (1988), figure 4.43. Van Hout *et al.* (2002) have suggested that drift velocity in stagnant liquid is different from the drift velocity in continuous slug due to the contribution of the small bubbles in the liquid slug. Since we are working with continuous slug flow, the higher drift velocity obtained can be associated with the dispersed bubbles contribution.

For the liquid superficial velocity 0.7 m/s, the cross correlation for the first conditions (at low gas superficial velocities) was not very good, as a consequence, it was not possible to calculate the structure velocity, observation showed however that small gas pockets appeared already. This particular behaviour of the correlation between the two signals for these flow conditions can be related to the change in flow pattern. The difference in the values of structure velocity between the two pipes is smaller when the liquid is increased, this might be due to the fact that the holdup in the liquid slug body increases as is shown in Section 5.6.

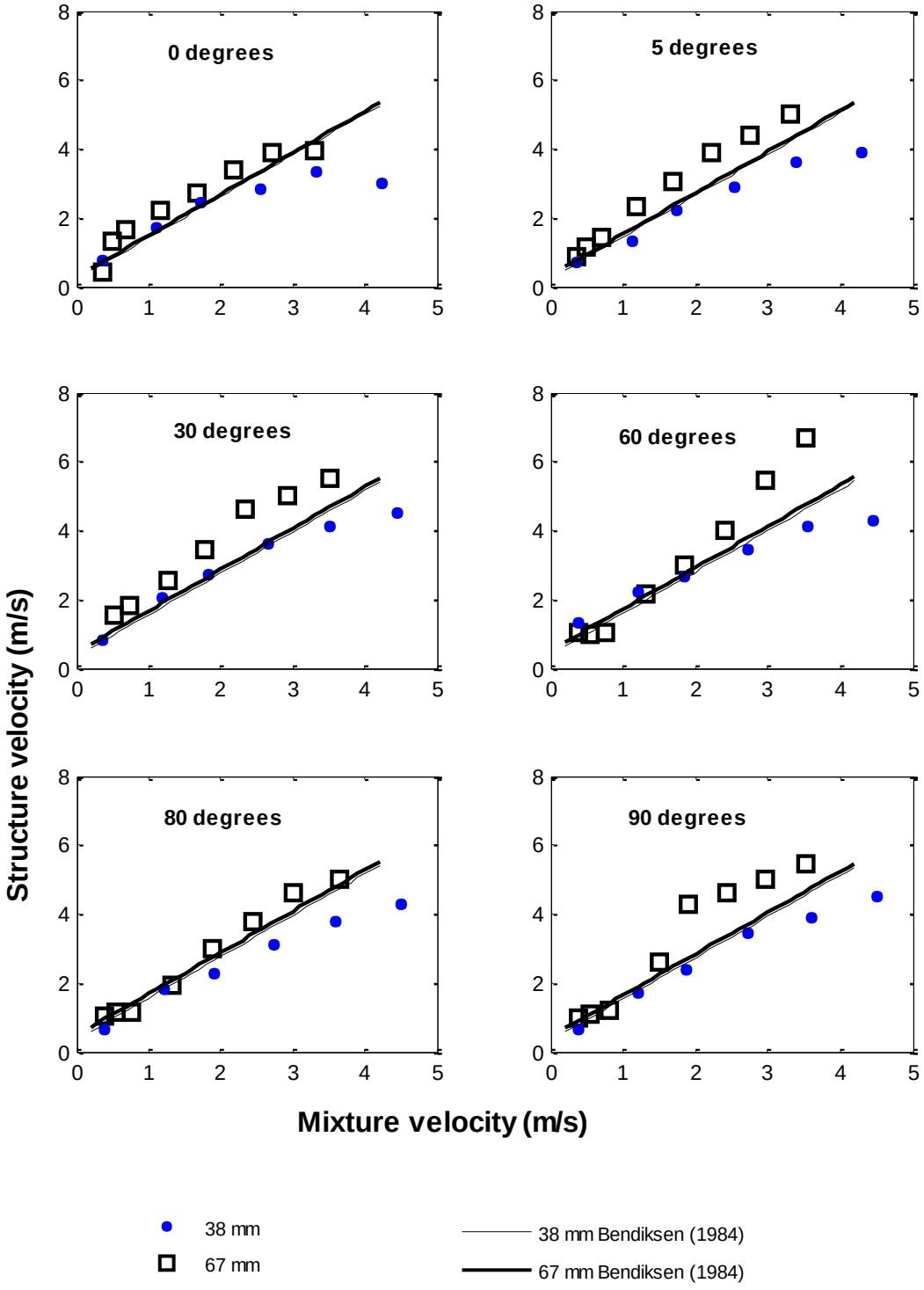

Figure 5.9 Structure velocity, U_{SL}=0.2 m/s and different inclination angles

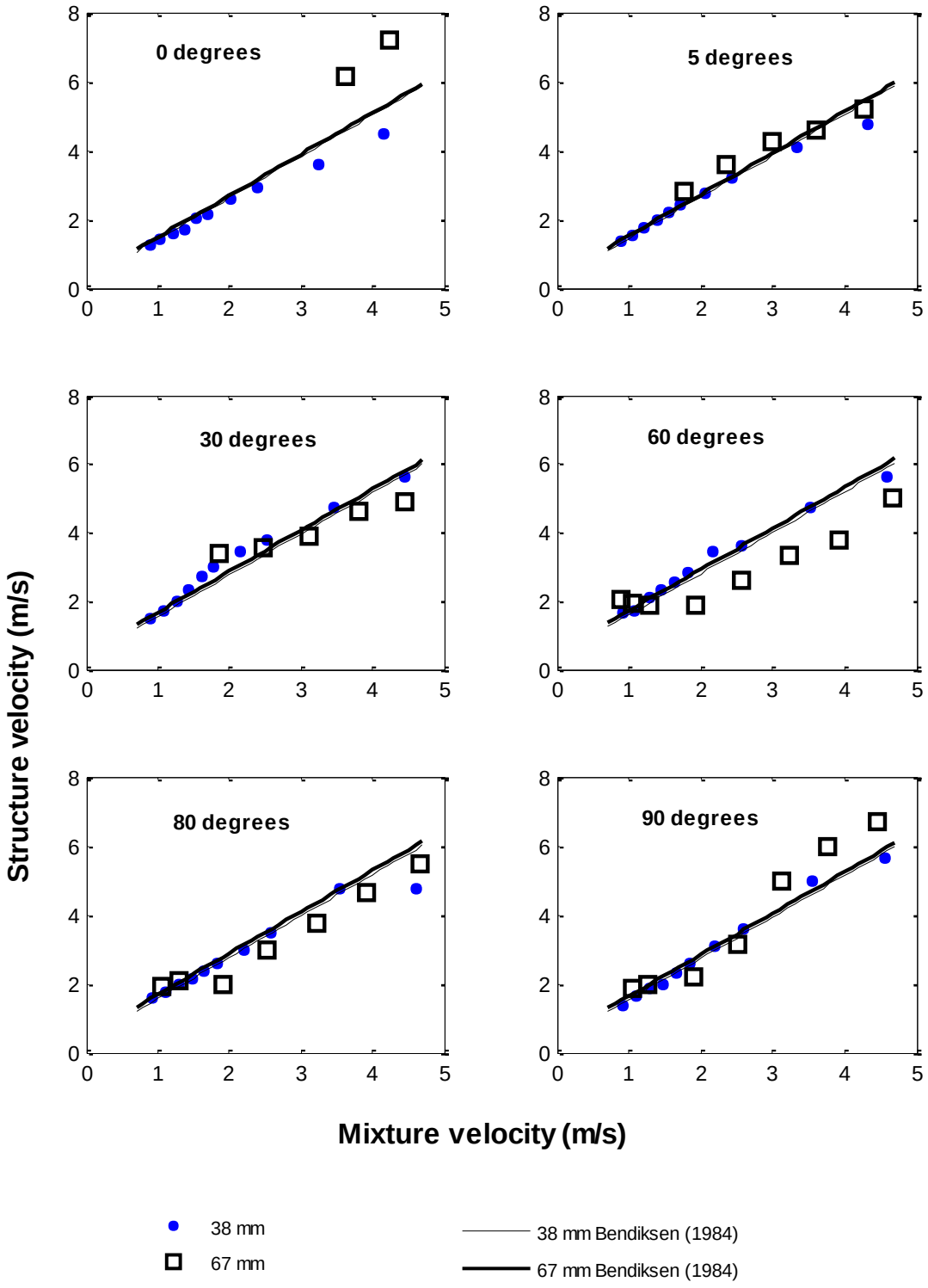

Figure 5.10 Structure velocity, U_{SL}=0.7 m/s and different inclination angles

5.4 Frequency

Knowledge of slugging frequency is required as an input variable in many mechanistic models such as those of Dukler and Hubbard (1975) and Cook and Behnia (2000) and is relied upon for the design of separator vessels, Wren *et al.* (2005). In this work, the frequency was determined as described in Section 4.5 and the results are plotted in Figures 5.13 and 5.14. It is in general affected by several parameters as described below.

For U_{SL}=0.2 m/s and the gas flow rates considered in this work, the frequency remains fairly constant for the horizontal case, the data for both pipes are overlapped. For the other inclinations, the tendency is not very clear at low values of U_{SG} but after U_{SG}=1 m/s seems to follow the slug frequency tendency found by other researchers such as Hubbard and Dukler (1966) and Gregory and Scott (1969), and the frequency does not change with the pipe diameter clearly. The biggest variation is found at the vertical position where it is clear that the frequency for 67mm pipe is bigger. This could be due to a combined effect of holdup and flow pattern.

In addition, it has been noted that at low gas superficial velocities, particularly for the 0.7 m/s liquid superficial velocity, there is some uncertainty about the values of the frequency. Indeed, the Power Spectral Density for those conditions is very small and there are several peaks on the PSD plot, see Figure 5.11 where the for the condition of U_{SL}= 0.73 m/s and U_{SG}=0.15 m/s the PSD is at least one order of magnitude lower with respect to the other conditions. For these cases it is not easy to determine the frequency and the final values chosen are based on the assumption that if we reduce the gas superficial velocity to zero, then the frequency would decrease to zero.

Also, as the gas superficial velocity approaches zero, bubbly flow exists and therefore the fluctuations are weaker over a wider range of frequencies.

For U_{SL}= 0.73 m/s, the frequency starts from a value of about 1 Hz for the lowest gas flow rate and then it grows very quickly, to a maximum as for this conditions bubble slug transition is passed and then it decreases gradually. For the horizontal case the behaviour is a bit different; for the 38mm pipe slug flow is obtained for all conditions,

having a frequency around 1 Hz whereas in 67 mm the flow starts with stratified flow, where the frequency is 0 Hz and then changes to slug with an increase in the frequency.

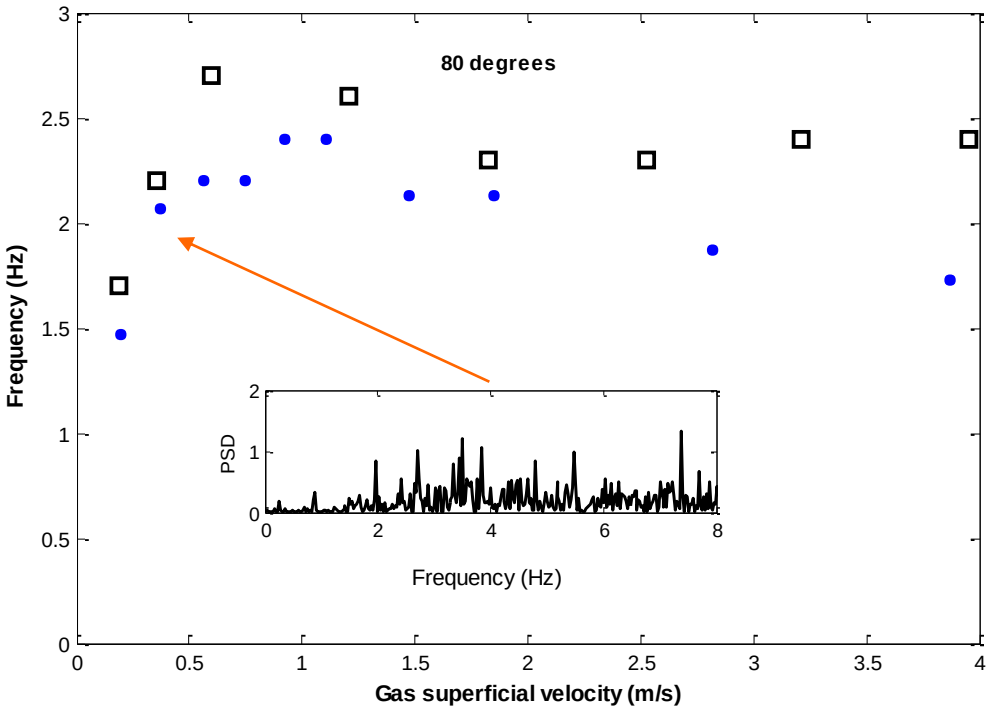

Figure 5.11 Frequency for liquid superficial velocity 0.7 m/s and 80 degrees inclination in the 67 mm pipe.

The literature (Section 2.5.4) reveals that slug frequency data have been reported by several authors as well as correlations and a comprehensive comparison of correlations for slug frequency has been made in section 4.5, and a wide disagreement with the present data was found. Particularly for inclined flow, which is expected from the fact that none of the correlations for slug frequency found in the literature (except Zabaras (1999) for small inclination angles from the horizontal) take into consideration the effect of inclination angle. However, all of them agree that as the pipe diameter increases, the frequency decreases. Comparatively little has been reported on slug frequency data in inclined pipes, Van Hout *et al.* (2003) reported data on slug frequency for inclined flow but no model or correlation was proposed, their data exhibit a tendency similar to the one found in the present work (Figure 4.24) though their superficial velocities are lower.

Examination of the frequency shows that it is strongly affected by the inclination angle as has been shown in Figure 4.24, therefore in this section, a correlation has been suggested to take into account the effect of inclination on the slug frequency from horizontal to vertical. Following a similar approach as that of Bendiksen (1984) and Malnes (1983) for drift velocity in inclined pipes, we correlate the slug frequency for inclined pipes from horizontal to vertical by using a linear combination of both horizontal and vertical frequencies.

Since the frequency and the velocity magnitude are directly proportional parameters, they are affected by the inclination angle in the same way. Similar to the velocity, for a particular inclination angle, the frequency can be multiplied by unity and apply the trigonometric relation $\cos^2\theta + \sin^2\theta = 1$ in order to be expressed as in equation (5.1).

$$f = (f\cos\theta)\cos\theta + (f\sin\theta)\sin\theta \tag{5.1}$$

In addition it must satisfy the conditions that

$$f(\theta = 0^\circ) = f_h \tag{5.2}$$

And

$$f(\theta = 90^\circ) = f_v \tag{5.3}$$

Where f_h and f_v are the frequencies for horizontal and vertical inclinations respectively, therefore

$$f = f_h\cos\theta + f_v\sin\theta \tag{5.4}$$

At this point we realise that there is no slug frequency correlation developed exclusively for the vertical case in the literature. By taking a look at Figure 5.13, it can be easily recognised that under the same flow conditions, frequencies in vertical flow are quite different from those in horizontal and as can be seen, literature correlations fail to predict the slug frequency for inclinations other than horizontal. Therefore the first step is to develop a correlation for vertical flow. Similarly to Manolis *et al.* (1995), Zabaras (1999) and Wren *et al.* (2005), we develop the correlation based on a

modification to the Gregory and Scott (1969) to adapt it to the vertical frequency data, which are plotted in Figure 5.12 as a function of the Froude number. Wren *et al.* (2005) also compared data for 5, 19 and 35 mm pipe diameter in horizontal and showed a nonlinear decrease of frequency with increase in pipe diameter.

Gregory and Scott (1969) correlation for frequency is given by

$$f_v = 0.0226\left[\frac{U_{SL}}{gd}\left(\frac{19.75}{U_m} + U_m\right)\right]^{1.2} \tag{5.5}$$

Examination of the present data in Figure 5.12 (from both 38 and 67 mm pipes) showed that for the vertical case, the more suitable values of the power and pre-constant were 0.2528 and 0.8428 respectively. This yields a new correlation for slug frequency in vertical pipes, which predicts considerably better than the correlations of the literature:

$$f_v = 0.8428\left[\frac{U_{SL}}{gd}\left(\frac{19.75}{U_m} + U_m\right)\right]^{0.25} \tag{5.6}$$

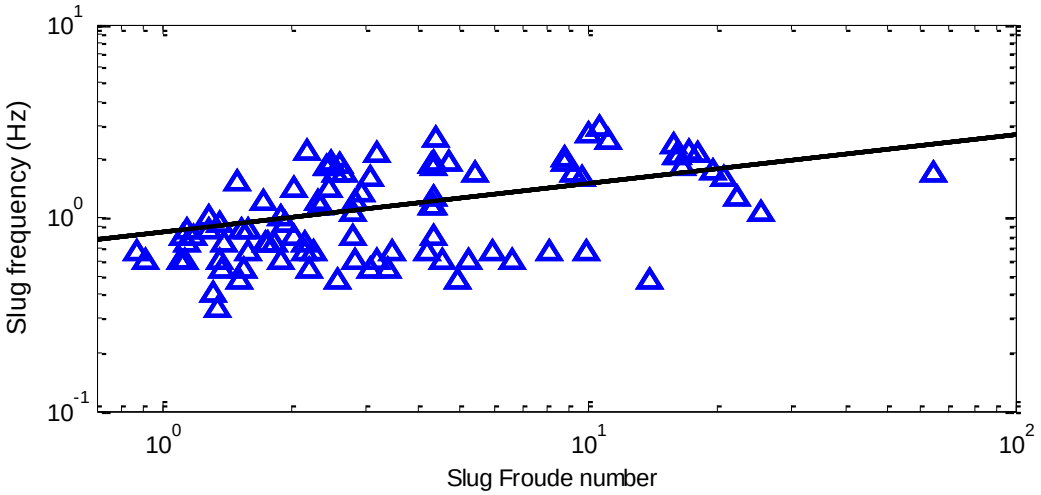

Figure 5.12 Slug frequency vs. slug Froude number for vertical flow including data from both 38 and 67 mm pipes.

The comparison between the values predicted by the correlations suggested by equations (5.4) and (5.5) and the experimental data gives a good agreement as can be seen in Figures 5.13 and 5.14. It seems that the effect of the pipe diameter on the frequency is that when increasing the pipe diameter, the frequency reaches its maximum at a steeper inclination angle; in Figures 5.13 and 5.14 it can be observed that the frequency has its maximum value at 60 degrees for 38mm and 80 degrees for 67 mm.

Further examination of Figures 5.13 and 5.14, shows that increasing the liquid superficial velocity from 0.2 to 0.7 m/s has a big effect on the frequency in horizontal but not in vertical. In vertical even if the liquid superficial velocity is zero, we could have an intermittent flow with an associated frequency. This suggests that the frequency depends on the liquid holdup rather than U_{SL}.

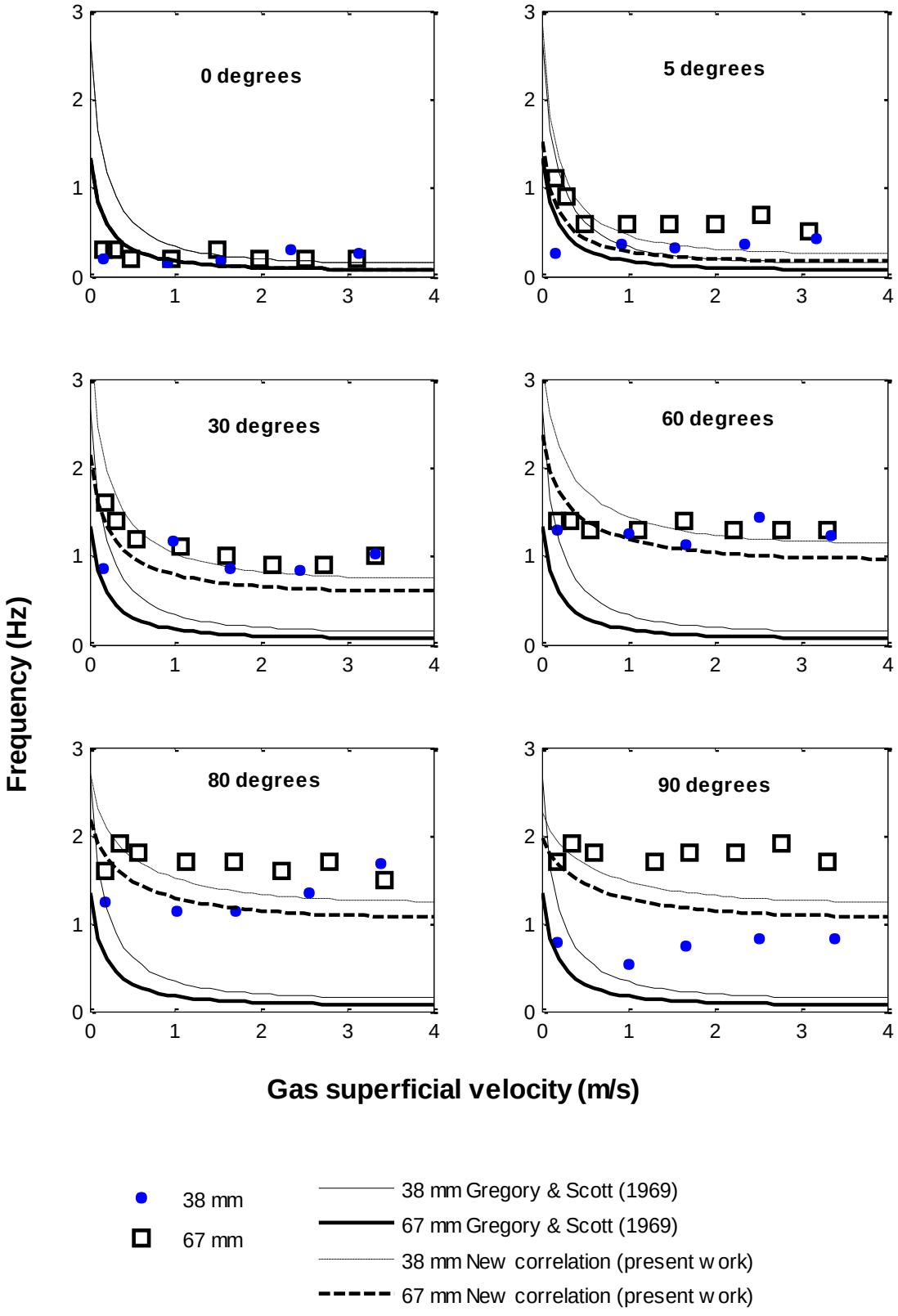

Figure 5.13 Frequency results, U_{SL}=0.2 m/s and several inclination angles

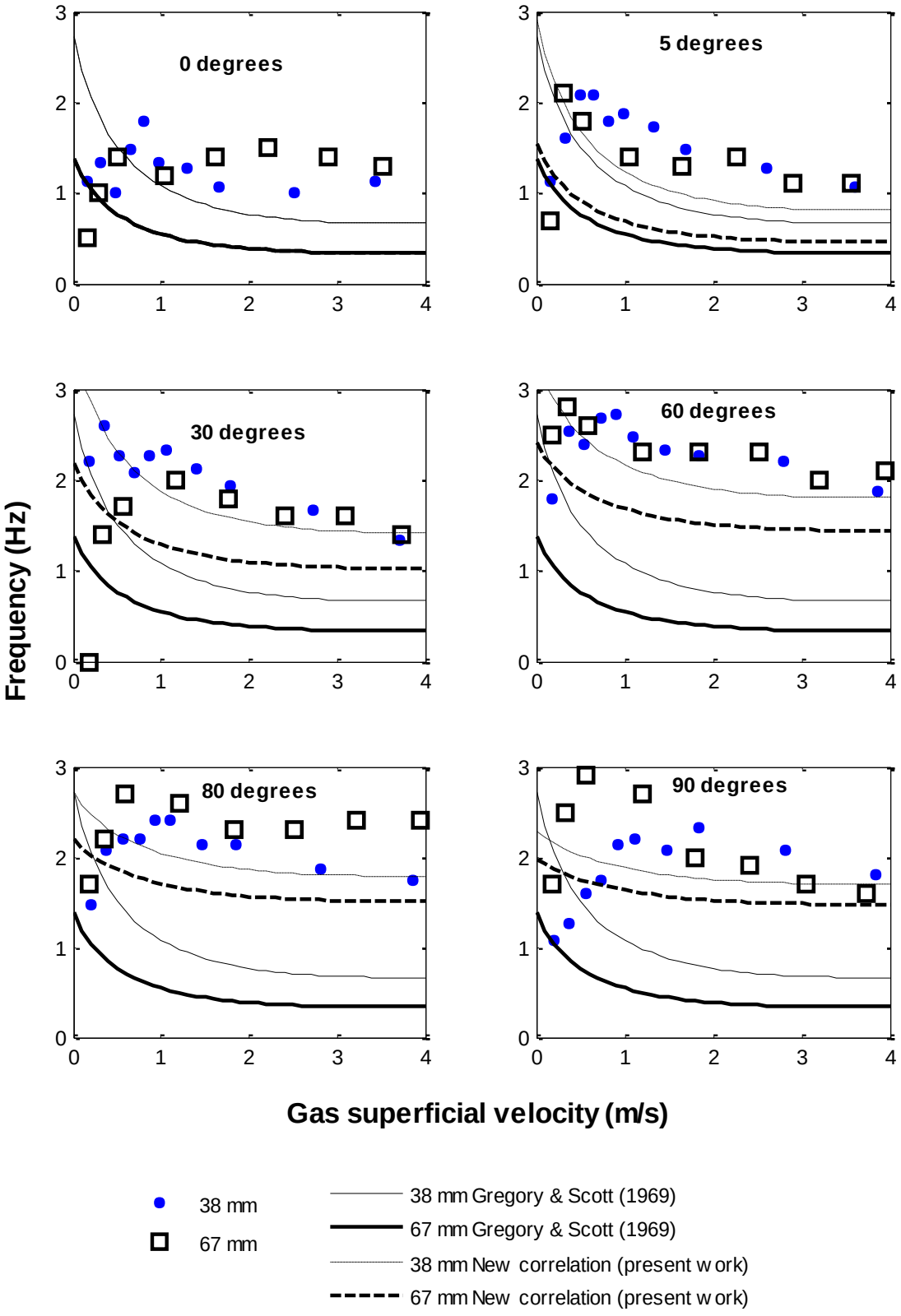

Figure 5.14 Frequency, U_{SL}=0.7 m/s and several inclination angles

5.5 Flow pattern map

Knowledge and possible identification of the flow regime of an approaching gas-liquid mixture is crucial in the operation of many pieces of plant equipment. Having presented and compared the data for liquid holdup, pressure drop, frequency, structure velocity in the 67 mm pipe, it is possible that whenever some small differences are observed when comparing the two pipe diameters, they are related to the flow pattern. Therefore the different flow behaviour for different pipe diameter can help to identify the change in the flow pattern with the pipe diameter. In practice however is difficult to identify the flow pattern since the transitions happen gradually.

In Figure 5.15 a set of PDF plots is presented. The liquid superficial velocity has been kept constant and the flow pattern can be deduced to be somehow intermittent from the shape of the PDFs for all the cases. However it is clear that a well defined second peak appears at lower gas superficial velocities for the smaller diameter pipe (38 mm).

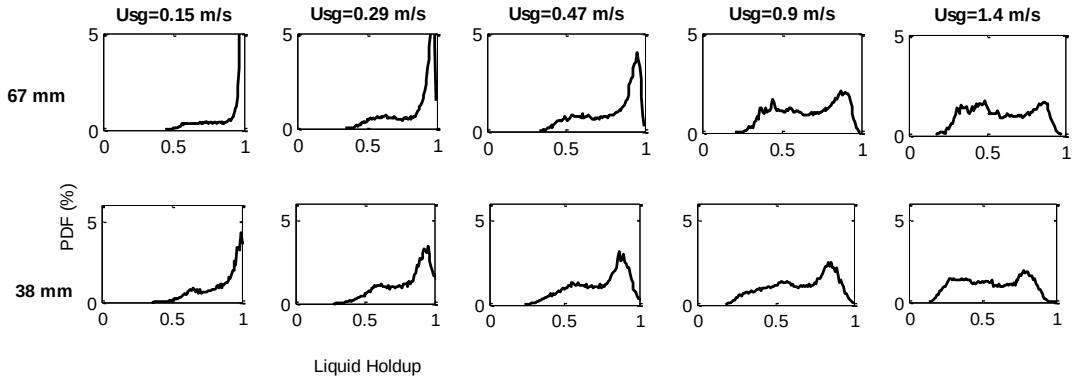

Figure 5.15 Probability Density Function (PDF) for U_{SL}=0.7 m/s and several gas superficial velocities at 60 °.

The behaviour illustrated in Figure 5.15 is consistent for all inclinations angles and the general effect of pipe diameter was that as diameter was increased from 38 to 67 mm, the bubbly-slug boundary moved to the right hand side on the flow pattern map in inclined flow. This is predicted well by the bubble-slug Taitel *et al.* (1980) transition in the flow pattern map expanded for all inclinations angles by Barnea (1987) as shown in Figure 5.16. For horizontal and inclined downwards flow in 67 mm pipe, slug flow is more difficult to achieve than in 38mm pipe, since it is more difficult for

the liquid to reach the top of the pipe to block the cross section area. Therefore the boundary between stratified and slug flow is in this case moved up. Finally a compacted representation of these conditions is given in the flow pattern maps of Figure 5.16 for different inclination angles.

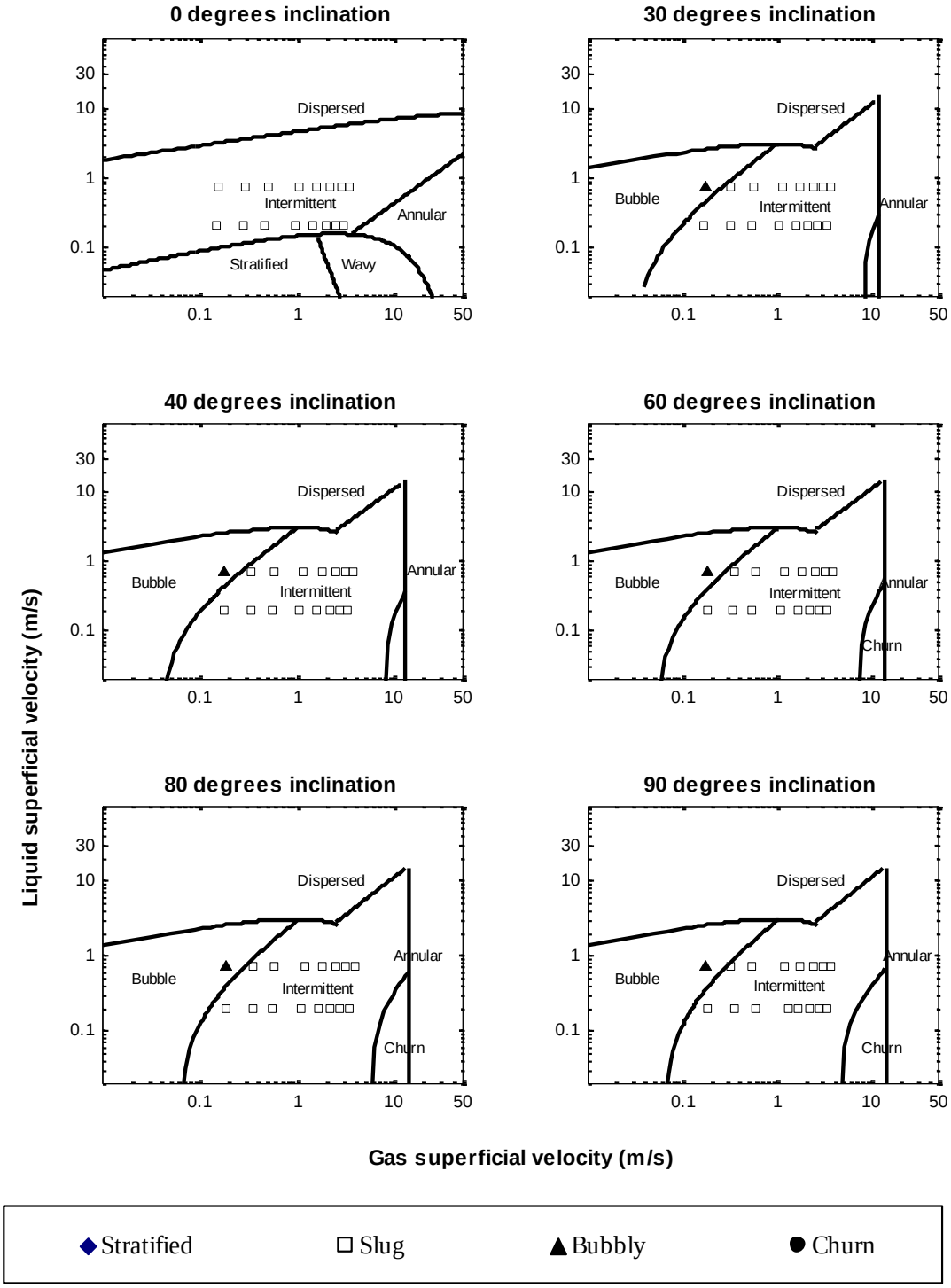

Figure 5.16 Flow pattern maps for different inclination angles, 67 mm pipe. Barnea (1987).

5.6 Liquid holdup in the slug

Another important parameter of slug flow that is required for input of mechanistic models is the liquid holdup in the slug body; this parameter has been calculated from the PDF of the liquid holdup time series as shown in Section 4.8. Figure 5.17 and 5.18 present the results for liquid holdup in the liquid slug body for different inclination angles, within the same figure, additional data taken from Nydal (1991) for different inclination angles (31 mm diameter) and Jepson and Taylor (1993) in horizontal flow (306 mm diameter) have been included in order to compare. The flow conditions have been chosen to match the ones used in the present work and they show good agreement.

The correlation of Gregory *et al.* (1978), which is independent of the pipe diameter and inclination angle, is also included in this comparison. The purely empirical approach of this correlation suggests limits in its generality. Compared with the present work, this correlation performs better for low inclination angles where the agreement with the present data is quite close, as well as for the highest liquid superficial velocity (U_{SL}=0.7 m/s)

In addition the correlation of Gomez *et al.* (2000) has been evaluated at the experimental conditions of the present work, it takes into account the effect of inclination and pipe diameter, however it does not produce satisfactory predictions; the predictions are too low.

The liquid holdup in the slug body appears to decrease with the gas superficial velocity (as expected) and slightly with pipe inclination, and more importantly it is observed to decrease slightly with the increase in the pipe diameter. Reasons for the holdup in the liquid slug body to be affected by the pipe diameter in such a way that it decreases for the bigger diameter are associated with the fact that the more turbulent flow in the bigger pipe induces more bubble entrainment in the slug body. Also, the pipe diameter seems to have more effect at higher gas superficial velocities. This tendency is in agreement with Andreussi and Bendiksen (1989) who used 50 and 90 mm pipes. At some conditons, PDF method is not accurate since the peaks in the histogram are not well defined due to the presence of waves.

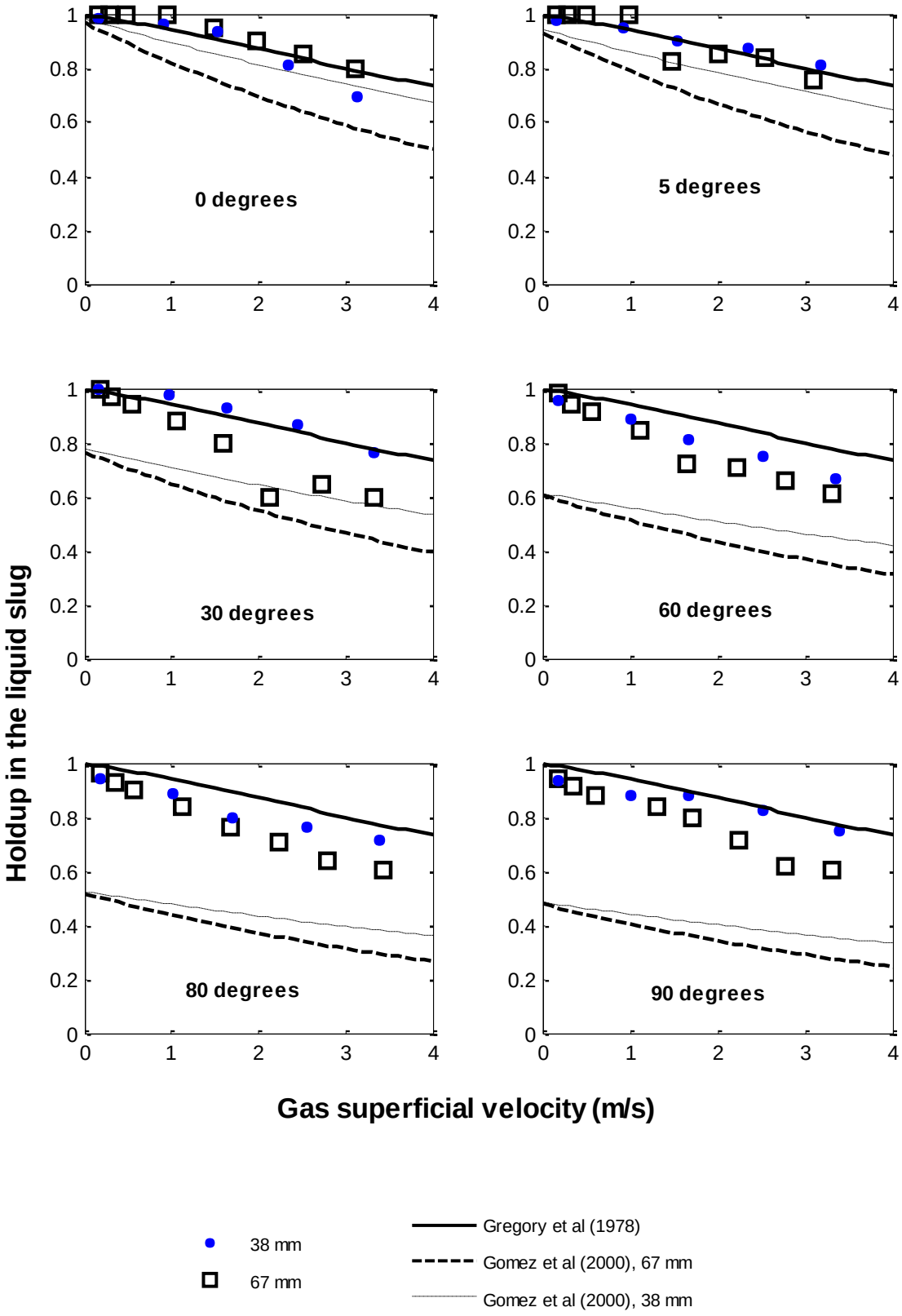

Figure 5.17 Liquid holdups in the slug for different inclination angles. U_{SL}= 0.2 m/s

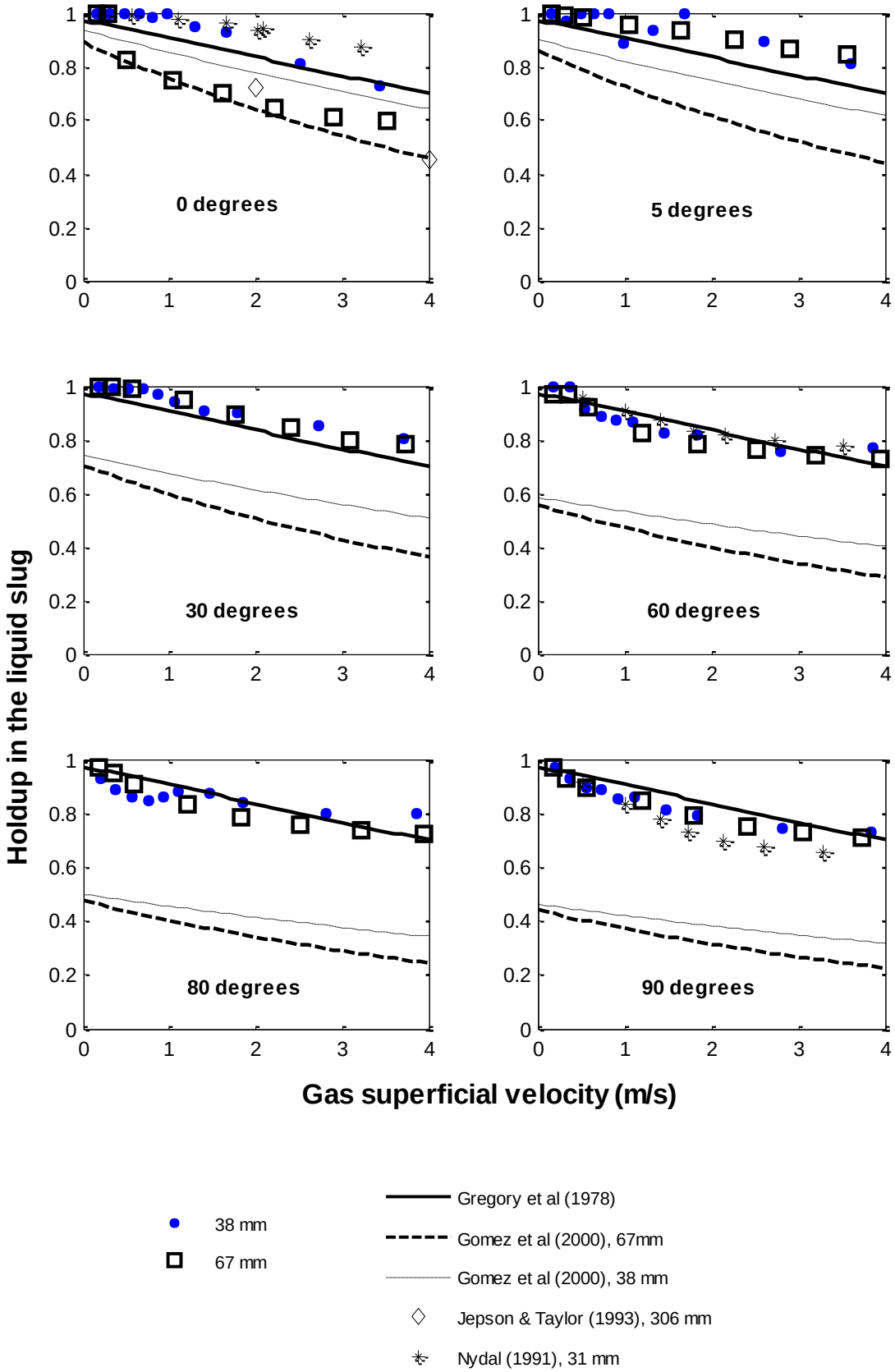

Figure 5.18 Liquid holdups in the slug for different inclination angles, U_{SL}= 0.7 m/s

5.7 Slug length

In order to calculate pressure drop in slug flow mechanistic models, it is necessary to know either the frequency or the slug length. Slug length will influence the size of downstream equipment used in a production facility. In fact some researchers such as Malnes (1983) think of the slug length as a more fundamental parameter than the frequency due to the fact that dimensionless slug length is expected to remain fairly constant for developed slug flow.

In this section the slug length has been calculated as done in Section 4.8. Also since we are calculating the slug length based on the frequency, it is obvious that we obtain the relationship between these parameters or between the slug length and the traslational velocity that was observed by Gregory and Scott (1969).

Since the main characteristics of gas-liquid slug flow are intermittency and irregularity, it is not a surprise to observe that the dimensionless liquid slug length exhibits an unclear function of the slug unit length and other variables, however as can be seen in Figures 5.19 to 5.22. Average slug lengths were in the order of 10 to 30 pipe diameters, and relatively independent of flow conditions. This is in agreement with other authors such as Dukler and Hubbard (1975), Taitel and Dukler (1977) for horizontal flow.

In Section 4.8, it was pointed out that slug length is also observed to change with the inclination angle. By looking at Figure 5.19, we can observe that slug length is bigger for horizontal flow than for vertical and intermediate values happen for other inclinations. For vertical flows Moissis and Griffith (1962) found the minimum stable slug length was about 8–16 d. Values for the minimum stable slug length obtained by Van Hout *et al.* (2003) in vertical and inclined flow are in the range of 10 pipe diameters.

Correlations for slug length and frequency are uncertain. In fact, not many models or correlations for slug length can be found in the literature review. Figures 5.21 and 5.22 show that the slug length remains fairly constant, whereas the bubble length and the total slug unit length increases with the gas superficial velocity.

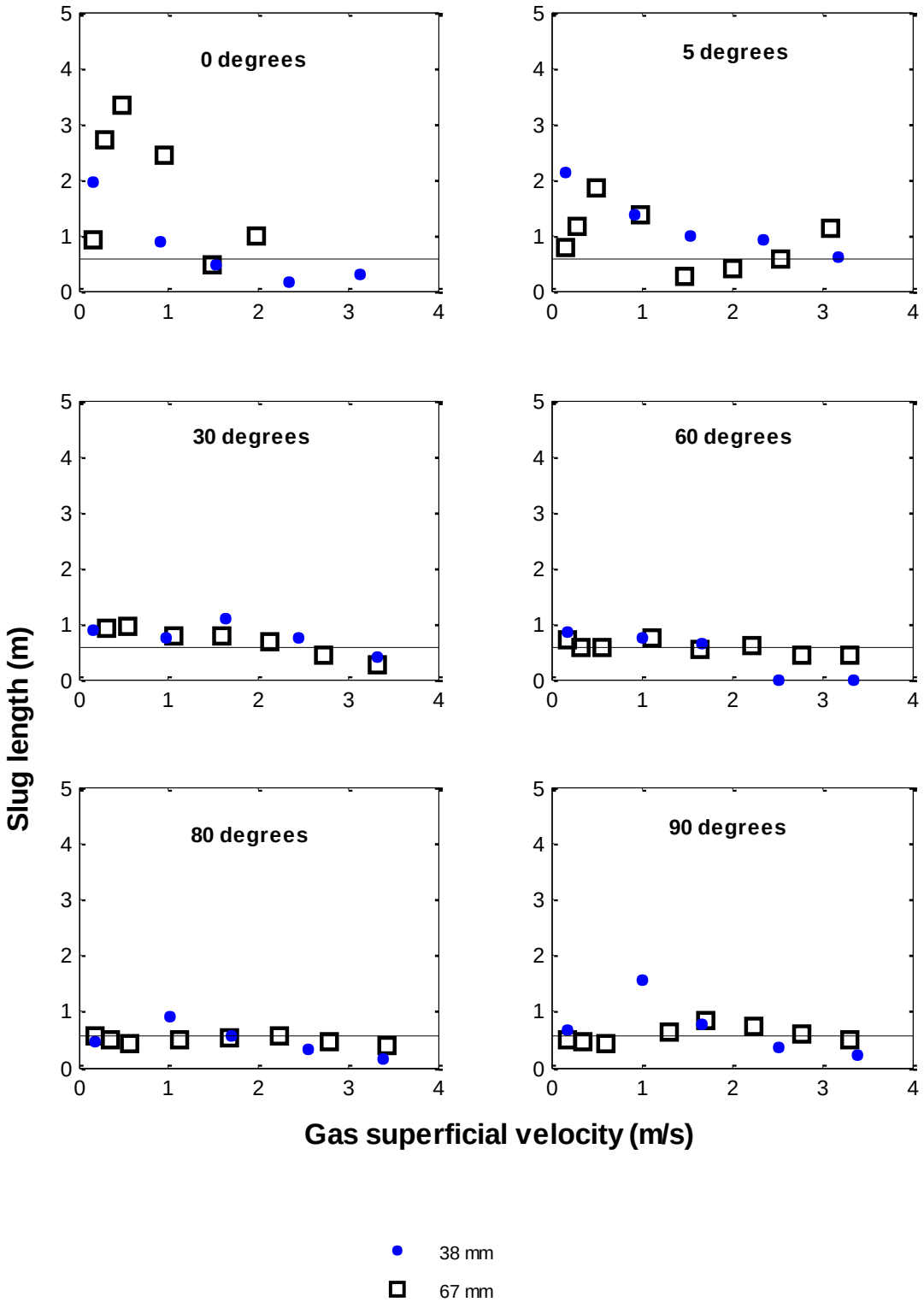

Figure 5.19 Slug lengths as a function of the gas superficial velocity. 67 mm pipe and U_{SL}=0.2 m/s

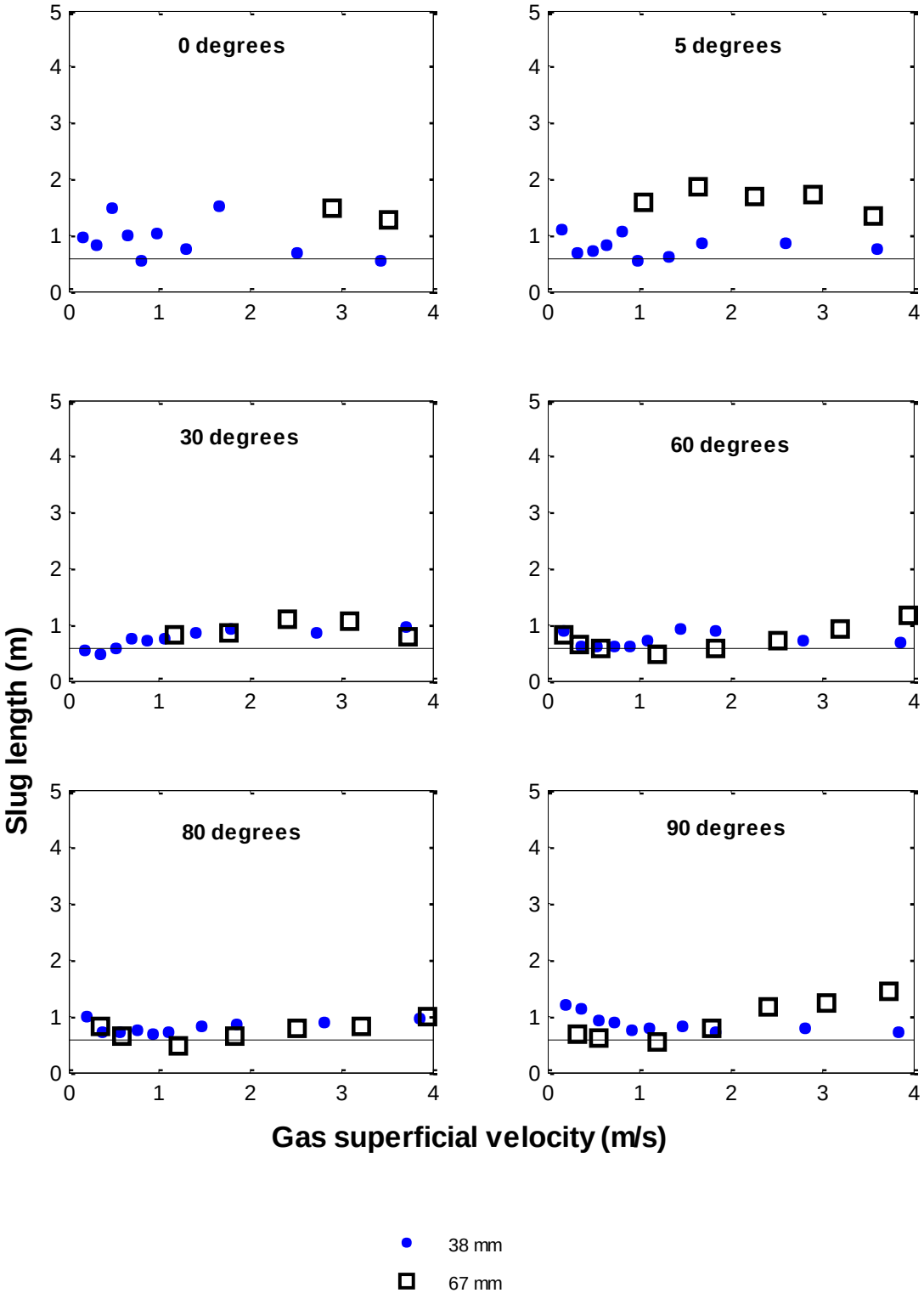

Figure 5.20 Slug lengths as a function of the gas superficial velocity. 67 mm pipe and U_{SL}=0.7 m/s.

The total slug unit length increases linearly with the gas superficial velocity. But it can be observed that it gets shorter when the liquid superficial velocity is increased from 0.2 to 0.7 m/s, this is due to the fact that the frequency of slugging gets bigger when the gas liquid velocity is increased. This happens in both pipes.

In Figures 5.19 to 5.22, the absolute values of total and slug liquid lengths are plotted. Both the liquid slug and total slug unit lengths are comparable. This implies that in dimensionless form slugs are longer for the 38 mm pipe. That means that the slug length is not linearly proportional to the pipe diameter.

It is interesting to note that the frequency and length are inversely proportional to each other. Even if we do not directly plot the slug length as a function of the inclination angle, by taking a look at the set of subplots in Figures 5.19 to 5.22 it can be seen that, the total slug unit take its highest values at low inclination angles such as horizontal and 5 degrees and the lowest ones are about 60 and possibly 80 degrees inclination.

By increasing the gas superficial velocity, there seems to be a tendency for the slug length, to increase this should be due to the entrainment of small bubbles. The total slug unit length seems to increase, since it depends on both the structure velocity and the frequency.

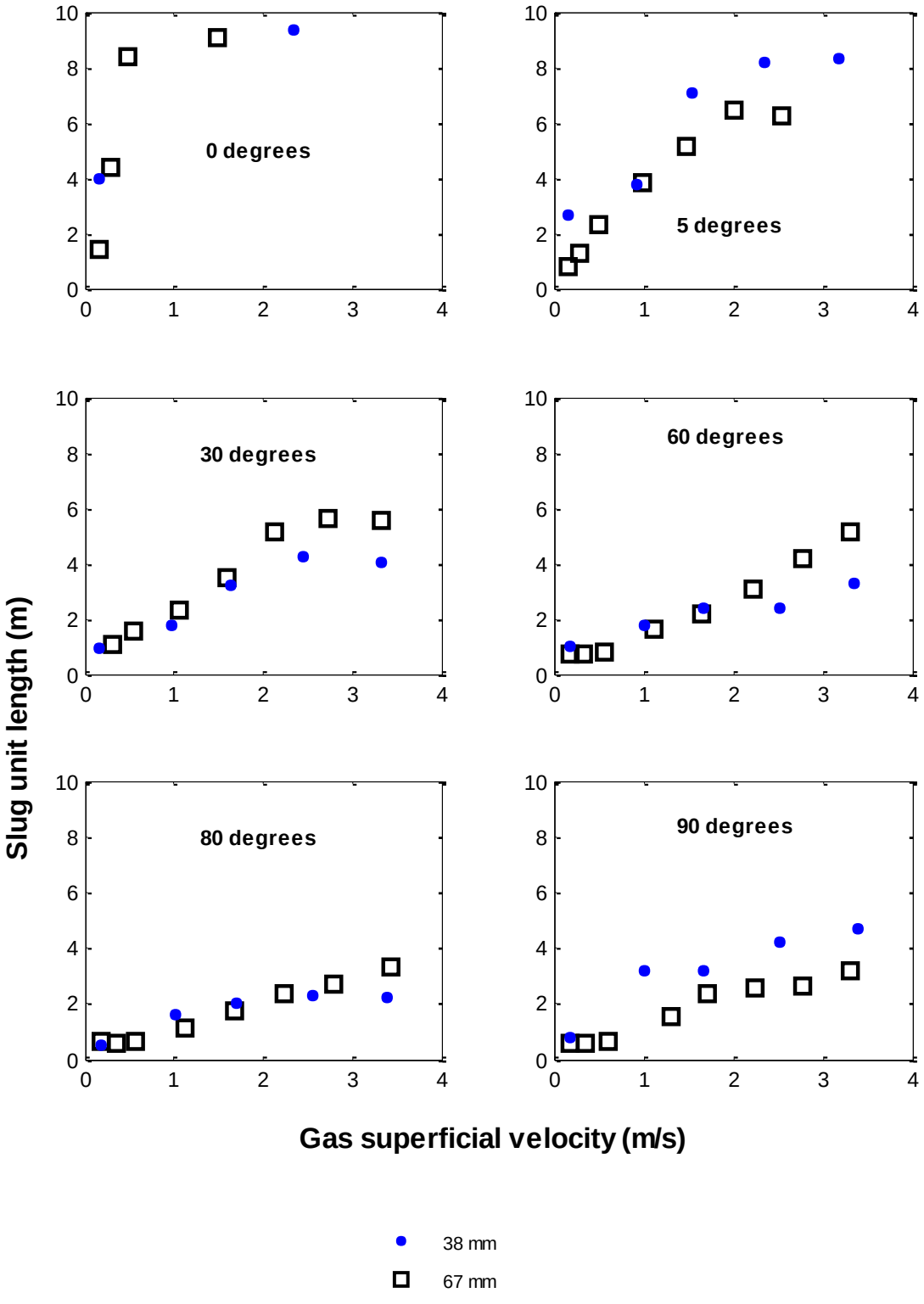

Figure 5.21 Slug unit length as a function of the gas superficial velocity. 67 mm pipe and U_{SL}=0.2 m/s.

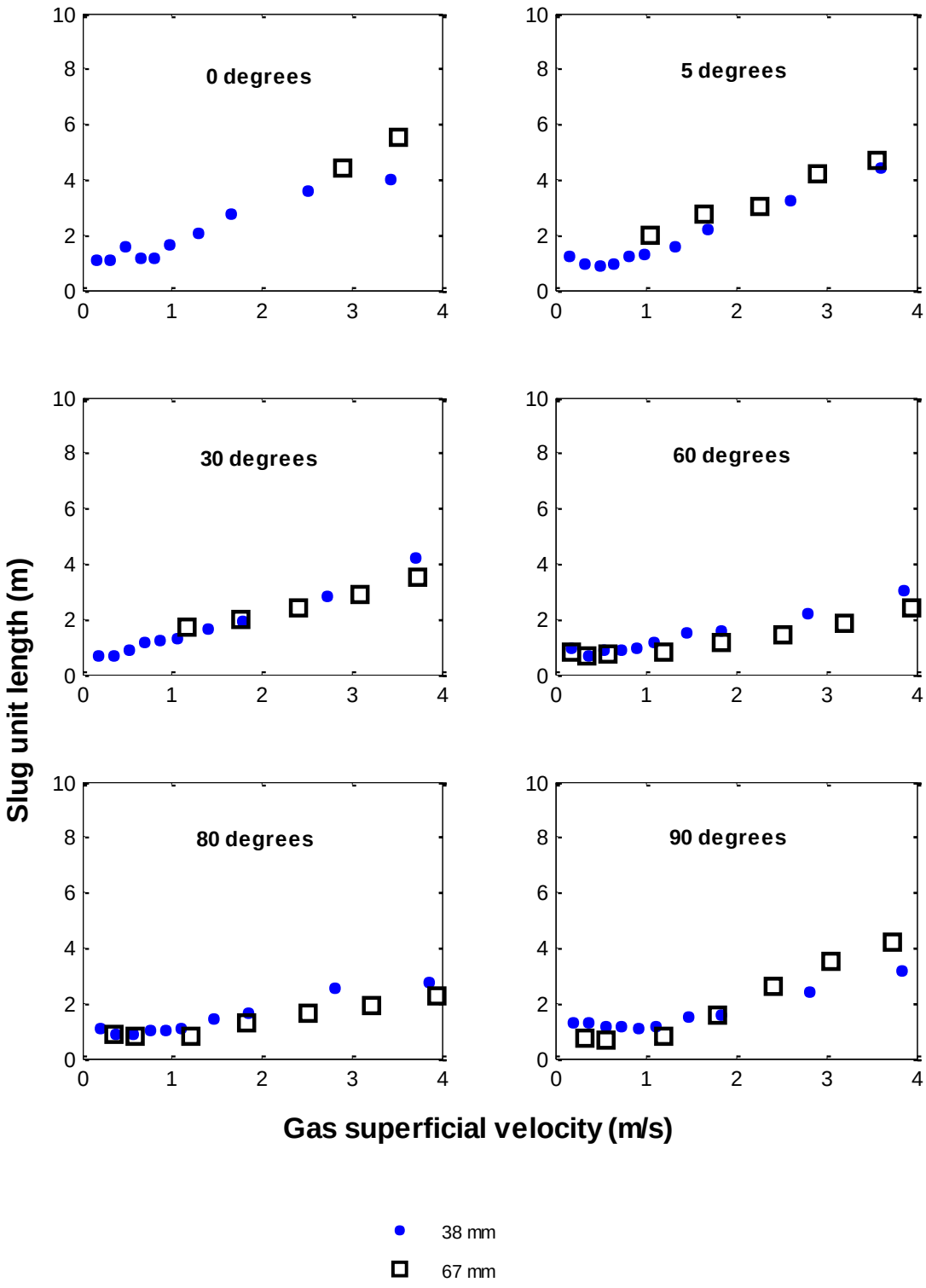

Figure 5.22 Slug unit length as a function of the gas superficial velocity. 67 mm pipe and U_{SL}=0.7 m/s.

5.8 Validation of the capacitance probes with Wire-Mesh Sensor

In order to validate the data obtained with the capacitance probes, a comparison was performed between the capacitance probes and a Wire-mesh sensor. The sensor consists of two electrode grids with 24 electrodes each, placed at an axial distance of 1.5 mm behind each other. Its function is based on the measurement of the local instantaneous conductivity of the two-phase mixture. The conductivity is measured at the crossing points of the wires of the two grids. This results in 24x24 sensitive points, which are equally distributed over the cross section (Figure 5.22).

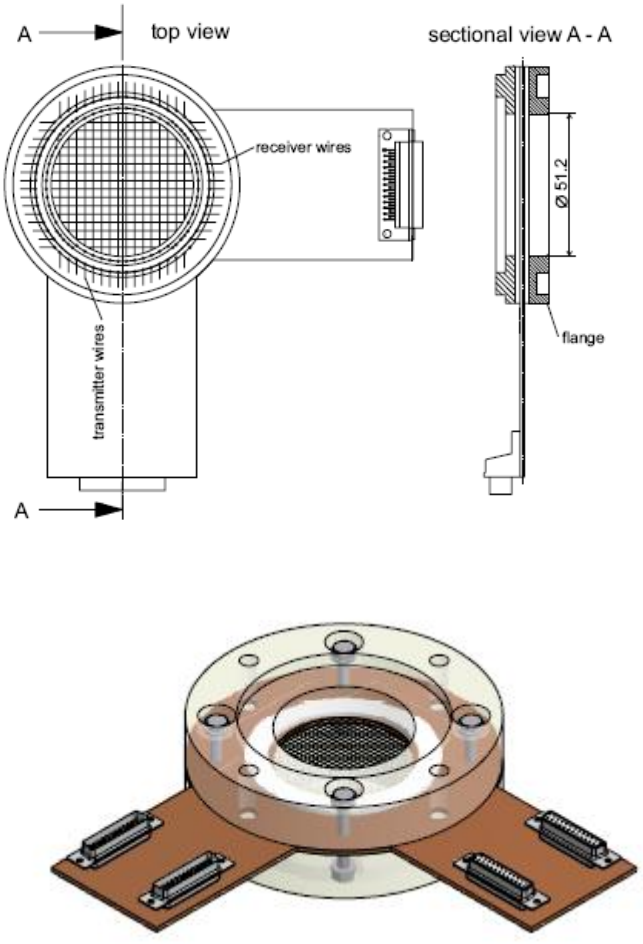

Figure 5.23 Wire-mesh sensor (2x24 electrode wires).

The wires have a diameter of 120 µm. For the conductivity measurement, one plane of electrode wires is used as transmitter, the other as receiver plane. A thorough description of the Wire-mesh sensor can be found in Prasser *et al.* (1998). In Figure

5.23 the comparison is presented, only the first probe is presented, the second probe is used mainly to determine the translational velocity by cross correlation with the first one. Even though there are some differences, the capacitance probes are good considering that they are much more simple devices. Based on this comparison, liquid holdup uncertainty is presented in appendix C.

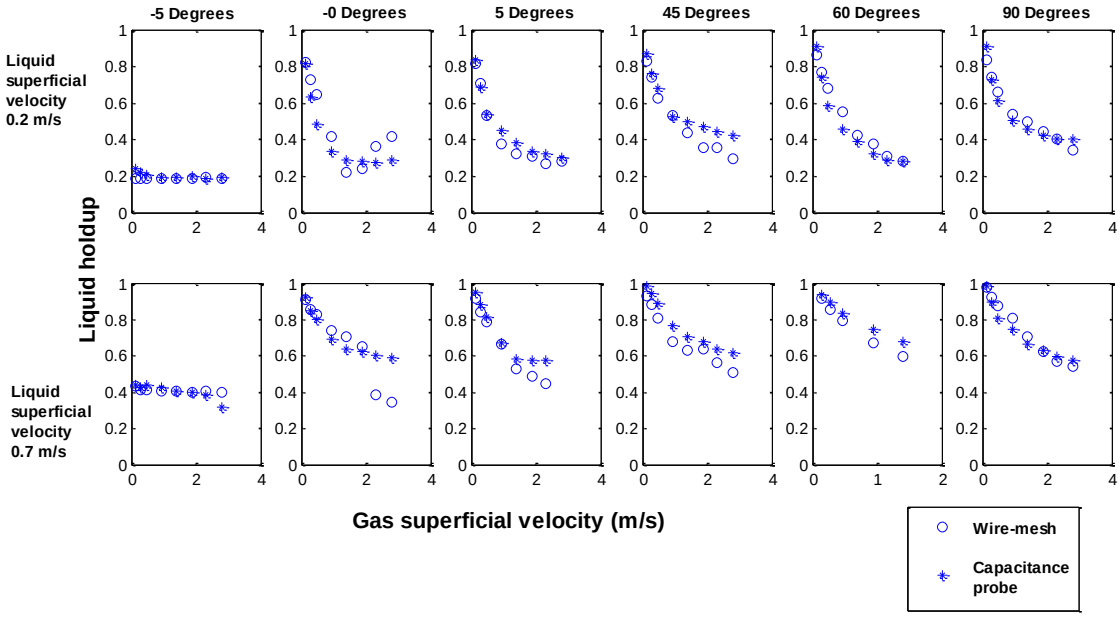

Figure 5.24 Comparison of the average liquid holdup obtained with the capacitance probes and wire-mesh-sensor.

The wire mesh sensor was used to take data for similar flow conditions and inclinations as the ones presented in the present chapter. These data are being processed and its analysis is suggested in section 7.2 as a recommendation for another future work.

5.9 Summary

Experimental data have been presented in this chapter for a 67mm diameter pipe and compared with data obtained with a 38 mm pipe. In this section, a brief summary of the results discussed in this chapter will be made.

For the range of flow conditions studied in the present work: It is an interesting finding to observe that at liquid superficial velocity of 0.2 m/s no effect of the pipe diameter on the average liquid holdup was observed, however when the liquid flow rate is increased to 0.7 m/s, the holdup tends to be slightly higher for the bigger pipe diameter. The same tendency occurs with the pressure gradient, since it strongly depends on the liquid holdup, particularly for steep inclination angles and lower gas flow rates.

The structure velocity follows a linear trend as a function of the mixture velocity for both pipes, but it is higher for the bigger pipe diameter. This due to the fact that as found by Van Hout *et al.* (2002), the drift velocity for continuous slug flow is enhanced by the dispersed bubbles in the liquid slug body. These dispersed bubbles contribute to the drift velocity by coalescing with the elongated bubble at its nose. Therefore, the drift velocity contribution calculated assuming stagnant liquid is very small compared to the discrepancies found.

In most cases no effect of the pipe diameter on the frequency was observed, it is with U_{SL}= 0.2 m/s and inclination angles close to vertical when the frequency for the bigger diameter pipe was higher. Frequency behaviour is slightly disturbed at low gas superficial velocities, however by increasing the gas superficial velocity at some point the frequency is fairly the same for both pipe diameters and follows the same tendency. Frequency values have been calculated for all the conditions, however not all of them might correspond to slug flow. A new correlation for slug frequency has been developed for vertical flow and it has been extended to cover inclination angles from 0 to 90 degrees

For a fixed flow condition, an increase in pipe diameter increases the turbulence of the flow. This in turn produces bubble breakup and therefore it takes a higher gas flow rate to form a gas pocket, for slug flow. As a result more dispersed bubbles will be present within the liquid slug body for the bigger pipe diameter. The liquid slug length does not appear to be affected by the pipe diameter. In general, the liquid slug length remains constant with the pipe diameter in absolute terms (m), but in dimensionless form there is more variation (10 to 20 pipe diameters for 67mm compared with 10 to 30 pipe diameters for 38 mm).

Since it is the structure velocity and the holdup in the liquid slug body that are more affected by the pipe diameter, it can be deduced that the increase in the slug length and structure velocity is due to a more aerated liquid slug. Another way to look at it is that in order to maintain continuity for the phases (liquid), faster slugs will contain more dispersed bubbles and they will be longer.

The liquid slug length is inversely proportional to the frequency and seems to have a minimum around 60° where the frequency has a maximum. The total slug unit length varies in a similar way with the inclination angle.

Increase of pipe diameter displaces the bubbly-slug transition to the right hand side on the flow pattern map for inclined flow, and for horizontal stratified-slug transition is moved up.

Increasing pipe diameter, from 38 to 67 mm, on the two-phase mixture behaviour has been found to have some influence, yet bigger changes in the pipe diameter can produce a more significant effect.

Chapter 6

Modelling slug two-phase flow with CFD

In the present work the hydrodynamics of slug two-phase flow has been simulated using Computational Fluid Dynamics. While gas-liquid flow behaviour, even in simple pipe geometries, is a very complex phenomenon to model, understanding the mechanisms governing co-current gas-liquid flow in inclined conduits is of great practical and industrial importance. However, the literature review reveals that no effort has been made (to the best of our knowledge) to arrive at a numerical modelling of continuous slug flow in inclined pipes. Most work has been directed to the motion of single Taylor bubble in vertical pipe, Mao and Dukler (1990), Clarke and Issa (1997), Brauner and Ullmann (2004), Ndinisa *et al.* (2005) and a few for horizontal flow, e.g., Frank (2005). Therefore the objective of this study involves both assessment of the capabilities of using CFD to simulate two-phase flow and its use to understand the flow by taking advantage of the capabilities of the numerical techniques to yield transient, 3D full volume information of the flow field for the two phases in slug flow regime.

In this chapter, a description of the CFD model and the results obtained will be presented. The results presented here include the phase distribution, velocity field and pressure. In order for the simulation to be useful, the results that it yields must be a realistic representation of a fluid in motion. Therefore, the simulation was run under similar conditions as those used in the experiments so that a proper comparison between experiments and CFD results can be performed. The agreement is found to be qualitatively good though.

6.1 Description of the problem

Before presenting the respective results in Section 6.2 some common generic features of the simulations will be stated in this section and the particular features for each individual case (inlet flow condition) will be revealed in the corresponding section. Several two-phase slug flow cases were simulated in this work using the commercial CFD code FLUENT 6.1 in order to solve the governing equations. The simulations were conducted on a Sun Microsystems Inc. server operating on UNIX Release 5.9 operating system. Since the UNIX server was a machine shared by multiple users, the run times were different depending upon the amount of load on the machine at the time a particular run was conducted. Estimated run times are included Table 6.6.

6.1.1 Geometry

The experimental arrangements were described in detail in Chapter 3. The general geometry for the case studies modelled is illustrated in Figure 6.1; it consists of a 38 mm internal diameter pipe and 6 m long. Two different cases were studied: a horizontal pipe and a pipe inclined at 45 degrees. The pipe axis is always aligned with the *x* axis and several measurements sections can be placed along the pipe.

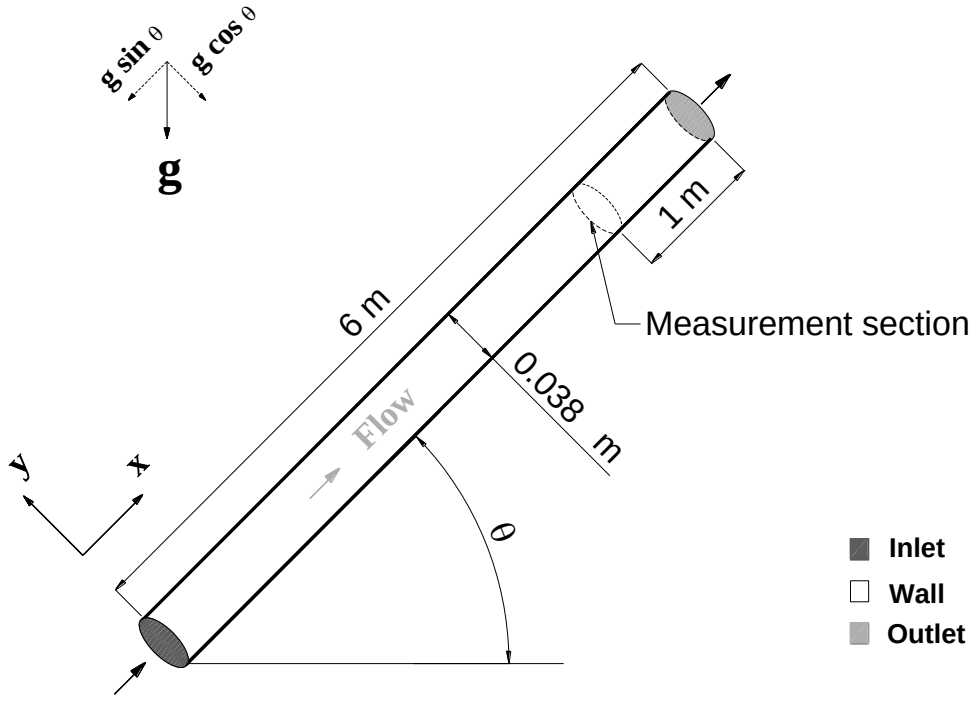

Figure 6.1 Inclined pipes geometry and zones of the computational flow domain**.**

6.1.2 Flow Specification

As it is done in the experimental work, the air and water flows are supplied at the inlet section of the computational flow domain (pipe), then the two-phase mixture flows along the pipe and is finally discharged through the outlet at atmospheric pressure.

6.1.2.1 Fluid properties

The relevant properties of the two fluids (air and water) used in the simulation are as given in Table 6.1.

Table 6.1 Materials properties

Fluid	Density (kg/m^3)	Viscosity (kg/ms)	Surface tension (N/m)
Air	1.224	0.000018	0.072
Water-liquid	999.98	0.001	

6.1.2.2 Boundary conditions

The boundary conditions are specifications of flow properties on the computational domain boundaries. They are, therefore, a critical component of the CFD simulations in terms of representing the experimental configuration of the two-phase flow through the pipe. Hence the boundary conditions were chosen based on the experimental setup described in Chapter 3. These conditions are summarized in Table 6.2.

At the inlet, a velocity-inlet boundary type is used in which the mixture velocity and the liquid volume fraction are specified. The velocity profile is assumed to be uniform. This approach requires no additional experimental knowledge about the slugs in order to setup the numerical simulation. This is also similar to the way experimental work has been carried out (see Chapter 3 for details about the mixing section design). The inlet values for turbulent kinetic energy, *k*, and its dissipation rate, ε, are estimated with the following equations, Launder and Spalding (1974):

$$k = \frac{3}{2} I^2 U^2_{in} \tag{6.1}$$

$$\varepsilon_{in} = 2k_{in}^{3/2} / d \tag{6.2}$$

Where *d* is the pipe diameter, and the turbulence intensity for fully developed pipe flow, $I = 0.16\mathrm{Re}^{-1/8}$. The walls of the pipe are assumed to be rigid and impermeable, in which the wall roughness was set as a smooth wall. A no-slip condition is applied to the velocity where there is contact at solid walls at any instant. Close to the wall, the standard wall function approach based on the proposal of Launder and Spalding (1974) and implemented in FLUENT was employed to predict flow accurately close to walls by modelling turbulent boundary layer. The pressure and liquid volume fraction at the wall are described by a zero gradient condition since the volume fraction can not diffuse into the wall. At the outlet, the remaining variables are transported out of the computational domain with zero average static pressure so that the mass balance is satisfied. Operating conditions were specified as being standard atmospheric pressure (101.3 kPa) and temperature 20 °C. Gravity effects are accounted for and the acceleration of gravity taken to be -9.81 m/s^2 on the vertical.

Table 6.2 Boundary conditions

```
      Zone Name          id   type
      ------------------------------------
      Fluid               2    Fluid
      Wall                3    Wall
      Outlet              4    outflow
      Inlet               5    velocity-inlet
Boundary Conditions
-------------------
      Wall
         Condition                      Value
        ------------------------------------
         Wall Roughness Constant         smooth wall
      Outlet
         Condition             Value
         --------------------------
         Flow rate weighting   1
      Inlet
         Condition                                Value
         ---------------------------------------------
         Velocity Magnitude                       1.6
         X-Component of Flow Direction            1
         Turb. Kinetic Energy                     0.025
         Turb. Dissipation Rate                   0.0072
```

6.1.2.3 Initial conditions

At *t=0* s all velocity components are set to 0 m/s. For the liquid volume fraction, the specified initial condition depended on the case under study; for horizontal pipe an

initial condition of perfectly mixed phases throughout the flow domain was set whereas for the inclined flow case the initial condition was the pipe full of either air or water. These initial conditions ease the convergence process. In addition, an initial guess for the turbulent kinetic energy and the dissipation rate was applied in all simulations studied.

6.1.3 Multiphase model

The first step in solving any multiphase problem is to determine which of the flow regimes best represents the investigated scenario. In the present work, isothermal motion of an incompressible two-phase flow is considered. The condition of slug two-phase flow has been simulated with the Volume of Fluid (VOF) model of Hirt and Nichols (1981) based on Eulerian-Eulerian approach, since it is a model suitable for this flow regime and computationally efficient, Cook and Behnia (2001). VOF is an interface tracking technique that captures the interface between the phases. This powerful tool allows the simulation of complex free surface flows with an arbitrary shape in any situation included folding or break-up, Kvicinsky *et al.* (1999). As long as the interface resolution and conservation of mass, momentum, and energy is ensured by use of proper numerical techniques, the VOF method is accurate enough to capture essential flow features around the free-surface Rhee *et al.* (2004). It is even possible to handle mass and heat transfer through the interface using the VOF method. Compared with the interpenetrating-continua (two-fluid model) formulation, the interface tracking approach (VOF) can be thought of as a Direct Numerical Simulation (DNS) of interface motion (not of turbulence), where no closure assumptions for the interfacial area evolution are needed, Lakehal *et al.* (2002).

The VOF formulation relies on the fact that two or more fluids (or phases) are not interpenetrating. For each additional phase that is added to the model, a variable is introduced: the volume fraction of the phase in the computational cell. The fields for all variables and properties are shared by the phases and represent volume-averaged values, as long as the volume fraction of each of the phases is known at each location. A single momentum equation is resolved throughout the domain, and the resulting velocity field is shared among the phases and to maintain the mass balance in the system the continuity equation is also solved. The body forces in the momentum

equation consist of gravitational force and surface tension, in VOF surface tension is introduced by adding a momentum source. The momentum equation, equation (6.4), is dependent on the volume fractions of all phases through the properties ρ and μ. Once the Reynolds averaging approach for turbulence modelling is applied, the Navier-Stoke equations can be written in Cartesian tensor form as:

$$\frac{\partial \rho}{\partial t} + \frac{\partial (\rho u_j)}{\partial x_j} = 0 \tag{6.3}$$

$$\frac{\partial}{\partial t}(\rho u_i) + \frac{\partial}{\partial x_j}(\rho u_i u_j) = -\frac{\partial P}{\partial x_i} + \frac{\partial}{\partial x_j}\left[\mu_{eff}\left(\frac{\partial u_i}{\partial x_j} + \frac{\partial u_j}{\partial x_i} - \frac{2}{3}\delta_{ij}\frac{\partial u_i}{\partial x_i}\right)\right] + \frac{\partial}{\partial x_j}\left(-\rho\overline{u'_i u'_j}\right)_i \tag{6.4}$$

where u_i is the i component of the fluid velocity u, x_j is the j spatial coordinate, P is the static pressure, μ_{eff} is the effective viscosity as detailed in 6.1.4, δ_{ij} is the Kronecker delta and $-\rho\overline{u'_i u'_j}$ the Reynolds stresses

The tracking of the interface(s) between the phases is accomplished by the solution of a continuity equation for the volume fraction (α) of one (or more) of the phases. For the q_{th} phase, this equation has the following form:

$$\frac{\partial \alpha_q}{\partial t} + \frac{\partial (\alpha_q u_j)}{\partial x_j} = \frac{S\alpha_q}{\rho_q} \tag{6.5}$$

Where S is a source, the volume fraction equation will not be solved for the primary phase; the primary-phase volume fraction will be computed based on the constraint:

$$\sum_{q=1}^{n} \alpha_q = 1 \tag{6.6}$$

For the calculation of fluxes at control volume faces required by the VOF model, the geometric reconstruction scheme was used.

6.1.4 Turbulence model

Turbulence must be considered in the numerical simulation since even in low flowing rate, the Taylor bubble rising through the liquid creates a developing film around itself and a wake at its tail. In order to simulate turbulence, the standard *k*-*ε* model (Launder and Spalding (1974)) was used for several reasons; the model is simple, is implemented in many commercial codes, the pipe geometry is not complicated and it has demonstrated capability to simulate properly many industrial processes, including multiphase flow, Ramos-Banderas *et al.* (2005), Cook and Behnia (2001) among others. The model is described by the following equations:

$$\rho u_j \frac{\partial k}{\partial x_j} = \frac{\partial}{\partial x_j}\left(\frac{\mu_t}{\sigma_k}\frac{\partial k}{\partial x_j}\right) + \mu_t \frac{\partial u_j}{\partial x_i}\left(\frac{\partial u_i}{\partial x_j} + \frac{\partial u_j}{\partial x_i}\right) - \rho\varepsilon \tag{6.7}$$

$$\rho u_j \frac{\partial \varepsilon}{\partial x_j} = \frac{\partial}{\partial x_j}\left(\frac{\mu_t}{\sigma_\varepsilon}\frac{\partial \varepsilon}{\partial x_j}\right) + C_1 \mu_t \frac{\varepsilon}{k}\frac{\partial u_j}{\partial x_i}\left(\frac{\partial u_i}{\partial x_j} + \frac{\partial u_j}{\partial x_i}\right) - C_2 \frac{\varepsilon}{k}\rho\varepsilon \tag{6.8}$$

In the above equations, k is the turbulent kinetic energy; ε is the dissipation rate of k. σ_k, σ_ε, C_1 and C_2 are constants whose values are 1.0, 1.3, 1.44 and 1.92 respectively, u_i is the i component of the fluid velocity u, x_j is the j spatial coordinate. The fluid viscosity must be corrected for turbulence in the Navier-Stokes equations employing an effective viscosity $\mu_{eff} = \mu + \mu_t$ where μ is the dynamic viscosity and μ_t is the turbulent viscosity.

Table 6.3 Models used in the simulation

Model	Settings
Space	3D
Time	Unsteady, 1st-Order Implicit
Viscous	*k*-*ε* turbulence model
Wall Treatment	Standard Wall Functions

6.1.5 Discretisation and method of solution

In order to numerically solve the system of partial and ordinary differential equations, discretisation of the equations has been carried out using a Finite Volume Method (FVM) with an algebraic segregated solver and co-located grid arrangement as implemented in FLUENT 6.1. In this grid arrangement pressure and velocity are both stored at cell centres. Details of the discretisation (FVM) can be found elsewhere (e.g. Versteeg and Malalasekera (1995)) and are hence omitted here. Since FLUENT uses a segregated solver, the continuity and momentum equations need to be linked. Various techniques are reported in the literature and available in FLUENT. However, The PISO algorithm which stands for Pressure Implicit with Splitting of Operators, of Issa (1986) was employed because of its good performance to find a fast converged solution, Ramos-Banderas *et al.* (2005). PISO is a pressure-velocity calculation procedure that involves one predictor step and two corrector steps. It is recommended in FLUENT for unsteady flow problems.

6.1.6 Solver controls

All simulations in this work are performed under time dependent conditions. For the time dependent solution scheme, the main controlling factor is the time step. This is set to give a small number of time steps as possible whilst maintaining a smoothly converging solution. If a large time step is chosen, then the solution changes too much and is therefore likely to diverge.

Inside each time interval iterations are carried out to resolve the transport equations for that time step. As long as the time step is small enough to get convergence, the smaller the time step, the fewer iterations, per time step are required. For this iteration process to converge, it may be necessary to control the change of the variables from one iteration to the next. This is achieved with under relaxation factors. Under relaxation factors of 0.3, 0.7 and 0.8 respectively were applied on pressure, momentum and turbulence kinetic energy parameters as recommended by FLUENT.

A measure of how well the solution is converged can be obtained by plotting the residuals errors for each equation at the end of each time step. For a well-converged

solution, the maximum residual obtained was set to be around 10^{-5}; typically the Root Mean Square residual will be an order of magnitude lower than this.

Table 6.4 Solver controls

Unsteady Calculation Parameters	
Time Step (s)	0.0001
Max. Iterations Per Time Step	100

Discretization Scheme	
Variable	Scheme
Pressure	Body Force Weighted
Pressure-Velocity Coupling	PISO
Momentum	Second Order Upwind
Turbulence Kinetic Energy	Second Order Upwind
Turbulence Dissipation Rate	Second Order Upwind

An increase of a residual after any particular time step does not necessarily imply that the solution is diverging. It is usual for residuals to occasionally get larger, especially at the beginning of a run. Reducing the under relaxation factors to extremely low values, say 0.01, will cause the residuals to drop. A typical residual plot for a run which has converged quickly is shown below.

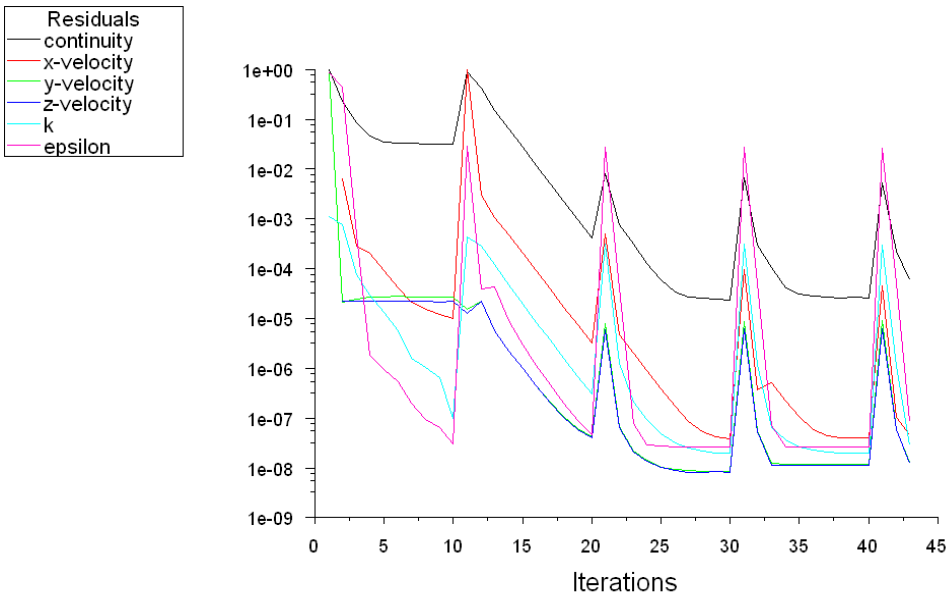

Figure 6.2 Example of plot of residuals

6.1.7 Mesh

The mesh is an integral part of the numerical solution and must satisfy certain criteria to ensure a valid, and hence accurate solution, Lun *et al.* (1996). In this work, the mesh was developed using Gambit 2.0 and imported into FLUENT 6.1 where the calculations were performed.

Gambit 2.0's mesh generation tools offer the capability to parametrically create grids from geometry in multi-block structured, unstructured hexahedral, tetrahedral, hybrid grids consisting of hexahedral, tetrahedral, pyramidal and prismatic cells and Cartesian grid formats combined with boundary conditions. Within the 3D geometries, different mesh schemes were tested ranging from unstructured tetrahedral to structure hexahedral arrangements.

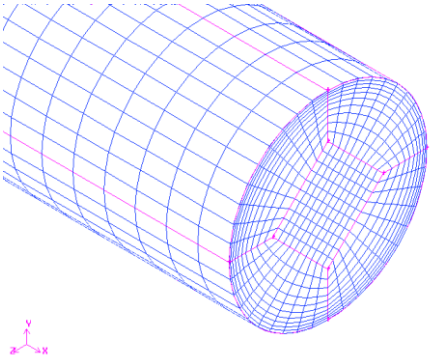

Figure 6.3 Typical computational domain grids representing the flow domain discretization for a deviated pipe

From the preliminary tests it was observed that for the case of tetrahedral unstructured scheme, it is more difficult to reach convergence, since rapid changes in cell volume between adjacent cells translate into larger truncation errors.

It was found that the ratio of elements to nodes is approximately 5:1 for a tetrahedral mesh. For example, when there were 34 000 tetrahedral elements in a mesh, there were approximately 7 000 nodes. This is in contrast to a hexahedral mesh where the ratio of elements to nodes approaches 1:1 as the grid becomes large, Table 6.5. The memory required for a tetrahedral mesh is about 0.4 times the memory required for a hexahedral mesh of the same number of elements. Alternatively a tetrahedral mesh has about twice the memory of a hexahedral mesh with the same number of nodes.

A structured hexahedral grid is more suitable when solving the case under study since there is more control to obtain a fine cross sectional mesh without the need to have and equivalent longitudinal one. Then it would make the solution process convergence faster. However due to the cylindrical shape of the geometry it is not easy to directly place a hexahedral mesh. For the cells at the corners, skweness (defined as the difference between the cell's shape and the shape of an equilateral cell of equivalent volume) will increase when the mesh density is increased as the hexahedral elements are opened out to almost 180 degrees and quality is poor, as a result accuracy decreases and the solution destabilizes.

Table 6.5 Comparison of tetrahedral and hexahedral grids

	Cells	Faces	Nodes	Memory (kB)
Tetrahedral	4347	9225	1029	297
	34776	71676	6935	2061
Hexahedral	6400	20580	7855	1169
	51200	159120	56889	5767

The final mesh adopted to perform the full 3dvolume simulations, shown in Figure 6.3, is called an O-Grid and is an ideal configuration to make use of the hexahedral mesh properties. The mesh has good aspect ratio cells with limited skewness. It allows for a good representation of the boundary layer and it is adequately stretched along the longitudinal axis. Grid refinement was used to achieve finer resolution. A full domain is considered as the flow was found not to be symmetrical.

The region near the wall is meshed finer than the rest of the cross section, as it contains the maximum amount of gradients. When using wall functions, we need to know the distance of the first node above the wall, $y(1)$ so that the normalized wall distance (y^+) values remain within 20-100. The following equation is used, Gambit manual (2003)

$$y = y^+ L/(\mathrm{Re}\sqrt{\frac{C_f}{2}}) \tag{6.9}$$

Here L is the characteristic length, the diameter in case of a circular pipe. In a pipe, $C_f/2 = 0.039 * (Re^{-0.2})$. This gives an approximate idea of the value of y.

6.2.8 Grid convergence study

CFD numerical simulations are computationally very expensive. One of the most significant factors influencing the computation time is the size of the computational grid specified by the user. In order to identify the minimum mesh density to ensure the solution is independent of the mesh resolution, a mesh sensitivity analysis has been carried out, in the construction and analysis of the CFD model.

Three 3D and three 2D meshes were investigated in the present study (Table 6.6) for the general case of a geometry consisting of a 45° inclined pipe as illustrated in Figure 6.1 and a suitable grid resolution has been found.

Since slug two-phase flow is characterised by liquid holdup fluctuation, one aspect that is interesting to look at is the time trace of liquid holdup. Furthermore time variant liquid holdup was obtained experimentally.

For the CFD model, in order to determine the holdup time series, the following procedure is performed: Within the pipe geometry, a cross sectional area (measurement section in Figure 6.1) is defined and the Area-Weighted Average value of the liquid volume fraction is calculated over the surface. The area-weighted average of the volumetric fraction of liquid is computed by dividing the summation of the product of the liquid volume fraction and facet area by the total area of the surface as follows:

$$\frac{1}{A}\int H_L A = \frac{1}{A}\sum_{i=1}^{n} H_L |A_i| \tag{6.10}$$

Finally the value of liquid holdup in this surface is recorded every time step.

Experimental liquid holdup time series was described in previous chapters. However it is important to point out the averaging over the probe electrodes length (50 mm). Then the capacitance sensor gives a volume averaged liquid holdup at each point in time.

First the meshes were tested with an inlet flow condition of small inlet velocity (U_m = 0.1 m/s and 0% liquid). An initial condition of domain full of water was used. This is similar to the simulation of a single Taylor bubble flowing in stagnant liquid. But in this case an initial gas bubble was formed at the bottom of the liquid filled pipe by entering a continuous flow of gas and the two-phase flow domain interaction allowed the development of the bubble over time until the terminal bubble rise velocity and shape were reached. Therefore, there was no need to specify a well defined 2D or 3D bubble.

Table 6.6 Mesh profiles

Case	Domain	Structure	Nodes	Cross section x length	Run time (hours) per 1 s real time*
Mesh-1	2D	Quadrilateral	3900	13x300	1
Mesh-2	2D	Quadrilateral	12000	20x600	4
Mesh-3	2D	Quadrilateral	36000	30x1200	100
Mesh-4	3D	Hexahedral	60000	100x600	50
Mesh-5	3D	Hexahedral	141000	189x746	100
Mesh-6	3D	Hexahedral	500000	500x1000	1000

The velocity of the Taylor bubble U_b is given quite accurately, Weber *et al.* (1986) by the relation from Nicklin *et al.* (1962)

$$U_b = C_0 U_m + U_d \tag{6.11}$$

Where is U_m is the mixture velocity and the coefficient C_0 accounts for the velocity and void fraction variations over the pipe cross section. In this equation, the second term in the RHS describes the velocity of Taylor bubble and it can be calculated as proposed by Bendiksen (1984):

* See section 6.1

$$U_d = U_d^h \cos\theta + U_d^v \sin\theta \tag{6.12}$$

Where U_d^h and U_d^v correspond to the drift velocity for the horizontal and the vertical case respectively. A calculation was performed to compare the performance of these meshes. The time calculated for the bubble to reach the measurement section turned out to be 11.4s. The plot of the time history of liquid volume fraction for the 5 meshes is shown in Figure 6.4, it can be seen that the full 3D simulation performs better than a 2D case as the Taylor bubble rise velocity calculated is closer to the one predicted by the theoretical expression.

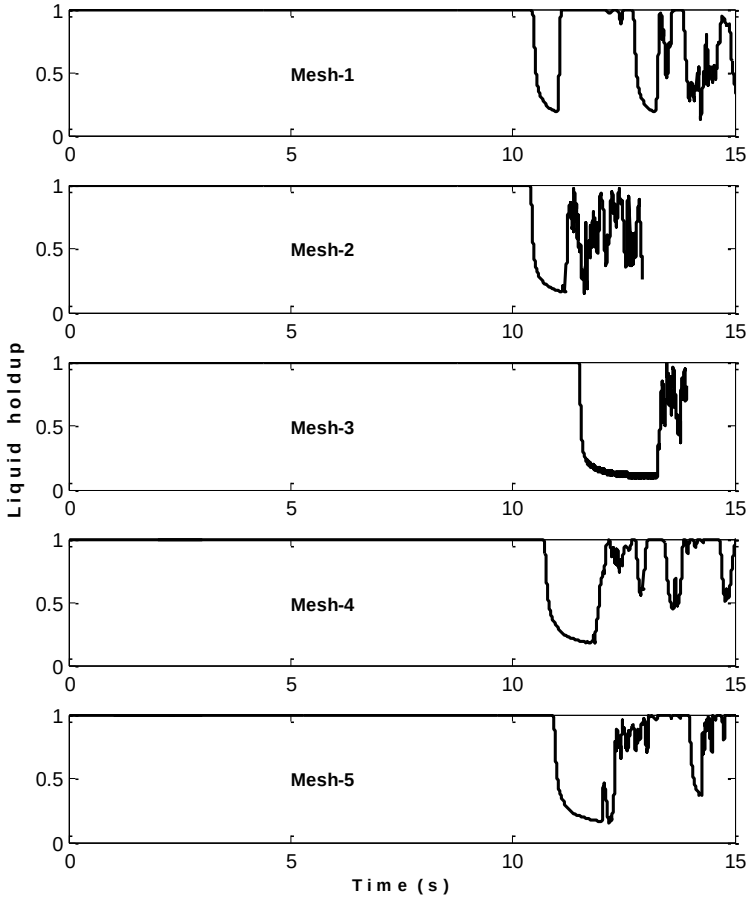

Figure 6.4 Effect of grid size on CFD simulation results. Time traces of liquid volume fraction for input liquid fraction 0 %, mixture velocity 0.1 m/s, 132d and 45° inclined flow.

In order to observe the response to the velocities the meshes were tested with a larger inlet flow condition. In this case an inlet flow condition (U_m = 1.63 m/s and Liquid

volume fraction=0.45) and initial condition of domain full of air was used. A comparison of the respective results is shown in Figure 6.5. It takes slightly less than 4s for the liquid to arrive to the measurement section located at x=132d from the inlet for mesh-1, mesh-2 and mesh-3 which are in 2D whereas for the meshes in 3D (mesh-4, mesh-5 and mesh-6) it takes about 4.5 s.

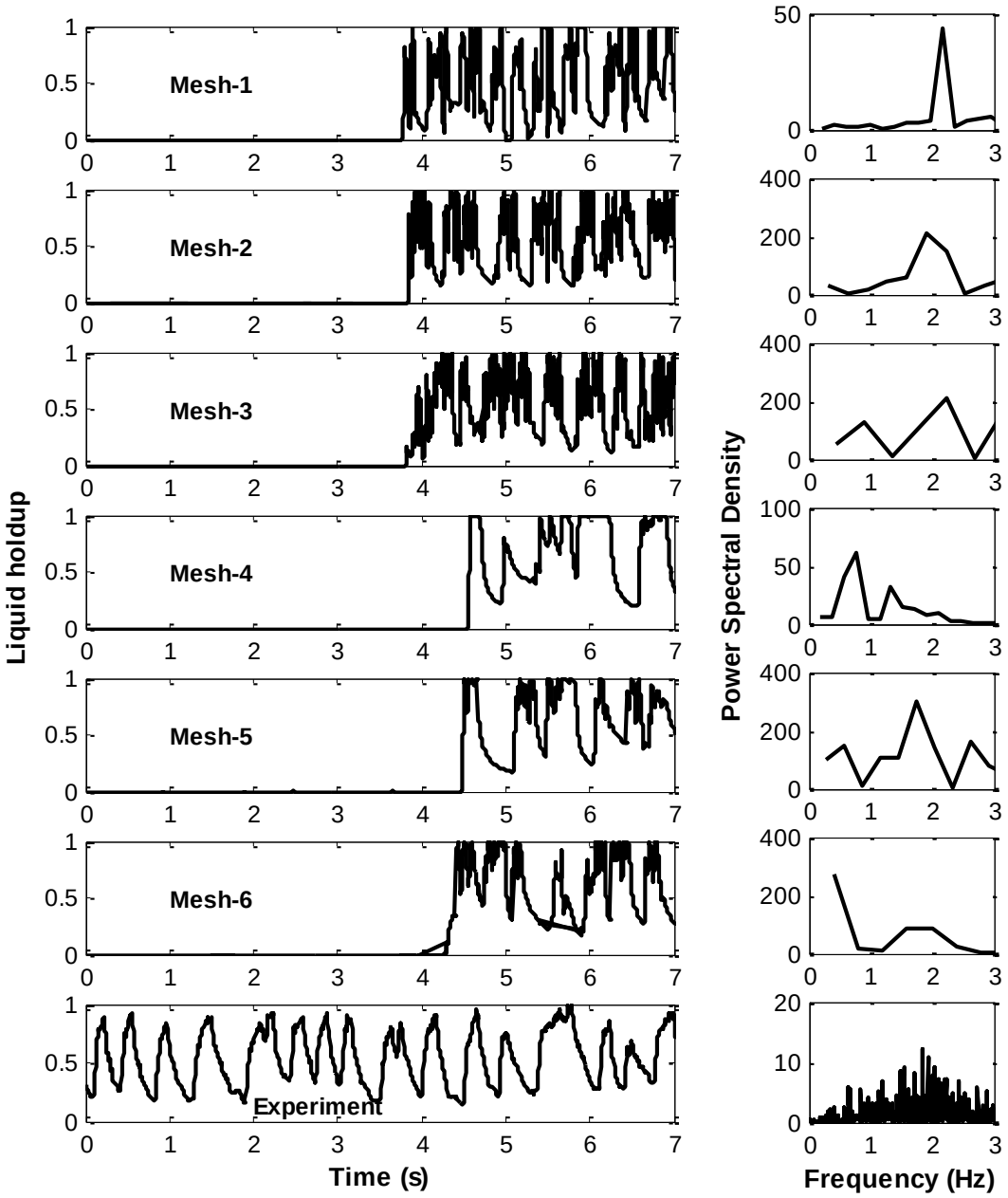

Figure 6.5 Effect of grid size on CFD simulation results. Time traces of liquid volume fraction for input liquid fraction 44.5 %, mixture velocity 1.63 m/s, 132d and 45 ° inclined flow**.**

The Power Spectral Density (PSD) predicts that the frequency is about 2 Hz for all of the cases including the experiment, except for mesh-4, which is a very coarse mesh. Thus the main difference is found between 2D and 3D meshes. This is not a surprise, since the 2D simulation does not take into account the shape of the cross sectional area of the pipe, which in turn affects the shape of the front of the bubbles. Therefore the flow is not symmetric and needs to be simulated with full 3D geometry.

It was observed that when the mesh is too coarse a refinement in the mesh can have a considerable influence on the result, as shown in Figure 6.5 from mesh-4 to mesh-5. However the time series of liquid holdup from mesh-5 and mesh-6 give a quite similar approximation to the experimental holdup time trace.

It was found from the comparison of results of mesh sensitivity analysis in Figures 6.4 and 6.5 that the mesh sensitivity does not appear to depend on the flow conditions (within this range of velocities). For both conditions, the mesh has an effect on the result, which is proportional to the result itself. This can be backed up by the fact that for a given grid size, the residence time of a fluid particle in a cell ($t=x/u$) decreases as the velocity increases as a result for a given time step (small enough to get convergence) the grid size required when the velocity increases will be larger. Also it was found that when the grid size is reduced, the maximum time step required to achieve convergence needs to be reduced accordingly.

Based on the mesh sensitivity analysis presented above, mesh-5 is chosen as it has been observed to perform better than or as well as the others and also it takes a shorter time than mesh-6 to complete each simulation. In addition, the basic idea was to develop a grid that can be suitable for the simulation of a wide range of inlet flow conditions which requires only a minimum of user attention in order to reduce the numerical restrictions of a correct code application.

It is not possible to give specific rules for the determination of both the grid size and the time step that will always give a converging solution; this can be explained by the fact that stability criteria of the Navier-Stokes equations cannot be found analytically. However it was found that a time step of the order of the residence time of a fluid

particle in a cell can give good convergence. Also it can be seen that for some parameters such as the translational velocity of the slug and the frequency, even a coarse mesh will provide useful information about the problem.

The numerical investigation of the distribution of the void fraction within an inclined pipe is also compared in Figure 6.6 and it can be seen, that phase interface is more grid dependent.

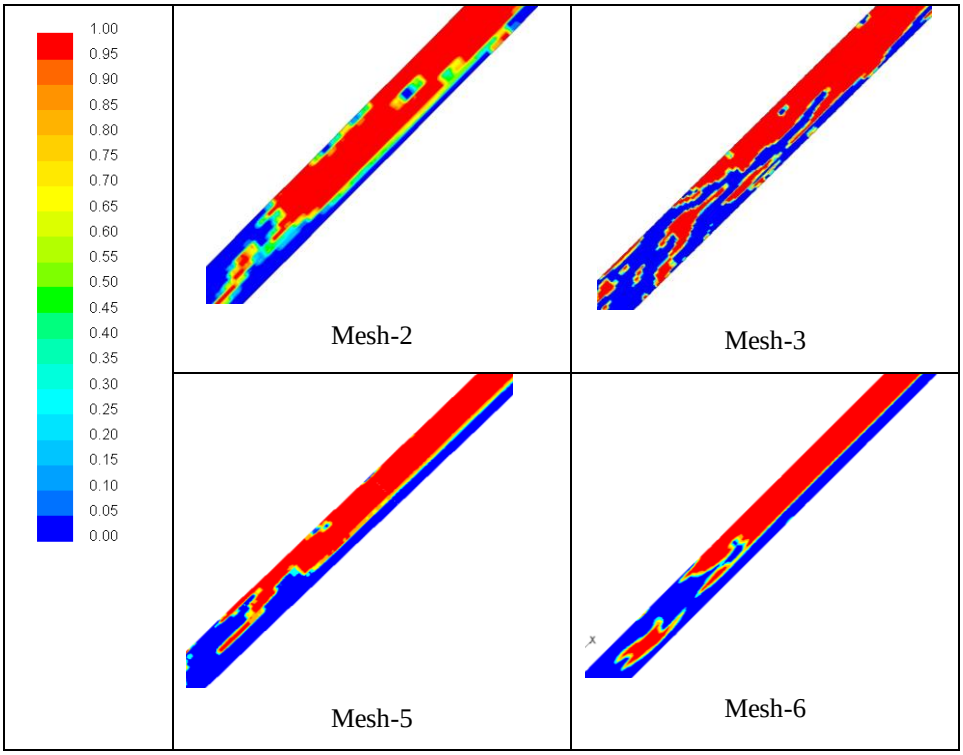

Figure 6.6 Effect of grid size on resolution of phase distribution for CFD simulation results. Contours of phase distribution of air for input liquid fraction 44.5 %, mixture velocity 1.63 m/s, and 45° inclined flow.

6.2 Validation and discussion of results

The test model was designed to provide a generic data set that exhibits general flow characteristics and also to investigate a particular flow scenario in detail. The prediction of how phases distribute in a flow field is of first order importance in developing a scientific approach to multiphase flow. This involves the specification of the type of flow pattern and a quantitative description of where the phases are located for a given pattern.

6.2.1 Horizontal pipe

After the first set of preliminary cases performed during the mesh sensitivity analysis, the next CFD case study performed in this work was the simulation of the slug two-phase flow in a horizontal pipe for the sake of simplicity compared to the inclined case.

In this case an inlet flow condition of U_m = 1.1 m/s and Liquid volume fraction=0.18 was used. As mentioned in Section 6.1, for the horizontal case an initial condition of fully dispersed flow inside the pipe was used. After an interval of liquid holdup fluctuation, the fluid in the domain eventually arranges itself into stratified flow regime and then slug initiates after a short period of time. The stratification process takes about 3 s. This process is shown in Figure 6.7 by means of the liquid holdup time series at a cross sectional area.

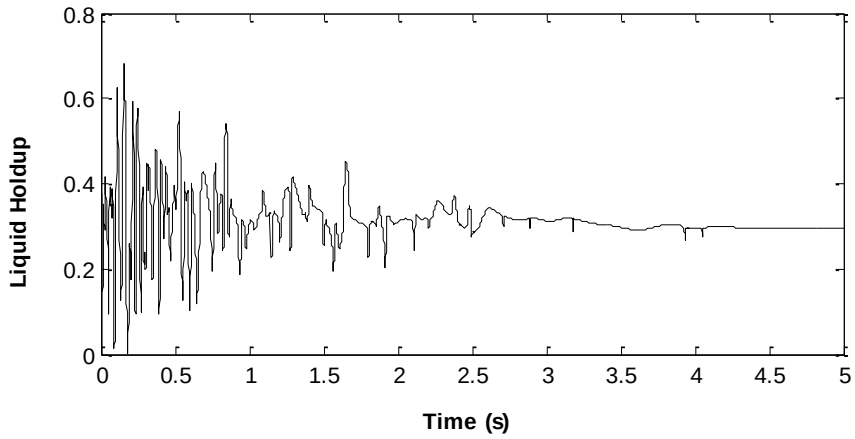

Figure 6.7 Stratification of the mixture from the initial condition of fully dispersed flow on horizontal pipe, Usl=0.2 m/s, Usg=0.9 m/s.

6.2.1.1 Slug formation

The process of slug formation occurring in a horizontal conduit following injection of air in a flowing liquid stream has been described by several investigators (Dukler and Hubbard (1975), Kordyban (1961), Kordyban (1985)). It is understood that slugs originate from unstable waves formed at the gas-liquid interface of a stratified flow, which eventually grows in amplitude to block the gas passage. This was confirmed by the results obtained with CFD as shown in Figure 6.8.

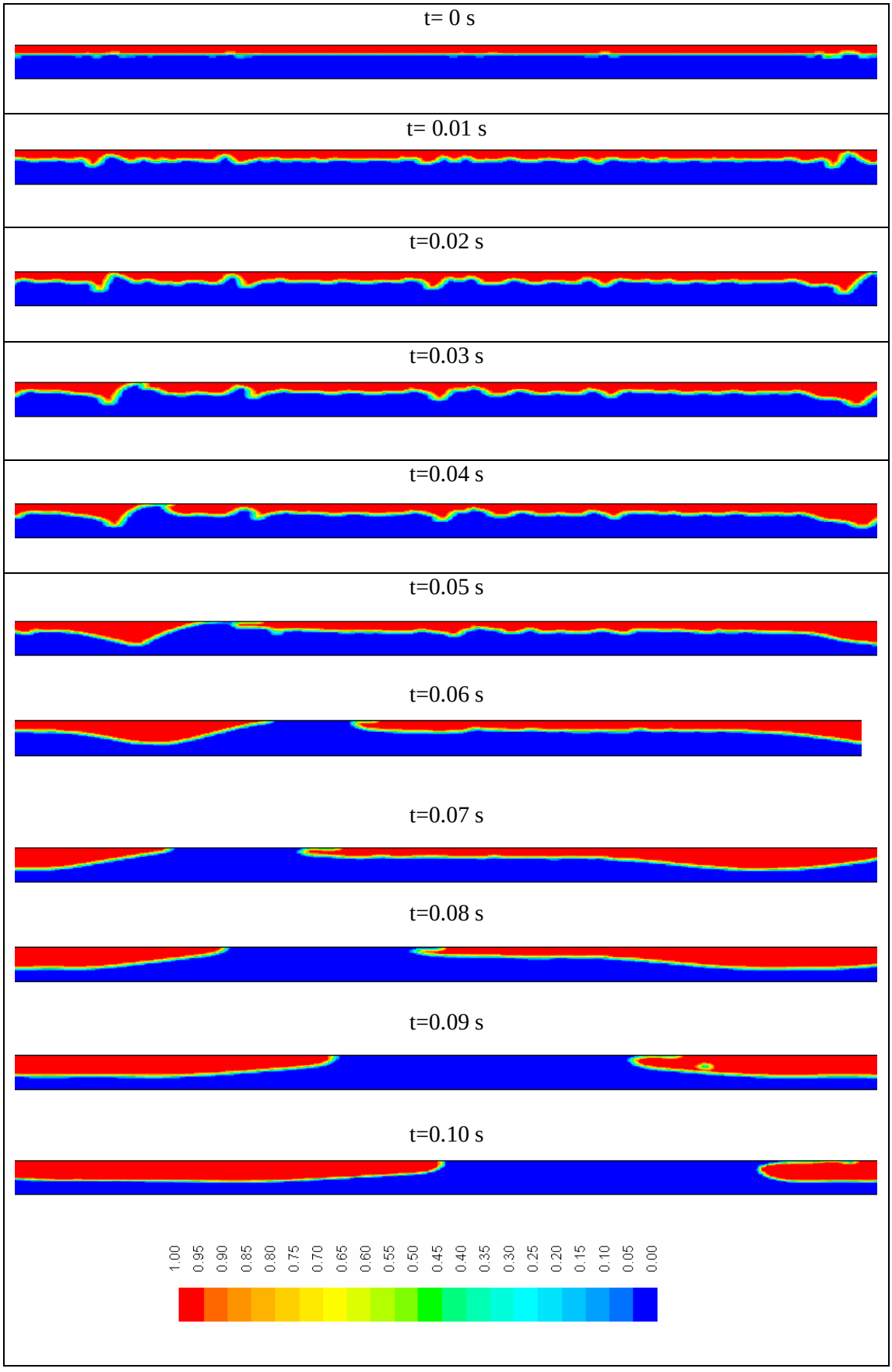

Figure 6.8 Contours of volume fraction of air for horizontal flow

In Figure 6.8 detail information on the phase distribution is presented by means of the contours of volume fraction of the phases. A sequence of instantaneous stages of the slug formation process is presented. These stages are 0.01 seconds separated from each other and both the liquid and gas velocities are kept constant at the inlet. The process is followed from a state where stratified flow exists in the domain, at that moment the time is considered as t=0 s.

The slug formation was studied by observing the behaviour of the gas-liquid interface initially under stratified conditions from the inlet until the slug was formed. Several disturbances appear in the gas-liquid interface along the pipe. Some of these disturbances develop into waves that begin to grow until eventually they reach the top of the pipe to form a liquid slug. The slug formation process occurs very quickly.

6.2.1.2 Development of the slug

Once a slug has been initiated, it is observed that it grows. In order to follow the development process of the slug, a set of time traces of liquid holdup are obtained at particular locations as indicated in Figure 6.9.

In the literature, it has been established that slugs grow by picking up more liquid in the front compare to the liquid that they leave behind, Dukler and Hubbard (1975).

The first cross sectional area, located 26 pipe diameters away from the inlet shows a series of insipient slugs, it can be seen that, these insipient slugs are characterised initially by slow growing but suddenly its growing rate changes to reach the peak and the wave bridges the whole section of the pipe. Therefore on the basis of the results in Figure 6.9, it is confirmed that slugs form as a result of local instability at the wave crest rather than due to instability of the whole wave, as suggested by, Kordyban (1985). The wave instability results from a "Bernoulli effect," which is responsible for a normal force component acting on the wave crest in the opposite direction of gravity.

On the contrary for a fully developed slug, Figure 6.9 (L/d=158), there is a fast growing holdup from a minimum value up to reach the peak and then it is followed by

a slow decrease of the holdup until it gets to the lowest value in the stratified liquid film.

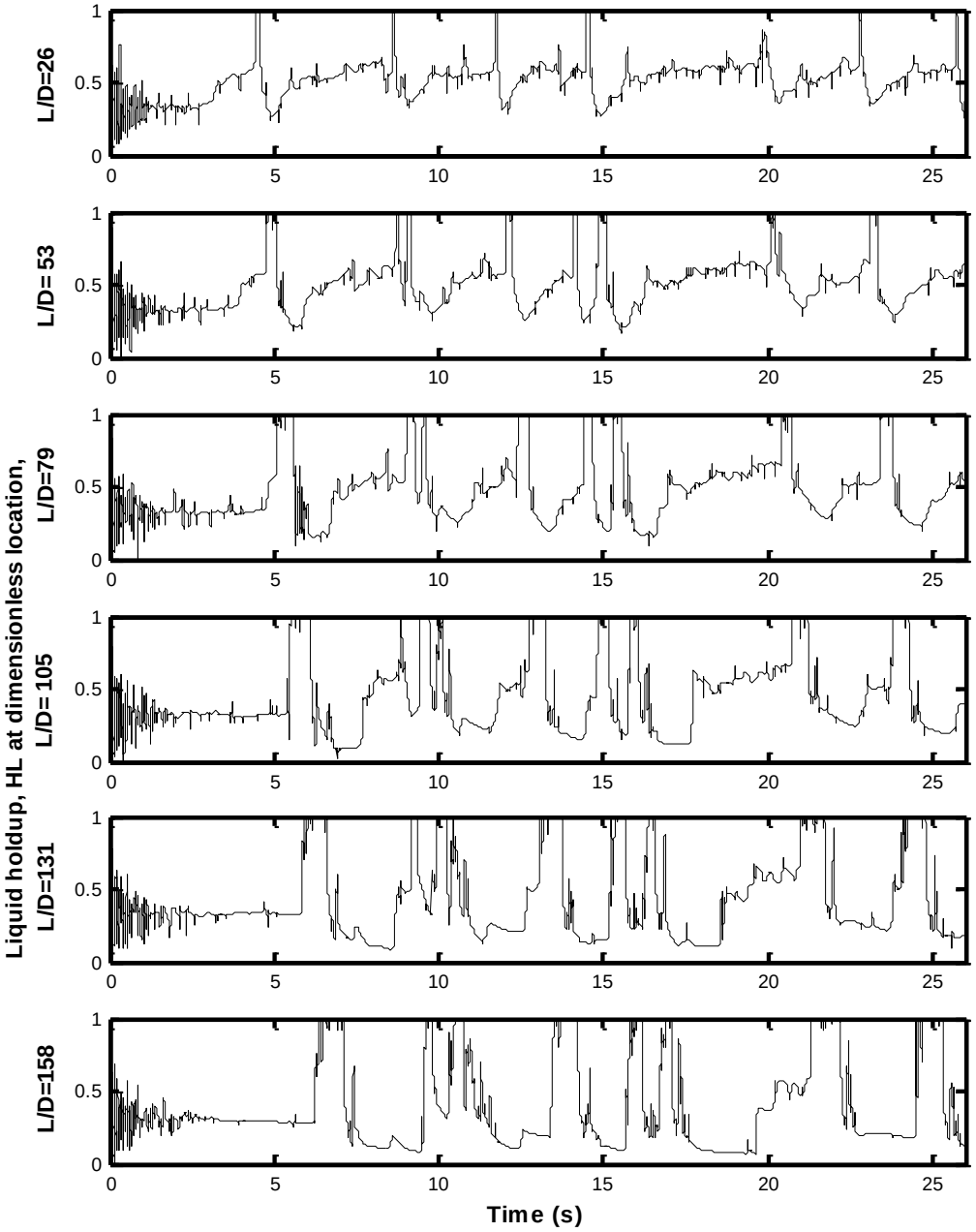

Figure 6.9 Liquid holdup traces for slug flow at U_{SL}=0.2 m/s U_{SG} and 0.9 m/s

It can be observed that in order to pick up liquid, there must be enough liquid in the stratified flow in front of the slug, which means a minimum liquid level of the liquid

film is required. This means that if a slug already exists, it will exist as long as the condition of equally picking up and shedding liquid is met. And if the film in front of the slug is not enough to maintain the slug, it will decay.

Another interesting observation is that under this condition, it can be seen that the slug is always initiated from the back of the pipe and then it follows a development process as it travels along the pipe.

Due to instability in the pressure over the gas-liquid interface, a small wave appears on the liquid surface. This is shown in Figures (6.10 and 6.11) where the pressure and velocity fields are shown for this section. It can be seen that the pressure decreases above the interface and the velocity increases. The gas velocity can reach values as high as 10 m/s under this conditions and the pressure decreases to values as low as 300 Pa.

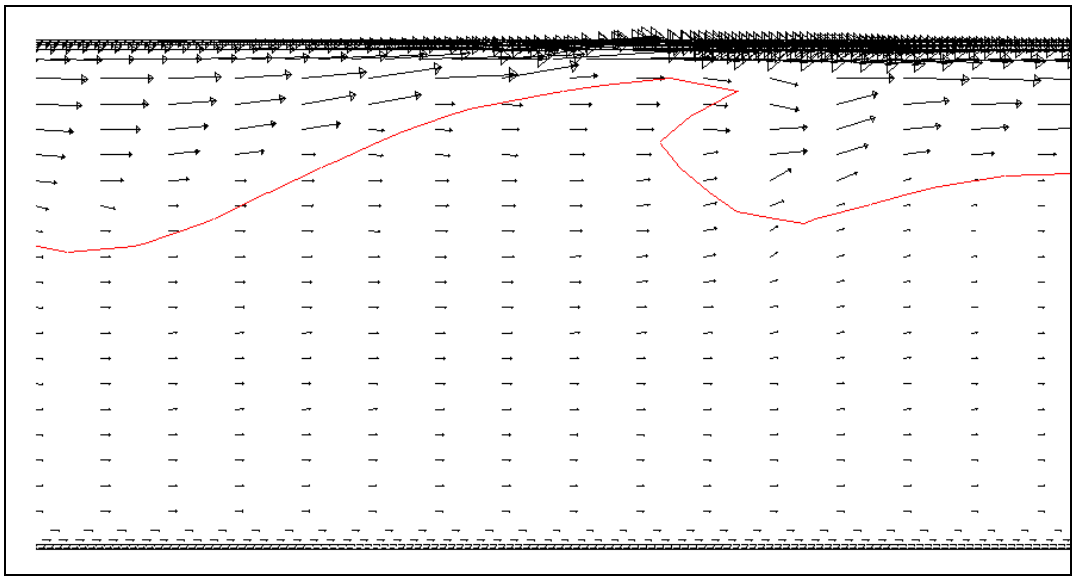

Figure 6.10 Velocity vectors for the onset of slug flow

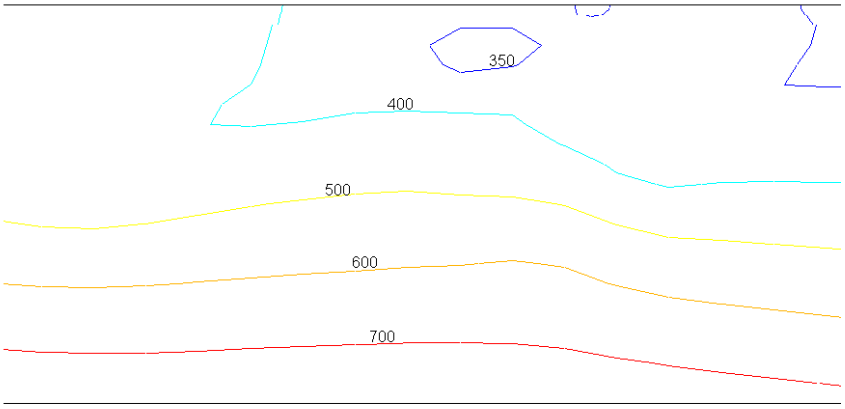

Figure 6.11 Contours of Pressure (Pa) for slug initiation

Regarding to the liquid film, it can be seen that it decreases continuously from the back of the slug to the front of the next liquid slug. It is obvious that different inlet flow conditions will produce different shape of the liquid film interface, even for the same condition. A comparison was made with the shape of the experimental liquid film interface.

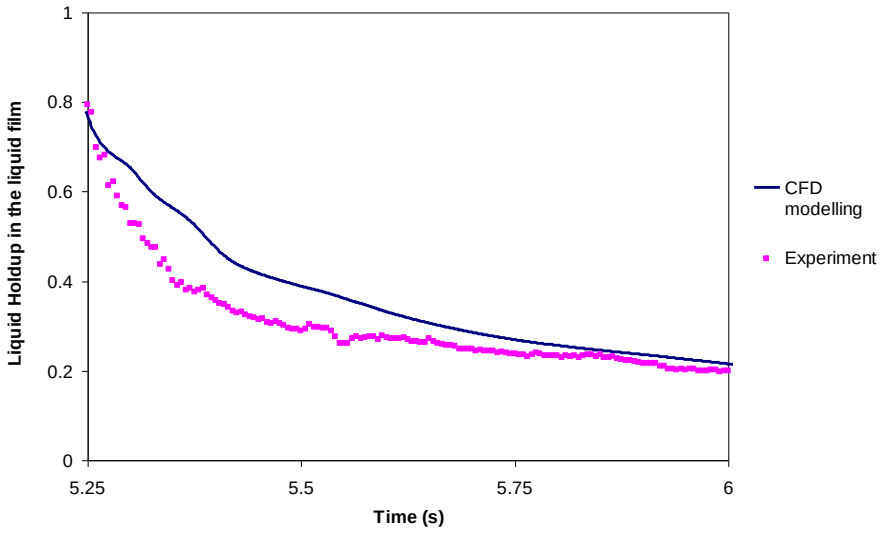

Figure 6.12 Film thickness profile

The profile of static pressure along the pipe: The profile of mean static pressure along the pipe for different times is shown in Figures (6.13 and 6.14) it can be observed that pressure continuously decreases and at the end of the tube, its gradient tends to be uniform.

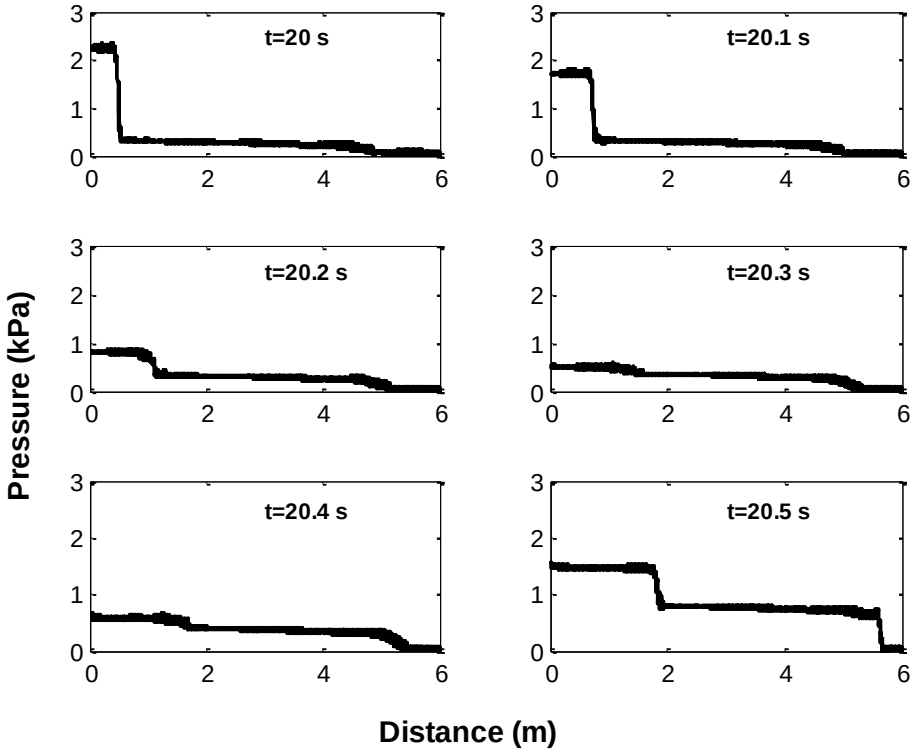

Figure 6.13 Plots profile of static pressure along the pipe.

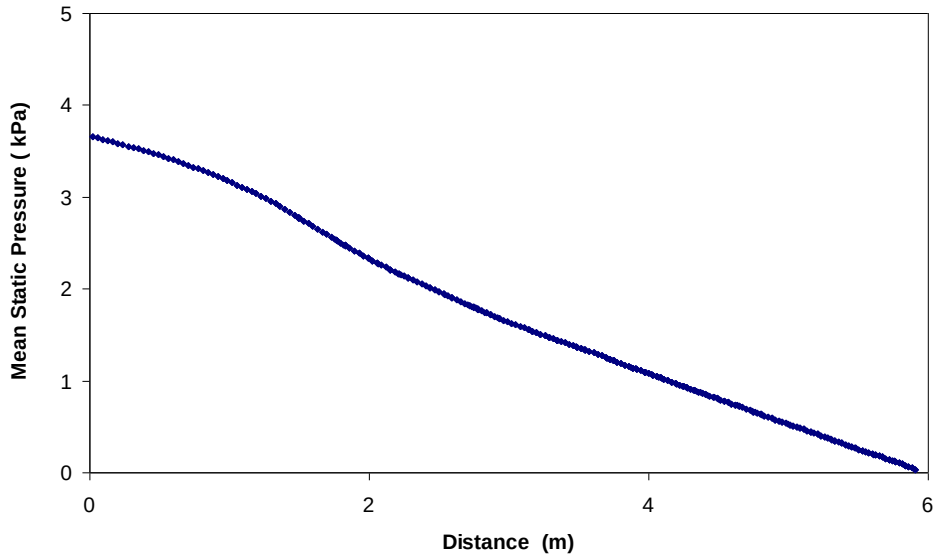

Figure 6.14 Pressure profile for mixture velocity, U_m= 1.1 m/s.

Like the liquid holdup, the velocity profile also changes with both space and time as it is a feature for slug flow. We can observe the different profiles at different times by focusing on one single fixed cross-sectional area of the pipe, Figure 6.15. At large enough liquid flow rates, the symmetric waves assume large amplitudes. One of these

waves can suddenly jump up to form a liquid bridge across the pipe. This bridge can either collapse or grow in length to form a slug. If it forms a slug, there is a sudden increase in the pressure and a calming of the liquid interface behind the slug.

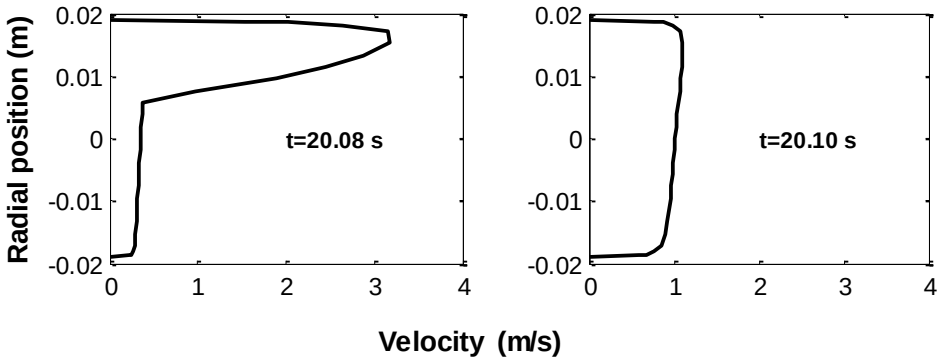

Figure 6.15 Plots of the velocity profile in the stratified region

In order to see the different velocity profiles along the pipe at a particular time instant, Figure 6.16 presents a slug unit together with the velocity profiles at different sections along it.

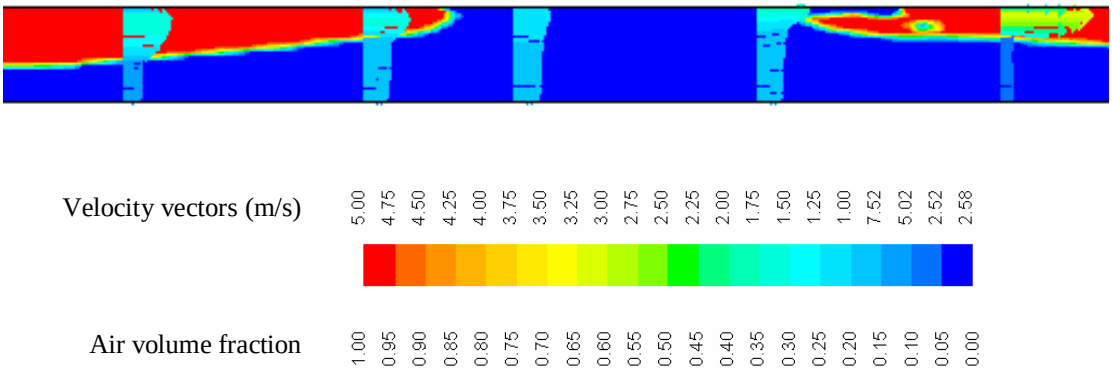

Figure 6.16 Velocity vector and contours of air volume fraction for different sections along the slug unit, the vectors are plotted and coloured by magnitude in m/**s.**

From figures 6.15 and 6.16, it can be observed that huge differences exist between the velocity profiles corresponding to the gas pocket and the liquid slug sections. For the liquid film and gas pocket region, the velocity profile obtained at any cross sectional

area of the pipe is divided into two parts, corresponding to the liquid film and gas pocket regions respectively, that can be identified by their different gradient of velocity in the y-direction. The velocity gradient is greater for the gas-pocket region than for the liquid film.

On the other hand, for the liquid slug, the velocity gradient in the y-direction changes in the same way as it does in the liquid film; however, it covers the whole pipe section. The figure below depicts the shape of the velocity profiles that were obtained at different sections along a slug unit for the case under study. It can be seen in figure 6.16 that the profile is basically parabolic, with the shape of a turbulent flow profile, where the velocity vectors are more homogeneous at the centre, due to the mixing phenomenon that occurs with high turbulence.

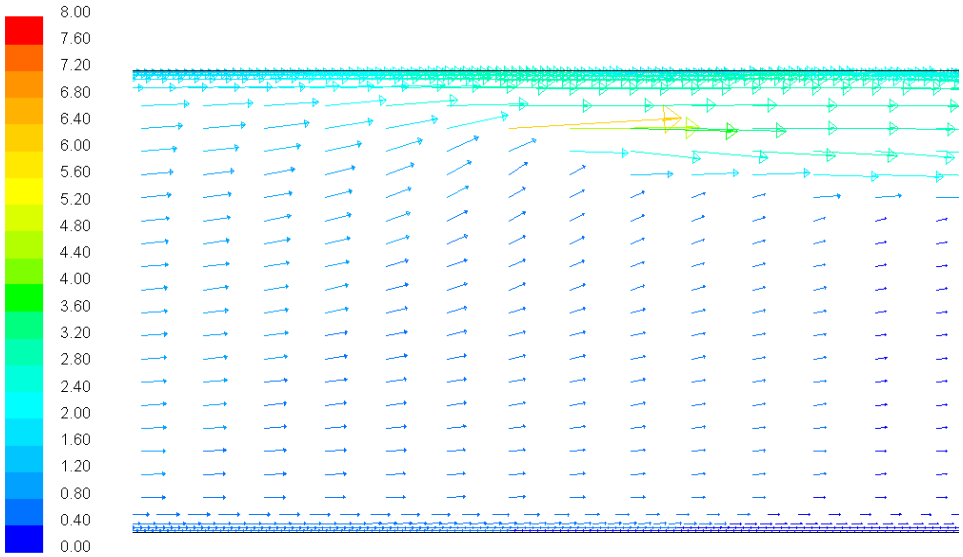

Figure 6.17 Velocity vector distributions within the mixing section at the front of the slug, the vectors are plotted and coloured by magnitude in m/s.

Figure 6.17 shows the velocity field within the mixing section at the front of the liquid slug for a mixture velocity of 1.6 m/s and liquid holdup 0.43. The results confirm that the average velocity field within the liquid slug (also known as liquid slug velocity) equals the mixture velocity. It is important to differentiate between the slug velocity and the translational velocity, which is not given explicitly by the CFD results but can

be calculated from the cross correlation of two liquid volume fraction time series, as done with the experimental time series, see Section 4.7. It can be seen that the liquid that is picked up is then accelerated from a low velocity in the liquid film to a very high velocity in the nose of the liquid slug. As the slugs propagate down the pipe, the liquid in the stratified flow is swept up and the liquid level in the whole pipe drops. This liquid is replenished and, when the level builds up, the whole cycle is repeated.

For certain problems, one may have to conduct "cascades" of computations at increasingly finer scales to resolve all issues. Therefore the CFD studies were conducted with increasing degree of sophistication and detail to clarify key issues such as the velocity profile. The mesh was adapted to ensure that the first computational node away from the wall was within the region necessary to use standard wall functions. It can be observed that even though in the VOF formulation, a unique set of conservation equations is used for the entire computational domain, the velocity field and fluid properties such as density and viscosity vary sharply when we move from one phase into the other. Such a sharp variation of the fluid properties across the interfaces might provoke numerical difficulties in the convergence of the equations.

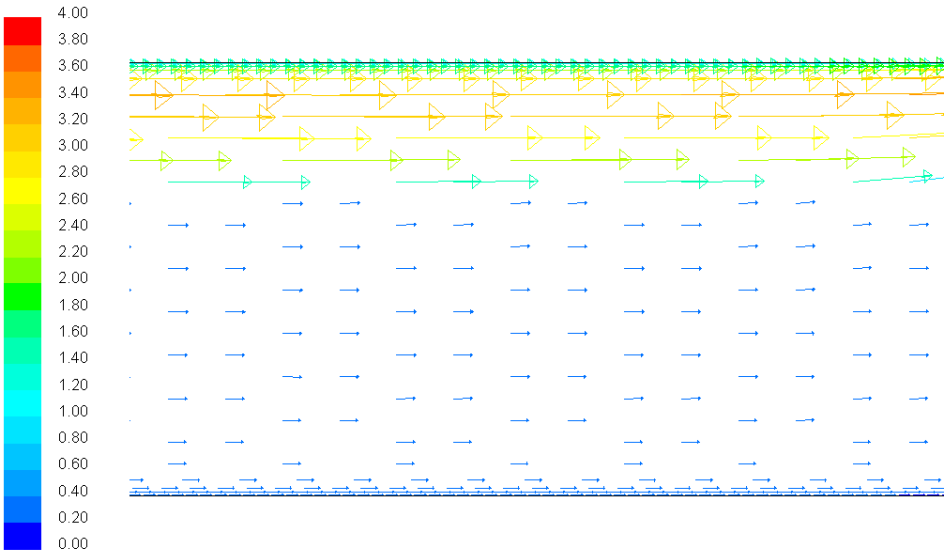

Figure 6.18 Velocity field within the film and gas pocket region.

6.2.3 Inclined pipe at 45°

Initial simulation results for the 45° inclination case were presented during the mesh sensitivity analysis process. In this section, further and deeper analysis of the simulation of the inclined pipe at 45° is presented. For the case presented in this section the inlet flow conditions are; U_{SL}=0.7 and U_{SG}=0.9 m/s with H_L (t=0) =0. The choice of this inlet conditions is due to the flow pattern found experimentally (see section 4.2 and 4.3). Inclined flow is more complicated than horizontal flow from CFD modelling point of view, due to the higher pressure gradient and turbulence that is generated for the inclined case under the same inlet flow conditions.

A remarkable aspect of the physics of two-phase flow is that macroscopic behaviour can be influenced by small scale interactions. For example the evolution of slug flow along a pipeline has been confirmed to strongly depend on the relative velocities between the elongated bubbles. At small separation distances, trailing elongated bubbles accelerate and eventually merge with the leading ones (Pinto and Campos (1996); Pinto *et al.* (1998); Fabre and Liné (1992); Polonsky *et al.* (1999)). Let us begin this section by taking a look at this phenomenon.

In Figure 6.19, it can be observed that in the developing stage of the flow the growing slugs coalesce at a further distance from the inlet. As a consequence, the slug frequency changes along the length of the pipe and it is actually decreasing, which can be explained by the fact that during the merging process, both the liquid slug and the elongated bubble lengths increase. This process is assumed to terminate once the liquid velocity profiles at the back of the liquid slug are fully developed and all elongated bubbles propagate at the same translational velocity. The slug frequency along the pipe tends to be constant for that inlet flow condition. This phenomenon was clearly observed in the 67 mm pipe that was transparent all the way, however it was not possible to physically observe this phenomenon through the 38 mm pipe due to the fact that it occurs before the transparent section. Experimental studies of this phenomenon in three dimensions become very complex due to the effect of free boundaries, significant density and viscosity difference and the effect of surface tension. Flow instabilities resulting mainly from pressure and temperature fluctuations cause the mixture to arrange itself into different phase distributions.

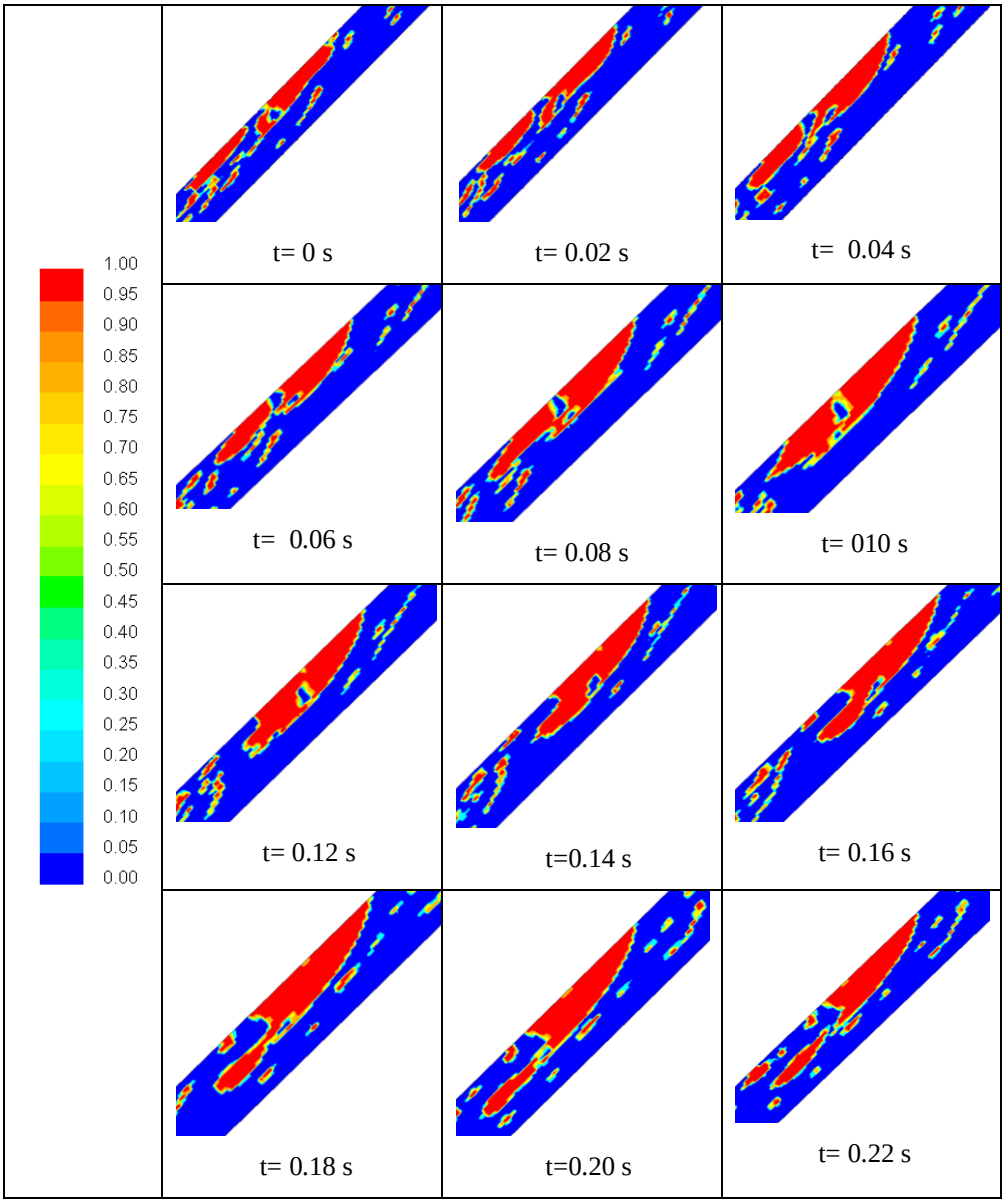

Figure 6.19 Bubble formation process

After formation, a large bubble rapidly accelerates to its terminal rise velocity, U_b. The value of U_b is influenced by the balance between the buoyant rise force, and the drag force. It can be observed that the translation motion of the air bubble along the pipe with water is accompanied by the deformation of the bubble itself. It is also affected by the presence of other bubbles. A bubble rising moving liquid stream, will move at a velocity made up of its basic rising velocity in still water, plus a contribution due to the motion of the liquid. However, the movement of bubbles and

the chaotic three-dimensional (3-D) structures dominate intermittent inclined two-phase flow hydrodynamics. It has been observed both with the experiment and with CFD that it is the Taylor bubble that captures small bubbles in front of it; Figures 6.19 and 6.20 respectively. This observation supports the previous works such as Van Hout *et al.* (2002) who takes into account the effect of dispersed bubbles in continuous slug for the calculation of the translational velocity of elongated bubbles and Brauner and Ullmann (2004) who modelled the gas entrainment.

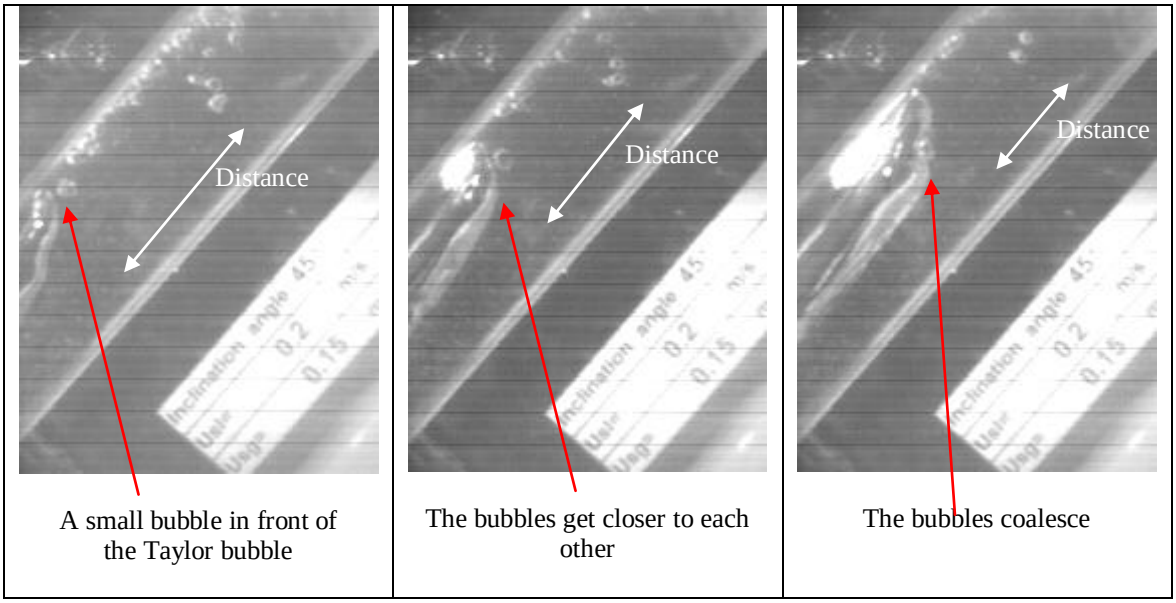

Figure 6.20 Bubble coalescence

In the experiments, the flow was observed through a transparent wall section both directly and using high speed videos. In order to better visualise and understand the flow behaviour, animations of the contours of phase distribution were performed. These animations were also compared to animations of images obtained experimentally with the high speed camera KODAK HS 4540. The camera was run at 256x256 pixels. A typical sequence snapshots recorded by the camera using a recording rate of 500 frames/s is presented in Figure 6.21 together with the ones produced by the simulations. It can be observed that, the bubble shape observed from the high speed video pictures over the area view of the pipe is nearly identical to the one predicted by the computations and the propagation velocity is very similar.

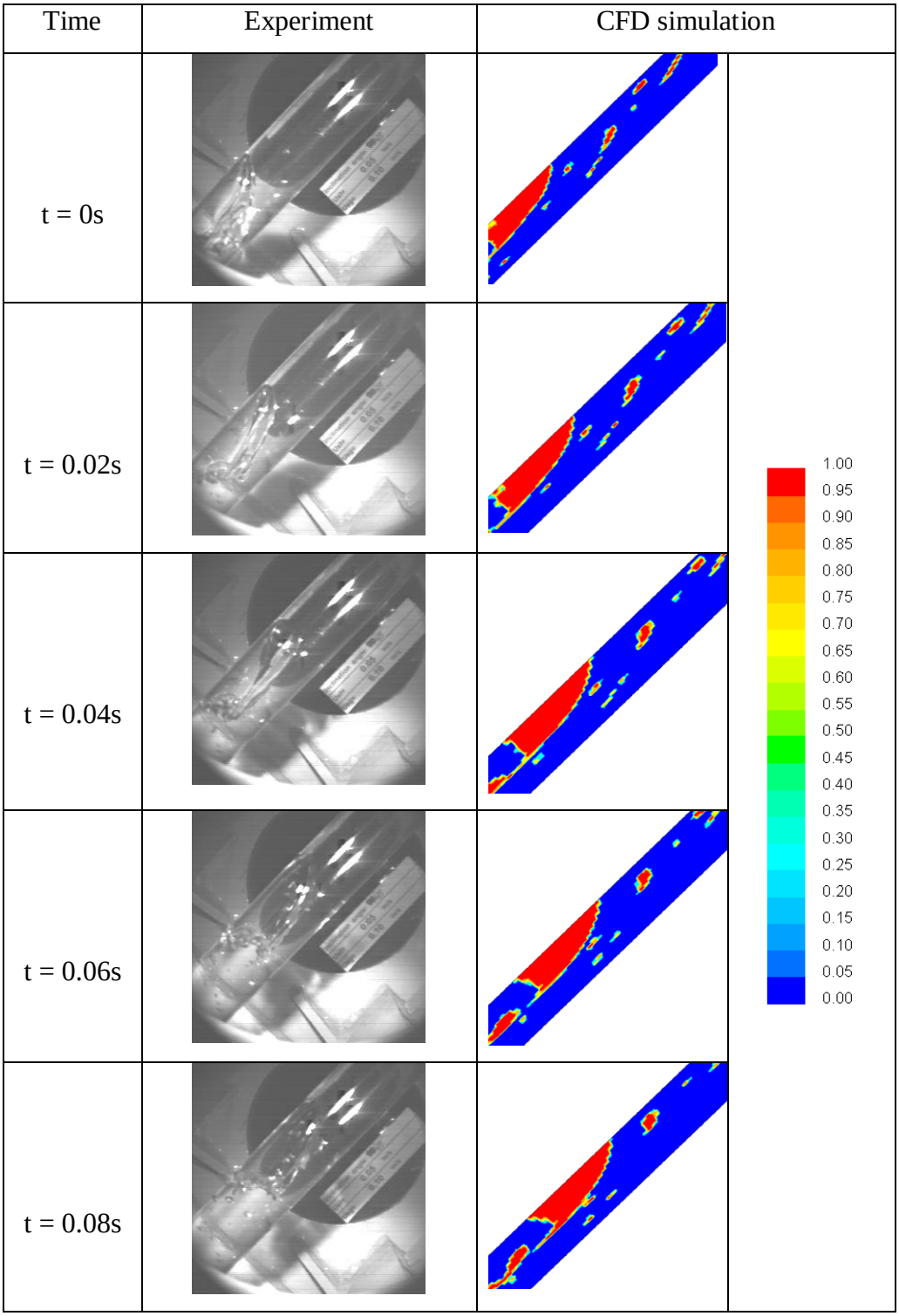

Figure 6.21 Comparison between experimental images and CFD simulation contours of air distribution for 45 ° inclination, U_{SL}=0.1 m/s and U_{SG}=0.15 m/s

In addition it can be observed that small bubbles are driven along the liquid film to the back of the Taylor bubble. The velocity field at the defined section shows that unlike

horizontal flow, reverse flow that can exist for this flow condition, Figure 6.22. There is also a long "backflow" along the liquid film.

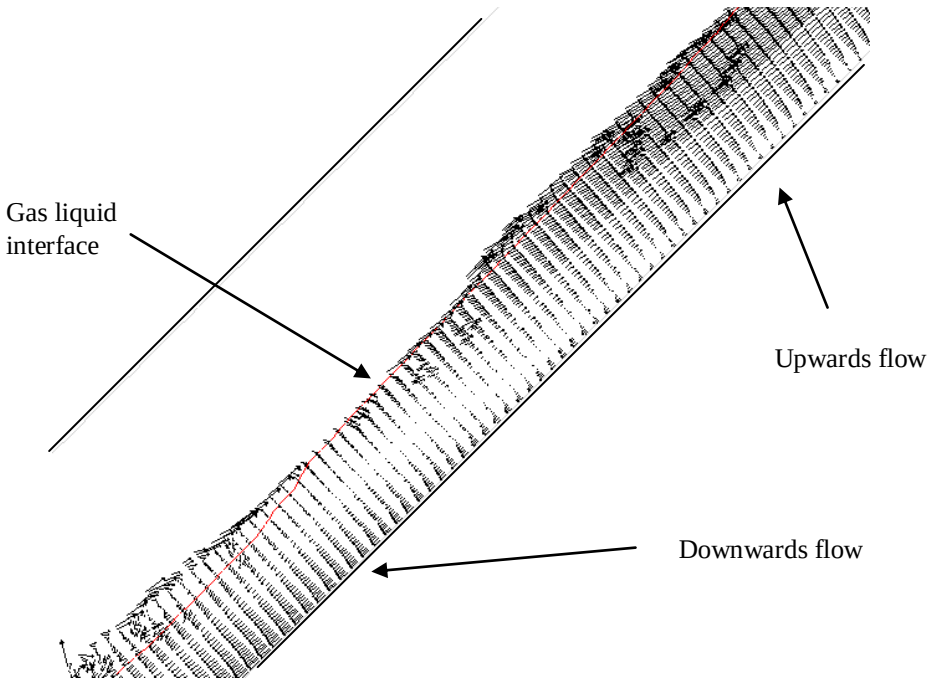

Figure 6.22 Velocity field in a section of the liquid film where the flow changes from upward to downwards

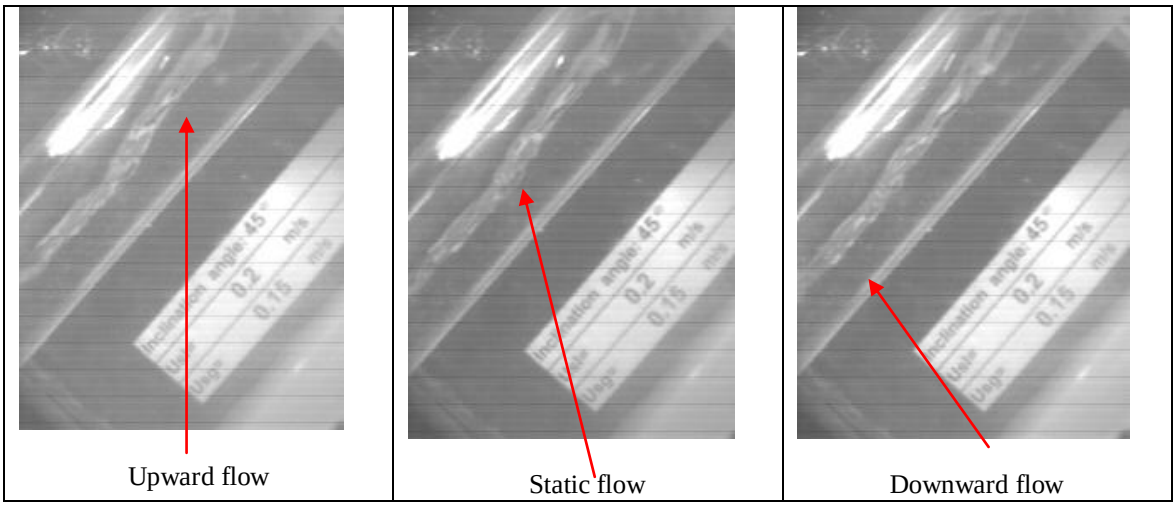

Figure 6.23 Observation of the liquid film behaviour

Down to the tail of the bubble (front of the liquid slug), it was observed during the experiments that due to the turbulent reversed jet of the liquid film at the rear of the bubble a highly agitated mixing zone is produced (Figure 6.24).

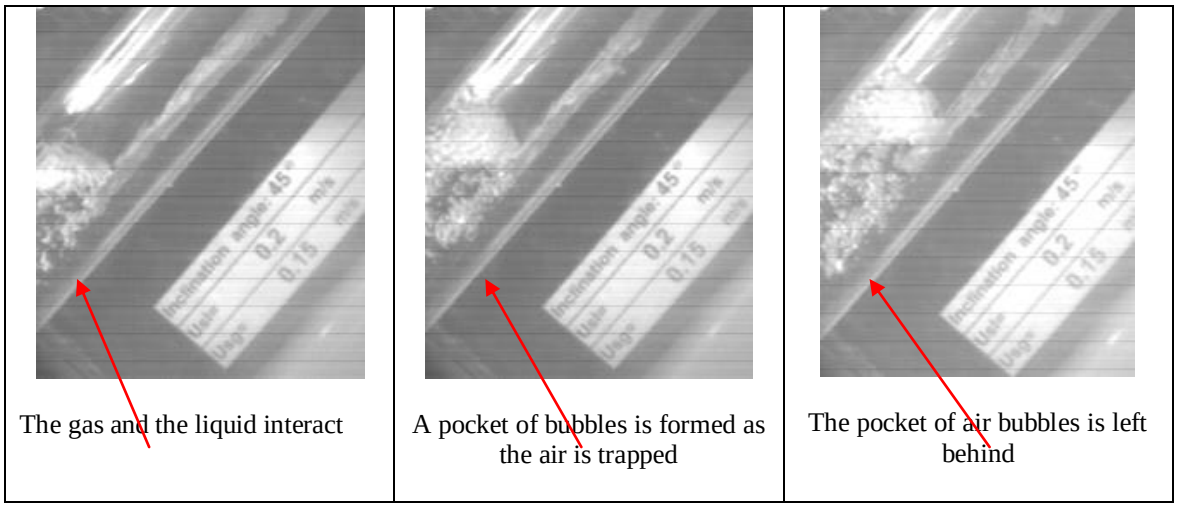

Figure 6.24 Observation of the wake of the Taylor bubble

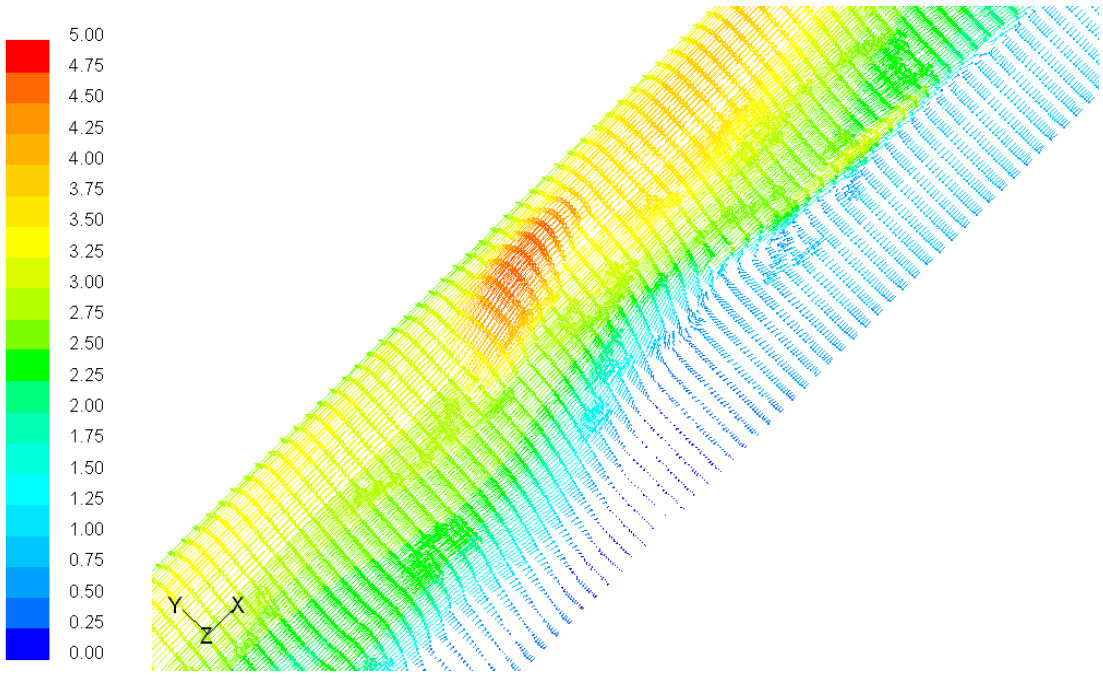

Figure 6.25 Velocity vectors in the wake of the slug bubble section, velocity magnitude (m/s)

It is difficult to measure experimentally the velocity field for these conditions due to the presence of the bubbles and the highly turbulent flow field; however this has been successfully modelled and is represented in Figure 6.24, by means of the velocity vectors. Figures 6.23 and 6.24 show that within the mixing section at the front of the liquid slug where the adjacent elements of air and water interact, the slug unit contains a zone of large recirculation. This is characterised by a strong rollup. The flow field behind the Taylor bubble controls both entrainment and dispersion of small bubbles. Some bubbles re-circulate back to the Taylor bubble while the remaining escapes to the liquid slug behind the wake.

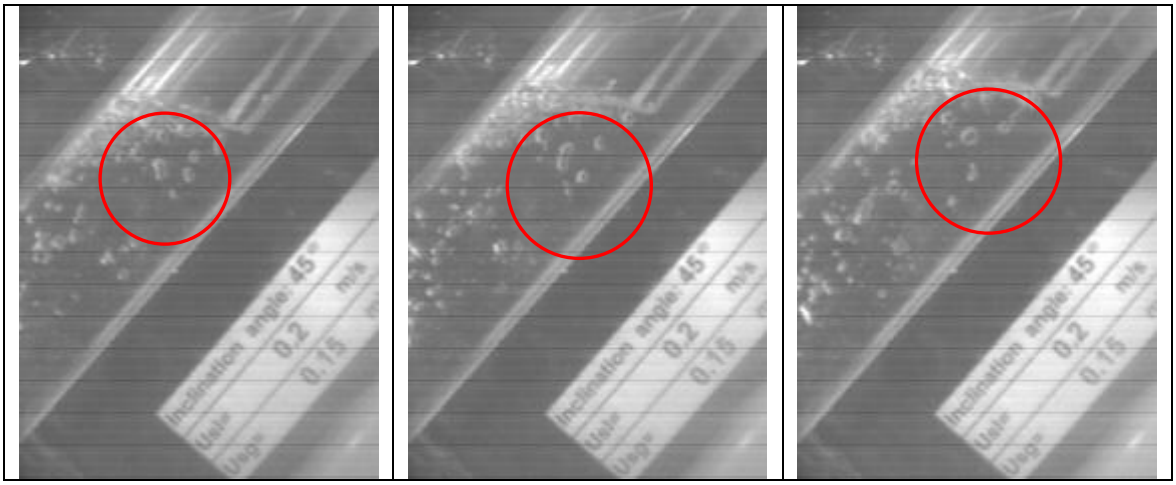

Figure 6.26 Sequential photographs of bubbles motion in the mixing section

It is worth noting that the study of bubble entrainment is beyond the scope of this work, which would involve the use of different models (two-fluid model). In theory (Lakehal *et al.* (2002)) if the mesh is fine enough, both the two-fluid model and VOF should give the same result. In practice the procedure is limited by the growing computational effort and by increasing convergence problems. For the flow conditions of the cases presented here, the macroscopic behaviour of the flow (for example the translational velocity, Section 6.10) does not seem to be affected too much by the small scale interactions of bubble entrainment. For flow conditions where more gas entrainment happens (at higher superficial velocities), the VOF model is not appropriate since the assumption of shared velocity field does not allow the fluids to interact properly, phases interact only through 3-dimensional motion and not by interpenetration of phases Frank (2005), whereas for general gas–liquid two-phase

flow five major bubble interaction mechanisms may be considered, Sun *et al.* (2004). This might lead to delayed demixing times and a generally different behaviour of the multiphase mixture. In such situations, the free surface model can be combined with the full Eulerian multiphase model to provide accurate solutions.

The effect of bubbles on the turbulent field is very complex since not only does the turbulence field in the liquid affect the distribution of bubbles, but also the bubbles affect the turbulence in the liquid phase. Shemer *et al.* (2004) used an experimental approach involving Particle Image Velocimetry (PIV) to measure the turbulent velocity field in vertical flow. Clarke and Issa (1997) performed a numerical study for vertical flow. A significant advantage of CFD simulations, besides the fact that they could potentially replace actual experiments, is that they offer a large amount of information on the turbulence, velocity and pressure fields.

As it is known, transition to turbulent flow for bounded flows occurs between Reynolds numbers ($\mathrm{Re} = \rho d u / \mu$) of 2000 and 3000 and are characterized by large fluctuations in velocity, pressure and fluid properties in both space and time in a random and chaotic way. These fluctuations arise from instabilities that grow until nonlinear interactions cause them to break down into finer and finer whirls that eventually are dissipated (into heat) by the action of viscosity. Figure 6.27 shows the time history of the velocity magnitude at a point located at the centre of the pipe in which turbulent flow exists. It can be observed that there is a sudden change in the velocity at a time about 4s, this is due to the fact that the case was run with initial condition of H_L (t=0) =0. Therefore when the liquid arrives at this point, the increase in velocity fluctuation is accompanied with a change in the phase present at the point under consideration.

By definition $\bar{u}_0 = 0$ m/s (the average of the fluctuation is zero). Consequently, a better measure of the strength of the fluctuation or turbulence intensity is the average of the *square* of a fluctuating variable. Figures 6.27 (b) and (c) show the time evolution of the velocity fluctuation, u_0, and the square of that quantity, u_0^2. Notice that the latter quantity is always greater than zero as is its average. Figure 6.28 presents the contours of turbulence intensity predicted in the pipe, it can be observed

that the turbulence intensity of the two-phase mixture spans over a wide range, however the maximum turbulence occurs in the region of the wake of the bubble, since the reversed liquid film flow is suddenly forced to change its direction from downwards to upwards. A turbulence intensity of 1% or less is generally considered low and turbulence intensities greater than 10% are considered high

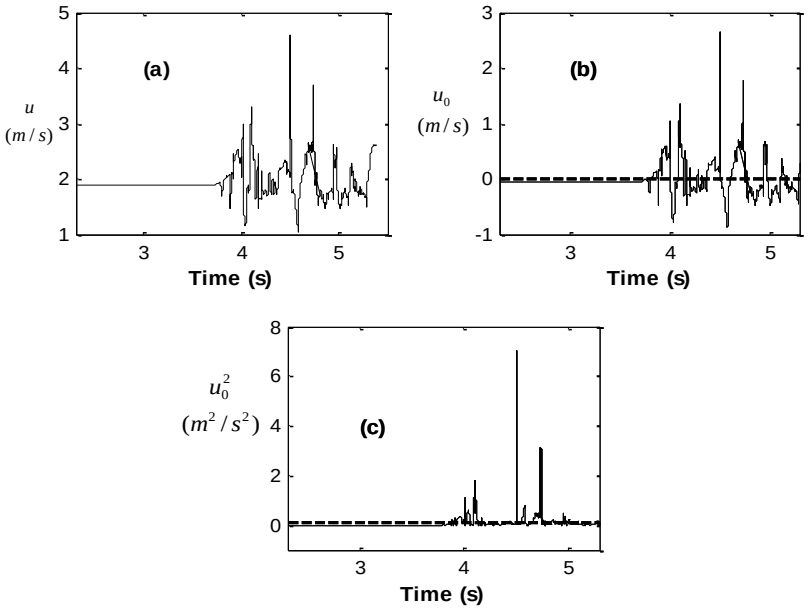

Figure 6.27 Time history of the fluctuation of the velocity magnitude at a point. (a) shows the velocity, (b) shows the fluctuating component and (c) the square of the fluctuating component. Dashed lines in (a) and (c) indicate time averaged

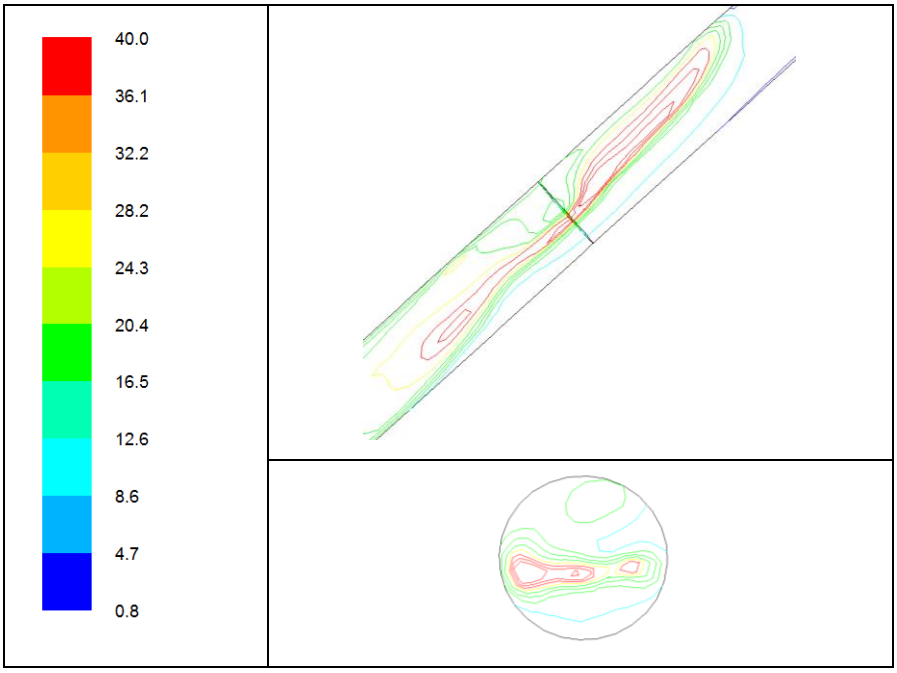

Figure 6.28 Contours of turbulence intensity (mixture), %.

As stated in previous chapters, both the pressure and pressure gradient are parameters of great concern in a multiphase system. The CFD modelled pressure profile along the pipe is shown in Figure 6.29 for different times. At any time, significant pressure gradient sections can be observed followed by sections of nearly constant pressure. The pressure drop sections correspond to the liquid slugs in the pipe whereas the sections of constant pressure correspond to the bubble section. It can also be observed that the pressure gradient is not the same along the liquid slug. At the front of the liquid slug, also known as the mixing section, the pressure drop presents a bigger slope.

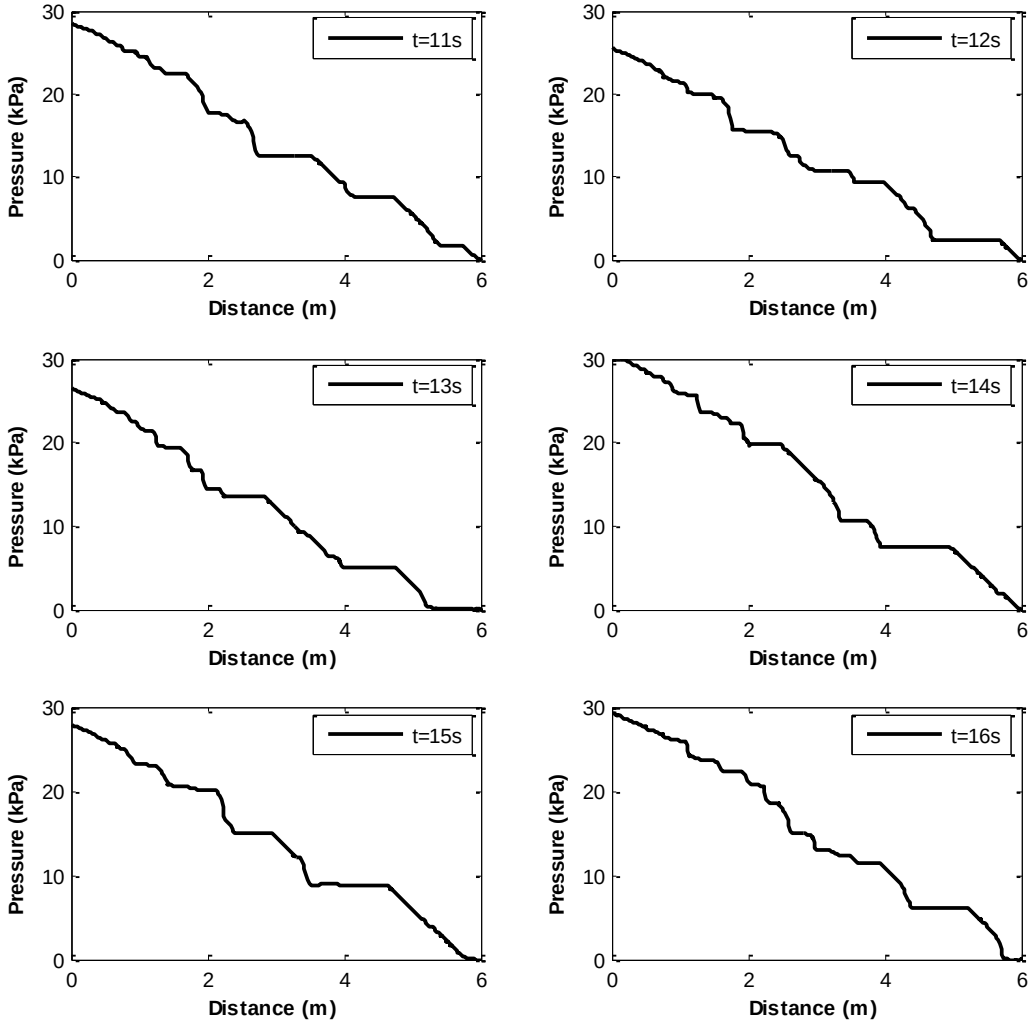

Figure 6.29 Pressure drop profiles along the pipe.

The entrainment of the gas phase into the slug is accompanied by a change in pressure analogous to that which occurs at any sudden enlargement of a single-phase pipe. It is the shearing motion of the viscous fluid within the eddies that is inevitably accompanied by a dissipation of mechanical energy. Simplified hydrodynamic models of pressure drop calculation for horizontal and inclined pipes were suggested by Dukler and Hubbard (1975), Nicholson *et al.* (1978) and Stanislav *et al.* (1986). These investigators proposed that pressure loses in the near wake region behind the elongated bubble are due to acceleration across the mixing zone. Taitel and Barnea (1990) proposed that pressure drop in the liquid film needs to considered, however in Figure 6.29 it can be observed that this pressure drop is very small.

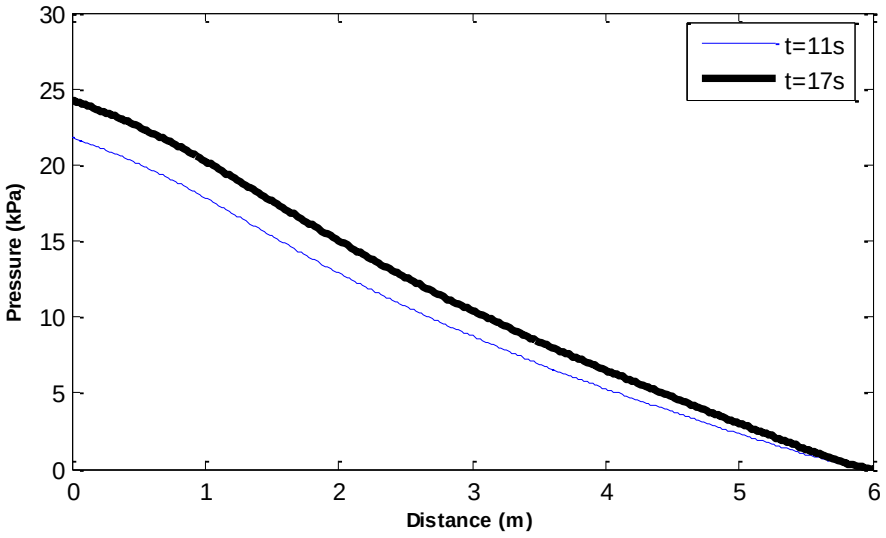

Figure 6.30 Pressure as a function of the distance along the pipe. Inclination of 45°, superficial velocities (m/s): gas =0.9; liquid = 0.73.

In Figure 6.30, the average pressure profile along the pipe can be seen to decrease linearly. The difference between the two profiles at two different times is due to the fact that the case was initiated with H_L *(t=0) =0* and *P (t=0) =0*, and as the liquid enters the flow domain, the pressure is built up eventually. The experimental pressure gradient for this particular case was 5.07 kPa/m, whereas for the simulation it was found to be 4.2 kPa/m from the pressure profile in figure 6.30.

6.3 Further comparison between CFD and the experiment

In spite of the current widespread use of Computational Fluid Dynamics, multiphase applications are not so developed. Therefore multiphase simulations, using this approach, require careful validation against experimental data. Since a wide variety of air-water experiments have been carried out in the Nottingham University Inclinable rig (see appendix A), it would be useful to compare those results with FLUENT multiphase flow simulations. As it was done in Chapters 4 and 5, more information about the slug parameters for this particular case can be obtained from the time series of liquid holdup such as frequency. And therefore further comparisons of the experimental results and CFD computations can be achieved with the Probability Density Function (PDF) of the time series and the PSD. As can be seen in Figure 6.31 and 6.32, the CFD results were taken during a shorter interval of time than that used in the experiments due to computing time limitations (experimental runs were taken for 180 s). However, the time simulated is enough to compare the time series of liquid holdup obtained.

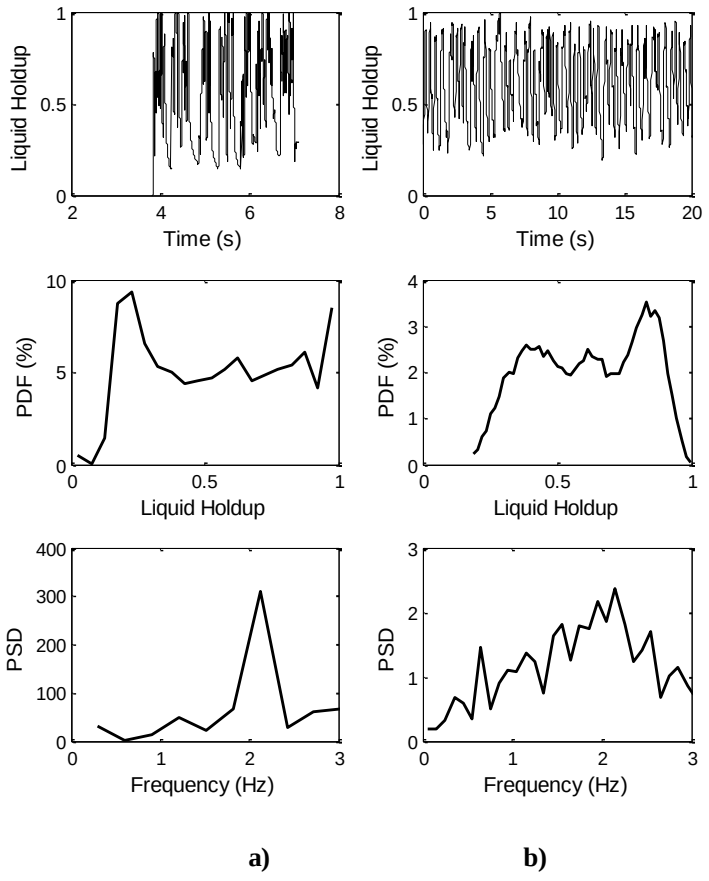

Figure 6.31 Liquid holdup time series: a) CFD simulation b) experiment for 45 ° inclination, U_{SL}=0.73 m/s and U_{SG}=0.9 m/s.

In Figure 6.31, the time series plots look quite similar for both CFD and experiment, however the PDF differs, this might be due to the short time interval simulated, the frequency compares quite well. In the case of Figure 6.32, for frequency, the experimental result is for this case 1.2, whereas the CFD simulation frequency obtained with the PSD is 1.6 which means that it over predicts.

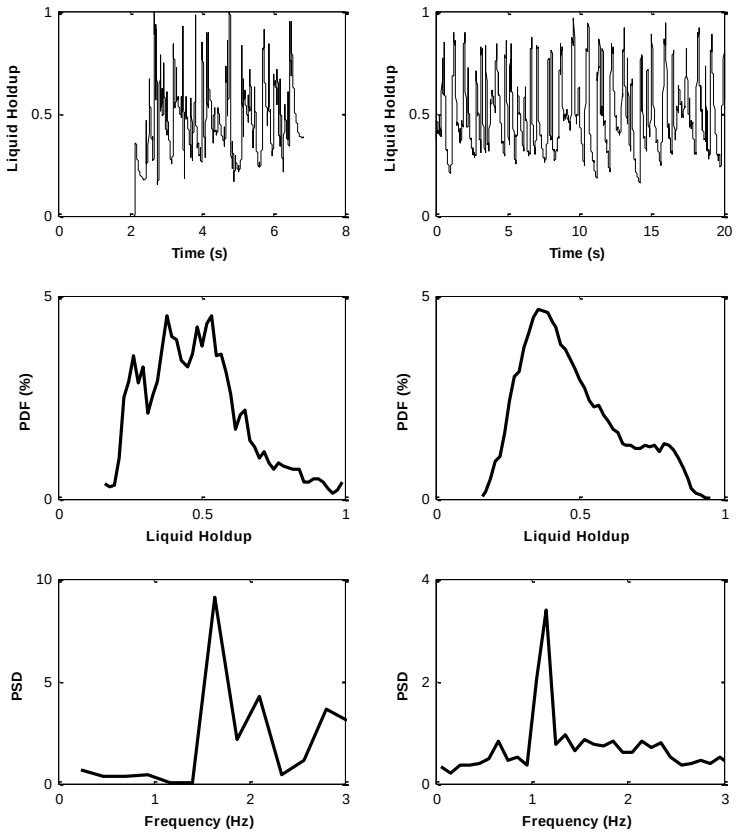

Figure 6.32 Liquid holdup time series: a) CFD simulation b) experiment for 45 ° inclination, U_{SL}=0.73 m/s and U_{SG}=2.9 m/s.

By using the time dependent holdup at two different cross sectional areas, separated by a known distance from each other, the slug translational velocity can also be obtained by applying the cross correlation technique as in Section 4.10. Figure 6.33 shows the comparison between CFD and experimental translational velocity, for this case the CFD prediction is quite accurate.

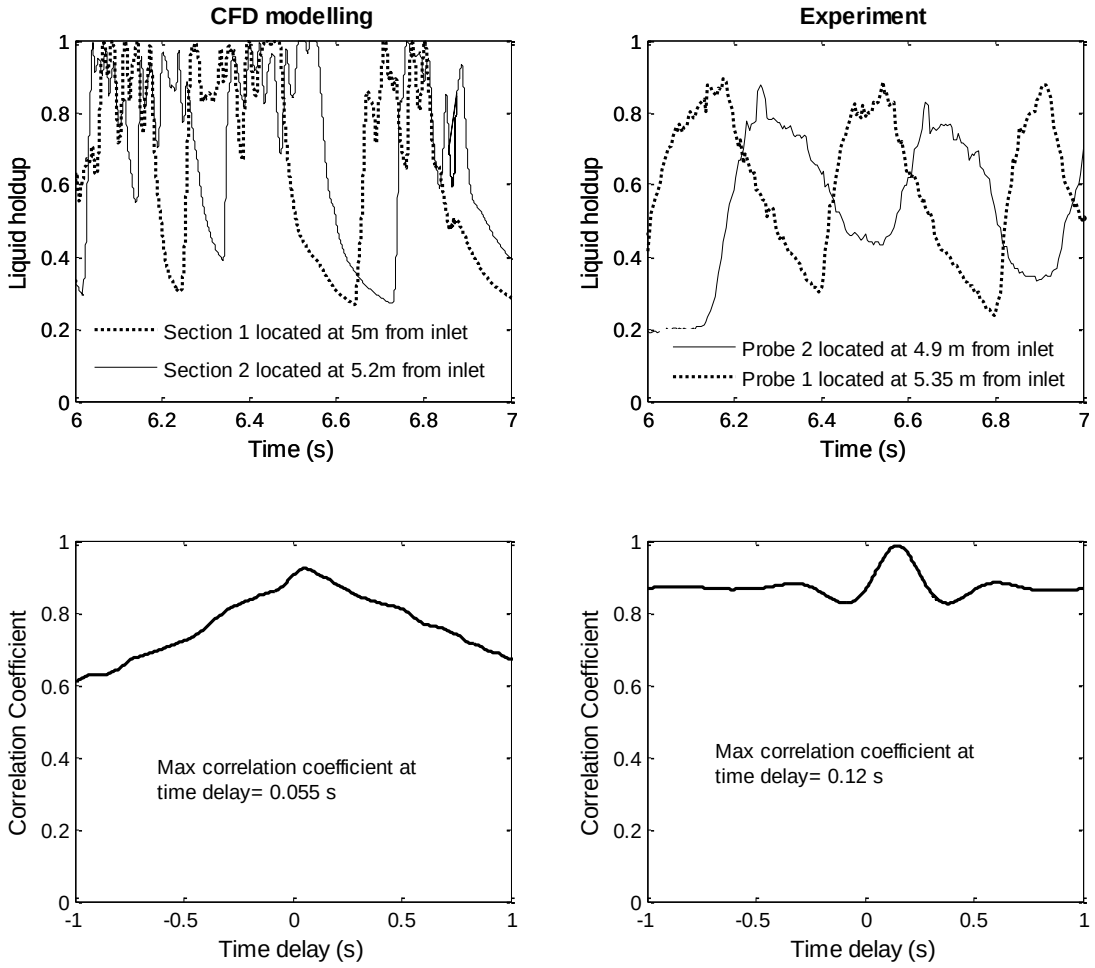

$U_b = \frac{\text{distance}}{\text{time delay}} = \frac{0.2m}{0.055s} = 3.66 m/s$	$U_b = \frac{\text{distance}}{\text{time delay}} = \frac{0.45m}{0.12s} = 3.75 m/s$
a)	**b)**

Figure 6.33 Translational velocity comparison: a) CFD simulation b) experiment for 45 ° inclination, U_{SL}=0.73 m/s and U_{SG}=0.9 m/s.

Unlike experimental data, CFD data were taken during a shorter interval of time due to computing time limitations. However, it can be observed that they differ in less than 2.5 per cent which is within the uncertainty range of the experiment itself, see appendix C.

6.4 Flow development

The "fully-developed" flow is defined as one when the flow pattern does not change with the distance and that evolves far enough downstream. This situation offers a simple system to test physical understanding. Furthermore, such studies provide results that can find direct use. In this section flow development was studied from a CFD simulation point of view and the results for different cases are presented. The advantage of the CFD simulation respect to the physical experiment is the possibility to record the liquid holdup time series at many measurement sections along the pipe. First we present in figure 6.34 the results of a simulation performed with a 6m long pipe (the same length as the one used in the experiments) at 45 ° inclination with the measurement sections located as indicated in the figure.

The difference between the holdup time series obtained at 4m (L/d=105) and 5m (L/d=132) distances is very small, similar differences can be observed between the PDF graph and the PSD frequency. This is a good indication of the flow development. What can be seen in the result of the flow development simulation is that, the flow remains quite similar at the different sections for measurement.

In addition, it can be observed from the liquid holdup time series that the average liquid holdup is decreasing when the flow is developing; this means the liquid tends to accumulate at the bottom of the pipe until the liquid slug is formed.

In the literature some researchers (Penmatcha *et al.* (1996)) have recommended a development distance of about 600 pipe diameters. However, due to physical limitations in the length of the rig, the question addressed was whether a sufficient length to diameter (L/d) ratio had been provided so that observations taken at the end of the pipeline could be considered to be representation of a fully developed flow situation. Therefore in order to observe what may happen with a longer distance, the flow was simulated for a pipe 10 m long as it is shown below for 5 degrees inclination. In this case study a two-dimensional structured grid was used and observations were taken at the locations shown along the pipeline. The results presented in Figure 6.35 show that the flow has been developed.

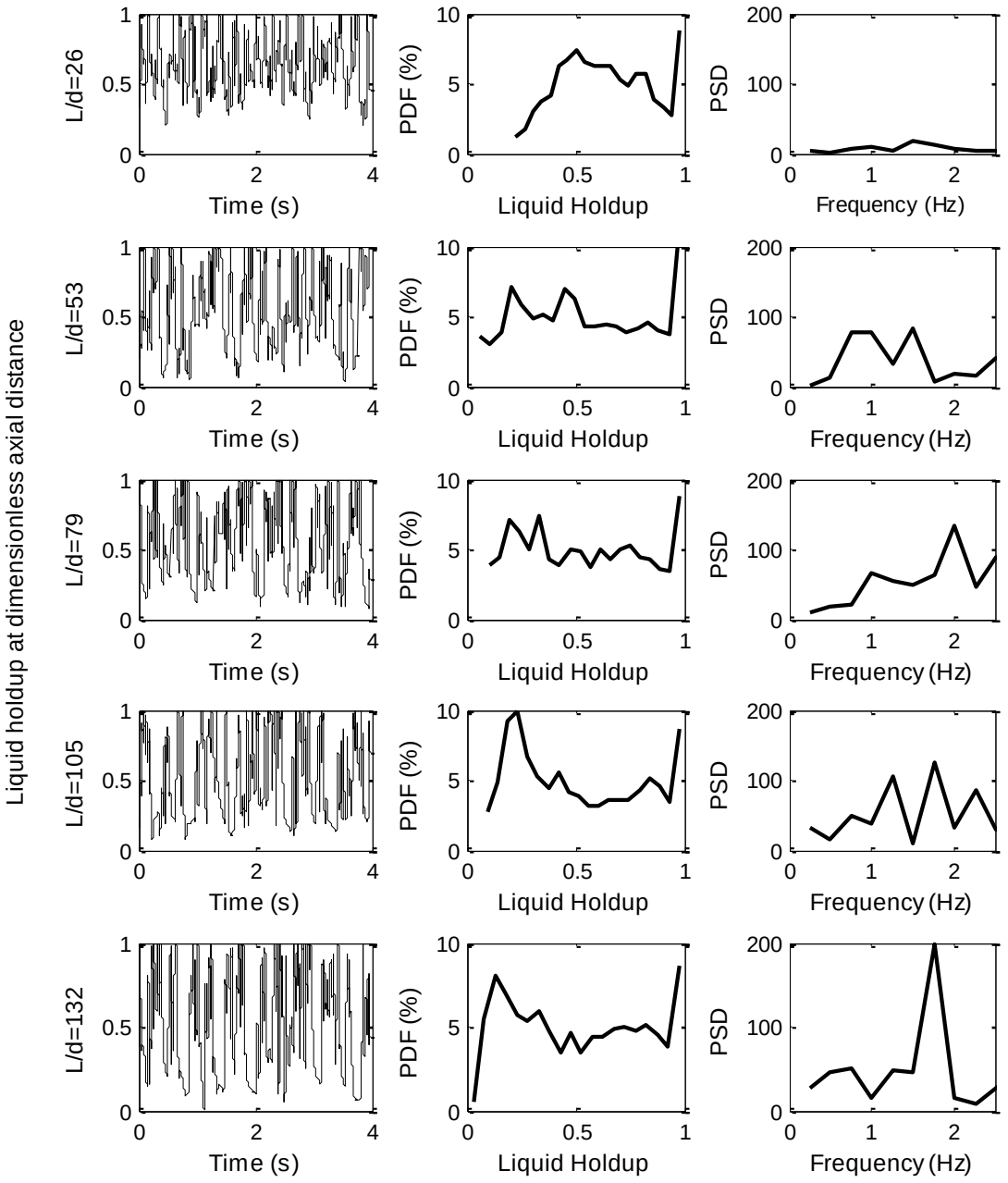

Figure 6.34 Flow development along the pipe, 45 degrees inclination. U_{SL}=0.7 m/s and U_{SG}=0.9 m/s

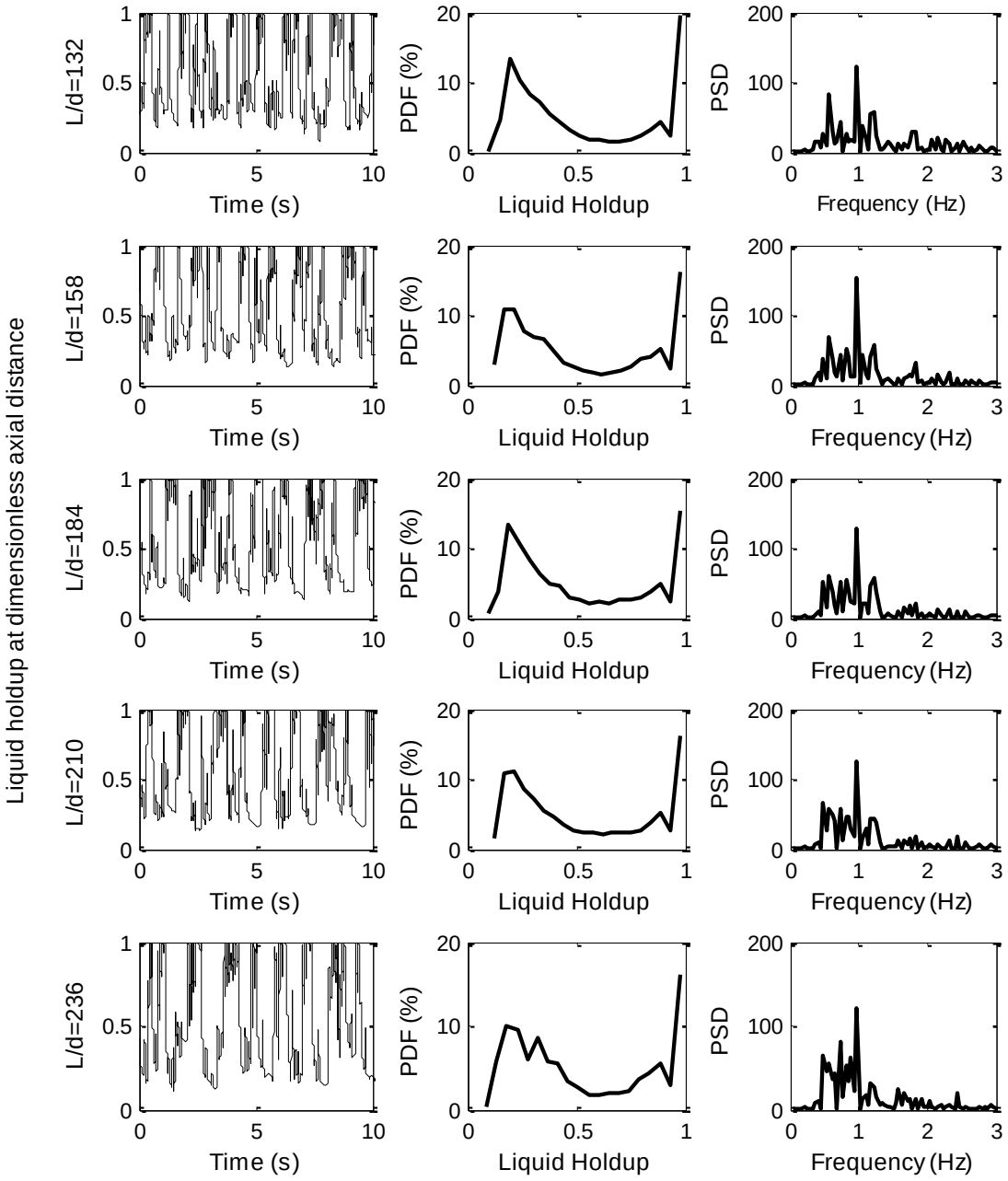

Figure 6.35 Flow development along the pipe. U_{SL}=0.7 m/s and U_{SG}=0.3 m/s

6.5 Summary

Several issues regarding features of slug flow in an inclined pipe have been addressed in this chapter. The numerical simulation of slug flow focused on both the validation of the VOF model with respect with experimental results and understanding of the slug motion phenomenon.

- A series of progressively more complex CFD simulations were conducted in accordance with the experimental conditions. The first and simplest case simulated the condition of air bubbles flowing in an inclined pipe initially full of static water. This case study examined the simulation dependence on the employed grid in predicting the motion of slugs. Further simulations evaluated the motion of slugs in horizontal and inclined pipes.

- From quantitative comparison of the computational and experimental results, it can be seen that in general CFD does predict the behaviour of multiphase flow. By using the VOF method, such stratified and slug flow can be simulated.

- The slug flow pattern has been successfully obtained by flow interaction from the specification of a homogenous mixture at the inlet boundary condition. In the case of horizontal pipe, stratified and subsequently slug flow have been attained from an initial fully dispersed flow.

- Comparison with experimental visualisation of different aspects of the flow behaviour such as the wake of the Taylor bubble and reversed flow in the liquid film suggests that a qualitatively good prediction of the velocity field was obtained.

- The computed frequency and translational velocity of the slugs are in very close agreement with the experiment; the difference is less than 5% of the actual value.

- For the simulation of air-water slug flow flowing through a pipe, the *k*-ε turbulence model used, which requires that the flow is fully turbulent, performs well.

- A qualitative prediction of the phase distribution at the front of the liquid slug body has been achieved in terms of air entrainment for the case of 45° inclined flow with U_m=1.6 m/s; in the simulation a single bubble is observed the entrain into the liquid slug and eventually brakes into a few smaller bubbles whereas the visualisation of the experiment shows that it is a pocket of small bubbles. However, the study of air entrainment is beyond the scope of this work.

- From the results obtained, flow development has been monitored along the pipe. This shows advantages of CFD compared with physical experimentation.

- The CFD modelling results are generally in accordance with the actual experimental findings. This demonstrates the capabilities of Computational Fluid Dynamics to model slug flows. The disadvantage of CFD is that it is still a computationally expensive tool due to the unsteady nature of slug flow.

Chapter 7

Conclusion and further work

In this work an extensive study of slug two-phase flow in inclined pipes has been presented; Experimental data on different variables (liquid holdup, pressure drop, structure velocity and frequency) for different inclination angles and flow rates were acquired and analysed, modelling of the slug flow regime has also been carried out. The analysis was carried out by varying liquid and gas mass flow rates and inclination. This has given a good insight into the phenomena that occur in inclined pipes. Such a comprehensive study had not been carried out previous to the present work. The great amount of data collected gives an idea of the number of experimental tests carried out; a total of 1120 experiments were performed in three campaigns, namely on a 38 mm pipe with low liquid flow rate, on a 38 mm pipe with high liquid flow rate and on a 67 mm pipe.

In this chapter the final conclusions drawn from this study are summarised. Further work is also proposed, in order to improve and expand the knowledge of multiphase flow in inclined pipes.

7.1 Conclusions

Special attention was paid to the effect of the inclination on the slug flow characteristics. Data from other authors were introduced, discussed and compared to the present data. Results from other works concerning frequency of slugs and structure velocity were confirmed. In addition, computational fluid dynamics modelling was performed in order to better understand multiphase flow interaction in inclined pipes.

7.1.1 Conclusions for gas-liquid flow in 38 mm pipe

- For a constant liquid superficial velocity, the average liquid holdup decreases as the gas velocity is increased. For downwards stratified flow, the liquid holdup becomes independent of the gas superficial velocity over the range of gas flow rate employed but is a function of the liquid flow rate.

- In upwards flow, the pipe inclination has just a slight effect on the liquid holdup. The liquid holdup increased slightly for the higher inclination angles.

- It is confirmed that intermittent flow exists as the dominant flow pattern in upward inclined flow.

- Unlike the liquid holdup, the frequency is strongly affected by the inclination angle. At low gas superficial velocities, the frequency depends on the angle of inclination in such a way that it tends to have a maximum at about 50 degrees. For high mixture velocities, the more deviated from horizontal, the higher the frequency.

- In slug flow the expected linear dependence of the structure velocity on the mixture velocity has been confirmed.

- The liquid holdup in the liquid slug body appears to decrease with the gas superficial velocity and slightly with pipe inclination.

- Average slug lengths were in the order of 10 to 30 pipe diameters, and relatively independent of flow conditions.

- The slug length tends to decrease as the frequency increases and also with the inclination angle.

- The frequency is significantly affected by the change in the liquid flow rate.

7.1.2 Conclusions for gas-liquid flow in 67 mm pipe

- For the range of flow conditions studied in the present work: No effect of the pipe diameter on the average liquid holdup was observed at liquid superficial velocity of 0.2 m/s, however when the liquid flow rate is increased to 0.7 m/s, the holdup tends to be slightly higher for the bigger pipe diameter. The same tendency is observed for the pressure gradient, since it strongly depends on the liquid holdup, particularly for steep inclination angles and lower gas flow rates.

- The structure velocity shows a trend with the mixture velocity for both pipes, but it is higher for the larger pipe diameter. This due to the fact that, as found by Van Hout *et al.* (2002), the drift velocity for continous slug flow is enhanced by the dispersed bubbles in the liquid slug body. These dispersed bubbles contribute to the drift velocity by coalesing with the elongated bubble at its nose. Therefore the drift velocity contribution calculated assuming stagnant liquid is very small compared to the discrepancies found.

- Since it is the structure velocity and the holdup in the liquid slug body that are more affected by the pipe diameter, it can be deduced that the increase in the slug length and structure velocity is due to a more aerated liquid slug. Another way to look at it is that in order to maintain continuity for the phases (liquid), faster slugs will contain more dispersed bubbles and they will be longer.

- Increase of pipe diameter displaces the bubbly-slug transition to the right hand side on the flow pattern map for inclined flow, and for horizontal the stratified-slug transition is moved up.

- Increasing pipe diameter, from 38 to 67 mm, on the two-phase mixture behaviour has been found to have some influence, yet bigger changes in the pipe diameter can produce a more significant significant effect.

7.1.3 Conclusions for modelling of slug flow with CFD

- A series of progressively more complex CFD simulations were conducted in accordance with the experimental conditions. The first and simplest case simulated the condition of air bubbles flowing in an inclined pipe initially full of static water. This case study examined the simulation dependence on the employed grid in predicting the motion of slugs. Further simulations evaluated the motion of slugs in horizontal and inclined pipes.

- From quantitative comparison of the computational and experimental results, it can be seen that in general CFD does predict the behaviour of multiphase flow. By using the VOF method, which tracks the interface between the phases, free surface flows, such as stratified and slug flow can be simulated.

- The slug flow pattern has been successfully obtained by flow interaction from the specification of a homogenous mixture at the inlet boundary condition. In the case of horizontal pipe, stratified and subsequently slug flow have been attained from an initial fully dispersed flow.

- Comparison with experimental visualisation of different aspects of the flow behaviour such as the wake of the Taylor bubble and reversed flow in the liquid film suggests that a qualitative good prediction of the velocity field was obtained.

- The computed frequency and translational velocity of the slugs are in very close agreement with the experiment; the difference is less than 5% of the actual value.

- For the simulation of air-water slug flow flowing through a pipe, the k-ε turbulence model used, which requires that the flow is fully turbulent, performs well.

- A qualitative prediction of the phase distribution at the front of the liquid slug body has been achieved in terms of air entrainment for the case of 45° inclined flow with U_m=1.6 m/s; in the simulation a single bubble is observed the entrain into the liquid slug and eventually brakes into a few smaller bubbles whereas the visualisation of the experiment shows that it is a pocket of small bubbles. However, the study of air entrainment is beyond the scope of this work.

- The CFD modelling results are in accordance with the actual experimental findings. This demonstrates the capabilities of Computational Fluid Dynamics to model slug flows. The disadvantage of CFD is that it is still a computationally expensive tool due to the unsteady nature of slug flow.

7.2 Recommendations for future work

Although we have performed an extensive study on slug two-phase flow in inclined pipes using two pipe diameters, there are still some issues that need further investigation:

- Since four capacitance probes have been developed in the laboratory, future works should consider the use of all four probes along the pipe. This would allow the observation of the flow development along the pipe.

- As for the capacitance probes, in order to get more accurate results, the capacitance probes should be calibrated at different inclination angles. The liquid should have low conductivity, otherwise it acts as a capacitor rather than as a dielectric. In addition these electrodes should also be wide as to cover the whole pipe perimeter.

- To add a pressure gauge transducer in the measurement section of the pipe in order to identify the flow pattern from the gauge pressure signal.

- The use of a DP cell with a narrower range of pressure drop measurement for near horizontal inclinations; for these inclinations, the pressure drop is small and therefore this would allow more accurate measurements.

- More sophisticated instrumentation should be used (wire mesh sensor). This will allow obtaining the volume fraction distribution in the cross sectional area of the pipe and bubble size distribution.

- Further experiments on pressure drop should be carried out for higher flow rates both of gas and liquid. A further investigation would confirm the results found on the effect of the inclination on pressure drop.

- Consideration should be paid to the use of more industrially relevant fluids such as silicon oil and kerosene. Investigating the effect of fluid properties (viscosity, density and surface tension) would be of particular interest in the oil & gas industry applications where liquids and gases have different properties from those involved in the present work.

- Different pipe diameters, both bigger and smaller should be tested in order to better characterise the effect of pipe diameter on the two-phase mixture parameters such as flow pattern and liquid holdup.

- In order to explore the capabilities of the CFD models, a natural step for future simulations will be to utilize the two-fluid model and compare it with the VOF model under the same conditions. This will establish advantages and disadvantages of each approach in future applications.

Nomenclature

Symbol	Description, Units
A	Cross sectional area, m^2
c	Constant, (section 3.2.7)
C	Capacitance, F
C_0	Accounts for velocity variations over pipe cross section
$C_{D\theta}$	Drag coefficient for the Taylor bubble
C_L	Input liquid volume fraction, $C_L=U_{SL}/U_m$
d	Diameter of the tube, mm
E_L	In-situ liquid volume fraction
f	Friction factor $f = 0.0014 + \frac{0.125}{(\mathrm{Re})^{0.32}}$; Frequency (Hz)
F	Force, N
G	Mass flux, kg/m^2
H_f	Liquid film holdup
H_L	Liquid holdup
H_S	Liquid holdup in the liquid slug body
h	Height, m
g	Gravity constant, 9.81 m/s^2
I	Turbulence intensity, %
k	Turbulent kinetic energy, J
K	Dielectric constant, Fm^{-1}
l	Characteristic length , m
L	Length of the tube, m
L_f	Liquid film length, m
L_S	Liquid slug length, m
$\dot{m}$	Mass flow rate, kg/s
P	Pressure (Pa)
ΔP	Pressure difference, pressure drop, Pa

$p(\alpha)$	Probability density function, %
P_w	Wetted perimeter, m
Q	Volumetric flow rate of the mixture, m^3/s
R	Result
Q_G	Volumetric flow rate of gas, m^3/s
Q_L	Volumetric flow rate of liquid, m^3/s
r	Radius of curvature, m
S	Source term, Standard deviation
t	Time, s
T	Sample period, s
u	Velocity, m/s; uncertainty, %
u_0	Velocity fluctuating component, m/s;
$\overline{U}$	Mean velocity, m/s
U_d	Drift velocity
U_d^h	Drift velocity for the horizontal, m/s
U_d^v	Drift velocity for the vertical, m/s
U_f	Film velocity, m/s
U_G	Mean velocity of gas, m/s
U_m	Mixture homogeneous velocity, m/s
U_L	Mean velocity of liquid, m/s
U_r	Relative velocity, m/s
U_S	Slug velocity, m/s
U_{SG}	Gas superficial velocity, m/s
U_{SL}	Liquid superficial velocity, m/s
U_∞	Bubble rise velocity, m/s
$U_{\infty T\theta}$	Taylor bubble rise velocity at inclination θ, m/s
U_t	Translational velocity, m/s
V	Volume, m^3; valve
X	Lockhart-Martinelli parameter
x	x-axis, measured variable
y	y-axis; distance from the wall in equation (6.9), m
y^+	Normalized wall distance

z	*z*-axis

Greek Symbols

α	Volume fraction
δ_{ij}	Kronecker delta
ε	Rate of dissipation of *k, J/s*
ε	Error in models and correlations, %
θ	Inclination angle with respect to horizontal, °
σ	Surface tension, N/m; Stress tensor; Standard deviation
γ	Distribution coefficient
ρ	Density, kg/m^3
ρ_n	Non slip mixture density, kg/m^3
μ	Viscosity, Pa·s
ω	Oscillation frequency, Hz
τ_i	Interfacial shear stress, Pa
τ_w	Wall shear stress, Pa
τ	Time displacement, s

Subscripts

b	Bubble
acc	Accelerational
fric	Frictional
grav	Gravitational
d	Drift
eff	Effective
f	Liquid film
G	Gas
h	Horizontal
i	Indicates velocity component; number of a variable

j	Indicates spatial coordinate
L	Liquid
m	Mixture
n	Number
N	Number
min	Minimum
max	Maximum
q	Indicates phase
s	Slug, Standard conditions
t	Translational, turbulent
tp	Two-phase
u	Slug unit
v	Vertical
p	point

Abbreviations

ac	Alternate Current
CFD	Computational Fluid Dynamics
dc	Direct Current
DFT	Discrete Fourier Transform
DNS	Direct Numerical Simulation
DP	Differential Pressure
ECT	Electrical Capacitance Tomography
FFT	Fast Fourier Transform
fps	Frames per second
FVC	Frequency to Voltage Converter
FVM	Finite Volume Method
LHS	Left Hand Side
PCB	Printed Circuit Board
PDF	Probability Density Function
PISO	Pressure Implicit with Splitting of Operators
PSD	Power Spectral Density
PVC	Polyvinyl Chloride

RC	Resistive-Capacitive
RHS	Right Hand Side
SIMPLE	Semi Implicit Pressure Linked Equations
SNR	Signal to Noise Ratio
VOF	Volume of Fluid

Dimensionless numbers

Re	Reynolds number Re = ρdv/μ
Fr	Froud Number, $Fr_m=U_m^2/gd$
Ku	Kutadelaze number
E_{OD}	Eotvos number, $E_{OD}=\frac{\rho_L g d^2}{\sigma}$
St	Strouhal Number, $St = \omega\, l / v$
X	Lockhart-Martinelli parameter

Appendix A

Test Matrix

Table A.1 Test matrix for 38 mm pipe, campaign 1

	U_{SG} [m/s]									
U_{SL} [m/s]	**0.15**	**0.88**	**1.52**	**2.28**	**3.04**	**3.97**	**4.91**	**6.89**	**9.33**	**12.32**
U_{SL}=0.04	0°	0°	0°	0°	0°	0°	0°	0°	0°	0°
	5°	5°	5°	5°	5°	5°	5°	5°	5°	5°
	10°	10°	10°	10°	10°	10°	10°	10°	10°	10°
	30°	30°	30°	30°	30°	30°	30°	30°	30°	30°
	45°	45°	45°	45°	45°	45°	45°	45°	45°	45°
	60°	60°	60°	60°	60°	60°	60°	60°	60°	60°
	75°	75°	75°	75°	75°	75°	75°	75°	75°	75°
	85°	85°	85°	85°	85°	85°	85°	85°	85°	85°
	90°	90°	90°	90°	90°	90°	90°	90°	90°	90°
U_{SL}=0.05	-5°	-5°	-5°	-5°	-5°	-5°	-5°	-5°	-5°	-5°
	0°	0°	0°	0°	0°	0°	0°	0°	0°	0°
	5°	5°	5°	5°	5°	5°	5°	5°	5°	5°
	10°	10°	10°	10°	10°	10°	10°	10°	10°	10°
	50°	50°	50°	50°	50°	50°	50°	50°	50°	50°
	75°	75°	75°	75°	75°	75°	75°	75°	75°	75°
	85°	85°	85°	85°	85°	85°	85°	85°	85°	85°
	90°	90°	90°	90°	90°	90°	90°	90°	90°	90°
U_{SL}=0.06	0°	0°	0°	0°	0°	0°	0°	0°	0°	0°
	5°	5°	5°	5°	5°	5°	5°	5°	5°	5°
	10°	10°	10°	10°	10°	10°	10°	10°	10°	10°
	30°	30°	30°	30°	30°	30°	30°	30°	30°	30°
	45°	45°	45°	45°	45°	45°	45°	45°	45°	45°
	60°	60°	60°	60°	60°	60°	60°	60°	60°	60°
	75°	75°	75°	75°	75°	75°	75°	75°	75°	75°
	85°	85°	85°	85°	85°	85°	85°	85°	85°	85°
	90°	90°	90°	90°	90°	90°	90°	90°	90°	90°
U_{SL}=0.08	0°	0°	0°	0°	0°	0°	0°	0°	0°	0°
	5°	5°	5°	5°	5°	5°	5°	5°	5°	5°
	10°	10°	10°	10°	10°	10°	10°	10°	10°	10°

	30°	30°	30°	30°	30°	30°	30°	30°	30°	30°
	45°	45°	45°	45°	45°	45°	45°	45°	45°	45°
	60°	60°	60°	60°	60°	60°	60°	60°	60°	60°
	75°	75°	75°	75°	75°	75°	75°	75°	75°	75°
	85°	85°	85°	85°	85°	85°	85°	85°	85°	85°
	90°	90°	90°	90°	90°	90°	90°	90°	90°	90°
U_{SL}=0.1	-5°	-5°	-5°	-5°	-5°	-5°	-5°	-5°	-5°	-5°
	0°	0°	0°	0°	0°	0°	0°	0°	0°	0°
	5°	5°	5°	5°	5°	5°	5°	5°	5°	5°
	10°	10°	10°	10°	10°	10°	10°	10°	10°	10°
	30°	30°	30°	30°	30°	30°	30°	30°	30°	30°
	45°	45°	45°	45°	45°	45°	45°	45°	45°	45°
	50°	50°	50°	50°	50°	50°	50°	50°	50°	50°
	60°	60°	60°	60°	60°	60°	60°	60°	60°	60°
	75°	75°	75°	75°	75°	75°	75°	75°	75°	75°
	85°	85°	85°	85°	85°	85°	85°	85°	85°	85°
	90°	90°	90°	90°	90°	90°	90°	90°	90°	90°
U_{SL}=0.13	0°	0°	0°	0°	0°	0°	0°	0°	0°	0°
	5°	5°	5°	5°	5°	5°	5°	5°	5°	5°
	10°	10°	10°	10°	10°	10°	10°	10°	10°	10°
	60°	60°	60°	60°	60°	60°	60°	60°	60°	60°
U_{SL}=0.15	-5°	-5°	-5°	-5°	-5°	-5°	-5°	-5°	-5°	-5°
	30°	30°	30°	30°	30°	30°	30°	30°	30°	30°
	45°	45°	45°	45°	45°	45°	45°	45°	45°	45°
	50°	50°	50°	50°	50°	50°	50°	50°	50°	50°
	60°	60°	60°	60°	60°	60°	60°	60°	60°	60°
	75°	75°	75°	75°	75°	75°	75°	75°	75°	75°
	85°	85°	85°	85°	85°	85°	85°	85°	85°	85°
	90°	90°	90°	90°	90°	90°	90°	90°	90°	90°
U_{SL}=0.2	-5°	-5°	-5°	-5°	-5°	-5°	-5°	-5°	-5°	-5°
	0°	0°	0°	0°	0°	0°	0°	0°	0°	0°
	5°	5°	5°	5°	5°	5°	5°	5°	5°	5°
	10°	10°	10°	10°	10°	10°	10°	10°	10°	10°
	30°	30°	30°	30°	30°	30°	30°	30°	30°	30°
	45°	45°	45°	45°	45°	45°	45°	45°	45°	45°
	50°	50°	50°	50°	50°	50°	50°	50°	50°	50°
	60°	60°	60°	60°	60°	60°	60°	60°	60°	60°
	75°	75°	75°	75°	75°	75°	75°	75°	75°	75°
	85°	85°	85°	85°	85°	85°	85°	85°	85°	85°
	90°	90°	90°	90°	90°	90°	90°	90°	90°	90°

	U_{SG} [m/s]				
	0.29	0.58	0.88	1.18	1.47
	-5°	-5°	-5°	-5°	-5°
	0°	0°	0°	0°	0°
	5°	5°	5°	5°	5°

U_{SL}=0.2	10°	10°	10°	10°	10°
	20°	20°	20°	20°	20°
	30°	30°	30°	30°	30°
	40°	40°	40°	40°	40°
	50°	50°	50°	50°	50°
	60°	60°	60°	60°	60°
	70°	70°	70°	70°	70°
	80°	80°	80°	80°	80°
	90°	90°	90°	90°	90°

Table A.2 Test matrix for 38 mm pipe, campaign 2

	U_{SG} [m/s]									
	0.15	0.29	0.44	0.59	0.73	0.88	1.17	1.47	2.2	2.93
U_{SL}=0.73	-5°	-5°	-5°	-5°	-5°	-5°	-5°	-5°	-5°	-5°
	0°	0°	0°	0°	0°	0°	0°	0°	0°	0°
	5°	5°	5°	5°	5°	5°	5°	5°	5°	5°
	10°	10°	10°	10°	10°	10°	10°	10°	10°	10°
	20°	20°	20°	20°	20°	20°	20°	20°	20°	20°
	30°	30°	30°	30°	30°	30°	30°	30°	30°	30°
	40°	40°	40°	40°	40°	40°	40°	40°	40°	40°
	50°	50°	50°	50°	50°	50°	50°	50°	50°	50°
	60°	60°	60°	60°	60°	60°	60°	60°	60°	60°
	70°	70°	70°	70°	70°	70°	70°	70°	70°	70°
	80°	80°	80°	80°	80°	80°	80°	80°	80°	80°
	90°	90°	90°	90°	90°	90°	90°	90°	90°	90°

Table A.3 Test matrix for 67 mm pipe

	U_{SG} [m/s]							
	0.15	0.29	0.44	0.88	1.17	1.47	2.2	2.93
U_{SL}=0.73	-5°	-5°	-5°	-5°	-5°	-5°	-5°	-5°
	0°	0°	0°	0°	0°	0°	0°	0°
	5°	5°	5°	5°	5°	5°	5°	5°
	20°	20°	20°	20°	20°	20°	20°	20°
	30°	30°	30°	30°	30°	30°	30°	30°
	45°	45°	45°	45°	45°	45°	45°	45°
	60°	60°	60°	60°	60°	60°	60°	60°
	80°	80°	80°	80°	80°	80°	80°	80°
	90°	90°	90°	90°	90°	90°	90°	90°

Appendix B

Rig operating procedure

B.1 Start up and shout down procedure

1. Examine the different parts of the apparatus to make sure they are in good condition. This includes checking the flow meters, pressure gauges, valves, pipes, flexible hoses, pump and the tanks.
2. Make sure that the liquid supply tank contains enough water or solution for the operation, that is it should not have a low liquid level.
3. Make sure that valve (X1) is open.
4. Start the air flow by opening (V1) valve and adjust flow rate to approximate correct value.
5. Open the bypass Valve (V5)
6. Turn on the pump
7. Select the appropriate flow meter and open valve (V2, V3 or V4) connected to it.
8. The rig is initially operated vertically to eliminate and control any air bubbles. The rig is then tilted.
9. To start controlling the gas and liquid flow rates until required values are reached.

B.2 Shout down

1. The rig should be return to the vertical position and fasten it with the large screw.

The water flow is shut down as follows:

2. Open the bypass valve (V5)

3. Close the flow meter valve (V2, V3 or V4)
4. Turn off the pump
5. The air flow should not be shutdown immediately so that the air discharges any water that is present in the rig to the separation tank.
6. Turn off the air by closing (V1) valve.

B.3 Emergency shut down:

1. Turn off the pump to stop water circulation.
2. Closing valve (V1) to stop the air flow.

Rig Diagrams

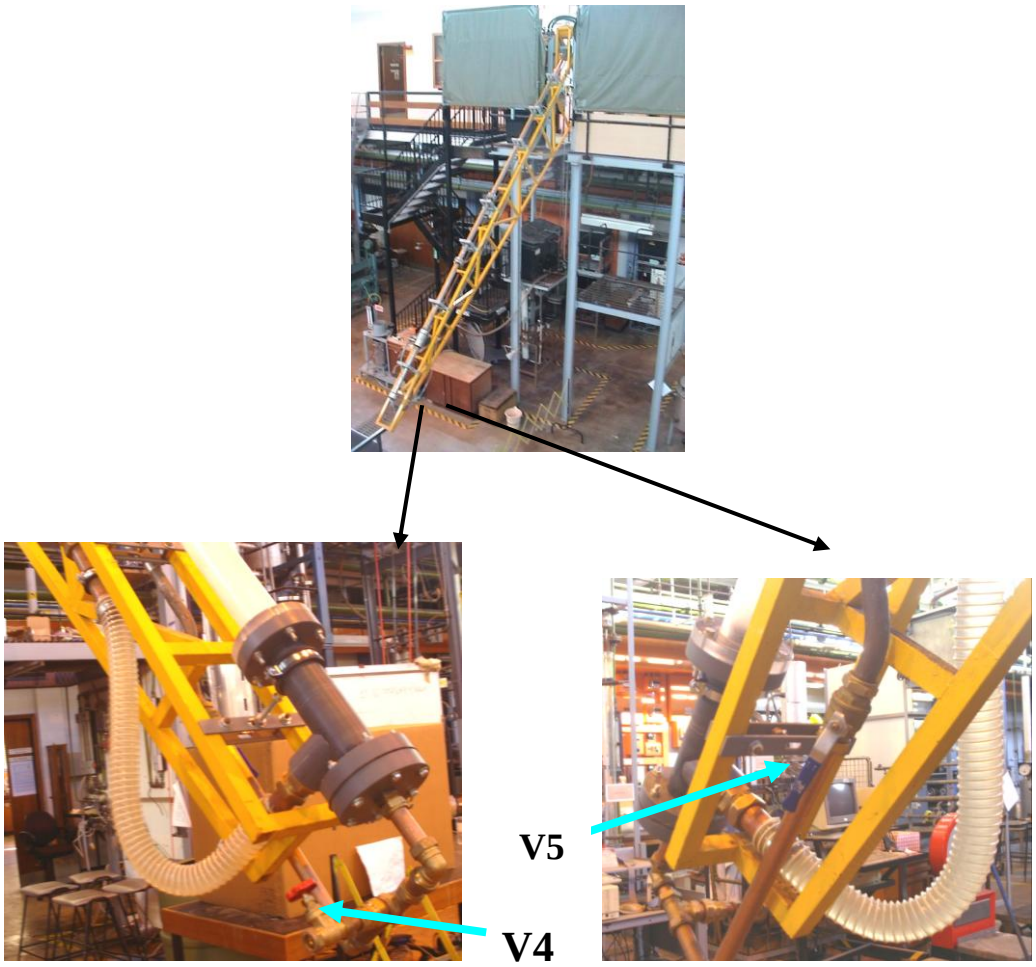

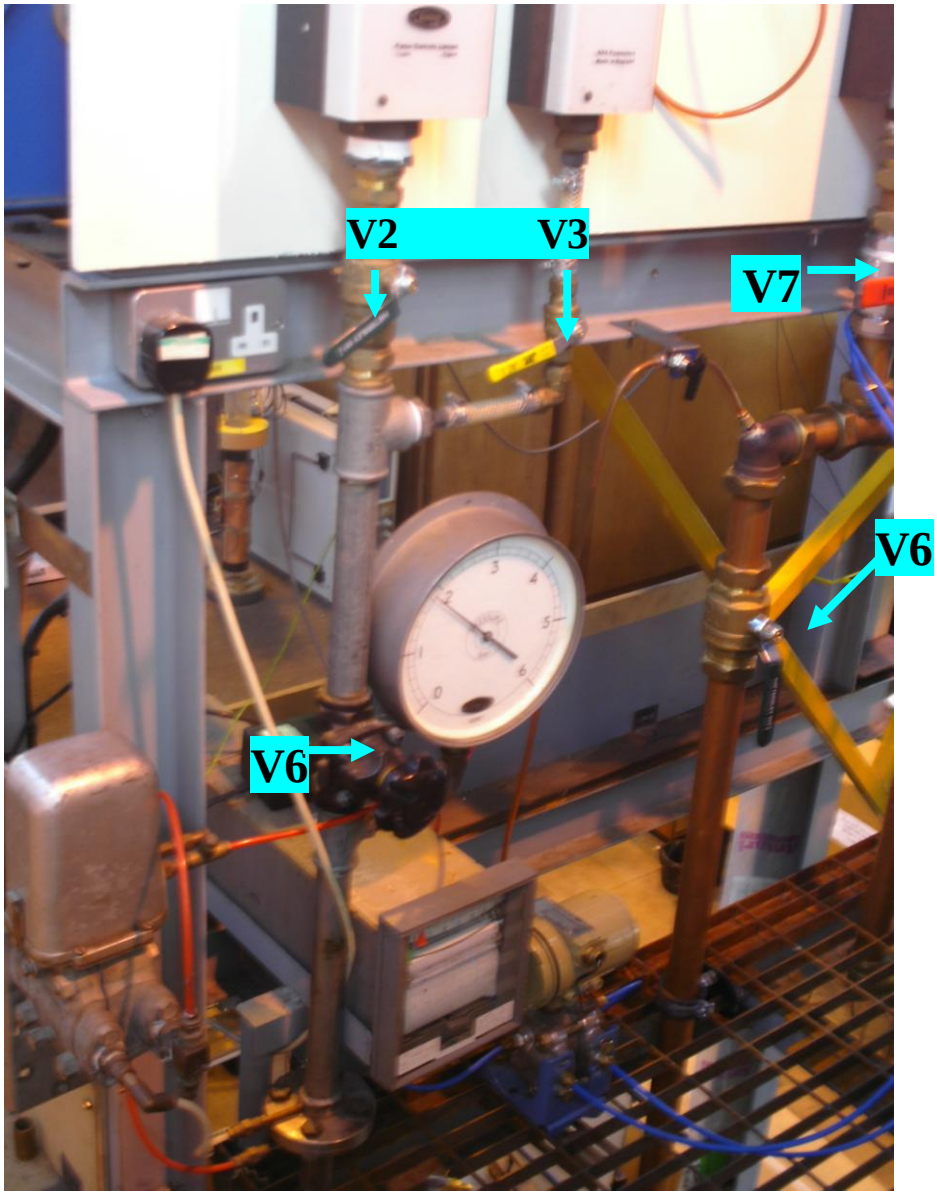
V2
V3
V7
V6
V6

Appendix C

Error analysis

The result obtained from measuring will only approach the truth. Measurement, by its nature, is inexact; the magnitude of that "inexactness" is the error. Error refers to the disagreement between a measurement and the true or accepted value. Since we must know the true or correct value to discuss the error, the concept of error is not that important in the discussion of experimental results and the concept of uncertainty is introduced.

$$Measured\ value = True\ value + Error$$

Uncertainty of a measured value is an interval around that value such that any repetition of the measurement will produce a new result that lies within this interval. This uncertainty interval is assigned following established principles of uncertainty estimation.

C.1 Estimation of the measurement uncertainty interval:

One possible way to find the uncertainty interval for each variable would be to repeat each measurement many times. The result would be a distribution of data for each variable. This distribution of data values is often represented by showing a single data point, representing the mean value of the data, and error bars to represent the overall distribution of the data. The data scatter for a normal distribution is characterized by the standard deviation, σ. The uncertainty interval for each measured variable, x_i, may be stated as $\pm n\sigma_i$, where n=1, 2 or 3. For normally distributed data, over 99 percent of measured values of x_i lie within $\pm 3\sigma_i$, of the mean value, 95 percent lie within $\pm 2\sigma_i$, and 68 percent lie within $\pm \sigma_i$, of the mean value data set. Thus it would be possible to quantify expected errors within any desired confidence limit if a statistically

significant sample were available.

The method of repeated measurements usually is impractical. In most applications, usually it is impossible to obtain enough data for a statistically significant sample owing to the excessive time and cost involved. However, the normal distribution suggests several important concepts: Small errors are more likely than large ones, plus and minus errors are about equally likely, no finite maximum error can be specified.

C.3 Sample calculation

In this section we present an example for the determination of the uncertainty for the measurements based on the concepts introduced above. For this sample let us consider a flow condition where the gas superficial velocity, U_{sg}, is 2.9 m/s, the liquid superficial velocity, U_{sl}, is 0.7 m/s, the air inlet pressure, P_{inlet}, is 1.6 bara and the pressure difference between the two tappings, ΔP_{cell}, is 1.05 kPa.

The measurements are used to calculate some result, *R*, for the experiment. Therefore it is necessary to analyse how errors in the x_is, propagate into the calculation of *R*. In general *R*, may be expressed mathematically as R(x_1, x_2, . . .,x_n). The effect on *R* of an error in measuring an individual x_i may be estimated by analogy to the derivative of a function. A variation, δx_i, in x_i would cause variation δR_i in *R*, Fox, R. W., McDonald, A. T., and Pritchard, P. J. (2006)

$$\delta R_i = \frac{\partial R}{\partial x_i} \delta x_i \tag{C.1}$$

The relative variation in R is

$$\frac{\delta R_i}{R} = \frac{1}{R} \frac{\partial R}{\partial x_i} \delta x_i = \frac{x_i}{R} \frac{\partial R}{\partial x_i} \frac{\delta x_i}{x_i} \tag{C.2}$$

Equation (C.2) may be used to estimate the relative uncertainty in the result due to uncertainty in x_i. Introducing the notation for relative uncertainty, we obtain

$$u_{R_i} = \frac{x_i}{R}\frac{\partial R}{\partial x_i}u_{x_i} \tag{C.3}$$

How do we estimate the relative uncertainty in R caused by the combined effects of the relative uncertainties in all the x_is. The random error in each variable has a range of values within the uncertainty interval. It is unlikely that all errors will have adverse values at the same time. It can be shown that the best representation for the relative uncertainty of the result is

$$u_R = \pm\left[\left(\frac{x_1}{R}\frac{\partial R}{\partial x_1}u_1\right)^2 + \left(\frac{x_2}{R}\frac{\partial R}{\partial x_2}u_2\right)^2 + \ldots + \left(\frac{x_n}{R}\frac{\partial R}{\partial x_n}u_n\right)^2\right]^{\frac{1}{2}} \tag{C.4}$$

C.3.1 Uncertainty on the air superficial velocity:

A reasonable estimate of the measurement uncertainty due to random error in a single sample experiment usually is plus or minus half the smallest scale division (or least count) of the instrument. If the measuring instrument is the limiting factor, we can use the manufacturer's documentation to determine its accuracy and precision.

The air superficial velocity is obtained by reading the number in the scale of the rotameter that has a least count of 5 l/min. The uncertainty in reading the air rotameter is thus, *u(Usg)* = 0.5 the least count. This error gives an uncertainty in the air superficial velocity of:

$$u(U_{sl}) = \pm 0.03 \text{ m/s} \tag{C.5}$$

The fraction uncertainty is, therefore:

$$\frac{u(U_{sl})}{U_{sl}} = \frac{0.03}{2.9} = 0.01 = 1\% \tag{C6}$$

The air superficial velocity can be written as U_{sl} = (2.9 ± 0.01) m/s

C.3.2 Uncertainty on the liquid superficial velocity:

The liquid superficial velocity is obtained by reading the number in the scale of the liquid rotameter that has a least count of 10 l/min. The uncertainty in reading the liquid rotameter is, *u(Usl)* = 0.5 the least count . This error gives an uncertainty in the liquid superficial velocity of:

$$u(U_{sl}) = \pm 0.06 \text{ m/s} \tag{C.7}$$

The fraction uncertainty is, therefore:

$$\frac{u(U_{sl})}{U_{sl}} = \pm \frac{0.06}{0.7} = \pm 0.08 = \pm 8\% \tag{C.8}$$

The liquid superficial velocity can be written as U_{sl} = (0.7 ± 0.06) m/s

C.3.3 Uncertainty on the mixture velocity:

The mixture velocity is obtained from the addition of the gas and liquid superficial velocities.

$$U_m = U_{SL} + U_{SG} \tag{C.9}$$

The propagation of the uncertainty from the gas and liquid superficial velocity gives:

$$u(U_m) = \pm \sqrt{u(U_{SL})^2 + u(U_{SG})^2} = \pm \sqrt{0.06^2 + 0.03^2} = \pm 0.067 \; m/s \tag{C.10}$$

The fraction uncertainty is, therefore:

$$\frac{u(U_m)}{U_m} = \pm \frac{0.067}{3.6} = \pm 0.018 = \pm 1.8\% \tag{C.11}$$

The mixture velocity can be written as U_m = (3.6 ± 0.067) m/s

C.3.4 Uncertainty on the liquid holdup:

The uncertainty of the liquid holdup comes from the uncertainty of the capacitance probe. In order to determine the uncertainty of the capacitance probes, several calibrations were performed as described in Chapter 3. During calibration, we also determined robustness of equation forms and coefficients and collect sufficient data to statistically define accuracy performance limits. In addition, the capacitance probes were compared with the wire mesh sensor (Section 5.8), they performed quite similar as can be seen in Figure C.2

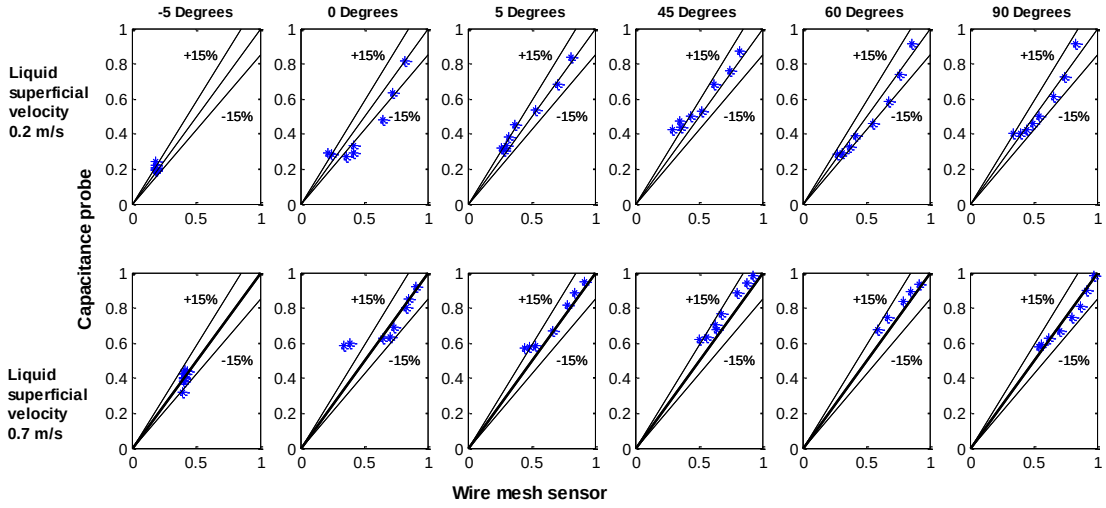

Figure C.2 Liquid holdup uncertainty

C.3.5 Uncertainty on the pressure gradient:

Manufacturers will usually specify the accuracy and precision to be expected from their equipment as a ±uncertainty. Both accuracy and precision affect how many significant digits can be reported. Precision is the ability to produce the same value within given accuracy bounds when successive readings of a specific quantity are measured.

For the pressure gradient, the uncertainty interval is given by the DP cell uncertainty, which in turn provided by the manufacturer as ± 0.025% of the range. The range is 0-70 kPa. A calibration process (Section 3.2.5) was used to check or adjust the output of a measuring device in convenient units of pressure.

Appendix D

Further flow pattern identification

In addition to the PDF of the liquid holdup, the following statistical parameters associated with the N samples of liquid holdup data were also obtained, since these parameters have been successfully used by Hasanein *et al.* (1997) among others to determine the flow pattern in small pipes.

Mean

$$\bar{\varepsilon} = \frac{1}{n}\sum_{i=1}^{n}\varepsilon_i \tag{D.1}$$

Standard deviation

$$S = \sqrt{\frac{\sum_{i=1}^{n}(\varepsilon_i - \bar{\varepsilon})^2}{n-1}} \tag{D.2}$$

Coefficient of skewness

$$S_a = \left[\sum_{i=1}^{N}(\varepsilon_i - \bar{\varepsilon})^3 / N\right] \Big/ \varepsilon^3 \tag{D.3}$$

Coefficient of kurtosis

$$K_a = \left[\sum_{i=1}^{N}(\varepsilon_i - \bar{\varepsilon})^4 / N\right] \Big/ \varepsilon^4 \tag{D.4}$$

In order to classify the PDF as to whether it is uni-modal (i.e. has one peak) or bimodal (i.e. has two peaks). These relations are:

$$K_a = (4/3) S_a^{\,2} + 2 \tag{D.5}$$

$$K_a = S_a^{\,2} + 1 \tag{D.6}$$

Equation (D.5) gives the boundary between intermittent flow and bubbly or annular flow while Equation (D.6) gives the lower bound for intermittent flows.

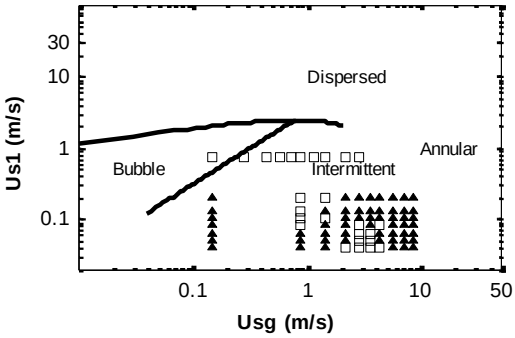

0 degrees inclination

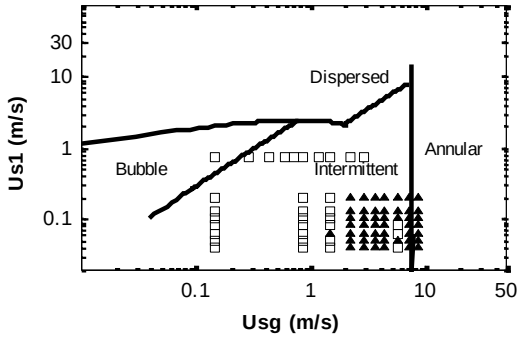

5 degrees inclination

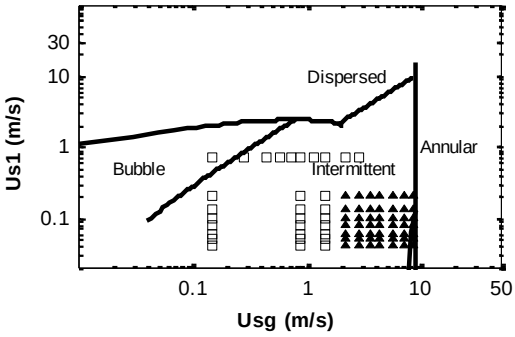

10 degrees inclination

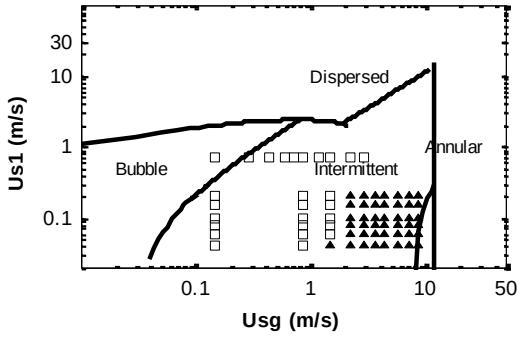

30 degrees inclination

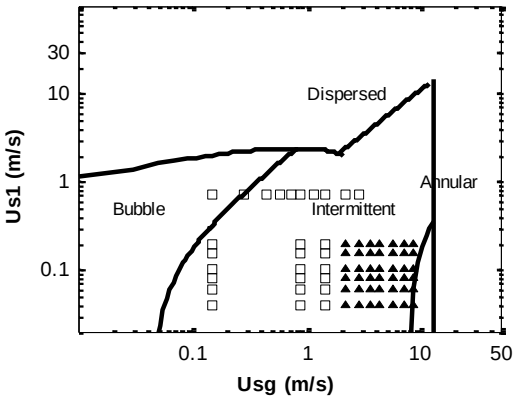

45 degrees inclination

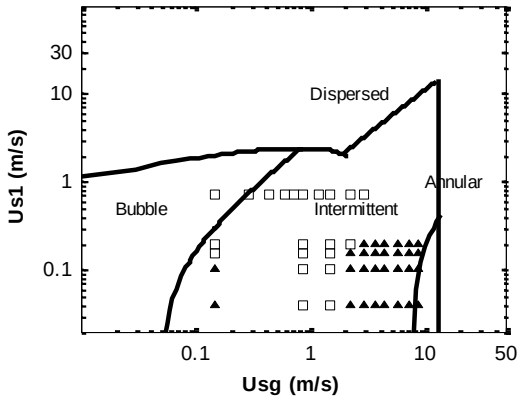

50 degrees inclination

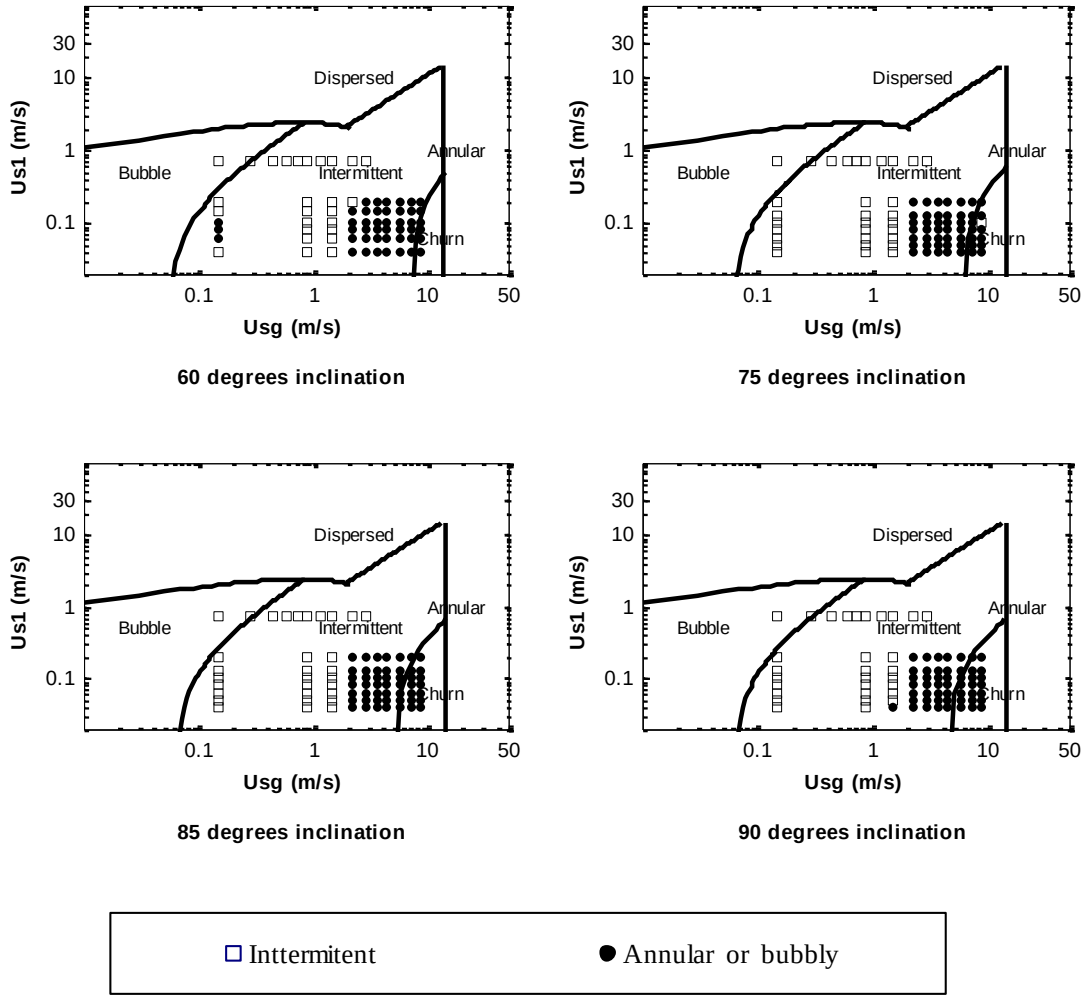

Figure D.1 Two-phase flow patterns in horizontal pipes

References

Andreussi, P. and Bendiksen, K., (1989), "**An investigation of void fraction in liquid slugs for horizontal and inclined gas-liquid pipe flow**", *International Journal of Multiphase Flow,* Vol. 15, No. 6, pp. 937-946.

Andreussi, P., Bendiksen, K. H., and Nydal O. J. (1993), "**Void distribution in slug flow**", *International Journal of Multiphase Flow,* Vol. 19, No. 5, pp. 817-828.

Ansari, A. M., Sylvester, N. D., Sarica, C., Shoham, O., and Brill, J. P., (1994), "**A Comprehensive Mechanistic Model for Upward Flow in Pipes**", *SPE Prod. Facil., Trans. AIME*, No. 297, pp. 217226.

Azzopardi, B. J., (1997), "Drops in annular two-phase flow", *International Journal of Multiphase Flow,* Vol. 23, pp. 1-53.

Azzopardi, B. J., Zaidi, S. H., and Jepson. D.M., (1997), "**Entrained fraction in inclined annular gas-liquid flow**", *ASME Int Mech. Eng. Congress and Exposition,* Dallas.

Baker, G., (2003), "**Separation and control of gas-liquid flows at horizontal T-junctions**", *Ph. D. Thesis,* University of Nottingham, Nottingham, England.

Baker, O., (1954), "**Simultaneous flow of oil and gas**", *Oil and Gas J.* Vol. 53, No. 12, pp. 185-195.

Baker, O., (1957), "**Discussion on how uphill and downhill flow affect pressure drop in two-phase pipelines in hilly country**", *Oil and Gas J.*, pp. 150-152.

Barnea, D., (1987), "**A unified model for prediction flow pattern transitions in the whole range of pipe inclination**", *International Journal of Multiphase Flow,* Vol. 13, pp. 1-12.

Barnea, D., Shoham, O., and Taitel, Y., (1982), "**Flow pattern transition for downward inclined two phase flow; horizontal to vertical**", *Chemical Engineering Science,* Vol. 37, No. 5, pp. 735-740.

Barnea, D., Shoham, O., Taitel, Y., and Dukler, A. E., (1980), " **Flow pattern transition for gas-liquid flow in horizontal and inclined pipes. Comparison of experimental data with theory**", *International Journal of Multiphase Flow,* Vol. 6, No. 3, pp. 217-225.

Barnea, D., Shoham, O., Taitel, Y., and Dukler, A. E., (1985), " **Gas-liquid flow in inclined tubes: Flow pattern transitions for upward flow**", *Chemical Engineering Science,* Vol. 40, No. 5, pp. 131-136.

Barnea, D. and Taitel, Y., (1993), "**A model for slug length distribution in gas-liquid slug flow**", *International Journal of Multiphase Flow,* Vol. 19, No. 5, pp. 829-838.

Beggs, H. D. and Brill, J. P., (1973), "**A Study of Two-Phase Flow in Inclined Pipes**", *J. Pet. Tech.,* pp. 607-617.

Bendiksen, K. H., (1984), "**An experimental investigation of the motion of long bubbles in inclined tubes**", *International Journal of Multiphase Flow,* Vol. 10, No. 4, pp. 467-483.

Benjamin, T. B., (1968), "**Gravity currents and related phenomena**", *Journal of Fluid Mechanics,* Vol. 31, pp. 209-248.

Bilicki, Z. and Kestin, J., (1987), "**Transition criteria for two-phase flow patterns in vertical upward flow**", *International Journal of Multiphase Flow,* Vol. 13, No. 3, pp. 283-294.

Bonnecaze, R. H., Erskine, W., and Grescovich, E. J., (1971), "**Holdup and pressure drop for two-phase slug flow in inclined pipelines**", *AIChE Journal*, Vol. 17, No. 5, pp. 1109-1113.

Brauner, N. and Barnea, D., (1986), "**Slug/Churn transition in upward gas-liquid flow**", *Chemical Engineering Science,* Vol. 41, No. 2, pp. 159-163.

Brauner, N. and Ullmann, A., (2004), "**Modelling of gas entrainment from Taylor bubbles. Part A: Slug flow**", *International Journal of Multiphase Flow,* Vol. 30, No. 3, pp. 239-272.

Butler, R. T., Chen, X., and Bril, J. P., (1995), "**Ratio-Arm bridge capacitance transducer for two-phase flow measurements**", *ISA International Instrumentation Symposium,* Aurora, Colorado.

Chen, J. J. J. and Speding, P. L., (1981), "**An extension of the Lockhart-Martinelli theory of two-phase pressure drop**", *International Journal of Multiphase Flow ,* Vol. 7, pp. 659-675.

Clarke, A. and Issa, R. I., (1997), "**A numerical model of slug flow in vertical tubes**", *Computers & Fluids,* Vol. 26, No. 4, pp. 395-415.

Cook, M. and Behnia, M., (2000), "**Pressure drop calculation and modelling of inclined intermittent gas-liquid flow**", *Chemical Engineering Science,* Vol. 55, No. 20, pp. 4699-4708.

Cook, M. and Behnia, M., (2001), "**Bubble motion during inclined intermittent flow**", *International Journal of Heat and Fluid Flow,* Vol. 22, No. 5, pp. 543-551.

Costigan, G. and Whalley, P. B., (1997), "**Slug flow regime identification from dynamic void fraction measurements in vertical air-water flows**", *International Journal of Multiphase Flow ,* Vol. 23, pp. 263-282.

Dukler, A. E. and Hubbard, M. G., (1975), "**A Model for Gas-Liquid Slug Flow in Horizontal and Near Horizontal Tubes**", *Ind. Eng. Chem. Fundamentals,* Vol. 14, No. 4, pp. 337-347.

Dukler, A. E., Maron D. M., and Brauner N., (1985), "**A Physical Model for Predicting the Minimum Stable Slug Length**", *Chemical Engineering Science*, Vol. 40, pp. 1379.

Fabre, J. and Liné, A., (1992), "**Modelling of Two Phase Slug Flow**", *Annu. Rev. Fluid Mech*, Vol. 24, pp. 21-46.

Flanigan, O., (1958), "**Effect of uphill flow on pressure drop in design of two-phase gathering systems**", *Oil and gas journal*, Vol. 56, No. 10, pp. 132.

Fox, R. W., McDonald, A. T., and Pritchard, P. J., (2006), "**Introduction to Fluid Mechanics**", John Wiley & Sons,

Frank, T., (2005), "**Numerical simulation of slug flow regime for an air-water two-phase flow in horizontal pipes**", *11th International Topical Meeting on Nuclear Reactor Thermal-Hydraulics (NURETH-11)*, Avignon, France.

Gambit manual., (2003), "*GAMBIT Users Guide*", FLUENT Inc., Lebanon, New Hampshire, USA, Report

Geraci, G., (2005), "**Gas-liquid Flows in Inclined Pipes and Venturis**", *Ph. D. Thesis*, University of Nottingham, Nottingham England.

Geraci, G., Azzopardi, B. J., and Van Maanen, H. R. E., (2007a), "**Inclination effects on circumferential film flow distribution in annular gas/liquid flows**", *AIChE Journal*, Vol. 53, No. 5, pp. 1144-1150.

Geraci, G., Azzopardi, B. J., and Van Maanen, H. R. E., (2007b), "**Effect of inclination on circumferential film thickness variation in annular gas/liquid flow**", *Chemical Engineering Science*, Vol. 62, No. 11, pp. 3032-3042.

Gomez, L. E., Shoham, O., and Taitel, Y., (2000), "**Prediction of slug liquid holdup horizontal to upward vertical flow**", *International Journal of Multiphase Flow*, Vol. 26, pp. 517-521.

Gould, T. L., Tek, M. R., and Katz, D. L., (1974), "**Two-phase flow through vertical, inclined or curved pipes**", *J. Pet. Tech.*, Vol. 19, pp. 815-828.

Govier, G. W., Radford, B. A., and Dun, J. S. C. , (1957), "**The upward flow of air-water mixture. I Effect of air and water rates on flow pattern, holdup and pressure drop.**", *Canadian Journal of Chemical Engineering*, Vol. 35, pp. 58-70.

Govier, G. W. and Short, W. L., (1958), " **The upward vertical flow of air-water mixture. II Effect of tubing diameter on flow pattern, holdup and pressure drop**", *Canadian Journal of Chemical Engineering*, Vol. 36, pp. 195.

Gregory, G. A., (1974), "**Comments on the predictions of liquid holdup for gas-liquid flow in inclined pipes**", *The Canadian Journal of chemical*

engineering, Vol. 52, pp. 438-448.

Gregory, G. A. and Mattar, L., (1973), "**An In-Situ Volume Fracture Sensor for Two-Phase Flows of Non-Electrolytes**", *The Journal of Canadian Petroleum Technology*, pp. 1-5.

Gregory, G. A., Nicholson, M. K., and Aziz, K., (1978), "**Correlation of the liquid volume fraction in the slug for horizontal gas-liquid slug flow**", *International Journal of Multiphase Flow*, Vol. 4, No. 1, pp. 33-39.

Gregory, G. A. and Scott, D. S., (1969), "**Correlation of liquid slug velocity and frequency in horizontal co-current gas-liquid slug flow**", *AIChE Journal* , Vol. 15, pp. 833-835.

Grescovich, E. J. and Shrier, A. L., (1971), "**Pressure drop and holdup in horizontal slug flow**", *AIChE Journal*, Vol. 17, No. 5, pp. 1214-1219.

Greskovich, E. J., (1973), "**Prediction of gas-liquid hold-up for inclined flows**", *AIChE Journal* , Vol. 19, No. 5, pp. 1060-1061.

Greskovich, E. J. and Shrier, A. L., (1972), "**Slug frequency in horizontal gas-liquid slug flow**", *Ind. Eng. Chem. Proc. Design Dev.*, Vol. 11, No. 2, pp. 317-318.

Griffith, P. and Wallis, G. B., (1961), "**Two-phase slug flow**", *Trans. ASME Journal of Heat Transfer*, Vol. 83, pp. 307-320.

Grolman, E. and Fortuin, Jan M. H., (1997), "**Liquid hold-up, pressure gradient, and flow patterns in inclined gas-liquid pipe flow**", *Experimental Thermal and Fluid Science*, Vol. 15, No. 3, pp. 174-182.

Guzhov, A. I., Mamayev, A. A., and Odishariya G.E., (1967), "**A study of transportation in gas-liquid systems**", *10th Intern. Gas Conf. Hamburg Germany*,

Hasan, A. R. and Kabir, C. S., (1988), "**Predicting multiphase flow behaviour in a deviated well**", *SPEPE*, pp. 474.

Hasanein, H. A., Kawaji, M., Chan, A. M. C., and Yoshioka, Y., (1997), "Flow regime identification of steam-water flow in a large vertical pipe at elevated pressures", 1997 ASME Fluids Engineering Division Summer Meeting FEDSM97-3558.

Hernández-Pérez, V. and Azzopardi, B. J., (2006), "**Effect of inclination on gas-liquid flows**", *10th Int. Conf. "Multiphase Flow in Industrial Plant*, Tropea, Italy .

Heywood, N. I. and Richardson, J. F., (1979), "**Slug Flow of Air-Water Mixtures in a Horizontal Pipe: Determination of Liquid Hold-up by -ray Absorption**", *Chemical Engineering Science*, Vol. 34, pp. 17-30.

Hirt, C. W. and Nichols, B. D., (1981), "**Volume of Fluid (VOF) Method for the**

Dynamics of Free Boundaries", *J. Comp. Phys.*, Vol. 39, pp. 201.

Huang, S. M., Stott, A. L., Green R. G., and Beck, M. S., (1988), "**Electronic Transducers for Industrial Measurement of Low Value Capacitance**", *J. Phys. E: Sci. Instrum.*, Vol. 21, pp. 212-250.

Hubbard, M. G., (1965), "**An analysis of horizontal gas-liquid slug**", *Ph. D. Thesis, University of Houston, Houston USA* .

Hubbard, M. G. and Dukler, A. E., (1966), "**The characterization of flow regimes for horizontal two-phase flow I. Statistical Analysis of Wall Pressure Fluctuations**", *Proceedings Heat transfer and fluid mechanics Institute. Standford University Press,* pp. 385-400.

Issa, R. I., (1986), "**Solution of the implicitly discretised fluid flow equations by operator splitting**", *J. Computational Physics*, Vol. 62, No. 1, pp. 40-65.

Jepson, W. P. and Taylor, R. E., (1993), "**Slug flow and its transitions in large-diameter horizontal pipes**", *International Journal of Multiphase Flow*, Vol. 19, No. 3, pp. 411-420.

Jones, Jr. O. C. and Zuber, N., (1975), "**The interrelation between void fraction fluctuations and flow pattern in two-phase flow**", *International Journal of Multiphase Flow*, Vol. 2, pp. 273-306.

Kaji, R., Omebere-Iyari, N. K., Hernandez-Perez, V., and Azzopardi, B. J., (2007), "**The effect of pipe diameter on flow pattern in vertical upflow**", *6th Int. Conf. Multiphase Flow*, Leipzig, Germany .

Kaya, A. S., Sarica, C., and Brill, J. P., (2001), "**Mechanistic modelling of two-phase flow in deviated wells**", *SPEPF*, Vol. 156,

Kokal, S. L. and Stanislav, J. F., (1989), "**An experimental study of two-phase flow in slightly inclined pipes II. Liquid holdup and pressure drop**", *Chemical Engineering Science*, Vol. 44, No. 3, pp. 681-693.

Kordyban, E. S., (1961), "**A model for two-phase slug flow in horizontal tubes**", *Journal of Basic Engineering, Transactions of the ASME,* Vol. pp. 613-618.

Kordyban, E. S., (1985), "**Some Details of Developing Slugs in Horizontal Two-Phase Flow**", *AIChE J.*, Vol. 31, pp. 802 .

Kouba, G. E., (1986), "**Dynamic calibration of two types of capacitance sensors used in measuring liquid holdup in two-phase**", *Proceedings of the 32nd ISA International*, Seattle.

Kouba, G. E., (1987), "**Horizontal slug flow modelling and metering**", *PhD thesis. Dept. of petroleum engineering. University of Tulsa*, Vol.

Kouba, G. E., Shoham, O., and Brill, J. P., (1990), "**A nonintrusive flow metering method for two-phase intermittent flow in horizontal pipes**", *SPE*

Production Engineering, Vol. pp. 373-380.

Kvicinsky, S., Longatte, F., Kueny, J. L., and Avellan, F., (1999), "**Free surface flows: Experimental validation of Volume of Fluid (VOF) method in the plane wall case**", *Proceedings of the 3rd ASME, JSME Joint fluids Engineering Conference*, San Francisco, California.

Lakehal, D., Meier, M., and Fulgosi, M., (2002), "**Interface tracking towards the direct simulation of heat and mass transfer in multiphase flows**", *International Journal of Heat and Fluid Flow,* Vol. 23, pp. 242-257.

Launder, B. and Spalding, D., (1974), "**The numerical computation of turbulent flows**", *Computer Methods in Applied Mechanics and Engineering* , Vol. 3, pp. 269-289.

Lun, I., Calay, R. K., and Holdo, A. E., (1996), "**Modelling two-phase flows using CFD** ", *Applied Energy,* Vol. 53, No. 3, pp. 299-314.

Malnes, D., (1983), "**Slug flow in vertical, horizontal and inclined pipes**", *Tech. Rep. IFE/KR/E-83/002 Rev. 1987, Institute for Energy Technology*.

Mandhane, J. M., Gregory, G. A., and Aziz, K., (1974), "**A flow pattern map for gas-liquid flow in horizontal pipes**", *International Journal of Multiphase Flow,* Vol. 1, pp. 537.

Manolis, I G., Mendes-Tatsis M A. , and Hewitt, G F., (1995), "**The effect of pressure on slug frequency on two-phase horizontal flow**", *The 2nd conference on multiphase flow, Kyoto, Japan, April 3-7, 1995*.

Mao, Z. S. and Dukler, A. E., (1990), "**The motion of Taylor bubbles in vertical tubes. I. A numerical investigation for the shape and rise velocity of Taylor bubbles in stagnant and flowing liquid**", *Journal of computational physics,* Vol. 91, pp. 132-160.

Marcano, R., Chen, X. T., Sarica, C., and Brill, J. P., (1996), "**A study of slug characteristics for two-phase horizontal flow**", *SPE 39856. In: Int. Petr. Conf., Mexico,* pp. 213-219.

Mattar, L. and Gregory, G. A., (1974), "**Air-oil slug flow in an upward inclined pipe I, slug velocity, holdup and pressure gradient**", *The Journal of Canadian Petroleum Technology,* pp. 69.

Moissis, R. and Griffith, P., (1962), "**Entrance effects in a two-phase slug flow**", *Journal of Heat Transfer, Trans. ASME, Series C,* Vol. 84, pp. 29-39.

Mukherjee, H. and Brill, J. P., (1985), "**Empirical equations to predict flow patterns in two-phase inclined flow**", *International Journal of Multiphase Flow,* Vol. 11, No. 3, pp. 299-315.

Ndinisa, N. V., Wiley, D. E., and Fletcher, D. F., (2005), "**Computational fluid dynamics simulations of Taylor bubbles in tubular membranes: Model**

validation and application to laminar flow systems", *Trans IChemE, Part I*, Vol. 83, No. A1, pp. 40-49.

Nicholson, M. K., Aziz, K., and Gregory, G. A., (1978), "**Intermittent two-phase flow in horizontal pipes: Predictive models**", *The Canadian Journal of chemical engineering*, Vol. 56, pp. 653-663.

Nicklin, O. J., Wilkes, J. O., and Davison, J. F., (1962), "**Two-phase flow in vertical tubes**", *Transactions of the institute of Chemical Engineers*, Vol. 40, pp. 61-68.

Nydal, O. J., (1991), "**An experimental investigation of slug flow**", *PhD thesis, University of Oslo*.

Penmatcha, V. R., Ashton, P. J., and Shoham, O., (1996), "**Two-phase stratified flow splitting at a T-Junction with an inclined branch arm**", *International Journal of Multiphase Flow*, Vol. 22, No. 6, pp. 1105-1122.

Pinto, A. M. F. R. and Campos, J. B. L. M., (1996), "**Coalescence of two gas slugs rising in a vertical column of liquid**", *Chemical Engineering Science*, Vol. 51, No. 45-54

Pinto, A. M. F. R., Coelho Pinheiro, M. N., and Campos, J. B. L. M., (1998), "**Coalescence of two gas slugs rising in a co-current flowing liquid in vertical tubes**", *Chemical Engineering Science*, Vol. 53, pp. 2973-2983.

Polonsky, S., Shemer, L., and Barnea, D., (1999), "**The relation between the Taylor bubble motion and the velocity field ahead of it**", *International Journal of Multiphase Flow*, Vol. 25, pp. 957-75.

Prasser, H. M., Bottger, A., and Zschau, J., (1998), "**A new electrode-mesh tomograph for gas-liquid flows**", *Flow measurements and Instrumentation*, pp. 111-119.

Ramos-Banderas, A., Morales, R. D., Sanchez-Perez, R., Garcia-Demedices, L., and Solorio-Diaz, G., (2005), "**Dynamics of two-phase downwards flows in submerged entry nozzles and its influence on the two-phase flow in the mold**", *International Journal of Multiphase Flow*, Vol. 31, pp. 643-665.

Reinecke, N., Petrisch, G., Boddem, M., and Mewes, D., (1998), "**Tomographic imaging of the phase distribution in a two-phase slug flow**", *International journal of multiphase flow*, Vol. 24, No. 4, pp. 617-634.

Rhee, S. H., Makarov, B. P., Krishnan, H., and Ivanov, I., (2004), "**Assessment of Numerical Techniques in Volume of Fluid Method for Free-Surface Wave Flows**", *9th Symposium on Practical Design of Ships and Other Floating Structures*, Luebeck-Travemuende, Germany.

Scott, S. L., Shoham, O., and Brill, J. P., (1986), "**Prediction of slug length in horizontal large-diameter pipes**", *In: 56th California Regional Meeting, SPE 15103*, Vol. pp. 105-114.

Scott, S. L., Shoham, O., and Brill, J. P., (1987), "**Modelling slug growth in large diameter pipes**", *In: 3rd International Conference on Multiphase Flow, The Hague, Netherlands. Vol. 1. BHRA,* pp. 55-64.

Shemer, L., Gulitski, A., and Barnea, D., (2004), "**Velocity field in the Taylor bubble wake measurements in pipes of various diameters**", *24nd European Two-phase Fow Group Meeting*, Genova.

Singh, G. and Griffith, P., (1970), "**Determination of pressure drop optimum pipe size for Two-phase slug flow in an inclined pipe**", *J. Eng. Ind., Trans. ASME,* pp. 92.

Spedding, P. L., ChenVan, J. J. J., and Nguyen, T., (1982), "**Pressure drop in two phase gas-liquid flow in inclined pipes**", *International Journal of Multiphase Flow,* Vol. 8, No. 4, pp. 407-431.

Spedding, P. L. and Nguyen, V. T., (1976), "**Regime maps for air-water two-phase flow**", *Chemical Engineering Science*, Vol. 35, pp. 779-793.

Stanislav, J. F., Kokal, S., and Nicholson, M. K., (1986), "**Intermittent gas-liquid flow in upward inclined pipes**", *International Journal of Multiphase Flow,* Vol. 12, No. 3, pp. 325-335 .

Sun, X., Kim, S., Ishii, M., and Beus, S. G., (2004), "**Modeling of bubble coalescence and disintegration in confined upward two-phase flow**", *Nuclear Engineering and Design*, No. 230, pp. 3-26.

Taitel, Y. and Barnea, D., (1990), "**A consistent approach for calculating pressure drop in inclined slug flow**", *Chemical Engineering Science*, Vol. 45, No. 5, pp. 1199-1206.

Taitel, Y., Barnea, D., and Dukler, A. E., (1980), "**Modelling flow pattern transitions for steady upward gas-liquid flow in vertical tubes**", *AIChE Journal*, Vol. 26 , No. 3, pp. 345-354.

Taitel, Y. and Dukler, A. E., (1976), "**A Model for Predicting Flow Regime Transition in Horizontal and Near Horizontal Gas-Liquid Flow**", *AIChE. Journal*, Vol. 22, No. 1, pp. 47-55.

Taitel, Y. and Dukler, A. E., (1977), "**A model for slug frequency during gas-liquid flow in horizontal and near horizontal pipes**", *International Journal of Multiphase Flow,* Vol. 3, No. 6, pp. 585-596.

Taitel, Y., Lee, N., and Dukler, A. E., (1978), "**Transient Gas-Liquid flow in horizontal pipes: Modelling the flow pattern transitions**", *AIChE Journal,* pp. 920.

Tronconi, E., (1990), "**Prediction of Slug Frequency in Horizontal Two-Phase Slug Flow**", *AIChE Journal*, Vol. 36, No. 5, pp. 701-709.

Van Hout, R., Barnea, D., and Shemer, L., (2002), "**Translational velocities of**

elongated bubbles in continuous slug flow", *International Journal of Multiphase Flow,* Vol. 28, No. 8, pp. 1333-1350.

Van Hout, R., Shemer, L., and Barnea, D., (2003), "**Evolution of hydrodynamic and statistical parameters of gas-liquid slug flow along inclined pipes**", *Chemical Engineering Science*, Vol. 58, No. 1, pp. 115-133.

Vermeulen, L. R. and Ryan, J. T., (1971), "**Two-phase slug flow in horizontal and inclined tubes**", *The Canadian Journal of chemical engineering*, Vol. 49, pp. 195-201.

Versteeg, H. K. and Malalasekera, W., (95), "**An introduction to Computational fluid Dynamics, The finite volume method**", Prentice Hall,

Wallis, G. B., (1969), "**One Dimensional Two-phase flow**", *McGraw Hill Book Company*.

Weber, M. E., (1981), "**Drift in intermittent two-phase flow in horizontal pipes**", *Canadian Journal of Chemical Engineering*, Vol. 59, pp. 398-399.

Weber, M. E., Alarie, A., and Ryan, M. E., (1986), "**Velocities of extended bubbles in inclined tubes**", *Chemical Engineering Science*, Vol. 41, No. 9, pp. 2235-2240.

Weisman, J. and Kang, S. Y., (1981), "**Flow pattern transitions in vertical and upwardly inclined lines**", *International Journal of Multiphase Flow*, Vol. 7, No. 3, pp. 271-291.

Wren, E., Baker, G., Azzopardi, B. J., and Jones, R., (2005), " **Slug flow in small diameter pipes and T-junctions** ", *Experimental Thermal and Fluid Science*, Vol. 29, No. 8, pp. 893-899 .

Zabaras, G. J., (1999), "**Prediction of slug frequency for gas-liquid flows**", *Annual Technical Conference, SPE 56462,* pp. 181-188.

Zheng, G., Brill, J. P., and Taitel, Y., (1994), "**Slug flow behaviour in a hilly terrain pipeline**", *International Journal of Multiphase Flow*, Vol. 20, No. 1, pp. 63-79.

Zuber, N. and Findlay, J. A., (1965), "**Average Volumetric Concentration in Two Phase Flow System**", *Journal of Heat Transfer*, Vol. 87, pp. 453-468.

Zukoski, E. E., (1966), "**Influence of viscosity, surface tension and inclination angle on motion of long bubbles in closed tubes**", *Journal of Fluid mechanics*, Vol. 25, pp. 821-837.